GDAŃSK UNIVERSITY OF TECHNOLOGY
Faculty of Civil and Environemental Engineering

The author of the PhD dissertation: mgr. inż. Mohammad Malikan
Scientific discipline: Mechanics of Smart Materials and Structures

DOCTORAL DISSERTATION

Title of PhD dissertation: Nonlocal Models of Plates and Shells with Applications in Micro- and Nanomechanics

Title of PhD dissertation (in Polish): Nielokalne modele płyt i powłok z zastosowaniami w mikro- i nanomechanice

Supervisor Victor Eremeev *signature*	Second supervisor No. *signature*
Prof. dr. hab. V. A. Eremeyev	
Auxiliary supervisor No. *signature*	Cosupervisor No. *signature*

Gdańsk, 2021

GDAŃSK UNIVERSITY OF TECHNOLOGY
Faculty of Civil and Environemental Engineering

STATEMENT

The author of the PhD dissertation: mgr. inż. Mohammad Malikan

I, the undersigned, agree that my PhD dissertation entitled:
"Nonlocal Models of Plates and Shells with Applications in Micro- and Nanomechanics"
may be used for scientific or didactic purposes.[1]

Gdańsk 20 Dec-2021 .....

signature of the PhD student

Aware of criminal liability for violations of the Act of 4th February 1994 on Copyright and Related Rights (Journal of Laws 2006, No. 90, item 631) and disciplinary actions set out in the Law on Higher Education (Journal of Laws 2012, item 572 with later amendments),[2] as well as civil liability, I declare, that the submitted PhD dissertation is my own work.

I declare, that the submitted PhD dissertation is my own work performed under and in cooperation with the supervision of Prof. dr. hab. V. A. Eremeyev.

This submitted PhD dissertation has never before been the basis of an official procedure associated with the awarding of a PhD degree.

All the information contained in the above thesis which is derived from written and electronic sources is documented in a list of relevant literature in accordance with art. 34 of the Copyright and Related Rights Act.

I confirm that this PhD dissertation is identical to the attached electronic version.

Gdańsk 20 Dec-2021 ....

signature of the PhD student

I, the undersigned, agree to include an electronic version of the above PhD dissertation in the open, institutional, digital repository of Gdańsk University of Technology, Pomeranian Digital Library, and for it to be submitted to the processes of verification and protection against misappropriation of authorship.

Gdańsk 20 Dec-2021 .....

signature of the PhD student

[1] Decree of Rector of Gdansk University of Technology No. 34/2009 of 9th November 2009, TUG archive instruction addendum No. 8.

[2] Act of 27th July 2005, Law on Higher Education: Chapter 7, Criminal responsibility of PhD students, Article 226.

Preface

Nowadays, the use of small-scale structures in micro/nanomachines has become more and more widespread. The most important applications of such small-sized parts are in micro-electro-mechanical systems (MEMS) as well as nano-electro-mechanical systems (NEMS) as actuators, sensors, energy harvesters. For example, nanosensors are nanoscale devices that measure physical quantities and convert these to signals that can be detected and analyzed. On the applications of micro/nanosensors in civil engineering, one can state that nanosensors can be developed and used in construction to monitor and/or control the environmental conditions and the materials/structures' performance. As an example, nanosensors can be used to monitor concrete corrosion and micro-cracking. The smart sensor can also be employed for structural health monitoring in bridges and other structures. In this regard, understanding the mechanical response of such structures in various environmental and physical situations is seriously required.

For the design and modelling of such a device, one can use various approaches. First, we mention straightforward experiments which need special equipment and result in high costs. Second, molecular dynamics could be used, which requires a lot of computational efforts, in general. Moreover, this method cannot be implemented for all types of nanostructures. Finally, the application of continuum models properly modified for modelling materials and structures at small scales is worth mentioning. Among various enhancements of classic mechanics of continua and structures, we mention the non-local approach related to the description of long-range interactions. In what follows, we apply the third technique based on non-local models and corresponding modelling to thin-walled structures as principal elements of MEMS and NEMS. Moreover, we consider the coupling between mechanical and electromagnetic fields. So this dissertation is based on this approach. Using it, the mechanical behavior of the MEMS and NEMS has been predicted.

This dissertation is organized as follows: it consists of three main parts. The problem and nonlocal continuum theories will be stated and reviewed in the first part. Here the attention to magneto-elastic phenomena is paid. The lower and higher-order magnetic effects will be considered. In the second part, the conclusions and scientific contributions are summarized, possible new works are discussed, and some novel topics are recommended. The list of main publications is also given. The third part collects those papers published in high-rank journals where the main results of the thesis were published.

Acknowledgments

The results of scientific research are never due to a single person's efforts. I would like to express my deep gratitude to my research colleagues. First, I should say thank to my supervisor Prof. Eremeyev. Thanks to him for establishing such a wonderful collaboration to conduct scientific research. I am also grateful for his supervision and support. He always made himself available to correct manuscripts and gave me his valuable comments. In addition, I wish to give my thanks to Prof. Rucka (head of the Department of Mechanics of Materials), who has always helped me with full responsibility. She has been a great boss. I appreciate her dedication and time associated to me.

Many thanks to the international collaborators of the thesis, Dr. Francesco Tornabene and Dr. Rossana Dimitri from the department of Engineering for Innovation, Università del Salento, Lecce, **Italy**. Prof. Jean-François Ganghoffer from LEM3 - UMR CNRS 7239. Université de Lorraine University of Lorraine, Nancy, **France**. Prof. Snehashish Chakraverty from the department of Mathematics, National Institute of Technology Rourkela, Sundargarh, **India**. Prof. Ömer Civalek from China Medical University, Taichung, **Taiwan**. Dr. Shahriar Dastjerdi and Dr. Bekir Akgöz from the department of Civil Engineering, Akdeniz University, Antalya, **Turkey**. Prof. Ahmed E. Abouelregal from the department of Mathematics, Mansoura University, Al Manşūrah, **Egypt**. Dr. Krzysztof Kamil Żur from Faculty of Mechanical Engineering, Bialystok University of Technology, Bialystok, **Poland**. Prof. Yaghoub Tadi Beni from Faculty of Engineering, Shahrekord University, Shahr-e Kord, **Iran**. Dr. M. E. Golmakani from the department of Mechanical Engineering, Islamic Azad University, Mashhad Branch, Mashhad, Iran. And Dr. Hamid M. Sedighi from the department of Mechanical Engineering, Shahid Chamran University of Ahvaz, Ahvaz, Iran

Streszczenie

W obecnych latach systemy mikro- i nanoelektromechaniczne (MEMS i NEMS) są szeroko stosowane w inżynierii. Przykładowo mikro/nanoczujniki można zastosować do pomiaru temperatury, wilgotności, siły, częstotliwości i ciśnienia z bardzo dużą precyzją. Materiały nanostrukturalne mogą również być stosowane jako wzmocnienie o wysokiej wytrzymałości dla zaawansowanych struktur kompozytowych. Ponieważ główne elementy MEMS i NEMS są elementami cienkościennymi, zazwyczaj są one modelowane jako konstrukcje belkowe, płytowe i powłokowe. Mechaniczne zachowanie tych elementów konstrukcyjnych w małej skali ma istotne znaczenie dla rzeczywistej mechaniki materiałów i konstrukcji. Powszechnie wiadomo, że modelowanie materiałowe materiałów w małych skalach wymaga odpowiedniego wzbogacenia modeli klasycznych. Na przykład, niektóre efekty wielkości powinny być prognozowane. Efekty te można opisać na podstawie nielokalnych modeli ciągłości, takich jak elastyczność gradientu naprężeń i odkształceń. Ponadto warto wspomnieć o różnych efektach sprzężenia, takich jak fleksoelektryczność i fleksomagnetyczność, które również są zależne od wielkości i obserwowane w nanoskali. Na przykład, flexoelektryczność jest ogólną właściwością wszystkich dielektryków i może dominować w małej skali.

Niniejsza rozprawa doktorska jest poświęcona nowemu podejściu do analiz mechanicznych struktur cienkościennych w oparciu o modele nielokalne. W rzeczywistości istnieje wiele nieznanych problemów w dziedzinie mechaniki elementów w saki mikro/nano. Nacisk położono na zastosowaniu podejścia nielokalnego do analiz dotyczących mechaniki magneto-elastycznych struktur w mikro/nanoskali. W szczególności przeprowadzono analizę dotyczącą badania odpowiedzi piezomagnetyczno-fleksomagnetycznych mikro/nanoczujników w powiązaniu z wpływami różnych warunków wewnętrznych/zewnętrznych. Te ostatnie obejmują wpływy środowiskowe (temperaturę), wibracje, obciążenia statyczne i dynamiczne, wady materiałowe (porowatość), efekty odkształceń ścinających, zewnętrzne pola magnetyczne, propagację fal, siły w płaszczyźnie i inne. Co więcej, w kilku pracach zaproponowano i zbadano inteligentny czujnik mikro/nanorozmiarowy z materiałów funkcyjnie zmiennych. Zważywszy na to, że zjawisko fleksomagnetyczności jest znacznie mniej zbadane w porównaniu z piezomagnetycznością, a nawet fleksoelektrycznością, analizy cienkich elementów fleksomagnetycznych stanowią istotną część pracy o charakterze nowatorskim. Ponieważ fleksoelektryczność odnosi się do polaryzacji elektrycznej i gradientu naprężeń, fleksomagnetyczność odpowiada wzajemnym relacjom gradientów naprężeń i namagnesowania. Oba zjawiska mogą być korzystne w małej skali. W pracy opracowano nowe modele matematyczne elementów cienkościennych (belek, płyt i powłok), uwzględniając te zjawiska i interakcje nielokalne. Zastosowane założenia kinematyczne w większości przypadków odpowiadają hipotezie Eulera-Bernoulliego lub Kirchhoffa-Love'a. Ponadto opracowano również modele odkształcalne przy ścinaniu. Efekty na małą skalę zbadano za pomocą nielokalnych modeli gradientu odkształceń. Zbadano również inne znaczące efekty, które mają kluczowe znaczenie w małej skali, takie jak efekty powierzchniowe.

Analizy zawarte w pracy zostały wykonane z wykorzystaniem różnych technik obliczeniowych, obejmujących podejście analityczne (Naviera, Galerkina), półanalityczne i numeryczne (Rayleigha-Ritza, kwadratura różnicowa). W celu rozwiązania problemów nieliniowych opracowano również nową półanalityczną metodę rozwiązywania, zwaną techniką analityczno-numeryczną, która została przeprowadzona w kilku pracach. Jednak nadaje się do niezbyt dużych ugięć. Przeprowadzono obszerną analizę literatury w celu zebrania odpowiednich danych w celu walidacji przeprowadzonych procesów matematycznych i rozwiązań dla niektórych przypadków.

Najistotniejsze wnioski opisano w sekcji podsumowującej Część II. Zawarto tam również przyszłe plany badawcze ukierunkowane na obliczenia problemów trójwymiarowych.

Słowa kluczowe rozprawy doktorskiej: Belki, płyty i powłoki; mikro/nanomechanika; Modele nielokalne; Piezomagnetyczność; Flexomagnetyczność; Rozwiązania analityczne i półanalityczne

Abstract

Nowadays, micro-and nano-electromechanical systems (MEMS and NEMS) are widely used in engineering. For example, micro/nanosensors can be deployed to measure temperature, humidity, force, frequency, and pressure with very high precision. Nanostructured materials can also be high-strength reinforcement for advanced composite structures. Usually, as principal elements of MEMS and NEMS are thin-walled elements, they are modelled as beams, plates, and shells. Thus, the mechanical behavior of these structural elements at small scales is of serious interest to the actual mechanics of materials and structures. It is well-established that material modelling of materials at small scales requires a proper enhancement of the classic models. For example, some size effects should be forecasted. These effects could be described on the base of nonlocal models of continua such as stress- and strain gradient elasticity. In addition, it is worth to mention about various coupling effects, such as flexoelectricity and flexomagneticity, which are also size-dependent and observed at the nanoscale. For example, flexoelectricity is a general property of all dielectrics and could be dominant at small scales.

Thus, this thesis is devoted to performing new mechanical analyses of thin-walled structures based on nonlocal models and representing new findings. In fact, there are vast unknown issues in the field of mechanics of micro/nanosized elements. An effort has been made to represent all of the analyses regarding the mechanics of magneto-elastic micro/nanoscale structures through the nonlocal approach. In particular, the analysis has been done on the investigation of the piezomagnetic-flexomagnetic responses of micro/nanosensors in connection with influences of various internal/external conditions. The latter include environmental impacts (temperature), vibrations, static and dynamic loads, material defects (porosity), shear deformation effects, external magnetic fields, wave propagations, in-plane forces, and others. Moreover, in a few works, an intelligent micro/nanosize sensor within a functionally graded composition has been studied to explore more efficiency of such smart parts through the new material structure. Let us note that the flexomagneticity phenomenon is much less studied in comparison with piezomagneticity or even flexoelectricity. So the study of flexomagnetic thin elements constitutes a significant novel part of the thesis. As flexoelectricity relates to the electric polarization and gradient of strains, the flexomagneticity corresponds to the interrelations of strain gradients and magnetization. Both phenomena could be beneficial at small scales. In the work, the new mathematical models of thin-walled elements (beams, plates, and shells) were developed, taking into account these phenomena and nonlocal interactions. The used kinematical assumptions in most cases correspond to Euler-Bernoulli or Kirchhoff-Love hypothesis. In addition, shear deformable models were also developed. The small-scale effects were studied by means of the nonlocal strain gradient models. Some other significant effects that are crucial at the small scales, such as surface effects, have also been investigated.

Furthermore, all the numerical results have been computed on the basis of different solution techniques, which include analytical (Navier, Galerkin residual), semi-analytical, and numerical (Rayleigh-Ritz, Differential quadrature) approaches. In order

to solve nonlinear problems, a new semi-analytical solving method has also been derived called the analytical-numerical solution technique and was carried out in a few papers. However, it suits for not very large deflections. An extensive analysis of literature was performed to collect relevant data in order to validate the performed mathematical and solution processes for some cases.

The most significant and valuable findings are briefly indicated in the conclusion section of Part II as well as future steps towards the three-dimensional problems.

Keywords of PhD dissertation: Beams, plates, and shells; Micro/Nanomechanics; Nonlocal models; Piezomagneticity; Flexomagneticity; Analytical and Semi-Analytical solutions

Contents Pages

Part I Introduction 1
I Thin-walled Structures Models with Applications to MEMS and NEMS 3
1 Beams/Plates/Shells 3
2 State of the art 6
2.1 Micro/nanomechanics 6
2.2 Magnetic structures 7
2.3 Micro/nanosensors 7
2.4 Applications of smart sensors 7
2.5 Applications in civil engineering 8
II Nonlocal models 11
1 Eringen's nonlocal elasticity theory 12
2 Nonlocal strain gradient elasticity theory 13
III Magneto-elastic coupling effects 16
1 Lower-order magneto-elastic effect 16
1.1 Piezomagneticity 16
2 Higher-order magneto-elastic effect 17
2.1 Flexomagneticity 17
Part II Summary, Discussions, Conclusions, and Outlook 19
1 Objectives of the thesis 21
2 List of published papers 21
3 Outlook of the published papers 25
4 Presented conferences 30
5 Scientific contributions of the thesis 30
6 New problems and future steps 32
Bibliography 34

Part III Publications.....40

I On the geometrically nonlinear vibration of a piezo-flexomagnetic nanotube.....42

II On nonlinear bending study of a piezo-flexomagnetic nanobeam based on an analytical-numerical solution.....72

III On instabilities and post-buckling of piezomagnetic and flexomagnetic nanostructures.....94

IV Effect of axial porosities on flexomagnetic response of in-plane Compressed piezomagnetic nanobeams.....128

V On thermal stability of piezo-flexomagnetic microbeams considering different temperature distributions.....144

VI Flexomagnetic response of buckled piezomagnetic composite Nanoplates.....173

VII Effect of surface on the flexomagnetic response of ferroic composite nanostructures; nonlinear bending analysis.....206

VIII Flexomagneticity in buckled shear deformable hard-magnetic soft structures.....237

IX Thermal buckling of functionally graded piezomagnetic micro- and nanobeams presenting the flexomagnetic effect.....273

X Torsional stability capacity of a nano-composite shell based on a nonlocal strain gradient shell model under a three-dimensional magnetic field.....299

Part I

Introduction

Chapter I

The dissertation addresses the development of new models of thin-walled structures, i.e., beams, plates, and shells, using non-local models of continua and magneto-elastic coupling. In order to discuss these topics in more details, in what follows, we briefly introduce the corresponding topics.

Thin-walled Structures Models with Applications to MEMS and NEMS

1 Beams/Plates/Shells

Beams, Plates, and Shells (Figures I.1-3)) have been considered as essential elements in engineering structures and thus have been paid significant attention by designers and researchers around the world [1]. In recent years, the extensively wide applications of these domains in several industries, including aerospace, shipbuilding, reactors, constructions, biomechanics, and many others, have required accurate approaches to analyze their mechanical behavior and begun to push the boundaries of available studied methods seriously. Heretofore, many approaches have been presented to investigate the beams, plates, and shells. These approaches included three-dimensional continuum theories and some two-dimensional procedures. Although three-dimensional elasticity analysis has confronted complexities and difficulties, it has been considered the most realistic and precise one so far. The simplest theory for analysis of the kinematic displacements is the classical hypothesis which is based on Euler-Bernoulli (for beams) and Kirchhoff's (for plates) assumptions in which the influences of transverse shear deformation are excluded. In this theory, it is supposed that each planar or perpendicular section to the mid-plane remains perpendicular on the middle surfaces during loading. This is an appropriate theory for studying thin models; however, due to the ignorance of the shear and transverse strains along with the thickness, this theory is accompanied by errors when using it for moderately thick and thick beams/plates. Therefore, another theory known as the shear deformation model is introduced to diminish the analysis's inaccuracy of relatively thick beams/plates [2]. In this theory, the transverse shear effects are taken into consideration. With regard to the number of sentences placed in the expansion of the displacement field along with the thickness, the order of the theory (first, second, etc.) is determined. Although the shear deformation theories in the analysis of thick beams/plates/shells have shown capturing the transverse shear effects and consequently reasonable results, they are still far from obtaining exact results due to the non-consideration of the effect of the transverse strain.

The first-order of the shear deformation theory called Timoshenko's (for beams) and Reissner-Mindlin's (for plates) is accompanied by a serious error (the assumption of constant value for shear stress along with the thickness of beams/plates from upper to bottom surfaces), and for that reason, the shear correction parameter has been used. This means that the assumption of constant shear stress through the entire thickness is not always correct. The most common higher-order shear deformation theory can be the third-order shear deformation theory raised by Reddy [3]. Although shear deformation theories have yielded good results in comparatively thick beams/plates/shells analysis, they are far from accurate answers yet because of the neglect of transverse strains and stretching effects across the thickness. To fix this problem and maximize the accuracy, quasi-3D elasticity came [4]. However, these theories work well only for isotropic thick materials and cannot be a general quasi-3d elasticity model appropriate for all materials such as laminated composites. Therefore, this theory complements previous theories and considers both the effects of shear and transverse deformation along with the thickness in the form of a higher-order theory.

The most capable of engineering structures, shells (Figures I.3-5), have shown a superb resistance and robustness in the matter of the ratio of strength-to-weight. Correspondingly, several scientific areas have exploited the shell structures. In the case of the shape of shell structures, there is an endless possibility, and infinite shapes shell compositions can be designed. In terms of engineering, shells can be generally divided into two classes, developable and non-developable shells. Developable shells are those that can be unrolled and flat without stretching and tearing in them, e.g., barrel shells. However, there is no ability and possibility to unroll the non-developable shells such as double curvature ones (Figure I.3). In order to generate a displacement field for a shell, it is possible to change the coordinates of the plate's deformation theories into spherical or cylindrical coordinates depending on the type of the shell.

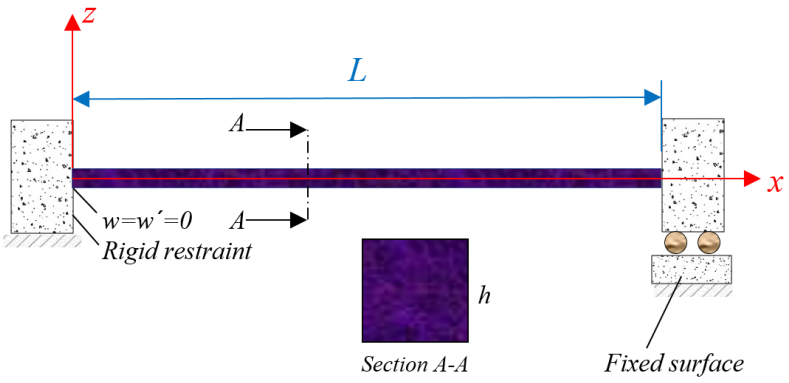

Figure I.1: A beam in the Cartesian coordinate system [5]

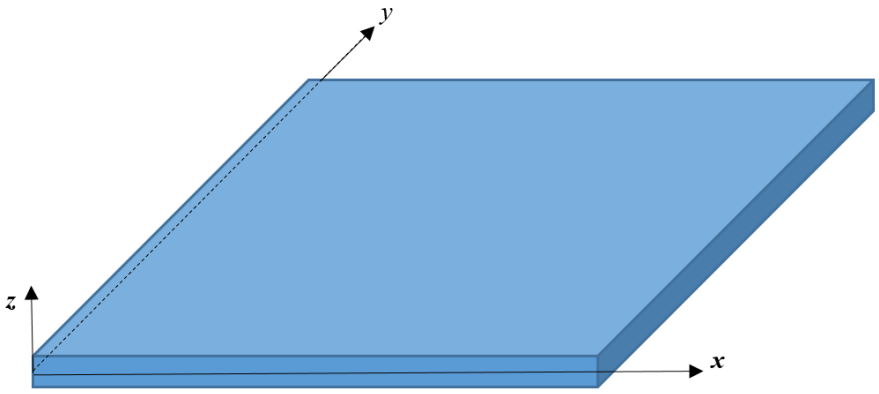

Figure I.2: A plate in the Cartesian coordinate system [6]

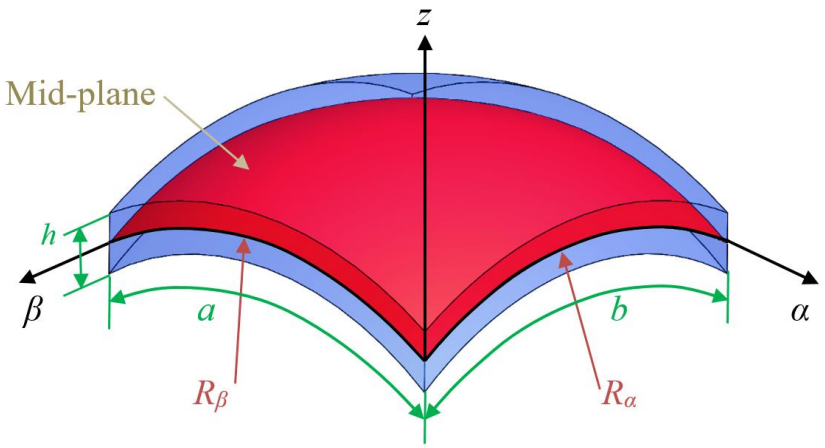

Figure I.3: A doubly-curved shell with spherical sections

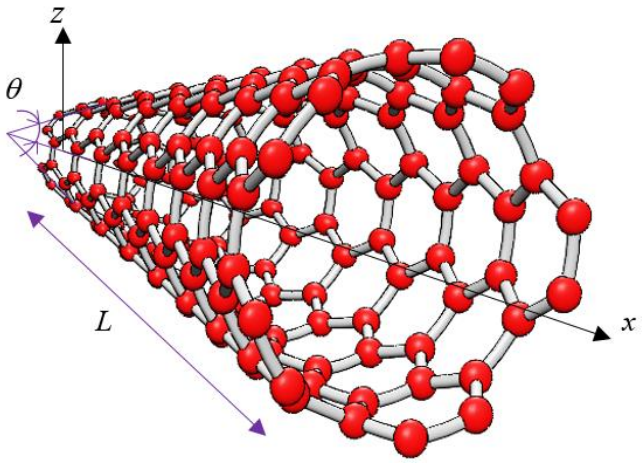

Figure I.4: A conic shell (SWCNTs) [7]

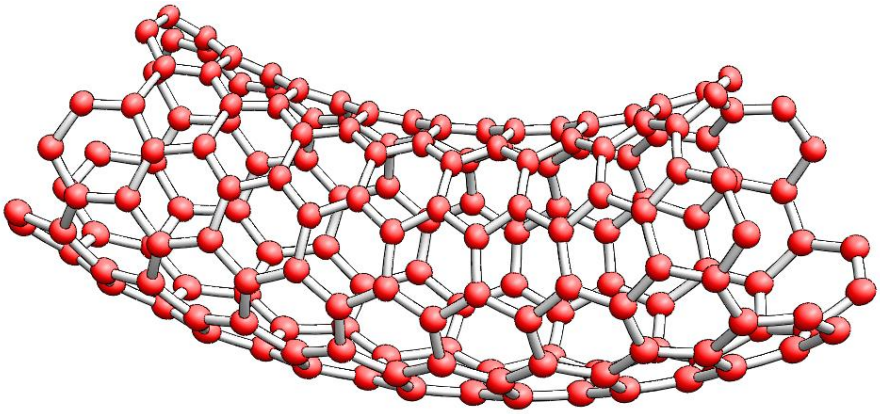

Figure I.5: A cylindrical curved shell (SWCNTs) [8]

2 State of the art

2.1 Micro/nanomechanics

Engineering knowledge always seeks to develop its boundaries to achieve the greatest benefit of human life and meet the growing needs of today, so that, without a doubt, one of the most effective tools to achieve these goals is the creation and expansion of interdisciplinary scientific fields and technology. Nanomechanical engineering is a branch of nanotechnology that studies the mechanical behaviors (structural, thermal, fluid, biological, mechatronics, etc.) of materials, structures, and systems with nano-dimensions and will pay their practical and engineering applications from an engineering point of view. This field is, in fact, an interdisciplinary field in which successful students and researchers, in addition to having classical knowledge of mechanical engineering tailored to their specific field of work, they also learn sciences related to quantum mechanics, solid-state physics, nanochemistry, and nanomaterials, nanobiotechnology, optics, electronics, etc. Various related topics can be listed under the micro/nanomechanics field as follows:

1- Atomic simulation of materials at the nanoscale (ab initio principles)
2- Experimental nanomechanics
3- Identifying the properties of nanoparticles, nanostructured materials, and structures
4- Computational nanomechanics (molecular dynamics)
5- Nano-composites (effective properties, optimization)
6- Energy transfer in nano dimensions
7- Micro and nanofluids
8- Micro and nano-electro-mechanical systems (MEMS / NEMS)
9- Bio micro and nano-electro-mechanical systems (BioMEMS / BioNEMS)
10- Nanobiomechanics
11- Basics of optics engineering and optomechanics
12- Micro and nanorobotics

2.2 Magnetic structures

In terms of magnetic properties, magnetic materials are divided into different categories: diamagnetic, paramagnetic, and ferromagnetic materials. Ferromagnetic materials are magnetic structures with high permeability, such as cobalt and iron. Ferromagnetic materials are divided into hard (e.g., $CoFe_2O_4$) and soft groups (e.g., Fe_3O_4). Hard magnetic materials are materials that become magnetized hardly ever; That is, a strong magnetic field is required to create magnetism in them. As these materials become magnetized hardly, they also lose scarcely ever their magnetic properties. These structures are suited to be used as a steady magnetic state, such as sensors and measuring instruments. Conversely, soft magnetic structures are easily magnetized and just as easily lose their magnetic properties [9-13].

$CoFe_2O_4$ magnetic nanostructures have received particular attention among different spinel ferrites, such as exclusive physical features, excellent mechanical hardness, significant magnetostrictive coefficient, high coercivity, moderate saturation magnetization, etc. [14, 15]. From a technological perspective, these characteristic properties cause the structure described above to be entirely significant, leading to its application in gas sensors, magnetic hyperthermia, biosensors, ferrofluid technology, and high-density magnetic media [16-19].

2.3 Micro/nanosensors

Micro/nanosensors have very high accuracy and responsiveness. Therefore, the sensor is a very delicate, precise, and sensitive device that is able to detect and respond to physical, chemical, and biological stimuli. The use of these types of sensors in engineering fields especially will help a lot to measure pressure, force, temperature, humidity accurately, and so on. Also, due to the advantages of wireless communication, this technology will be much cheaper, easier, and more convenient than other methods. Nanosensors used include carbon and graphene nanotubes, wireless sensors, and nanotechnology-based micro/nano-electro-mechanical systems. Nanotechnology-based micro/nano-electro-mechanical systems can, for example, measure soil temperature and humidity simultaneously. These systems consist of micro and nanosensors and an actuator that are sensitive to environmental changes. The sensor of micro-electro-mechanical systems uses the principle of shear stress to measure water vapor, in which the microsensor chip is combined with a particular nano-polymer and piezo resistor circuit, and the resulting voltages with relative humidity from zero to 100% and temperature from +30 to +100 degrees Celsius have a linear relationship. Sensor response time is speedy (about two to three minutes). For example, graphene nanofibers are suitable for fast and accurate moisture measurement [20].

2.4 Applications of smart sensors

The recognition of intelligent structures in material science and engineering applications in the last few years has taken place as the most noteworthy accomplishment by researchers all over the world. The importance of smart materials such as piezoelectric and magneto-electro-elastic ceramics in the development of advanced precise structures in material science and engineering technologies would be more explicit when noting that access to High Tech in all areas without the use of a

piece of smart ceramics in its original structures has not been possible before. The existence of electrical, electronic, chemical, mechanical, and magnetic properties of these materials have made them more and more widespread tendency in a wide range of applications as they not only transformed electronics, optics, and magnetism but also significantly changed their applications, resulting in constructing the small-scale devices with self-controlling and self-monitoring capabilities [1]. The below flowchart will briefly represent the applications of the nanosensors.

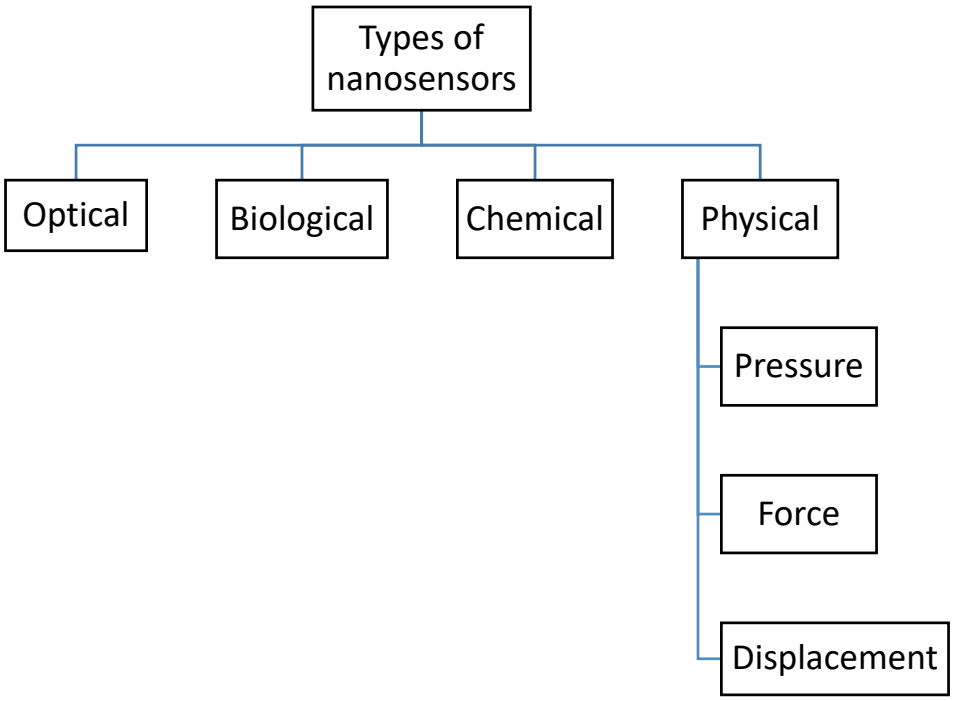

2.5 Applications in civil engineering

Civil engineering structures have a long service life and are difficult to replace once they are built. However, the performance of any civil structure can deteriorate over time. This is mainly due to aging, excessive use, overloading, environmental erosion, and lack of maintenance and inspection methods. An effective structural health monitoring system (Figures I.6-8) for civil engineering can diagnose the location and extent of defects (cracks, damage, rust, etc.) in real time so that the structure can be repaired and reinforced in time to ensure structural integrity and safety. At present, many structural health detection methods are applied to various civil engineering structures or their components, such as classical static strain (or displacement) testing, vibration identification methods, and non-destructive testing methods: acoustic emission, ultrasonic, impedance, infrared thermal imaging, pulse radar and X-ray [21]. Mentioned above methods have some limitations; for example, it is difficult to carry out real-time detection. Smart materials such as piezoelectric/piezomagnetic materials, optical fiber sensors, magnetostrictive materials, and cement-based intelligent composites all provide a new method for long-term, real-time health monitoring of civil engineering structures. These intelligent material devices have sensing, or sensing and driving the dual function, and they are integrated with the civil structure to form an intelligent structural system. Such a structural health detection system also includes signal

processing, signal interpretation software, and user interface. To achieve long-range detection, signal transmission should also be considered. Among the many smart materials, piezoelectric materials, which are mainly represented by piezoelectric ceramics, have the advantages of integrated sensing and driving integration, making them suitable for structural health monitoring. At the same time, piezoelectric/piezomagnetic materials have a fast response and good linear relationship. Most of these materials have low energy consumption, low cost, and easy processing. Therefore, the piezoelectric/piezomagnetic material working as the essential components, the development of a convenient and practical structural health monitoring system is also in line with current standard conditions. Based on the above definitions, this dissertation is devoted to researching piezoelectric/piezomagnetic micro/nano-ceramics used for structural health monitoring technology.

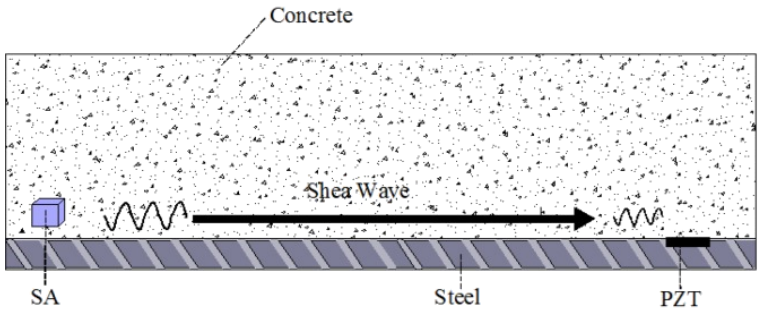

Figure I.6: Structural health monitoring with smart micro/nanobeam-like sensors (PZT) [22]

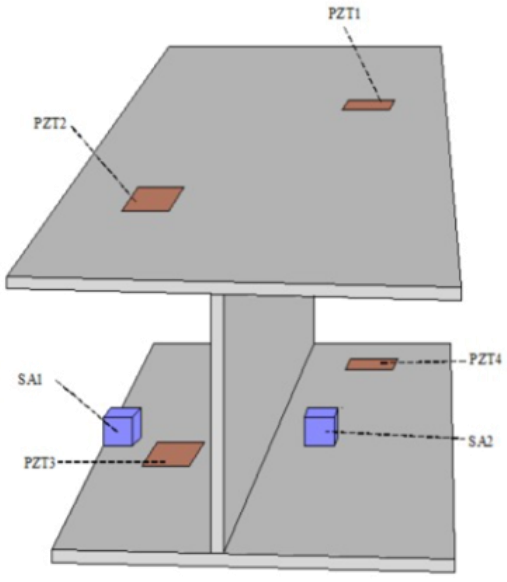

Figure I.7: Structural health monitoring for an I-shaped beam with smart micro/nano plate-like sensors (PZT1 up to PZT3) [22]

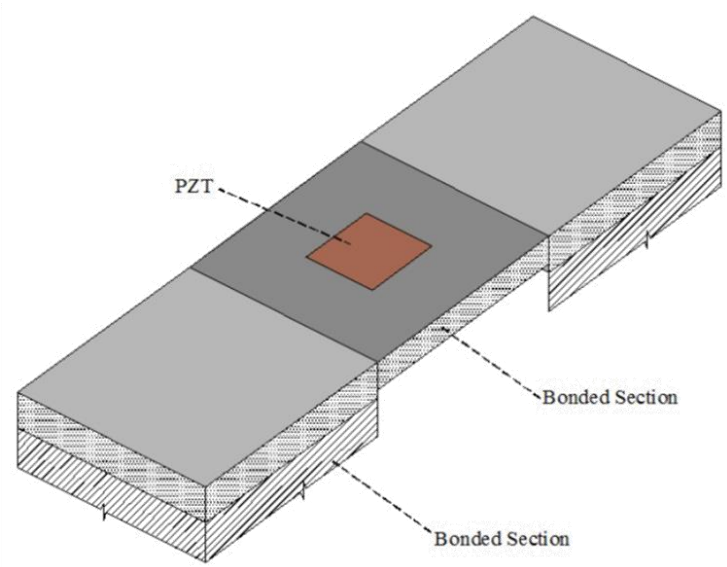

Figure I.8: Structural health monitoring for a pedestal with smart micro/nano plate-like sensors (PZT) [23]

Chapter II

Nonlocal models

Owing to the magnificent mechanical, electrical, chemical, and thermal properties of the nanostructures, they have obtained the attention of many researchers. Therefore, to exploit the incredible industrial characteristics of nanostructures, it can be highly recommended that their mechanical behavior be analyzed.

Besides experimental efforts, which may be formidable and expensive at the nanoscale, there are three main approaches for mechanical modeling of nanostructures: (a) atomistic modeling, (b) hybrid atomistic-continuum mechanics, and (c) continuum mechanics. Both atomistic and hybrid atomistic-continuum mechanics are computationally expensive and are not suitable for analyzing large-scale systems, in general. Computationally, the continuum mechanics technique is less expensive than the former two approaches. It was earned that the results of continuum mechanics are in good agreement with atomistic and hybrid approaches [24].

Upon physical view, extensive interactions between lattice atoms and large strain gradients oblige the theoretical studies on the nanoscale to a different constitutive formulation based on size-dependent continuum models. Mathematically, these models are up to differential or integral forms. From a macro scale point of view, interactions in a material plane are short and mostly between neighbor crystalline. Hence, strain non-localization implemented by nonlocal theories can help us to study large strain gradients. High contrast composite nanostructures such as FGMs may be worthy of investigation in the case of size dependency. Strain gradient phenomena occur in beam-lattice structures with homogeneity. The nanobeam/plate continua include large strain gradient resists against mechanical deformations, and because of the strain gradient, the structure's intrinsic reaction will alter. Generally, modeling the nanoscale on the basis of the strain gradient leads to accuracy in forecasting mechanical deformation of micro/nanostructures.

The influence of inter-atomic and/or intermolecular interactions must be taken into the investigation while the size of a structure is diminished from macroscale up to nanoscale. This is to precisely and properly predict the nanosize structure's mechanical response. The role of nonlocal impacts is significant in examining the mechanical behavior of small-scale domains. This property has been confirmed via simulations by molecular dynamics (MD) and experimental works.

Moreover, the nonlocal influences do not exist in the classical elasticity theory that is called local mechanics. Thus, it has been necessary to reform the local elasticity models. The size-dependent results due to the considerable interaction of atoms can be mathematically yielded by means of nonlocal models.

1 Eringen's nonlocal elasticity theory

The basis of the nonlocal elasticity theory is that the stress at a point in a continuous elastic medium depends not only on the strain at that point but on all other strains on the whole elastic domain (interactions between atoms (Figure I.9)). This position is in line with atomic theories and laboratory observations [25].

The general form of the fundamental equation in nonlocal elasticity theory involves integrals over the elastic media. This integral contains a kernel function (Figure I.10) that shows the effects of strains at different positions on stresses. The basic equations for a nonlocal and homogeneous elastic body without considering external forces are as follows [25-29]:

$$\sigma_{ij}(X) = \int_{v} k\left(\left|X' - X\right|\right) C_{ijkl}\varepsilon_{ij}\left(X'\right)dV\left(X'\right) \tag{1}$$

Respectively, $\sigma_{ij}(X)$, $k\left(\left|X' - X\right|\right)$, C_{ijkl}, and $\varepsilon_{ij}\left(X'\right)$ depicts nonlocal stresses, kernel function, fourth-order tensor of elasticity modulus, and elastic strains. Furthermore, the expression $\left|X' - X\right|$ is a Euclidean distance.

A differential form of Eq. (1) on the basis of Eringen's assumptions can be expressed as follows [25-29]:

$$\left(1 - \mu\nabla^2\right)\sigma_{ij} = C_{ijkl}\varepsilon_{ij}\ ,\ \mu(nm)^2 = (e_0 a)^2 \tag{2}$$

in which $e_0 a$ term is called nonlocal parameter and is equal to ($0 < e_0 a \leq 2$nm) [25-29]. Also, ∇^2 is the Laplace operator as follows:

$$\nabla^2 = \frac{\partial^2}{\partial x^2} + \frac{\partial^2}{\partial y^2} \tag{3}$$

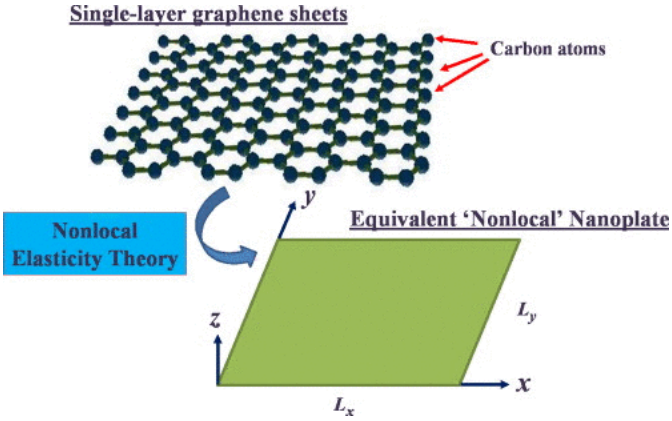

Figure I.9: Nonlocal elasticity in a plate domain [30]

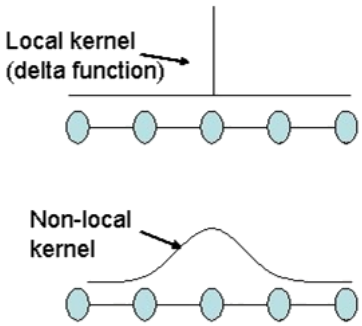

Figure I.10: Kernel function [31]

2 Nonlocal strain gradient elasticity theory

It is clear that nonlocal theories such as Eringen's nonlocal elasticity theory have been widely employed for studying nanoscale materials [32-34]. However, the ability of nonlocal elasticity theory in determining the size-dependence of nanostructures is limited due to that the strain gradient elasticity is not included in the energy density in Eringen's formulation [35], and the fact is that it can be only possible to predict the interaction effects of atoms in a domain by using the stress gradient parameter. Furthermore, unlike the nonlocal elasticity theory, the strain gradient theory enabled including the strain gradient effect by utilizing an additional factor called strain gradient length scale (SGLS) parameter. On the other hand, the modified couple stress theories are forms of strain gradient theories but have been rarely used for nanoscale materials as they only included the first strain gradient. In fact, the couple stress theories are weak in examining nanomaterials due to the lack of surface nonlocality in the theory [36].

Surface nonlocality can be defined with second gradient parameters due to the physical explanation of Laplacian, and the couple stress theories just represented the material hardness increased with decreasing material size from macro to micro [37]. On the other hand, Micro and nano tests have shown that the material hardness increased with decreasing size [38-40]. Generally, the classical continuum theory is unable to predict the size dependency since it does not possess an intrinsic material length scale.

As an explicit definition of the Laplacian operator, the Laplacian term in size-dependent theories means that the potential energy-density value at a reference point is equal to the average energy of all the points around it. In two dimensions, the around points are considered as a circle with radius R around the reference point. The primary aim of using nonlocal strain gradient theory is to synthesize stress nonlocality and strain gradient parameters in a unique theory.

It is also clear that the length scale in Eringen's nonlocal elasticity theory and the strain gradient theories (strain gradient and couple stress theories) represent two entirely different physical characteristics of materials at the nanoscale. Therefore, there has been a serious need to apply both of the length scales into a single theory so that the actual effect of the two length scales on the structural response can be assessed [41-

43]. Nonlocal strain gradient theory opened a way to develop such a size-dependent theory for investigating the nanoscale behavior. According to this non-classical hypothesis, the stress-gradient and strain-gradient parameters can be used together. In fact, by considering both second stress and strain gradient parameters, there can be a robust investigation for nanostructures.

In the present, the higher-order size-dependent theory is considered in order to reveal the length scale parameters in the aspect of the following equations [41-43]:

$$\left[1-\mu_1^2\nabla\nabla\right]\left[1-\mu_0^2\nabla\nabla\right]\sigma_{ij} = C_{ijkl}\left[1-\mu_1^2\nabla\nabla\right]\varepsilon_{kl} - C_{ijkl}\,l^2\left[1-\mu_0^2\nabla\nabla\right]\nabla\nabla\varepsilon_{kl} \tag{4}$$

$$\mu_0(nm) = e_0 a,\ \mu_1(nm) = e_1 a,\ \nabla\nabla = \frac{\partial^2}{\partial x^2} + \frac{\partial^2}{\partial y^2} \tag{5}$$

where μ_0, μ_1, and l are lower and higher-order stress nonlocality factors and strain gradient length scale (SGLS) parameter, respectively. e_0 and e_1 are nonlocal elasticity constants associated with the types of materials [44]. Also, a is a determined interior length regarding intrinsic properties of the material such as lattice parameter, connection length of two atoms, etc. [41-44]. As a matter of fact, the amounts of these three small scale parameters are independent and changeable for minor scale effects that define the dependence of mechanical responses on the structure size. Moreover, using a single separate small-scale parameter in size-dependent theories (Eringen's nonlocal elasticity, couple stress, and pure strain gradient theories) cannot appropriately predict the wide range of small-scale phenomena behavior [45-46].

Therefore, a size-dependent theory with multiple length-scale parameters was necessary to capture the size effects of structures' mechanical, electric, and magnetic behavior at the nanoscale [47]. These parameters are directly related to the internal properties of small-sized materials (granular distances, lattice parameters, and many other properties [25, 48]). Moreover, a fixed value for these parameters is not always realistic because different problems can require different values. Eq. (4) can be therefore converted into other forms of theories:

a) Eringen's nonlocal elasticity theory (ENET) [49] (strong nonlocality considering second stress gradient parameter, that is suitable for nanostructures [25]).

$$\left\{l = \mu_1 = 0 \rightarrow \left(1-\mu_0^2\nabla^2\right)\sigma_{ij} = C_{ijkl}\,\varepsilon_{kl}\right. \tag{6}$$

b) Strain gradient elasticity theory (considers the strain gradient parameter based on the first and second strain gradient parameters of Mindlin [50, 51]). As mentioned earlier, the couple stress theories are forms of strain gradient theories by taking Mindlin's first strain gradient parameter [6, 37, 52]. In couple stress theory, the cell of the material can be interpreted as a molecule of a polymer, a crystallite of a polycrystal, or a grain of a granular material [53-56]. In this theory, the unit cell is taken to be a parallelepiped to represent a crystal lattice's unit cell. The potential energy density is assumed to be a function of the strain and the curl of the strain instead of the strain alone [53-56]. In Mindlin's first strain gradient theory, the first gradient of the displacement enters the potential energy-density only in the symmetric form of strains. In fact, the potential

energy density depends on the gradient of the strain in addition to the strain itself [50, 51].

$$\left\{\mu_0 = \mu_1 = 0 \rightarrow \sigma_{ij} = C_{ijkl}\left(1 \pm l^2\nabla^2\right)\varepsilon_{kl}\right. \tag{7}$$

It is now vivid that the nonlocal continuum mechanics has been treated with two different approaches [57, 58]; the stress nonlocality (Eq. (6)) [25, 26, 48, 59] and the gradient elasticity theory (Eq. (7)) [60]. The strain gradient in Eq. (7) with the negative sign was derived from the positive-definite deformation energy density, and this model of strain gradient is stable. However, the positive sign of the strain gradient term in the equation made this term destabilizing [61, 62]. By consolidating Eq. (4), the nonlocal strain gradient elasticity theory can be achieved in the equation below.

c) Nonlocal strain gradient theory [63]:

$$\begin{cases}\mu_0 = e_0 a \\ \mu_1 = e_1 a\end{cases} \rightarrow \mu_0 = \mu_1 = \mu \rightarrow \left(1 - \mu^2\nabla^2\right)\sigma_{ij} = C_{ijkl}\left(1 - l^2\nabla^2\right)\varepsilon_{kl} \tag{8}$$

By applying nonlocal strain gradient theory, the problem might have stronger nonlocality against cases a, b by having stress-gradient and strain-gradient as second gradient parameters. It was because stress and strain gradient tensors are coupled together in the energy density of the nanomaterial. Mathematically interpreted based on the Taylor series expansion, it is permissible to incorporate the second deformation gradient (strain gradient) in the energy density to quantify size-dependent characteristics [47].

Chapter III

Magneto-elastic coupling effects

Magneto-elastic effect (ME) is a phenomenon that relates the magnetic field to elastic strains and vice versa. Among these effects, the piezomagneticity and flexomagneticity should be first mentioned among others. These effects can be linear or nonlinear with respect to external fields. Combined magnetic is a combination of magnetic tensile materials (materials that are deformed by magnetism), such as ferromagnetic materials. The microscopic mechanism determines the value of the aforesaid effect. This effect is due to coupling between the elastic strain and magnetic parameters in single-phase magneto-elastic, as observed in some multiferroics. In composite materials, this effect is due to the effect of surface coupling, such as tension. Some promising applications of the ME effect include sensitive magnetic field search, advanced logic devices, and adjustable microwave filters.

1 Lower-order magneto-elastic effect

1.1 Piezomagneticity

Piezomagnetic materials represent a particularly interesting class of smart materials, possessing highly efficient magneto-mechanical coupling, i.e., piezomagneticity, which is a unique feature for non-centrosymmetric dielectric materials (Figure I.11). A range of piezomagnetic nanoparticles has been created under various growth circumstances thanks to advancements in nanotechnology and synthesis techniques. Nanostructured materials are those with morphological features on the nanoscale in general, which are smaller than one-tenth of a micrometer in at least one direction.

Because of their nanoscale characteristics, such nanostructured materials may have unique physical and mechanical capabilities. In particular, piezomagnetic nanomaterials' enhanced electro-magneto mechanical coupling makes them attractive for potential applications as generators, sensors, and transducers, in micro and nano-electro-mechanical systems (MEMS/NEMS). In order to further explore the piezomagnetic nanomaterials and apply them commercially, it is of great importance to get a comprehensive understanding of their electro-magneto-mechanical coupling properties at the nanoscale.

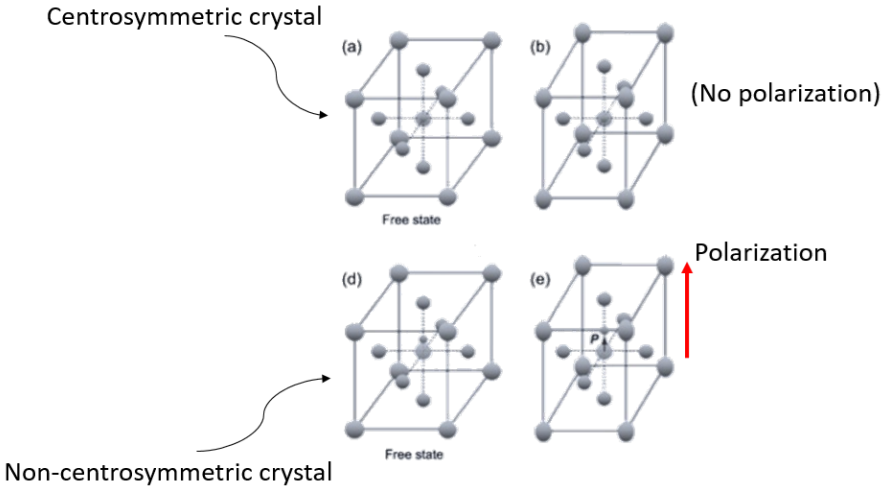

Figure I.11: PM effect [64]

2 Higher-order magneto-elastic effect

2.1 Flexomagneticity

A higher-order multiphysics impact, flexomagneticity (FM), is a novel discovery in micro/nanotechnology. To study the flexomagnetic effect and to better identify it, one can use the family close to it, that is, the piezomagnetic effect. In piezomagnetic, an internal magnetic field is created in the materials simply by compressing or stretching the structure. The piezomagnetic effect and its application can be seen in many materials and structures. However, besides these beneficial applications, there is a significant drawback; that is, this effect can only exist in about 20 crystal structures with a specific symmetrical classification. However, there is no such limit to the FM effect, and materials with broader symmetry classes can cause such a phenomenon. Therefore, the flexomagnetic effect can be powerful and effective so that it can be used in nanosensors or nanometer actuators. As a brief explanation of the FM effect, it can be noted that by bending an ionic crystal, the atomic layers are drawn inside it (Figure I.12), and it is clear that the outermost layer will have the most tension. This difference in traction in different atomic layers can cause ions to transfer to the crystal so much that they eventually create a magnetic field. In other words, strain gradient in some materials creates a magnetic field, a corresponding phenomenon called the flexomagnetic effect.

The effect of strain gradients shows that the importance of the FM effect in micro and nanosystems is comparable to that of piezomagnetic and even beyond. Additionally, unlike piezomagnetic, flexomagnetic can be found in a wider class of materials. This means that compared to piezomagnetic, which is invalid and inefficient in materials with central symmetry, there is an FM effect in all biological materials and systems. These traits have led to a growing interest in and research into the flexomagnetic effect in recent years. Currently, the role of the flexomagnetic effect in the physics of dielectrics has been investigated in some studies and has shown promising practical applications. On the other hand, the difference between theoretical

and experimental results shows a limited understanding in this field. This thesis improves the current knowledge of FM in engineering [65].

The flexomagnetic effect exists in many solid dielectrics, soft membranes, and biological filaments. The flexomagnetic effect is introduced as the effect of size-dependent electromagnetic coupling due to the presence of strain gradients and magnetic fields and promises many applications in nano-electronic devices (with strong strain gradients). Just as the piezomagnetic effect is expected to have important applications in nano-engines and particles, the FM effect can also play this role. Different fields of science are used to study nanodielectrics by considering the FM effect. These significant parts can be examined from a chemistry and physics point of view or put under a magnifier in the engineering and industrial aspects. In the engineering aspects, the study of external factors on dielectrics and their mechanical and physical behavioral responses will naturally be the criterion for evaluation. The purpose of this dissertation is to evaluate this aspect in static and dynamic analyses of micro/nano actuator beams/plates and shells [65].

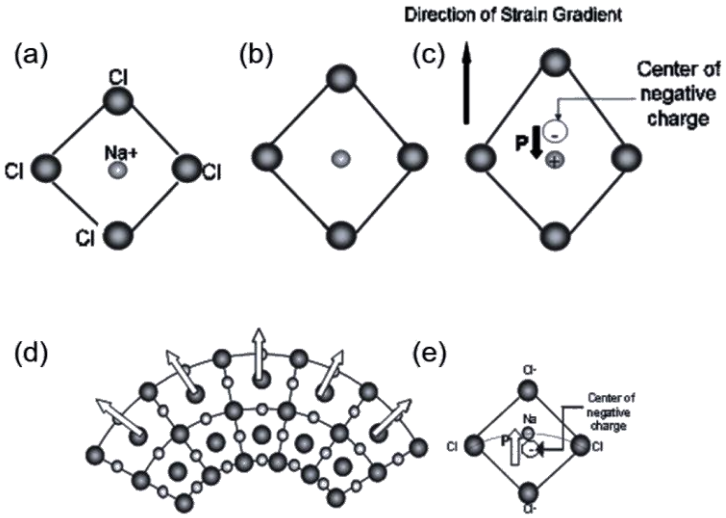

Figure I.12: FM effect [66]

Part II

Summary, Discussions, Conclusions, and Outlook

1 Objectives of the thesis

The point aim of this thesis is to provide new concepts on the nonlocal models applied to thin-walled structures. A particular attention will be paid to magneto-elastic coupling. These concepts include forecasting the mechanical response of MEMS/NEMS structures in several and different conditions. Within performing this thesis, it has now able to answer the below questions that were ambiguous before this dissertation and are helpful for MEMS/NEMS industries;

- How significant is the flexomagneticity (FM) role when a piezomagnetic nanosensor is confronted with linear and nonlinear vibrations?
- Is there any connection between shear deformations and FM in a structure?
- As the literature analyzed a piezomagnetic material containing FM based on linear bending, it has shown that FM could play a vital role in nonlinear bending and large deflections.
- How is FM in mechanical stability and post-stability situations of a micro/nanosensor?
- What will be the FM's role if a structure involves imperfection and porosities?
- What is the relationship of FM to the temperature of the environment?
- How does FM act in 2d nanostructures such as nanoplates?
- Is there any linkage between FM and surface effects through micro/nanostructures?
- Is the FM more dominant if the nanosensor is produced based on FGMs?
- What is the mechanical response of a piezomagnetic nanoshell against 3d external magnetic fields?

Moreover, the works done during this thesis also provided a new semi-analytical solution applied for nonlinear bending problems. The mentioned objectives were obtained in the chosen arbitrarily part of the thesis. As shown later, the results of the PhD works can be collected as more than one dissertation. Thus, the current results are related to this thesis's part of MEMS/NEMS.

2 List of published papers

During the work within the PhD school, various scientific activities were performed. These attempts have resulted in a series of published papers listed below. In order to present a compact and consistent study, we restricted ourselves to some of these results in the dissertation related to

- Mechanics of magneto-elastic smart micro/nanostructures (no. 1 to 13)

Note that ten works out of this topic are in the form of articles, and the rest are book chapters that are excluded in the outlook due to their shortness.

- Mechanics of electro-elastic smart micro/nanomaterials (no. 14)
- Mechanics of functionally graded materials (no. 15 to 21)
- Mechanics of carbon nanostructures (no. 22 to 35)

- Mechanics of shell structures (no. 36 to 38)
- Mechanics of thermoelastic problems (no. 39 and 40)
- Miscellaneous works (no. 41 to 43)

1. Malikan, M., & Eremeyev, V. A. (2021). Flexomagnetic response of buckled piezomagnetic composite nanoplates. *Composite Structures*, *267*, 113932. **Points: 140**

2. Malikan, M., Wiczenbach, T., & Eremeyev, V. A. (2021). Flexomagneticity in Functionally Graded Nanostructures. In book: *Advanced Materials Modelling for Mechanical, Medical and Biological Applications*, Springer Nature Switzerland AG. https://doi.org/10.1007/978-3-030-81705-3_17. **Points: 80**

3. Malikan, M., & Eremeyev, V. A. (2021). Effect of surface on the flexomagnetic response of ferroic composite nanostructures; nonlinear bending analysis. *Composite Structures*, *271*, 114179. **Points: 140**

4. Malikan, M., Wiczenbach, T., & Eremeyev, V. A. (2021). On thermal stability of piezo-flexomagnetic microbeams considering different temperature distributions. *Continuum Mechanics and Thermodynamics*, *33*, 1281-1297. **Points: 100**

5. Malikan, M., Wiczenbach, T., & Eremeyev, V. A. (2021). Thermal buckling of functionally graded piezomagnetic micro- and nanobeams presenting the flexomagnetic effect. *Continuum Mechanics and Thermodynamics*. https://doi.org/10.1007/s00161-021-01038-8. **Points: 100**

6. Malikan, M., & Eremeyev, V. A. (2021). Flexomagneticity in buckled shear deformable hard-magnetic soft structures. *Continuum Mechanics and Thermodynamics*. https://doi.org/10.1007/s00161-021-01034-y. **Points: 100**

7. Malikan, M., & Eremeyev, V. A. (2020). On Nonlinear Bending Study of a Piezo-Flexomagnetic Nanobeam Based on an Analytical-Numerical Solution. *Nanomaterials*, *10*, 1762. **Points: 70**

8. Malikan, M., Eremeyev, V. A., & Żur, K. K. (2020). Effect of Axial Porosities on Flexomagnetic Response of In-Plane Compressed Piezomagnetic Nanobeams. *Symmetry*, *12*, 1935. **Points: 70**

9. Malikan, M., Uglov, N. S., & Eremeyev, V. A. (2020). On instabilities and post-buckling of piezomagnetic and flexomagnetic nanostructures. *International Journal of Engineering Science*, *157*, 103395. **Points: 200**

10. Malikan, M., & Eremeyev, V. A. (2020). On the geometrically nonlinear vibration of a piezo-flexomagnetic nanotube. *Mathematical Methods in the Applied Sciences*. https://doi.org/10.1002/mma.6758. **Points: 100**

11. Malikan, M., Krasheninnikov, M., & Eremeyev, V. A. (2020). Torsional stability capacity of a nano-composite shell based on a nonlocal strain gradient shell model under a three-dimensional magnetic field. *International Journal of Engineering Science*, *148*, 103210. **Points: 200**

12. Malikan, M., & Eremeyev, V. A. (2020). Free Vibration of Flexomagnetic Nanostructured

Tubes Based on Stress-driven Nonlocal Elasticity. In book: *Analysis of Shells, Plates, and Beams*, Springer Nature Switzerland AG. https://doi.org/10.1007/978-3-030-47491-1_12.**Points: 80**

13. Malikan, M., & Eremeyev, V. A. (2021). On forced vibrations of piezo-flexomagnetic nano-actuator beams. In book: *Modeling and Computation in Vibration Problems*, IOP Publishing. DOI: 10.1088/978-0-7503-3483-9ch7. **Points: 80**

14. Malikan, M., & Eremeyev, V. A. (2020). On the dynamics of a visco-piezo-flexoelectric nanobeam. *Symmetry*, *12*, 643. **Points: 70**

15. Dastjerdi, S., Malikan, M., Eremeyev, V. A., Akgöz, B., & Civalek, Ö. (2021). On the generalized model of shell structures with functional cross-sections. *Composite Structures*, *272*, 114192. **Points: 140**

16. Golmakani, M. E., Malikan, M., Pour, S. G., & Eremeyev, V. A. (2021). Bending analysis of functionally graded nanoplates based on a higher-order shear deformation theory using dynamic relaxation method. *Continuum Mechanics and Thermodynamics*. https://doi.org/10.1007/s00161-021-00995-4. **Points: 100**

17. Dastjerdi, S., Malikan, M., Dimitri, R., & Tornabene, F. (2021). Nonlocal elasticity analysis of moderately thick porous functionally graded plates in a hygro-thermal environment. *Composite Structures*, *255*, 112925. **Points: 140**

18. Jena, S. K., Chakraverty, S., & Malikan, M. (2020). Application of shifted Chebyshev polynomial-based Rayleigh–Ritz method and Navier's technique for vibration analysis of a functionally graded porous beam embedded in Kerr foundation. *Engineering with Computers*, *37*, 3569-3589. **Points: 70**

19. Jena, S. K., Chakraverty, S., Malikan, M., & Sedighi, H. (2020). Implementation of Hermite–Ritz method and Navier's technique for vibration of functionally graded porous nanobeam embedded in Winkler–Pasternak elastic foundation using bi-Helmholtz nonlocal elasticity. *Journal of Mechanics of Materials and Structures*, *15*, 405–434. **Points: 70**

20. Dastjerdi, S., Tadi Beni, Y., & Malikan, M. (2020). A comprehensive study on nonlinear hygro-thermo-mechanical analysis of thick functionally graded porous rotating disk based on two quasi-three-dimensional theories. *Mechanics Based Design of Structures and Machines*, 1–30. https://doi.org/10.1080/15397734.2020.1814812. **Points: 70**

21. Malikan, M., & Eremeyev, V. A. (2020). A new hyperbolic-polynomial higher-order elasticity theory for mechanics of thick FGM beams with imperfection in the material composition. *Composite Structures*, *249*, 112486. **Points: 140**

22. Malikan, M. (2020). On the plastic buckling of curved carbon nanotubes. *Theoretical and Applied Mechanics Letters*, *10*, 46–56. **Points: 40**

23. Dastjerdi, S., & Malikan, M. (2020). Mechanical analysis of eccentric defected bilayer graphene sheets considering the van der Waals force. *Proceedings of the Institution of Mechanical Engineers, Part N: Journal of Nanomaterials, Nanoengineering and Nanosystems*. https://doi.org/10.1177/2397791420926067. **Points: 20**

24. Jena, S. K., Chakraverty, S., & Malikan, M. (2020). Vibration and buckling characteristics of nonlocal beam placed in a magnetic field embedded in Winkler–Pasternak elastic

foundation using a new refined beam theory: an analytical approach. *The European Physical Journal Plus*, *135*, 164. **Points: 70**

25. Sedighi, H. M., & Malikan, M. (2020). Stress-driven nonlocal elasticity for nonlinear vibration characteristics of carbon/boron-nitride hetero-nanotube subject to magneto-thermal environment. *Physica Scripta*, *95*, 055218. **Points: 40**

26. Sedighi, H. M., Malikan, M., Valipour, A., & Żur, K. K. (2020). Nonlocal vibration of carbon/boron-nitride nano-hetero-structure in thermal and magnetic fields by means of nonlinear finite element method. *Journal of Computational Design and Engineering*, *7*, 591-602. **Points: 70**

27. Jena, S. K., Chakraverty, S., Malikan, M., & Tornabene, F. (2020). Effects of surface energy and surface residual stresses on vibro-thermal analysis of chiral, zigzag, and armchair types of SWCNTs using refined beam theory. *Mechanics Based Design of Structures and Machines*, https://doi.org/10.1080/15397734.2020.1754239. **Points: 70**

28. Jena, S. K., Chakraverty, S., Malikan, M., & Mohammad-Sedighi, H. (2020). Hygro-Magnetic Vibration of the Single-Walled Carbon Nanotube with Nonlinear Temperature Distribution Based on a Modified Beam Theory and Nonlocal Strain Gradient Model. *International Journal of Applied Mechanics*, *12*, 2050054. **Points: 70**

29. Malikan, M., & Eremeyev, V. A. (2020). Post-critical buckling of truncated conical carbon nanotubes considering surface effects embedding in a nonlinear Winkler substrate using the Rayleigh-Ritz method. *Materials Research Express*, *7*, 025005. **Points: 70**

30. Jena, S. K., Chakraverty, S., & Malikan, M. (2020). Implementation of non-probabilistic methods for stability analysis of nonlocal beam with structural uncertainties. *Engineering with Computers*, *37*, 2957-2969. **Points: 70**

31. Jena, S. K., Chakraverty, S., & Malikan, M. (2020). Stability analysis of nanobeams in hygrothermal environment based on a nonlocal strain gradient Timoshenko beam model under nonlinear thermal field. *Journal of Computational Design and Engineering*, *7*, 685-699. **Points: 70**

32. Malikan, M., Eremeyev, V. A., & Sedighi, H. M. (2020). Buckling analysis of a non-concentric double-walled carbon nanotube. *Acta Mechanica*, *231*, 5007-5020. **Points: 100**

33. Golmakani, M. E., Ahmad Pour, M., & Malikan, M. (2021). Thermal buckling analysis of circular bilayer graphene sheets resting on an elastic matrix based on nonlocal continuum mechanics. *Journal of Applied and Computational Mechanics*, *7*, 1862-1877. **Points: 20**

34. Jena, S. K., Chakraverty, S., & Malikan, M. (2019). Implementation of Haar wavelet, higher order Haar wavelet, and differential quadrature methods on buckling response of strain gradient nonlocal beam embedded in an elastic medium. *Engineering with Computers*, *37*, 1251-1264. **Points: 70**

35. Jena, S. K., Chakraverty, S., Malikan, M., & Tornabene, F. (2019). Stability analysis of single-walled carbon nanotubes embedded in winkler foundation placed in a thermal environment considering the surface effect using a new refined beam theory. *Mechanics Based Design of Structures and Machines*, *49*, 581–595. **Points: 70**

36. Dastjerdi, S., Akgöz, B., Civalek, Ö., Malikan, M., & Eremeyev, V. A. (2020). On the non-linear dynamics of torus-shaped and cylindrical shell structures. *International Journal of Engineering Science*, *156*, 103371. **Points: 200**

37. Dastjerdi, S., Malikan, M., Eremeyev, V. A., Akgöz, B., & Civalek, Ö. (2020). Mechanical simulation of artificial gravity in torus-shaped and cylindrical spacecraft. *Acta Astronautica*, *179*, 330-344. **Points: 100**

38. Dastjerdi, S., Malikan, Akgöz, B., & Civalek, Ö., M., Eremeyev, V. A., Wiczenbach, T. (2022). On the deformation and frequency analyses of SARS-CoV-2 at nanoscale. *International Journal of Engineering Science*, *170*, 103604. **Points: 200**

39. Abouelregal, A. E., Mohammad-Sedighi, H., Shirazi, A. H., Malikan, M., & Eremeyev, V. A. (2021). Computational analysis of an infinite magneto-thermoelastic solid periodically dispersed with varying heat flow based on non-local Moore–Gibson–Thompson approach. *Continuum Mechanics and Thermodynamics*. https://doi.org/10.1007/s00161-021-00998-1. **Points: 100**

40. Abouelregal, A. E., Mohammad-Sedighi, H., Malikan, M., & Eremeyev, V. A. (2021). Nonlocalized thermal behavior of rotating micromachined beams under dynamic and thermodynamic loads. *Mathematical Methods in the Applied Sciences*. https://doi.org/10.1002/zamm.202100310. **Points: 100**

41. Golmakani, M. E., Wiczenbach, T., Malikan, M., Mahoori, S. M., & Eremeyev, V. A. (2021). Experimental and Numerical Investigation of Tensile and Flexural Behavior of Nanoclay Wood-Plastic Composite. *Materials*, *14*, 2773. **Points: 140**

42. Golmakani, M. E., Wiczenbach, T., Malikan, M., Aliakbari, R., & Eremeyev, V. A. (2021). Investigation of Wood Flour Size, Aspect Ratios, and Injection Molding Temperature on Mechanical Properties of Wood Flour/Polyethylene Composites. *Materials*, *14*, 3406. **Points: 140**

43. Alibakhshi, A., Dastjerdi, S., Malikan, M., Eremeyev, V. A. (2021) Nonlinear Free and Forced Vibrations of a Hyperelastic Micro/Nanobeam Considering Strain Stiffening Effect. *Nanomaterials*, *11*, 3066. **Points: 70**

3 Outlook of the published papers

Developing studies on the mechanical behavior of micro/nano-electro-mechanical systems (MEMS/NEMS) based on the nonlocal media models and thin-walled structural mechanics was the main objective of this dissertation. In addition, magneto-elastic coupling was considered. This thesis, albeit theoretical, can help designers of micro/nanosensors and actuators produce a highly efficient and accurate tool. To do this, the sensors have been mathematically built based on the beam, plate, and shell geometries. The models of the intelligent structures have been established dependent on the thin and moderately thick beam/plate approaches. Furthermore, many conditions have been investigated to predict the sensors' mechanical response. There are ten published papers in Part II consisting of the studies as mentioned earlier explained in the following.

1. Malikan, M., & Eremeyev, V. A. (2020). On the geometrically nonlinear vibration of a piezo-flexomagnetic nanotube. *Mathematical Methods in the Applied Sciences*. https://doi.org/10.1002/mma.6758

The first work examined the nonlinear natural frequencies of a nanosensor in the form of nanotubes. This investigation contained the Euler-Bernoulli hypothesis and accomplished the small-scale effects on the basis of nonlocal strain gradient theory. The obtained nonlinear partial differential relations were converted into algebraic ones concerning the Rayleigh-Ritz technique. Several boundary conditions were imposed, such as clamped, simple, and their combination. Finally, the results have been verified by using the literature regarding nonlinear vibrations of a macro/local beam.

In this work, the authors' contributions are as follows:
Mohammad Malikan: Conceptualization, Methodology, Investigation, Software, Visualization, Validation, Data curation, Resources, Formal analysis, Original draft. **Victor A. Eremeyev:** Investigation, Review & editing, Supervision, Funding acquisition.

2. Malikan, M., & Eremeyev, V. A. (2020). On Nonlinear Bending Study of a Piezo-Flexomagnetic Nanobeam Based on an Analytical-Numerical Solution. *Nanomaterials*, *10*, 1762. https://doi.org/10.3390/nano10091762

The second work is a well-considered paper by which the first time of investigating FM in a nonlinear bending analysis has been demonstrated. Both piezomagnetic and flexomagnetic effects have been taken into account together for a reduced scale thin beam. The geometrical nonlinearity which induces the large deformations was also assessed. Applying the variational formulation derived the favorable governing equations. The NSGT was inserted into the mathematical model to capture the consistent nanoscale effect. Transmuting the acquired relations based on the NSGT into the displacement relationship granted an eligible equation, which stood to compute large deflections. The translation and shifting of the nonlinear system of ordinary differential equations into the algebraic ones have been performed based on the Galerkin weighted residual method (GRWM). The GRWM concerning an analytical flow estimated clamped, simply-supported, and free end conditions. Afterward, the numerical solution regarding the Newton-Raphson technique (NRT) was investigated.

In this work, the authors' contributions are as follows:
Mohammad Malikan: Conceptualization, Methodology, Investigation, Software, Visualization, Validation, Data curation, Resources, Formal analysis, Original draft. **Victor A. Eremeyev:** Investigation, Review & editing, Supervision, Funding acquisition.

3. Malikan, M., Uglov, N. S., & Eremeyev, V. A. (2020). On instabilities and post-buckling of piezomagnetic and flexomagnetic nanostructures. *International Journal of Engineering Science*, *157*, 103395. https://doi.org/10.1016/j.ijengsci.2020.103395

The third paper is a simultaneous study for buckling and post-buckling of magnetic

nanosensors. It was supposed that the sensor has been made of cobalt-ferrite structures. The results have been discussed while the magnetic nanoparticle accommodated flexomagneticity influence. The mathematical model has been established in regard to the Euler-Bernoulli beam, nonlinear Lagrangian-von Kármán strains, and nonlocal strain gradient theory. The stability and post-stability were analytically evaluated for variations in size-dependent parameters, slenderness ratio, the magnetic field in the absence and presence of the FM when the boundary conditions of the beam-like nanosensor were differed.

In this work, the authors' contributions are as follows:
Mohammad Malikan: Conceptualization, Methodology, Investigation, Software, Visualization, Validation, Data curation, Resources, Formal analysis, Original draft. **N. S. Uglov:** Original draft, **Victor A. Eremeyev:** Investigation, Review & editing, Supervision, Funding acquisition.

4. Malikan, M., Eremeyev, V. A., & Żur, K. K. (2020). Effect of Axial Porosities on Flexomagnetic Response of In-Plane Compressed Piezomagnetic Nanobeams. *Symmetry*, *12*, 1935. https://doi.org/10.3390/sym12121935

The fourth study presented the stability capacity of a porous nanosensor beam involving piezomagnetic as well as flexomagnetic properties. To date, it is known that the mechanism of action of nanostructures is based on two principles of hardening and softening. This research applied these features to a piezo-flexomagnetic nanobeam. Substituting Lagrangian and nonlocal theory of strain gradient elasticity, the stability relation of the piezo-flexomagnetic nanobeam was obtained. Thereafter, the Navier method expanded numerical amounts of the in-plane static buckling of the nanosize sensor in the presence of imperfections.

In this work, the authors' contributions are as follows:
Mohammad Malikan: Conceptualization, Methodology, Investigation, Software, Visualization, Validation, Data curation, Resources, Formal analysis, Original draft. **K. K. Ż:** Funding acquisition, **Victor A. Eremeyev:** Investigation, Review & editing, Supervision.

5. Malikan, M., Wiczenbach, T., & Eremeyev, V. A. (2021). On thermal stability of piezo-flexomagnetic microbeams considering different temperature distributions. *Continuum Mechanics and Thermodynamics*. https://doi.org/10.1007/s00161-021-00971-y

The fifth paper is totally a different work as it expressed thermal effects on a microsensor exploring different distributions of the external temperature. Herein a distinct investigation has been reported on piezomagnetic-flexomagnetic micro-size beam-shaped sensors based on thin beam theory. Concerning the strain gradient theory, the microstructural effect was studied. The microbeam physical structure was defined based on magnetic microparticles. The constitutive equation, which is dominant on the problem, was obtained by linear Lagrangian strain, and the critical temperature was computed for clamped and simple boundary supports. The distribution of thermal loading in line with thickness was in linear, uniform, and parabolic states.

In this work, the authors' contributions are as follows:
Mohammad Malikan: Conceptualization, Methodology, Investigation, Software, Visualization, Validation, Data curation, Resources, Formal analysis, Original draft. **T. Wiczenbach:** Original draft, **Victor A. Eremeyev:** Investigation, Review & editing, Supervision, Funding acquisition.

6. Malikan, M., & Eremeyev, V. A. (2021). Flexomagnetic response of buckled piezomagnetic composite nanoplates. *Composite Structures*, *267*, 113932. https://doi.org/10.1016/j.compstruct.2021.113932

In the sixth work, a biaxial buckling analysis-based mathematical modeling has been depicted for converse flexomagnetic influence on a piezomagnetic nanoparticle composition of cobalt and ferrite. The equation of motion was obtained based on the classical plate theory and plane strain assumptions. Furthermore, after the analytical solution of the equation, the analytical relation was obtained for the first mode of the buckling load of this sheet based on the clamped and simply-supported edge conditions. Finally, a MATLAB code was written to calculate the flexomagneticity response in the two-dimensional domain.

In this work, the authors' contributions are as follows:
Mohammad Malikan: Conceptualization, Methodology, Investigation, Software, Visualization, Validation, Data curation, Resources, Formal analysis, Original draft. **Victor A. Eremeyev:** Investigation, Review & editing, Supervision, Funding acquisition.

7. Malikan, M., & Eremeyev, V. A. (2021). Effect of surface on the flexomagnetic response of ferroic composite nanostructures; nonlinear bending analysis. *Composite Structures*, *271*, 114179. https://doi.org/10.1016/j.compstruct.2021.114179

The seventh work reported the effects of the surface layer on the various significance items included in a ferromagnetic structure for providing the flexomagnetic response. On the basis of the available data of a flexo-ferroic material, an appropriate consideration was performed to predict the surface layer effect on the flexomagneticity. The Euler-Bernoulli beam assumption was used to find out large deflections of clamped–clamped and pinned–pinned nanoscale beams. When the nonlocal strain gradient model is applied, it can generate the stress nonlocality and large gradient of atoms in the nanoscale. When the magnetic field gradient is applied, one can observe the converse flexomagnetic effect, which was the studied case in this article. The contribution of the nonlinear von-Kármán strain aided us in modeling the problem mathematically. With the substitution of the differential quadrature method (DQM), which has been widely used and its precision has been entirely approved, the partial differential relations have been converted into algebraic equations. After that, the algebraic relations were solved vis-à-vis the Newton-Raphson technique to compute the large deflections. Further, investigations were warranted via a simple structure using a finite element commercial software before the results and discussion section. This study argued and demonstrated massive potential in affecting the flexomagnetic effect based on the surface layer.

In this work, the authors' contributions are as follows:
Mohammad Malikan: Conceptualization, Methodology, Investigation, Software, Visualization, Validation, Data curation, Resources, Formal analysis, Original draft. **Victor A. Eremeyev:** Investigation, Review & editing, Supervision, Funding acquisition.

8. Malikan, M., & Eremeyev, V. A. (2021). Flexomagneticity in buckled shear deformable hard-magnetic soft structures. *Continuum Mechanics and Thermodynamics*. https://doi.org/10.1007/s00161-021-01034-y

The eighth work aimed to extend the shear deformation effect on the flexomagneticity response of a piezomagnetic ultrasmall scale elastic beam. The governing equations have been established by using the Timoshenko beam. The nonlocal mechanics of the nanobeam was concerned with the nonlocal strain gradient approach by which there was an ability to transfer the discretized atomic lattice into a continuum region. The solution of the obtained equations corresponds to a closed-form solution within which the numerical results were reported for simply-supported boundary conditions. In addition, some tabulated verifications have been organized to corroborate the numerical results.

In this work, the authors' contributions are as follows:
Mohammad Malikan: Conceptualization, Methodology, Investigation, Software, Visualization, Validation, Data curation, Resources, Formal analysis, Original draft. **Victor A. Eremeyev:** Investigation, Review & editing, Supervision, Funding acquisition.

9. Malikan, M., Wiczenbach, T., & Eremeyev, V. A. (2021). Thermal buckling of functionally graded piezomagnetic micro- and nanobeams presenting the flexomagnetic effect. *Continuum Mechanics and Thermodynamics*. https://doi.org/10.1007/s00161-021-01038-8

Through ninth work, a more remarkable flexomagnetic response was looking by assuming functionality and grading compositions of the material in line with the thickness of the beam. Based on the Galerkin weighted residual method, the numerical results have been warranted in the framework of analytical solutions for fully fixed ends conditions. The beam's mechanical behavior was assumed to be dependent on the shear deformations; therefore, the Timoshenko beam was taken into the model. The examination in nanoscale was revealed by exerting both stress nonlocality and strain gradient in the media of the nonlocal strain gradient approach. The implementation of the material composition was presumed as exponential functionality concerning the rule of mixture. Inclusive of flexomagneticity was performed in terms of reverse field effect. Under the axially compressed conditions of the system, the critical buckling temperature was explored. Notwithstanding that the functionally graded materials (FGMs) can be correctly analyzed so that the mid-plane plays the role of the neutral surface, this research took into account the physical neutral plane that differs from the mid-surface.

In this work, the authors' contributions are as follows:
Mohammad Malikan: Conceptualization, Methodology, Investigation, Software, Visualization, Validation, Data curation, Resources, Formal analysis, Original draft. **T.**

Wiczenbach: Original draft, **Victor A. Eremeyev:** Investigation, Review & editing, Supervision, Funding acquisition.

10. Malikan, M., Krasheninnikov, M., & Eremeyev, V. A. (2020). Torsional stability capacity of a nano-composite shell based on a nonlocal strain gradient shell model under a three-dimensional magnetic field. *International Journal of Engineering Science*, *148*, 103210. https://doi.org/10.1016/j.ijengsci.2019.103210

Moreover, the tenth/last work performed a study on the torsional buckling of a piezomagnetic nano-composite shell under a three-dimensional magnetic field based on the first-order shear deformation shell approach in combining with the nonlocal theory of strain gradient. In order to take the numerical findings, an analytical process was used. After validation of numerical outcomes, the role of key parameters was investigated on the torsional behavior of the shell. The results focused on both buckling and wave propagation of the nanoscale shell.

In this work, the authors' contributions are as follows:
Mohammad Malikan: Conceptualization, Methodology, Investigation, Software, Visualization, Validation, Data curation, Resources, Formal analysis, Original draft. **M. Krasheninnikov:** Original draft, **Victor A. Eremeyev:** Investigation, Review & editing, Supervision, Funding acquisition.

4 Presented conferences

The results of the dissertation were discussed within two online conferences listed below.

- The conference ICCS23 - 23rd International Conference on Composite Structures & MECHCOMP6 - 6th International Conference on Mechanics of Composites held 1-4 September 2020 on Faculty of Engineering, University of Porto, Portugal. Conference chairs were António J.M. Ferreira, (University of Porto, Portugal), Nicholas Fantuzzi, (University of Bologna, Italy), Michele Bacciocchi, (University of San Marino, San Marino). Two presentations were delivered.

- The conference ICCS24 - 24rd International Conference on Composite Structures, 14 - 18 June 2021, on Faculty of Engineering, University of Porto, Portugal. Conference chairs were António J.M. Ferreira, (University of Porto, Portugal), Nicholas Fantuzzi, (University of Bologna, Italy), Michele Bacciocchi, (University of San Marino, San Marino), Carlos Santiuste (Universidad Carlos III de Madrid, Spain)

5 Scientific contributions of the thesis

The thesis developed new models of thin-walled structures such as beams, plates, and shells using non-local models of continua and magneto-elastic coupling. In particular, we paid a significant attention to the flexomagneticity, which could be very important at small scales. Let us note that up to our knowledge, the flexomagneticity phenomenon is much less studied than piezoelectricity, piezomagneticity, and even flexoelectricity. To the analysis of this phenomenon with application to thin-walled structures is quite topical.

More specifically, we found that:

- Increasing the numerical value of the nonlocal parameter leads to a softening effect on the nanomaterial, and in contrast, increasing the numerical value of the strain gradient parameter leads to the appearance of stiffness in the nanomaterial.

- The effect of nonlinear analysis is more extraordinary in large values of the nonlocal parameter and smaller values of strain gradient parameter.

- The effect of nonlinear analysis on a nonlocal study is greater than a local one.

- The effect of nonlinear analysis in the positive magnetic field decreases. However, the opposite is true in the case of a negative magnetic field.

- The flexomagnetic effect leads to more material stiffness and thus reduces the numerical values of deflections in static analysis.

- The less "flexible" the boundary condition, the higher the flexomagneticity effect.

- The post-buckling and failure resulting from it would happen sooner for nanostructures whilst the strain gradient and the nonlocal parameters are respectively substantial and negligible.

- In so-called lengthy micro/nanosensors, critical buckling and post-buckling loads can occur simultaneously. This means that the structure will fail exactly at the time of critical buckling.

- The variations of thickness of the nanobeam affected the flexomagneticity, and this property is further noticeable for lower thicknesses of nanostructures.

- The results showed that this imperfection could affect the flexomagnetic behavior of micro/nanomaterials in some porosity patterns.

- The importance of piezomagnetic-flexomagnetic properties depends on the surrounding temperature distribution.

- The uniaxial buckling makes the flexomagnetic response of the nanoplate more notable.

- In the case of the uniaxial buckling of intelligent nanoplates, the magnetic field has further affected the critical buckling load.

- In terms of the biaxial buckling of smart nanoplates, while β (L_x/L_y) < 1, the flexomagnetic response is more evident in contrast to $\beta > 1$.

- Under uniaxial loading, whenever the nanoplate is rectangular and $\beta < 1$, an increase of aspect ratio leads to softening, and this is vice versa for rectangular nanoplate with $\beta > 1$.

- Suppose the end conditions are selected as less flexible, and values of nonlocal or SGLS parameters are big and small enough. In that case, the surface layer can affect and develop a further flexomagnetic response.

- For the smart nanostructures, the flexomagneticity will affect the existence of shear deformations, and the effect is to increase its importance.

- The most important magnetic effect can be the transverse effect in the three-dimensional magnetic analysis of a nano-composite shell.

- The flexomagneticity would be more visible in FGMs, while shear deformations exist. Thus, the piezomagnetic FGMs nanosensors provide and offer new principal aspects that improve the designing of small-scale actuators/sensors.

- It was observed that flexomagneticity could be even more vital in a ferroic functionally graded material based on the exponential material composition.

The provided results could be useful for the design and further manufacturing of some devices such as sensors, actuators, energy harvesters, and some others

6 New problems and future steps

There would also be numerous new challenges and extensive opportunities to design MEMS/NEMS sensors and actuators. Therefore, upcoming scientific efforts could be focused on the following topics:

- How would be the efficiency of a micro/nanosensor if it is made of laminated structures incorporating an FGM layer and a piezomagnetic layer with FM effect.

- What is the mechanical response of a piezomagnetic FGM micro/nanosensor based on the functionality in line with the length instead of thickness.

- Within this thesis, the differential form of nonlocality has been scrutinized, which is a weak nonlocality versus the integral form. On the other hand, the integral form of nonlocal models gives a strong nonlocality. Therefore, the difference between these two schemas of nonlocal domains when considering micro/nanosensors is a new topic that can extend studies done in this thesis. In fact, based on the integral form of nonlocal strain gradient theory, there is the possibility to continue current studies.

- In a thermoelastic problem, different kinds of heat sources can affect the mechanical response of a micro/nanosensor. Thus, this topic can be considered and discussed.

- What would be the response of flexomagneticity through a three-dimensional study.

- Penta-graphene as a newly discovered nanostructure can be considered for any possible piezomagnetic-flexomagnetic effects.

- What is the impact of rotary inertia in a shear deformable micro/nanostructure, including FM effect subject to vibrational modes.

- What would be the amount of FM response if the micro/nanosensor is implemented into a resonance zone of nonlinear forced vibrations.

Bibliography

[1] M. Malikan, V. B. Nguyen, Buckling analysis of piezo-magnetoelectric nanoplates in hygrothermal environment based on a novel one variable plate theory combining with higher-order nonlocal strain gradient theory, Physica E: Low-dimensional Systems and Nanostructures 102 (2018) 8-28.

[2] S. P. Timoshenko, On the correction for shear of the differential equation for transverse vibrations of prismatic bars, The London, Edinburgh, and Dublin Philosophical Magazine and Journal of Science 41 (1921) 744-746.

[3] J. N. Reddy, A simple higher-order theory for laminated composite plates, Journal of Applied Mechanics 45 (1984) 745–52.

[4] M. Malikan, V. A. Eremeyev, A new hyperbolic-polynomial higher-order elasticity theory for mechanics of thick FGM beams with imperfection in the material composition, Composite Structures 249 (2020) 112486.

[5] M. Malikan, N. S. Uglov, V. A. Eremeyev, On instabilities and post-buckling of piezomagnetic and flexomagnetic nanostructures, International Journal of Engineering Science 157 (2020) 103395.

[6] M. Malikan, Electro-mechanical shear buckling of piezoelectric nanoplate using modified couple stress theory based on simplified first order shear deformation theory, Applied Mathematical Modelling 48 (2017) 196–207.

[7] M. Malikan, V. A. Eremeyev, Post-critical buckling of truncated conical carbon nanotubes considering surface effects embedding in a nonlinear Winkler substrate using the Rayleigh-Ritz method, Materials Research Express 7 (2020) 025005.

[8] M. Malikan, On the plastic buckling of curved carbon nanotubes, Theoretical and Applied Mechanics Letters 10 (2020) 46–56.

[9] L. L.-P. Diandra, R. D. Rieke, Magnetic properties of nanostructured materials, Chemistry of materials 8 (1996) 1770-1783.

[10] C. Fei, Y. Zhang, Z. Yang, Y. Liu, R. Xiong, J. Shi, X. Ruan, Synthesis and magnetic properties of hard magnetic (CoFe2O4)–soft magnetic (Fe3O4) nano-composite ceramics by SPS technology, Journal of Magnetism and Magnetic Materials 323 (2011) 1811-1816.

[11] V. Reddy, N. P. Annapu, Pathak, R. Nath, Particle size dependent magnetic properties and phase transitions in multiferroic BiFeO3 nano-particles, Journal of Alloys and Compounds 543 (2012) 206-212.

[12] Z. Karimi, Y. Mohammadifar, H. Shokrollahi, Sh. Khameneh Asl, Gh. Yousefi, L. Karimi, Magnetic and structural properties of nano sized Dy-doped cobalt ferrite synthesized by co-precipitation, Journal of Magnetism and Magnetic Materials 361 (2014) 150-156.

[13] I. Obaidat, I. Bashar, Y. Haik, Magnetic properties of magnetic nanoparticles for efficient hyperthermia, Nanomaterials 5 (2015) 63-89.

[14] P. C. Rajath, R. S. Manna, D. Banerjee, M. R. Varma, K. G. Suresh, A. K. Nigam, Magnetic properties of CoFe2O4 synthesized by solid state, citrate precursor and polymerized complex methods: A comparative study, Journal of Alloys and Compounds 453 (2008) 298-303.

[15] J. Wang, T. Deng, Y. Dai, Comparative study on the preparation procedures of cobalt ferrites by aqueous processing at ambient temperatures, Journal of Alloys and Compounds 419 (2006) 155-161.

[16] M. S. Khandekar, R. C. Kamble, J. Y. Patil, Y. D. Kolekar, S. S. Suryavanshi, Effect of calcination temperature on the structural and electrical properties of cobalt ferrite synthesized by combustion method, Journal of Alloys and compounds 509 (2011) 1861-1865.

[17] D. H. Kim, D. E. Nikles, D. T. Johnson, C. S. Brazel, Heat generation of aqueously dispersed CoFe2O4 nanoparticles as heating agents for magnetically activated drug delivery and hyperthermia, Journal of Magnetism and Magnetic Materials 320 (2008) 2390-2396.

[18] P. C. Morais, Photoacoustic spectroscopy as a key technique in the investigation of nanosized magnetic particles for drug delivery systems, Journal of Alloys and Compounds 483 (2009) 544-548.

[19] N. M. Deraz, Glycine-assisted fabrication of nanocrystalline cobalt ferrite system, Journal of Analytical and Applied Pyrolysis 88 (2010) 103-109.

[20] A. C. Peixoto, A.F. Silva, 11 - Smart devices: Micro- and nanosensors, Editor(s): Lígia Rodrigues, Manuel Mota, Bioinspired Materials for Medical Applications, Woodhead Publishing, 2017, Pages 297-329.

[21] B. M. Song, S. A. Pikuz, T. A. Shelkovenko, D. A. Hammer, Determination of the size and structure of an X-pinch x-ray source from the diffraction pattern produced by microfabricated slits, Applied Optics 44 (2005) 2349-2358.

[22] L. Zeng, S. M. Parvasi, Q. Kong, L. Huo, I. Lim, M. Li, G. Song, Bond slip detection of concrete-encased composite structure using shear wave based active sensing approach, Smart Materials and Structures 24 (2015) 125026.

[23] T. C. Huynh, N. L. Dang, J. T. Kim, Preload Monitoring in Bolted Connection Using Piezoelectric-Based Smart Interface, Sensors 18 (2018) 2766.

[24] B. Arash, Q. Wang, A review on the application of nonlocal elastic models in modeling of carbon nanotubes and graphenes, Computational Materials Science 51 (2012) 303–313.

[25] S. C. Pradhan, A. Kumar, Vibration analysis of orthotropic graphene sheets using nonlocal elasticity theory and differential quadrature method, Composite Structures 93 (2011) 774–779.

[26] A. C. Eringen, Nonlocal Continuum Field Theories, Springer-Verlag, New York, (2002).

[27] A. C. Eringen, Linear theory of non-local elasticity and dispersion of plane waves, International Journal of Engineering Science 10 (1972) 425-435.

[28] W. H. Duan, C. M. Wang, Y. Y. Zhang, Calibration of nonlocal scaling effect parameter for free vibration of carbon nanotubes by molecular dynamics, Journal of Applied Physics 101 (2007) 24305-24311.

[29] W. H. Duan, C. M. Wang, Exact solutions for axisymmetric bending of micro/nanoscale circular plates based on nonlocal plate theory, Nanotechnology 18 (2007) 385704.

[30] C. Y. Wang, T. Murmu, S. Adhikari, Mechanisms of nonlocal effect on the vibration of nanoplates, Applied Physics Letters 98 (2011) 153101.

[31] V. Sundararaghavan, A. Waas, F. Pawlowski, Computation of Spatial Kernel of Carbon Nanotubes in Non-Local Elasticity Theory, University of Michigan, Ann Arbor, Multi-scale structural simulations laboratory, (2014).

[32] M. Malikan, F. Tornabene, R. Dimitri, Nonlocal three-dimensional theory of elasticity for buckling behavior of functionally graded porous nanoplates using volume integrals, Materials Research Express 5 (2018) 095006.

[33] M. Malikan, V. B. Nguyen, A novel one-variable first-order shear deformation theory for biaxial buckling of a size-dependent plate based on Eringen's nonlocal differential law, World Journal of Engineering 15 (2018) 633-645.

[34] Sh. Dastjerdi, M. Malikan, Mechanical analysis of eccentric defected bilayer graphene sheets considering the van der Waals force, Proceedings of the Institution of Mechanical Engineers, Part N: Journal of Nanomaterials, Nanoengineering and Nanosystems 235 (2021) 41-51.

[35] Q. Deng, Size-dependent flexoelectric response of a truncated cone and the consequent ramifications for the experimental measurement of flexoelectric properties, Journal of Applied Mechanics 84 (2017) 101007.

[36] F. Ebrahimi, M. R. Barati, Free vibration analysis of couple stress rotating nanobeams with surface effect under in-plane axial magnetic field, Journal of vibration and control 24 (2017) 5097-5107.

[37] M. Malikan, Temperature influences on shear stability of a nanosize plate with piezoelectricity effect, Multidiscipline modeling in materials and structures 14 (2018) 125-142.

[38] Q. Ma, D. R. Clarke, Size Dependent Hardness in Silver Single Crystals, Journal of Materials Research 10 (1995) 853-863.

[39] W. J. Poole, M. F. Ashby, N. A. Fleck, Micro-Hardness of Annealed and Work-Hardened Copper Polycrystals, Scripta Materialia 34 (1996) 559-564.

[40] Y. Y. Lim, Y. Y. Chaudhri, The Effect of the Indenter Load on the Nanohardness of Ductile Metals: An Experimental Study of Polycrystalline Work-Hardened and Annealed Oxygen-Free Copper, Philosophical Magazine A 79 (1999) 2979-3000.

[41] C. W. Lim, G. Zhang, J. N. Reddy, A Higher-order nonlocal elasticity and strain gradient theory and Its Applications in wave propagation, Journal of the Mechanics and Physics of Solids 78 (2015) 298-313.

[42] M. Malikan, V. B. Nguyen, F. Tornabene, Damped forced vibration analysis of single-walled carbon nanotubes resting on viscoelastic foundation in thermal environment using nonlocal strain gradient theory, Engineering Science and Technology, an International Journal 21 (2018) 778-786.

[43] M. Malikan, V. B. Nguyen, R. Dimitri, F. Tornabene, Dynamic modeling of non-cylindrical curved viscoelastic single-walled carbon nanotubes based on the second gradient theory, Materials Research Express 6 (2018) 075041.

[44] M. Malikan, M. Jabbarzadeh, Sh. Dastjerdi, Non-linear Static stability of bi-layer carbon nanosheets resting on an elastic matrix under various types of in-plane shearing loads in thermo-elasticity using nonlocal continuum, Microsystem Technologies 23 (2017) 2973-2991

[45] N. Fleck, J. Hutchinson, A reformulation of strain gradient plasticity, Journal of the Mechanics and Physics of Solids 49 (2001) 2245–2271.

[46] L. Zhang, B. Wang, Sh. Zhou, Y. Xue, Modeling the Size-Dependent Nanostructures: Incorporating the Bulk and Surface Effects, Journal of Nanomechanics and Micromechanics 7 (2017) 04016012.

[47] Y. Zhou, X. Yang, D. Pan, B. Wang, Improved incorporation of strain gradient elasticity in the flexoelectricity based energy harvesting from nanobeams, Physica E: Low-dimensional Systems and Nanostructures 98 (2018) 148–158.

[48] A. C. Eringen, On differential equations of nonlocal elasticity and solutions of screw dislocation and surface waves, Journal of Applied Physics 54 (1983) 4703–4710.

[49] Ch.-P. Wu, W.-Ch. Li, Asymptotic nonlocal elasticity theory for the buckling analysis of embedded single-layered nanoplates/graphene sheets under biaxial compression, Physica E: Low-dimensional Systems and Nanostructures 89 (2017) 160-169.

[50] R. D. Mindlin, Second gradient of train and surface-tension in linear elasticity, International Journal of Solids and Strucutres 1 (1965) 417-438.

[51] R. D. Mindlin, N. N. Eshel, On first strain-gradient theories in linear elasticity, International Journal of Solids and Strucutres 4 (1968) 109-124.

[52] J. Guo, J. Chen, E. Pan, Free vibration of three-dimensional anisotropic layered composite nanoplates based on modified couple-stress theory, Physica E: Low-dimensional Systems and Nanostructures 87 (2017) 98-106.

[53] R. D. Mindlin, Micro-structure in linear elasticity, Archive for Rational Mechanics and Analysis 16 (1964) 51-78.

[54] R. A. Toupin, Elastic materials with couple stresses, Archive for Rational Mechanics and Analysis 11 (1962) 385-414.

[55] R. A. Toupin, Theories of elasticity with couple-stress, Archive for Rational Mechanics and Analysis 17 (1964) 85-112.

[56] R. D. Mindlin, H. F. Tiersten, Effects of couple-stresses in linear elasticity, Archive for Rational Mechanics and Analysis 11 (1962) 415-448.

[57] D. Rogula, Nonlocal theory of material media, Springer, New York, (2002).

[58] H. Askes, E. C. Aifantis, Gradient elasticity in statics and dynamics: An overview of formulations, length scale identification procedures, finite element implementations and new results, International Journal of Solid and Structures 48 (2011) 1962-1990.

[59] R. Ansari, J. Torabi, A. Norouzzadeh, Bending analysis of embedded nanoplates based on the integral formulation of Eringen's nonlocal theory using the finite element method, Physica B: Condensed Matter 534 (2018) 90-97.

[60] V. E. Tarasov, General lattice model of gradient elasticity, Modern Physics Letters B 28 (2014) 1450054.

[61] M. Rubin, P. Rosenau, O. Gottlieb, Continuum model of dispersion caused by an inherent material characteristic length, Journal of Applied physics 77 (1995) 4054-4063.

[62] A. V. Metrikine, H. Askes, One-dimensional dynamically consistent gradient elasticity models derived from a discrete microstructures. Part 1: Generic formulation, European journal of mechanics – A/Solids 21 (2002) 555-572.

[63] M. Malikan, R. Dimitri, F. Tornabene, Transient response of oscillated carbon nanotubes with an internal and external damping, Composites Part B: Engineering 158 (2019) 198-205.

[64] Wang Z.L., Liu Y. (2016) Piezoelectric Effect at Nanoscale. In: Bhushan B. (eds) Encyclopedia of Nanotechnology. Springer, Dordrecht. https://doi.org/10.1007/978-94-017-9780-1_273

[65] M. Malikan, V. A. Eremeyev, On Nonlinear Bending Study of a Piezo-Flexomagnetic Nanobeam Based on an Analytical-Numerical Solution, Nanomaterials 10 (2020) 1762.

[66] R. Maranganti, N. D. Sharma, P. Sharma, Electromechanical coupling in nonpiezoelectric materials due to nanoscale nonlocal size effects: Green's function solutions and embedded inclusions, Physical Review B 74 (2006) 014110.

Part II

Publications

Postprint for: Malikan M., Eremeyev V. A. On the geometrically nonlinear vibration of a piezo-flexomagnetic nanotube. Mathematical Methods in the Applied Sciences. https://doi.org/10.1002/mma.6758

On the geometrically nonlinear vibration of a piezo-flexomagnetic nanotube

Mohammad Malikan[1], Victor A. Eremeyev[1,2*]

[1]Department of Mechanics of Materials and Structures, Faculty of Civil and Environmental Engineering, Gdansk University of Technology, 80-233, Gdansk, Poland

[2]Don State Technical University, Gagarina sq., 1, Rostov on Don 344000, Russia

*Corresponding author: victor.eremeev@pg.edu.pl, eremeyev.victor@gmail.com

Abstract

In order to describe the behavior of thin elements used in MEMS and NEMS, it is essential to study a nonlinear free vibration of nanotubes under complicated external fields such as magnetic environment. In this regard, the magnetic force applied to the conductive nanotube with piezo-flexomagnetic elastic wall is considered. By the inclusion of Euler-Bernoulli beam and using Hamilton's principle, the equations governing the system are extracted. More importantly, a principal effect existed in a nonlinear behavior such as axial inertia is thoroughly analyzed which is not commonly investigated. We then consider the effects of nanoscale size using the nonlocal theory of strain gradient (NSGT). Hereafter, the frequencies are solved as semi-analytical solutions on the basis of Rayleigh-Ritz method. The piezo-flexomagnetic nanotube (PF-NT) is calculated with different boundary conditions. In order to validate, the results attained from the present solution have been compared with those available in the open literature. We realized that the nonlinear frequency analysis is so significant when a nanotube has fewer degrees of freedom at both ends, and its length is long.

Keywords: Nonlinear vibration; Piezo-flexomagnetic nanotubes; Axial inertia; NSGT; Rayleigh-Ritz method

1. Introduction

Nano-electro-mechanical systems (NEMS) are the technology of very small nanometer-sized machines. NEMS is a step ahead of micro-electro-mechanical systems (MEMS) and usually encompasses a combination of transistors (electric), sensors and motors (mechanical). Due to its very small size, NEMS is expected to have a major impact on large sections of science and technology and eventually replace MEMS [1].

Contemporarily, a discovered and explored phenomenon known in the elements of electro-mechanical coupling with taking magnetic effect is flexomagneticity. Uniform strain makes magnetic polarization, and the response is reflected by piezomagneticity. This occurrence exists only in dielectrics with non-centrosymmetric structures. A lot of studies showed that a non-zero magnetic field can be induced by the inclusion of non-uniform strains. Flexomagnetic (FM) effect defines this type of coupling of an induced magnetic field and distribution of the non-uniform strain [2-4]. Flexomagneticity in comparison with piezomagneticity, demonstrates the coupling features of induced magnetic polarization and strain gradient. Flexomagneticity becomes a remarkable and overcoming influence when the material size is scaled down to nanoscale, although this effect is meager and negligibly small on macro scale. Therefore, a further conceptual understanding of the FM on NEMS is necessary.

In a general understanding through FM, during polarization in the material, strain gradient induces magnetic field and magnetic field gradient induces the strain. The former is named as the direct impact and the later one as the converse effect. The FM already is on the novel threshold of its research.

To predict the mechanical response of NEMS, a great deal can be observed done on piezomagneticity during the contemporary decade [5-20], though the literature on FM is much less developed, see, e.g., [21-23]. The analysis of nanomaterials containing FM was commenced by Sidhardh and Ray [21] by surveying a cantilever nanoscale size piezomagnetic Euler-Bernoulli beam subjected to transverse static loading. The surface elasticity was developed on the model. Moreover, both converse and direct magnetic effects were discussed. Zhang et al. [22] extended FM studies to asses bending analysis of a small scale piezomagnetic Euler-Bernoulli beam under several conditions of boundaries. They investigated both reverse and direct FM. Malikan and Eremeyev [23] modeled the linear dynamic conditions for a nanotube involving FM and evaluated scale

effect on the basis of stress-driven nonlocal elasticity. The size-dependency behavior of FM was corroborated by their findings as well.

As far as very limited studies are found on FM, one can acquisition many opportunities to account for such the effect. This research intends to expand the FM on a nanosize Euler-Bernoulli beam. More importantly, the vibration problem is described with respect to nonlinear strains of Lagrangian based von Kármán assumptions [24-33]. It is worth to mention that the effect of axial inertia may become important in parts of vibrating machines. So, this effect is estimated as well. Plus, size-dependence is modeled with exerting nonlocal strain gradient theory (NSGT). In view of nonlinear partial differential equations, the analytical solution methods are unable to give a solution. By virtue of this, numerical solution techniques should come in hand, such as differential quadrature method (DQM) [34, 35], finite difference method (FDM) [36], finite element method (FEM) [37, 38], mesh free method [39], dynamic relaxation method (DRM) [40], Homotopy method [41], etc. These techniques take a long time to give the numerical results due to their massive computations. Amidst solution approaches, semi-analytical techniques require lower time to grant the numerical outcomes. The Rayleigh-Ritz technique is a one that based on a few convergence rate solves the equations with shorter formulation. On the basis of very general assumptions, the Rayleigh-Ritz shows its advantage. In terms of the approximation features, this method produces optimal solutions. Thus, the solution process is here accomplished by means of Rayleigh-Ritz technique. Thereby, a validation section is provided to render the correctness of the formulation. Thereupon, numerical results are reported by creating different pictorial figures for momentous parameters.

2. Mathematical model

Let us consider a typical nanotube of length L, of thickness h and of diameter d. Figure 1 shows a schematic image of the considered structure [42].

In what follows we consider the Euler-Bernoulli beam model for the considered nanotube. Moreover, we restrict ourselves to in-plane deformations. So, the middle neutral beam line coincides with the x-axis whereas z-axes relates to the transverse direction. The corresponding Cartesian displacements are denoted as u_1 and u_3,

respectively, see [43-46] for detail. The axial and transverse displacements of the middle neutral line are denoted by *u* and *w*, respectively. So, the kinematical relations are given by

$$u_1(x,z,t) = u(x,t) - z\frac{\partial w(x,t)}{\partial x} \tag{1}$$

$$u_3(x,z,t) = w(x,t) \tag{2}$$

Based on the von Kármán nonlinear strains, in the Lagrangian strain formula, the nonlinear term related to *u* is adequately small and can be ignorable. Accordingly, the nonlinear components of the axial strain and its gradient are calculated as

$$\varepsilon_{xx} = \frac{\partial u}{\partial x} - z\frac{\partial^2 w}{\partial x^2} + \frac{1}{2}\left(\frac{\partial w}{\partial x}\right)^2 \tag{3}$$

$$\eta_{xxz} = \frac{\partial \varepsilon_{xx}}{\partial z} = -\frac{\partial^2 w}{\partial x^2} \tag{4}$$

where η_{xxz} means gradient of the elastic strain. Following [21, 22] the one-dimensional stress-strain magneto-mechanical relations are prepared as

$$\sigma_{xx} = C_{11}\varepsilon_{xx} - q_{31}H_z \tag{5}$$

$$\xi_{xxz} = g_{31}\eta_{xxz} - f_{31}H_z \tag{6}$$

$$B_z = a_{33}H_z + q_{31}\varepsilon_{xx} + f_{31}\eta_{xxz} \tag{7}$$

where σ_{xx} and ξ_{xxz} are the stress and hyper stress, B_z and H_z are the magnetic flux and the magnetic field, respectively, and material parameters are introduced. In particular, $C_{11} = C_{1111}$ is the elastic modulus, $f_{31} = f_{3311}$ denotes the component of the fourth-order flexomagnetic coefficients tensor, a_{33} represents the component of the second-order magnetic permeability tensor, $q_{31} = q_{311}$ depicts the component of the third-order piezomagnetic tensor, and $g_{31} = g_{311311}$ is the component the sixth-order gradient elasticity tensor.

In order to precisely extract the particularized equation of piezo-flexomagnetic type nanotubes (PF-NTs), the variational formulation can be expanded adequately on the base of Hamilton's principle as

$$\int_{t_1}^{t_2}\left(\delta K-\delta U+\delta W\right)dt=0 \tag{8}$$

in which δ denotes the symbol of variation. In (8), the first variation of the total internal of the beam is equal to zero, and the other factors are the kinetic and strain energies (K and U) and the created work by outer forces (δW).

The first variation of the strain energy can be written in an integral form according to magneto-mechanical coupling as

$$\delta U=\int_V\left(\sigma_{xx}\delta\varepsilon_{xx}+\xi_{xxz}\delta\eta_{xxz}-B_z\delta H_z\right)dV \tag{9}$$

Using assumed 1D kinematics and integrating by parts, we can transform (9) in to a sum

$$\delta U=\delta\Pi_{U_1}^{Mech}+\delta\Pi_{U_1}^{Mag}+\delta\Pi_{U_2}^{Mech}+\delta\Pi_{U_2}^{Mag}$$

where

$$\delta\Pi_{U_1}^{Mech}=-\int_0^L\left(\frac{\partial N_x}{\partial x}\delta u+\frac{\partial^2 M_x}{\partial x^2}\delta w+\frac{\partial}{\partial x}\left(N_x\frac{\partial w}{\partial x}\right)\delta w+\frac{\partial^2 T_{xxz}}{\partial x^2}\delta w\right)dx \tag{10a}$$

$$\delta\Pi_{U_1}^{Mag}=-\int_0^L\int_{-h/2}^{h/2}\frac{\partial B_z}{\partial z}\delta\Psi\,dzdx \tag{10b}$$

$$\delta\Pi_{U_2}^{Mech}=\left(N_x\delta u-M_x\frac{\partial\delta w}{\partial x}-T_{xxz}\frac{\partial\delta w}{\partial x}+N_x\frac{\partial w}{\partial x}\delta w+\frac{\partial M_x}{\partial x}\delta w+\frac{\partial T_{xxz}}{\partial x}\delta w\right)\Bigg|_0^L \tag{11a}$$

$$\delta\Pi_{U_2}^{Mag}=\int_0^L\left(B_z\delta\Psi\right)\Big|_{-h/2}^{h/2}dx \tag{11b}$$

and we also have introduced normal axial force, moment and hyperstress as follows

$$N_x=\int_{-h/2}^{h/2}\sigma_{xx}dz \tag{12}$$

$$M_x=\int_{-h/2}^{h/2}\sigma_{xx}z\,dz \tag{13}$$

$$T_{xxz}=\int_{-h/2}^{h/2}\xi_{xxz}dz \tag{14}$$

In our case the work of external forces has the functional

$$W = -\frac{1}{2}\int_0^L N_x^0 \left(\frac{\partial w}{\partial x}\right)^2 dx \tag{15}$$

which first variation has the form

$$\delta W = -\int_0^L N_x^0 \left(\frac{\partial \delta w}{\partial x}\frac{\partial w}{\partial x}\right) dx \tag{16}$$

where N_x^0 presents the initial in-plane axial force.

In addition in (11b) we introduced the magnetic potential Ψ. The relationship between magnetic potential and magnetic field component can be given by

$$H_z + \frac{\partial \Psi}{\partial z} = 0 \tag{17}$$

By accounting a reverse flexomagnetic state for a closed circuit, one can attribute the following conditions

$$\Psi\left(+\frac{h}{2}\right) = \psi, \ \Psi\left(-\frac{h}{2}\right) = 0 \tag{18a-b}$$

in which the potential on the top surface as a result of the magnetic field is symbolized by ψ. The change of the magnetic potential along the thickness of the nanotube and then the component of the magnetic field can be feasible by the use of Eqs. (7), (10b), (11b), (17), and (18) [21, 22]

$$\Psi = -\frac{q_{31}}{2a_{33}}\left(z^2 - \frac{h^2}{4}\right)\frac{\partial^2 w}{\partial x^2} + \frac{\psi}{h}\left(z + \frac{h}{2}\right) \tag{19}$$

$$H_z = z\frac{q_{31}}{a_{33}}\frac{\partial^2 w}{\partial x^2} - \frac{\psi}{h} \tag{20}$$

Thereafter, Eqs. (5)-(7) on the basis of Eqs. (19) and (20) can be expanded as

$$B_z = q_{31}\left[\frac{\partial u}{\partial x} + \frac{1}{2}\left(\frac{\partial w}{\partial x}\right)^2\right] - f_{31}\frac{\partial^2 w}{\partial x^2} - \frac{a_{33}\psi}{h} \tag{21}$$

$$\xi_{xxz} = -\left(g_{31} + \frac{q_{31}f_{31}z}{a_{33}}\right)\frac{\partial^2 w}{\partial x^2} + \frac{f_{31}\psi}{h} \tag{22}$$

$$\sigma_{xx} = C_{11}\left[\frac{\partial u}{\partial x} + \frac{1}{2}\left(\frac{\partial w}{\partial x}\right)^2\right] - z\left(C_{11} + \frac{q_{31}^2}{a_{33}}\right)\frac{\partial^2 w}{\partial x^2} + \frac{q_{31}\psi}{h} \tag{23}$$

which are magnetic induction, the component of higher-order moment stress tensor and the component of stress field, respectively.

Therefore, magneto-mechanical stress resultants (Eqs. (12)-(14)) can be re-written as

$$N_x = C_{11}A\left[\frac{\partial u}{\partial x} + \frac{1}{2}\left(\frac{\partial w}{\partial x}\right)^2\right] + q_{31}\psi \tag{24}$$

$$M_x = -I_z\left(C_{11} + \frac{q_{31}^2}{a_{33}}\right)\frac{\partial^2 w}{\partial x^2} \tag{25}$$

$$T_{xxz} = -g_{31}h\frac{\partial^2 w}{\partial x^2} + f_{31}\psi \tag{26}$$

where $I_z = \int_A z^2 dA$ is dedicated for area moment of inertia.

According to Eq. (24), axial stress resultant involves mechanical and magnetic parts. Thus, the magnetic axial stress resultant can be presented as

$$N^{Mag} = q_{31}\psi \tag{27}$$

where we suppose the above value as axial magnetic force acted on both ends of the nanotube (due to longitudinal magnetic field), hence

$$N_x^0 = N^{Mag} \tag{28}$$

The kinetic energy can be associated with the nanotube as follows

$$K = \frac{1}{2}\int\int_A \rho(z)\left[\left(\frac{\partial u_1}{\partial t}\right)^2 + \left(\frac{\partial u_3}{\partial t}\right)^2\right] dA dz \tag{29}$$

or with (1) and (2) as

$$K = \frac{1}{2}\int\int_A \rho(z)\left[\left(\frac{\partial u}{\partial t} - z\frac{\partial^2 w}{\partial x \partial t}\right)^2 + \left(\frac{\partial w}{\partial t}\right)^2\right] dA dz \tag{30}$$

Finally, the first variational schema of kinetic energy would be

$$\delta K = \int_A \left[-I_0\frac{\partial^2 u}{\partial t^2}\delta u + I_1\frac{\partial^3 w}{\partial x \partial t^2}\delta u - I_1\frac{\partial^3 u}{\partial x \partial t^2}\delta w + I_2\frac{\partial^4 w}{\partial x^2 \partial t^2}\delta w - I_0\frac{\partial^2 w}{\partial t^2}\delta w\right] dA \tag{31}$$

where $\left\{I_0, I_1, I_2 = \int_{-h/2}^{h/2}\rho(z)\left(1, z, z^2\right)dz\right\}$ is depicted for the mass moments of inertia.

The corresponding magneto-mechanical governing equations can be derived by imposing Eq. (8) as

$$\frac{\partial N_x}{\partial x} = I_0 \frac{\partial^2 u}{\partial t^2} - I_1 \frac{\partial^3 w}{\partial x \partial t^2} \tag{32}$$

$$\frac{\partial^2 M_x}{\partial x^2} + \frac{\partial^2 T_{xxz}}{\partial x^2} + \frac{\partial}{\partial x}\left(N_x \frac{\partial w}{\partial x} \right) = I_0 \frac{\partial^2 w}{\partial t^2} + I_1 \frac{\partial^3 u}{\partial x \partial t^2} - I_2 \frac{\partial^4 w}{\partial x^2 \partial t^2} \tag{33}$$

Due to their premier chemical, electrical and mechanical properties, nanostructured elements such as nanobeams, nanotubes, nanoshells, and nanosheets are customarily used as components in nano-electro-mechanical devices. Therefore, accurate prediction of the vibrational characteristics of nanostructures is essential for engineering and production design. On the other hand, classical mechanic theory cannot predict the size-effect at the nanoscale. At the nanoscale, size-effects became important and even dominated. Both the experimental results and the results of the molecular dynamics simulation show that the size-effect on the mechanical properties of materials is extraordinary and meaningful when the dimensions of these structures are scaled down. To tackle this problem, there can be found three methods proposed for analyzing nanostructures, namely atomic mechanics [47, 48], atomic-continuum mechanics (multiscale methods) [49, 50] and continuum mechanics [51]. However, the third method has a lower computational cost than the previous two methods. In this research, the theory of non-classical continuum mechanics is utilized. It should be noted that this theory itself is divided into several sub-theories. Some researchers have used couple stress theories to examine the effect of scale [52-57], others have employed Eringen's nonlocal theory [58-64], some have utilized the theory of first and second strain gradient elasticity [65-68], and some other researchers have exerted a combination of these theories. They have merged and incorporated more up-to-date theories, such as the nonlocal theory of strain gradient [69], or the stress-driven nonlocal elasticity theory [70, 71]. Some also have developed Eringen's nonlocal theory [72, 73]. In this study, the nonlocal theory of strain gradient is used, which may simulate more accurate the mechanical behavior of nanostructures in continuous models. The nature of this theory is based on two principles: first, stress at any point is a function of strain at the same point and also in all parts of the body, which is known as the nonlocal section; and second, strain gradients in a material particle are substantial which this part is well-known as gradient section. Researchers in the

field of nanomechanics of continuous models have significantly moved toward this theory in recent years and have benefited from it [74-82].

In this section, the nonlocal elasticity model of strain gradient for the PF-NT is expanded in a general form as follows [69, 83-85]:

$$\left(1-\mu\frac{\partial^2}{\partial x^2}\right)\sigma_{xx}^{NonLocal}=\left(1-l^2\frac{\partial^2}{\partial x^2}\right)\left\{C_{11}\left[\frac{\partial u}{\partial x}+\frac{1}{2}\left(\frac{\partial w}{\partial x}\right)^2\right]-z\left(C_{11}+\frac{q_{31}^2}{a_{33}}\right)\frac{\partial^2 w}{\partial x^2}+\frac{q_{31}\psi}{h}\right\} \quad (34)$$

where $l(nm)$ is the gradient parameter and $l>0$ establishes non-zero strain gradient into the model; and $\mu(nm^2)$ allocates nonlocality. Noted that $\mu(nm)^2=(e_0a)^2$ in which e_0 and a are two small scale factors that determine the nonlocal parameter. It is germane to note that both factors are dependent on the nature of the model and physical conditions and cannot be material constants [86, 87]. This means they are not a constant value for each material something like elasticity modulus.

The effect of small scale on the stress resultants can be implemented by plugging Eq. (34) to Eqs. (24)-(26) as

$$N_x-\mu\frac{\partial^2 N_x}{\partial x^2}=\left(1-l^2\frac{\partial^2}{\partial x^2}\right)\left\{C_{11}A\left[\frac{\partial u}{\partial x}+\frac{1}{2}\left(\frac{\partial w}{\partial x}\right)^2\right]+q_{31}\psi\right\} \quad (35)$$

$$M_x-\mu\frac{\partial^2 M_x}{\partial x^2}=\left(1-l^2\frac{\partial^2}{\partial x^2}\right)\left\{-I_z\left(C_{11}+\frac{q_{31}^2}{a_{33}}\right)\frac{\partial^2 w}{\partial x^2}\right\} \quad (36)$$

$$T_{xxz}-\mu\frac{\partial^2 T_{xxz}}{\partial x^2}=\left(1-l^2\frac{\partial^2}{\partial x^2}\right)\left\{-g_{31}h\frac{\partial^2 w}{\partial x^2}+f_{31}\psi\right\} \quad (37)$$

Note that due to lack of a third additional equation, the small scale effects for Eq. (37) are omitted. Eqs. (35) and (36) with respect to Eqs. (32) and (33) can be simplified as

$$\begin{aligned}N_x=&\mu\left(I_0\frac{\partial^3 u}{\partial x\partial t^2}-I_1\frac{\partial^4 w}{\partial x^2\partial t^2}\right)\\&+C_{11}A\left[\frac{\partial u}{\partial x}+\frac{1}{2}\left(\frac{\partial w}{\partial x}\right)^2-l^2\left(\frac{\partial^3 u}{\partial x^3}+\frac{\partial^2 w}{\partial x^2}\frac{\partial^2 w}{\partial x^2}+\frac{\partial w}{\partial x}\frac{\partial^3 w}{\partial x^3}\right)\right]+q_{31}\psi\end{aligned} \quad (38)$$

$$\begin{aligned}M_x=&-\mu\left(\frac{\partial^2 T_{xxz}}{\partial x^2}-N_x^0\frac{\partial^2 w}{\partial x^2}-I_0\frac{\partial^2 w}{\partial t^2}-I_1\frac{\partial^3 u}{\partial x\partial t^2}+I_2\frac{\partial^4 w}{\partial x^2\partial t^2}\right)\\&-I_z\left(C_{11}+\frac{q_{31}^2}{a_{33}}\right)\left(\frac{\partial^2 w}{\partial x^2}-l^2\frac{\partial^4 w}{\partial x^4}\right)\end{aligned} \quad (39)$$

In this paper, we discuss PF-NT with reference to homogeneity in the material; therefore, I_1 will disappear.

In the case of a nonlinear conservative system, we can consider nonlinear oscillations as follows. First, let us note that in this case we have non-harmonic oscillations, that is $u(x,t) \neq v_1(x)\cos(\omega t)$, and $w(x,t) \neq v_2(x)\cos(\omega t)$ in general. Nevertheless, for conservative systems we have periodic solutions as

$$u(x,t) = v_1(x,t) = v_1(x,t+T) \tag{40}$$

$$w(x,t) = v_2(x,t) = v_2(x,t+T) \tag{41}$$

where T is a minimal period. We replace T using the relation $T = 2\pi/\omega$ in which ω is frequency. Moreover, v_1 and v_2 are the vibration amplitudes.

The following change of variable $\omega t \to \tau$ can be made. In this case, we get

$$\frac{\partial v_1}{\partial t} = \omega \frac{\partial v_1}{\partial \tau} \tag{42}$$

$$\frac{\partial v_2}{\partial t} = \omega \frac{\partial v_2}{\partial \tau} \tag{43}$$

Thus, strain and kinetic energies can be written in the framework of below

$$U = \frac{1}{2}\int_0^L \left\{ \sigma_{xx} \left[\frac{\partial v_1}{\partial x} - z\frac{\partial^2 v_2}{\partial x^2} + \frac{1}{2}\left(\frac{\partial v_2}{\partial x}\right)^2 \right] \right\} dx \tag{44}$$

$$K = \frac{1}{2}\int_0^L \left\{ I_0\omega^2 \left[\left(\frac{\partial v_1}{\partial \tau}\right)^2 + \left(\frac{\partial v_2}{\partial \tau}\right)^2 \right] + I_2\omega^2 \left(\frac{\partial^2 v_2}{\partial x \partial \tau}\right)^2 \right\} dx \tag{45}$$

$$W = -\frac{1}{2}\int_0^L N_x^0 \left(\frac{\partial v_2}{\partial x}\right)^2 dx \tag{46}$$

As approximate solutions we can use

$$v_1(x,\tau) = V_1(x)\cos\tau \tag{47}$$

$$v_2(x,\tau) = V_2(x)\cos\tau \tag{48}$$

Then integrating by time from the obtained equation over (0, 2π) will exclude the time from the equations.

Note that in the following the real part of frequency is considered only. Finally, putting Eqs. (37)-(39) into Eqs. (44)-(46), then connecting Eqs. (44)-(46) together ($K+U+W=0$) and imposing Hamiltonian gives the characteristic equation of frequency of the PF-NT which can be shortened and simplified as below

$$\left(\omega^2 M + K_1\right)\{X\} + \{X\} K_2 \{X\} = 0 \tag{49}$$

in which K_1, K_2, and M are coefficients related to stiffness and mass, respectively, and $X = \begin{Bmatrix} V_1 \\ V_2 \end{Bmatrix}$.

3. Rayleigh-Ritz approach

To catch a general solution for the aforesaid nonlinear equation (Eq. (49)), the analytical solutions are mostly incapable and restricted to get a solution. Moreover, numerical methods consume a large time to present a solution [88, 89]. On the other side, semi-analytical techniques, e.g., the Rayleigh-Ritz method presented its simplicity and speed of solving to compute the eigenvalue problems that existed in engineering problems [90-94]. This method in what follows will be indicated.

$$V_1(x) = \sum_{j=1}^{N} a_j \varphi_j(x) \tag{50a}$$

$$V_2(x) = \sum_{j=1}^{N} b_j \psi_j(x) \tag{50b}$$

in which N denotes a number of considered base elements and will determine the convergence to the exact solution, a_j and b_j are the unknown variables to be determined and, φ_j and ψ_j denote the basic mode shapes demonstrated as below

$$\varphi_j(x) = f_\varphi T_j(x) \tag{51a}$$

$$\psi_j(x) = f_\varphi T_j(x) \tag{51b}$$

where

$$f_\varphi = \left(\frac{x}{L}\right)^{\eta} \times \left(1 - \frac{x}{L}\right)^{\xi} \tag{52}$$

in which η and ξ associates an exponent to convey various boundary conditions (BCs) as seen in Table 1. Here SS, CS, CC denote the simply supported – simply supported, clamped-simply supported, and clamped–clamped BCs, respectively. Other polynomial base function is defined as

$$T_j = x^{j-1} \tag{53}$$

The dedicated kinematic and nonlocal strain gradient constitutive boundary conditions can be expressed by Table 2 [95-98]

Herein, by means of the simple solution of the quadratic polynomial equation (Eq. (49)), the results of nonlinear frequency can be determined. The positive values are considered only.

4. Numerical results

4.1. Results' accreditation

In this subsection in order to validate the model and the proposed technique, Eq. (49) will be reduced to a simple case to receive the validation. To achieve the simple case, we avoid the strain gradient effect, piezomagnetic and FM properties of the problem; however, we take the nonlocality into account. To do this, on the basis of Rayleigh-Ritz formulation, the simple case can be converted into two subcases, namely nonlinear and linear parts as shown by Eq. (54) and (55). In addition to these, we also investigate the results of the Navier solution technique for this simple case as illustrated by Eq. (56). Furthermore, in order to identify the accuracy of the present Rayleigh-Ritz formulation, a reference is dedicated as [99] and the numerical comparison is tabulated by Table 3. It is to be noted that here N=5 as [93, 100].

- Rayleigh quotient based on the nonlinear strains and simple case:

$$\omega_{NL}^2 = \frac{C_{11}I_z\int_0^L\left(\frac{\partial^2 V_2}{\partial x^2}\right)^2 dx + C_{11}A\int_0^L\left[\frac{\partial V_1}{\partial x}+\frac{1}{2}\left(\frac{\partial V_2}{\partial x}\right)^2\right]^2 dx}{\int_0^L\left[I_0 {V_2}^2 + I_2\left(\frac{\partial V_2}{\partial x}\right)^2 - \mu\left(I_0 V_2\frac{\partial^2 V_2}{\partial x^2} - I_2\left(\frac{\partial^2 V_2}{\partial x^2}\right)^2\right)\right]dx} \tag{54}$$

- Rayleigh quotient based on the linear strains and simple case:

$$\omega_L^2 = \frac{I_z C_{11} \int_0^L \left(\frac{\partial^2 v_2}{\partial x^2} \right)^2 dx}{\int_0^L \left[I_0 {v_2}^2 + I_2 \left(\frac{\partial v_2}{\partial x} \right)^2 - \mu \left(I_0 v_2 \frac{\partial^2 v_2}{\partial x^2} - I_2 \left(\frac{\partial^2 v_2}{\partial x^2} \right)^2 \right) \right] dx} \tag{55}$$

- Navier-type solution with linear strains and simple case:

$$\omega^2 = \frac{I_z C_{11} \left(\frac{\pi}{L} \right)^4}{\mu \left[I_0 \left(\frac{\pi}{L} \right)^2 + I_2 \left(\frac{\pi}{L} \right)^4 \right] + I_0 + I_2 \left(\frac{\pi}{L} \right)^2} \tag{56}$$

The tabular validation is regarding the growth of slenderness ratio (L/h), and nonlocal parameter (μ). Also, the following elasticity property; $E=1TPa$ is used, and the thickness is considered as $h=1nm$. Moreover, the frequencies are dimensionless using $\Omega = \omega L^2 \sqrt{\frac{\rho A}{EI}}$.

Clearly, the comparative results between outputs of Navier-type solution in the present paper and those attained by the literature present a completely acceptable correlation. On the other side, there cannot be observed any difference among the outputs of linear Rayleigh-Ritz method compared with the Navier cases even for higher values of nonlocal parameter as well as of slenderness ratio.

Elseway, the nonlinear frequencies are indicated by Table 4 by [101-103] and the ratio between nonlinear and linear instances are calculated. To indicate an approvement for the values of nonlinear frequency computed and obtained in this work, we consider SS edge conditions. Based on the demonstrated and tabulated results, the outcomes of present nonlinear analysis can be confirmed.

4.2. Discussion of the problem

Obviously, no one can find a frequency analysis of a PF-NT while geometrically nonlinearity is taken into account. To estimate the present problem, the existence quantities in Table 5 are employed [21, 22]. Note that all the eigenfrequencies extracted in the section are respecting the first mode only.

To consider a NSGT case, both nonlocal and strain gradient parameters perform outstanding roles. In point of fact, the values of both factors determine the value of frequency. As far as it was mentioned before about depending of these factor's values on many situations, Thus, exploring among the literature to pick up a logical limit for both parameters can be a time-effective choice. For nonlocal parameter the 0.5 nm$<e_0a<$0.8 nm [90], and $0<e_0a\leq$2 nm [104, 105], were found and then can be applied. However, there was no reference for strain gradient parameter values. Therefore, a lower bound limit is chosen for the values.

4.2.1 The effect of nonlocal parameter

Figure 2 carries out the influence of the nonlocal parameter versus both linear and nonlinear analyses of eigenfrequency. It is visible that the nonlinear case demonstrates greater results. This may be due to the fact that physically the geometrically nonlinear analysis gives the material axial forces because of presence of tension in mid-surface. So, the frequency capability of material will be higher which will lead to higher frequencies. Moreover, the nonlinear analysis eliminates the strain as a result of rigid displacements in a large deflection study (Note that in our work the mean of rigid displacement is any movement without deformation). Thus, e.g., in a nonlinear bending analysis the deflections will be lesser compared to the linear case. In a nonlinear vibration problem, the mode shapes will be bigger and the material because of large deformations, can capture higher frequencies.

As seen by the figure, any incremental change in the amount of nonlocal parameter leads to a decrease in dimensionless frequency values. This effect and the decreasing trend are more apparent when the less flexible end condition is considered. In fact, the slope is steeper. The most obvious result of the figure is the lesser effect of nonlinear analysis against the linear one for simple supported–simple supported end conditions. Physically, it can be interpreted that when the type of boundary condition is more flexible, the displacements and deflections are further rigid. Therefore, the difference between results of nonlinear and linear states is smaller in such the boundaries. This means that the beam has little stability and the material of the beam does not show significant resistance to large displacement, and therefore we do not see a substantial difference between nonlinear

and linear frequencies in these cases. When the boundary condition has fewer degrees of freedom, the stretching effect more appears in the layers of thickness and large deformations are established more, which results in a noticeable difference in the results of nonlinear frequency versus linear in such the boundary conditions. Finally, as a last case in the figure, it can be said that the greatest frequencies are related to the boundary condition with the lowest degrees of freedom.

4.2.2 The effect of strain gradient parameter

One of the most important results of comparing nonlinear to linear frequency analysis in Figure 3 has been shown by changing the numerical values of the strain gradient parameter. In the figure, the range of the value of the strain gradient parameter is considered from zero to 2 nm for different boundary conditions. Returning to the figure, it is visible that increase of the values of the strain gradient parameter leads to augmenting the distance between nonlinear and linear frequency results. It may be how interpreted that when the numerical value of the strain gradient parameter increments, the hardening effect of the material enhances and the frequencies naturally become more pronounced. Thus, it enlarges the effect of nonlinear analysis, and the results of linear and nonlinear analysis move away from each other. Purely, the higher the fundamental natural frequencies of the system, the further visible the nonlinear frequencies. More valuable point that can be extracted from this figure is that the effect of rising in value of the strain gradient parameter is greater on the boundary condition with lower degrees of freedom. According to the figure, the clamped-clamped boundary condition is affected largely by growing the value of the strain gradient parameter and the incremental trend occurs more rapidly in this less flexible boundary condition.

4.2.3 The effect of magnetic field

Figure 4 provides the effect of the magnetic field on the linear and nonlinear frequencies and a comparison between these two frequency modes by changing the amount of magnetic potential. Based on the data in the figure, it can be realized that increasing the values of the magnetic potential will lead to a rise in the eigenfrequency of the system in both linear and nonlinear states. In addition, the slope of the increment in the values of the frequencies in the nonlinear case is steeper than the linear one. Physically, it can be

deduced that since the positive magnetic potential, in general, the positive magnetic field has a tightening effect on materials due to the contraction, the large amounts of positive magnetic potential can make greater natural frequencies and provide clearly the nonlinear frequency impact. Hence, the results of linear and nonlinear frequencies move away from each other. To conclude the discussion on the effect of magnetic potential, the boundary conditions can be considered through which several boundary conditions are studied. As can be observed from the figure, the incremental slope of the nonlinear frequency values resulting from the increase in the magnetic potential at all boundary conditions will be steeper. Therefore, it can be concluded that in high values of magnetic potential and in general in strong magnetic fields, the difference between the nonlinear frequencies and the linear ones is further notable.

4.2.4 The effect of slenderness ratio

Figure 5 displays a consideration of the effect of length-to-diameter ratio (slenderness ratio) for the problem. It is worthy to note that the difference between nonlinear and linear cases increments by enlarging the length of the beam. It can be said that when the beam's length is long, the effect of nonlinear analysis is considerable. This can display the role of nonlinear analysis in vibrating behavior and emphasize on using this model of study.

4.2.5 The effect of axial inertia

In this work, we implemented the axial inertia effect in the formulation of eigenfrequencies contrarily to what has been usually accomplished. To demonstrate this effect, Figure 6 is plotted. This effect has been ignored in many studies performed on nonlinear vibrations of small or macro scale structures. As seen by Figure 6, while the effect is included, the nonlinear frequencies decrease. One can see the more pronounced discrepancy for lower values of slenderness ratio where the axial inertia causes appreciable reductions into the frequencies. This conclusion corresponds to the foregoing numerical data [106].

To make the effect of axial inertia rather obvious, some tabular results are presented by Table 6 in which assorted boundary conditions are inspected. As seen by the table, the presence of axial inertia is more prominent for tubes with fully fixed ends. All

in all, how we can terminate this discussion is that the axial inertia can be an effective factor in nonlinear vibration studies of macro/nano-structures.

5. Conclusions

This study analyzed nonlinear frequencies for a nanotube concerning the Euler-Bernoulli motion field. To accomplish the nanoscale size effect, the motion equations were shifted into NSGT relations. The relations governing the problem which are the nonlinear partial differential equations, were obtained by which the nonlinear vibrational equations of the PF-NT were computed. It was then converted to nonlinear algebraic equations by the Rayleigh-Ritz method. Free vibrations have been investigated in two cases, linear and nonlinear, for some kinds of boundary conditions: simply supported –simply supported, clamped–clamped, and clamped–simply supported. The results were compared with those of Navier's solution and the parametric analysis of the results was presented. The most superior shortened points harvested by our work can be implied as follows which can aid the designers in the MEMS/NEMS industries:

* Whenever the fundamental natural frequencies of a nanotube are enough big, the nonlinear frequencies will be more vital. In this category, the less flexible boundary conditions, the higher values of strain gradient, the longer nanotube, and a stronger positive magnetic field bring about greater fundamental natural frequencies.

* The shorter the length of the nanotube, the larger the effect of axial inertia.

Conflict of Interest Statement

The authors declare that they have no known competing financial interests or personal relationships that could have appeared to influence the work reported in this paper.

Acknowledgements

V.A.E acknowledges the support of the Government of the Russian Federation (contract No. 14.Z50.31.0046).

References

[1] W. Fahrner, Nanotechnology and Nanoelectronics, Springer, (2005). DOI: 10.1007/b137771

[2] A. F. Kabychenkov, F. V. Lisovskii, Flexomagnetic and flexoantiferromagnetic effects in centrosymmetric antiferromagnetic materials, Technical Physics, 64 (2019) 980-983.

[3] E. A. Eliseev, A. N. Morozovska, M. D. Glinchuk, R. Blinc, Spontaneous flexoelectric/flexomagnetic effect in nanoferroics, Physical Review B, 79 (2009) 165433.

[4] P. Lukashev, R. F. Sabirianov, Flexomagnetic effect in frustrated triangular magnetic structures, Physical Review B, 82 (2010) 094417.

[5] L.-L. Ke, Y.-S. Wang, Free vibration of size-dependent magneto-electro-elastic nanobeams based on the nonlocal theory, Physica E: Low-dimensional Systems and Nanostructures, 63 (2014) 52-61.

[6] T.-P. Chang, Nonlinear free vibration analysis of nanobeams under magnetic field based on nonlocal elasticity theory, Journal of Vibroengineering, 18 (2016) 1912-1919.

[7] M. Baghani, M. Mohammadi, A. Farajpour, Dynamic and Stability Analysis of the Rotating Nanobeam in a Nonuniform Magnetic Field Considering the Surface Energy, International Journal of Applied Mechanics, 8 (2016) 1650048.

[8] F. Ebrahimi, M. R. Barati, Porosity-dependent vibration analysis of piezo-magnetically actuated heterogeneous nanobeams, Mechanical Systems and Signal Processing, 93 (2017) 445-459.

[9] A. M. Zenkour, M. Arefi, N. A. Alshehri, Size-dependent analysis of a sandwich curved nanobeam integrated with piezomagnetic face-sheets, Results in Physics, 7 (2017) 2172-2182.

[10] X.-P. Sun, Y.-.Z. Hong, H.-L. Dai, L. Wang, Nonlinear frequency analysis of buckled nanobeams in the presence of longitudinal magnetic field, Acta Mechanica Solida Sinica, 30 (2017) 465-473.

[11] M. Arefi, A. M. Zenkour, Transient sinusoidal shear deformation formulation of a size-dependent three-layer piezo-magnetic curved nanobeam, Acta Mechanica, 228 (2017) 3657-3674.

[12] H. Liu, H. Liu, J. Yang, Vibration of FG magneto-electro-viscoelastic porous nanobeams on visco-Pasternak foundation, Composites Part B: Engineering, 155 (2018) 244-256.

[13] M. Arefi, A. H. Soltan Arani, Higher order shear deformation bending results of a magnetoelectrothermoelastic functionally graded nanobeam in thermal, mechanical, electrical, and magnetic environments, Mechanics Based Design of Structures and Machines, an International Journal, 46 (2018) 669-692.

[14] B. Alibeigi, Y. T. Beni, On the size-dependent magneto/electromechanical buckling of nanobeams, The European Physical Journal Plus, 133 (2018) 398.

[15] A. Azar, M. Ben Said, L. Azrar, A. A. Aljinaidi, Dynamic instability analysis of magneto-electro-elastic beams with uncertain parameters under static and parametric electric and magnetic fields, Composite Structures, 226 (2019) 111185.

[16] Y.-X. Zhen, S.-L. Wen, Y. Tang, Free vibration analysis of viscoelastic nanotubes under longitudinal magnetic field based on nonlocal strain gradient Timoshenko beam model, Physica E: Low-dimensional Systems and Nanostructures, 105 (2019) 116-124.

[17] M. Malikan, V. B. Nguyen, Buckling analysis of piezo-magnetoelectric nanoplates in hygrothermal environment based on a novel one variable plate theory combining with higher-order nonlocal strain gradient theory, Physica E: Low-dimensional Systems and Nanostructures, 102 (2018) 8-28.

[18] S. S. Mirjavadi, M. Forsat, M. Nikookar, M. Reza Barati, AMS Hamouda, Nonlinear forced vibrations of sandwich smart nanobeams with two-phase piezo-magnetic face sheets, The European Physical Journal Plus, 134 (2019) 508.

[19] S. S. Mirjavadi, M. Forsat, M. Nikookar, M. Reza Barati, AMS Hamouda, Post-buckling analysis of piezo-magnetic nanobeams with geometrical imperfection and different piezoelectric contents, Microsystem Technologies, 25 (2019) 3477-3488.

[20] M. Ghane, A. Reza Saidi, R. Bahaadini, Vibration of fluid-conveying nanotubes subjected to magnetic field based on the thin-walled Timoshenko beam theory, Applied Mathematical Modelling, 80 (2020) 65-83.

[21] S. Sidhardh, M. C. Ray, Flexomagnetic response of nanostructures, Journal of Applied Physics, 124 (2018) 244101.

[22] N. Zhang, Sh. Zheng, D. Chen, Size-dependent static bending of flexomagnetic nanobeams, Journal of Applied Physics, 126 (2019) 223901.

[23] M. Malikan, V. A. Eremeyev, Free Vibration of Flexomagnetic Nanostructured Tubes Based on Stress-driven Nonlocal Elasticity, Springer Nature, Analysis of Shells, Plates, and Beams, Advanced Structured Materials, 134 (2020). https://doi.org/10.1007/978-3-030-47491-1_12

[24] R. Ansari, M. Faraji Oskouie, R. Gholami, Size-dependent geometrically nonlinear free vibration analysis of fractional viscoelastic nanobeams based on the nonlocal elasticity theory, Physica E: Low-dimensional Systems and Nanostructures, 75 (2016) 266-271.

[25] M. Faraji Oskouie, R. Ansari, F. Sadeghi, Nonlinear vibration analysis of fractional viscoelastic Euler–Bernoulli nanobeams based on the surface stress theory, Acta Mechanica Solida Sinica, 30 (2017) 416–424.

[26] J. Wang, H. Shen, Nonlinear vibrations of axially moving simply supported viscoelastic nanobeams based on nonlocal strain gradient theory, Journal of Physics: Condensed Matter, 31 (2019) 485403.

[27] D. D. Nguyen, D. Q. Vu, D. N. Pham, M. C. Trinh, Nonlinear Dynamic Response of Functionally Graded Porous Plates on Elastic Foundation Subjected to Thermal and Mechanical Loads, Journal of Applied and Computational Mechanics, 4 (2018) 245-259.

[28] Hanif S. Hoseini, Dewey H. Hodges, Nonlinear flutter and limit-cycle oscillations of damaged highly flexible composite wings, Nonlinear Dynamics, 97 (2019) 247–268.

[29] G. Ferrari, P. Balasubramanian, S. Le Guisquet, L. Piccagli, K. Karazis, B. Painter, M. Amabili, Non-linear vibrations of nuclear fuel rods, Nuclear Engineering and Design, 338 (2018) 269–283.

[30] V. A. Eremeyev, W. Pietraszkiewicz, The nonlinear theory of elastic shells with phase transitions, Journal of Elasticity, 74 (2004) 67-86.

[31] H. M. Sedighi, A. Koochi, F. Daneshmand, M. Abadyan, Non-linear dynamic instability of a double-sided nano-bridge considering centrifugal force and rarefied gas flow, International Journal of Non-Linear Mechanics, 77 (2015) 96-106.

[32] H. M. Sedighi, K. Heidari Shirazi, A. Noghrehabadi, A. Yildirim, Asymptotic investigation of buckled beam nonlinear vibration, Iranian Journal of Science and Technology: Transactions of Mechanical Engineering, 36 (2012) 107-116.

[33] H. M. Sedighi, F. Daneshmand, Nonlinear transversely vibrating beams by the homotopy perturbation method with an auxiliary term, Journal of Applied and Computational Mechanics, 1 (2014) 1-9.

[34] Y. Li, M. Li, Dynamic analysis of rotating double-tapered cantilever Timoshenko nano-beam using the nonlocal strain gradient theory, Mathematical Methods in the Applied Sciences, (2020). https://doi.org/10.1002/mma.6616

[35] B. Safaei, N. A. Ahmed, A. M. Fattahi, Free vibration analysis of polyethylene/CNT plates, The European Physical Journal Plus, 134 (2019) 271.

[36] J. Guo, D. Xu, W. Qiu, A finite difference scheme for the nonlinear time-fractional partial integro-differential equation, Mathematical Methods in the Applied Sciences, (2020). https://doi.org/10.1002/mma.6128

[37] R. Rezzag Bara, S. Nicaise, I. Merabet, Finite element approximation of a prestressed shell model, Mathematical Methods in the Applied Sciences, (2020). https://doi.org/10.1002/mma.6196

[38] B. Safaei, The effect of embedding a porous core on the free vibration behavior of laminated composite plates, Steel and Composite Structures, 35 (2020) 659-670.

[39] B. Safaei, R. Moradi-Dastjerdi, K. Behdinan, Z. Qin, F. Chu, Thermoelastic behavior of sandwich plates with porous polymeric core and CNT clusters/polymer nanocomposite layers, Composite Structures, 226 (2019) 111209.

[40] M. E. Golmakani, M. N. Sadraee Far, M. Moravej, Dynamic relaxation method for nonlinear buckling analysis of moderately thick FG cylindrical panels with various boundary conditions, Journal of Mechanical Science and Technology, 30 (2016) 5565–5575.

[41] H. M. Sedighi, K. Heidari Shirazi, Using homotopy analysis method to determine profile for disk cam by means of optimization of dissipated energy, International Review of Mechanical Engineering (I.RE.M.E.), Vol. 05, 2011, n. 5

[42] A. Johan, W. Ari Adi, F. Suryani Arsyad, D. Setiabudidaya, Analysis crystal structure of magnetic materials $Co_{1-x}Zn_xFe_2O_4$, Journal of Physics: Conference Series, 1282 (2019) 012032.

[43] X. Song, S.-R. Li, Thermal buckling and post-buckling of pinned–fixed Euler–Bernoulli beams on an elastic foundation, Mechanics Research Communications, 34 (2007) 164–171.

[44] J. N. Reddy, Nonlocal nonlinear formulations for bending of classical and shear deformation theories of beams and plates, International Journal of Engineering Science, 48 (2010) 1507-1518.

[45] M. Moory-Shirbani, H. M. Sedighi, H. M. Ouakad, F. Najar, Experimental and mathematical analysis of a piezoelectrically actuated multilayered imperfect microbeam subjected to applied electric potential, Composite Structures, 184 (2018) 950-960.

[46] H. M. Ouakad, H. M. Sedighi, Static response and free vibration of MEMS arches assuming out-of-plane actuation pattern, International Journal of Non-Linear Mechanics, 110 (2019) 44-57.

[47] R. Ansari, S. Ajori, B. Arash, Vibrations of single- and double-walled carbon nanotubes with layerwise boundary conditions: A molecular dynamics study, Current Applied Physics, 12 (2012) 707-711.

[48] S. Seifoori, F. Abbaspour, E. Zamani, Molecular dynamics simulation of impact behavior in multi-walled carbon nanotubes, Superlattices and Microstructures, 14 (2020) 106447.

[49] F. Ebrahimi, A. Dabbagh, Vibration analysis of multi-scale hybrid nanocomposite plates based on a Halpin-Tsai homogenization model, Composites Part B: Engineering, 173 (2019) 106955.

[50] F. Ebrahimi, A. Dabbagh, An analytical solution for static stability of multi-scale hybrid nanocomposite plates, Engineering with Computers (2019). https://doi.org/10.1007/s00366-019-00840-y

[51] H. Altenbach, V. A. Eremeyev, On the Continuum Mechanics Approach in Modeling Nanosized Structural Elements, New Frontiers of Nanoparticles and Nanocomposite Materials. Advanced Structured Materials, 4 (2012). https://doi.org/10.1007/8611_2012_67

[52] H. Zeighampour, Y. Tadi Beni, Size-dependent vibration of fluid-conveying double-walled carbon nanotubes using couple stress shell theory, Physica E: Low-dimensional Systems and Nanostructures, 61 (2014) 28-39.

[53] B. Akgöz, Ö. Civalek, Free vibration analysis for single-layered graphene sheets in an elastic matrix via modified couple stress theory, Materials and Design 42 (2012) 164-171.

[54] M. Malikan, Electro-mechanical shear buckling of piezoelectric nanoplate using modified couple stress theory based on simplified first order shear deformation theory, Applied Mathematical Modelling, 48 (2017) 196-207.

[55] A. Skrzat, V. A. Eremeyev, On the effective properties of foams in the framework of the couple stress theory, Continuum Mechanics and Thermodynamics (2020). https://doi.org/10.1007/s00161-020-00880-6

[56] H. M. Sedighi, A. Bozorgmehri, Dynamic instability analysis of doubly clamped cylindrical nanowires in the presence of Casimir attraction and surface effects using modified couple stress theory, Acta Mechanica, 227 (2016) 1575–1591.

[57] Y. Yuan, K. Zhao, Y. Han, S. Sahmani, B. Safaei, Nonlinear oscillations of composite conical microshells with in-plane heterogeneity based upon a couple stress-based shell model, Thin-Walled Structures, 154 (2020) 106857.

[58] A. M. Fattahi, B. Safaei, N. A. Ahmed, A comparison for the non-classical plate model based on axial buckling of single-layered graphene sheets, The European Physical Journal Plus, 134 (2019) 555.

[59] B. Safaei, F. Hamed Khoda, A. M. Fattahi, Non-classical plate model for single-layered graphene sheet for axial buckling, Advances in Nano Research, 7 (2019) 265-275.

[60] N. Radić, D. Jeremić, S. Trifković, M. Milutinović, Buckling analysis of double-orthotropic nanoplates embedded in Pasternak elastic medium using nonlocal elasticity theory, Composites Part B: Engineering, 61 (2014) 162-171.

[61] M. Aydogdu, A general nonlocal beam theory: Its application to nanobeam bending, buckling and vibration, Physica E: Low-dimensional Systems and Nanostructures, 41 (2009) 1651-1655.

[62] J. N. Reddy, S. El-Borgi, Eringen's nonlocal theories of beams accounting for moderate rotations, International Journal of Engineering Science, 82 (2014) 159-177.

[63] M. S. Atanasov, V. Stojanović, Nonlocal forced vibrations of rotating cantilever nano-beams, European Journal of Mechanics - A/Solids, 79 (2020) 103850.

[64] S. A. M. Ghannadpour, Ritz Method Application to Bending, Buckling and Vibration Analyses of Timoshenko Beams via Nonlocal Elasticity, Journal of Applied and Computational Mechanics, 4 (2018) 16-26.

[65] R. D. Mindlin, Second gradient of train and surface-tension in linear elasticity, International Journal of Solids and Structures, 1 (1965) 417-438.

[66] R. D. Mindlin, N. N. Eshel, On first strain-gradient theories in linear elasticity, International Journal of Solids and Structures, 4 (1968) 109-124.

[67] B. Akgöz, Ö. Civalek, Longitudinal vibration analysis for microbars based on strain gradient elasticity theory, Journal of Vibration and Control, 20 (2014) 606-616.

[68] H. M. Sedighi, Size-dependent dynamic pull-in instability of vibrating electrically actuated microbeams based on the strain gradient elasticity theory, Acta Astronautica, 95 (2014) 111-123.

[69] C. W. Lim, G. Zhang, J. N. Reddy, A Higher-order nonlocal elasticity and strain gradient theory and Its Applications in wave propagation, Journal of the Mechanics and Physics of Solids, 78 (2015) 298-313.

[70] G. Romano, R. Barretta, Nonlocal elasticity in nanobeams: the stress-driven integral model, International Journal of Engineering Science, 115 (2017) 14-27.

[71] R. Barretta, F. Fabbrocino, R. Luciano, et al. Closed-form solutions in stress-driven two-phase integral elasticity for bending of functionally graded nano-beams, Physica E, 97 (2018) 13-30.

[72] C. C. Koutsoumaris, K.G. Eptaimeros, A research into bi-Helmholtz type of nonlocal elasticity and a direct approach to Eringen's nonlocal integral model in a finite body, Acta Mechanica, 229 (2018) 3629-3649.

[73] M. Lazar, G. A. Maugin, E. C. Aifantis, On a theory of nonlocal elasticity of bi-Helmholtz type and some applications, International Journal of Solids and Structures, 43 (2006) 1404-1421.

[74] M. Şimşek, Some closed-form solutions for static, buckling, free and forced vibration of functionally graded (FG) nanobeams using nonlocal strain gradient theory, Composite Structures, 224 (2019) 111041.

[75] B. Karami, M. Janghorban, On the dynamics of porous nanotubes with variable material properties and variable thickness, International Journal of Engineering Science, 136 (2019) 53-66.

[76] M. Malikan, M. Krasheninnikov, V. A. Eremeyev, Torsional stability capacity of a nano-composite shell based on a nonlocal strain gradient shell model under a three-dimensional magnetic field, International Journal of Engineering Science, 148 (2020) 103210.

[77] S. Sahmani, B. Safaei, Nonlinear free vibrations of bi-directional functionally graded micro/nano-beams including nonlocal stress and microstructural strain gradient size effects, Thin-Walled Structures, 140 (2019) 342-356.

[78] H. Tang, L. Li, Y. Hu, W. Meng, K. Duan, Vibration of nonlocal strain gradient beams incorporating Poisson's ratio and thickness effects, Thin-Walled Structures, 137 (2019) 377-391.

[79] B. Karami, M. Janghorban, T. Rabczuk, Dynamics of two-dimensional functionally graded tapered Timoshenko nanobeam in thermal environment using nonlocal strain gradient theory, Composites Part B: Engineering, 182 (2020) 107622.

[80] F. Ebrahimi, M. R. Barati, Hygrothermal effects on vibration characteristics of viscoelastic FG nanobeams based on nonlocal strain gradient theory, Composite Structures, 159 (2017) 433-444.

[81] P. R. Saffari, M. Fakhraie, M. A. Roudbari, Nonlinear vibration of fluid conveying cantilever nanotube resting on visco-pasternak foundation using non-local strain gradient theory, Micro & Nano Letters, 15 (2020) 181.

[82] M. H. Ghayesh, A. Farajpour, Nonlinear coupled mechanics of nanotubes incorporating both nonlocal and strain gradient effects, Mechanics of Advanced Materials and Structures, 27 (2020) 373-382.

[83] M. Malikan, R. Dimitri, F. Tornabene, Transient response of oscillated carbon nanotubes with an internal and external damping, Composites Part B: Engineering, 158 (2019) 198-205.

[84] M. Malikan, V. A. Eremeyev, On the dynamics of a visco-piezo-flexoelectric nanobeam, Symmetry, 12 (2020) 643. doi: 10.3390/sym12040643

[85] J. Zare, A. Shateri, Y. Tadi Beni, A. Ahmadi, Vibration analysis of shell-like curved carbon nanotubes using nonlocal strain gradient theory, Mathematical Methods in the Applied Sciences, (2020). https://doi.org/10.1002/mma.6599

[86] R. Ansari, S. Sahmani, B. Arash, Nonlocal plate model for free vibrations of single-layered graphene sheets, Physics Letters A, 375 (2010) 53-62.

[87] M. Akbarzadeh Khorshidi, The material length scale parameter used in couple stress theories is not a material constant, International Journal of Engineering Science, 133 (2018) 15-25.

[88] S. K. Jena, S. Chakraverty, F. Tornabene, Vibration characteristics of nanobeam with exponentially varying flexural rigidity resting on linearly varying elastic foundation using differential quadrature method, Materials Research Express, 6 (2019) 085051.

[89] R. Dimitri, F. Tornabene, J. N. Reddy, Numerical study of the mixed-mode behavior of generally-shaped composite interfaces, Composite Structures, 237 (2020) 111935.

[90] R. Ansari, S. Sahmani, H. Rouhi, Rayleigh–Ritz axial buckling analysis of single-walled carbon nanotubes with different boundary conditions, Physics Letters, A 375 (2011) 1255–1263.

[91] M. Teifouet, A. Robinson, S. Adali, Buckling of nonuniform and axially functionally graded nonlocal Timoshenko nanobeams on Winkler-Pasternak foundation, Composite Structures, 206 (2018) 95-103.

[92] Y. Wang, D. Cao, J. Peng, H. Cheng, H. Lin, W. Huang, Nonlinear random responses and fatigue prediction of elastically restrained laminated composite panels in thermo-acoustic environments, Composite Structures, 229 (2019) 111391.

[93] M. Malikan, V. A. Eremeyev, Post-critical buckling of truncated conical carbon nanotubes considering surface effects embedding in a nonlinear Winkler substrate using the Rayleigh-Ritz method, Materials Research Express, 7 (2020) 025005.

[94] S. K. Jena, S. Chakraverty, F. Tornabene, Buckling Behavior of Nanobeams Placed in Electromagnetic Field Using Shifted Chebyshev Polynomials-Based Rayleigh-Ritz Method, Nanomaterials, 9 (2019) 1326.

[95] R. Barretta, F. Marotti de Sciarra, Constitutive boundary conditions for nonlocal strain gradient elastic nano-beams, International Journal of Engineering Science, 130 (2018) 187–198.

[96] R. Barretta, F. Marotti de Sciarra, Variational nonlocal gradient elasticity for nano-beams, International Journal of Engineering Science, 143 (2018) 73–91.

[97] F. Marotti de Sciarra, R. Barretta, A new nonlocal bending model for Euler–Bernoulli nanobeams, Mechanics Research Communications, 62 (2014) 25–30.

[98] G. Romano, R. Barretta, M. Diaco, F. Marotti de Sciarra, Constitutive boundary conditions and paradoxes in nonlocal elastic nanobeams, International Journal of Mechanical Sciences, 121 (2017) 151-156.

[99] L. Lu, X. Guo, J. Zhao, Size-dependent vibration analysis of nanobeams based on the nonlocal strain gradient theory, International Journal of Engineering Science, 116 (2017) 12–24.

[100] S. K. Jena, S. Chakraverty, M. Malikan, Application of shifted Chebyshev polynomial-based Rayleigh–Ritz method and Navier's technique for vibration analysis of a functionally graded porous beam embedded in Kerr foundation, Engineering with Computers (2020). https://doi.org/10.1007/s00366-020-01018-7

[101] T. Pirbodaghi, M.T. Ahmadian, M. Fesanghary, On the homotopy analysis method for non-linear vibration of beams, Mechanics Research Communication, 36 (2009) 143–148.

[102] H. Rafieipour, S. M. Tabatabaei, M. Abbaspour, A novel approximate analytical method for nonlinear vibration analysis of Euler–Bernoulli and Rayleigh beams on the nonlinear elastic foundation, Arabian Journal for Science and Engineering, 39 (2014) 3279–3287.

[103] A. Mirzabeigy, R. Madoliat, Large amplitude free vibration of axially loaded beams resting on variable elastic foundation, Alexandria Engineering Journal, 55 (2016) 1107–1114.

[104] W. H. Duan, C. M. Wang, Exact solutions for axisymmetric bending of micro/nanoscale circular plates based on nonlocal plate theory, Nanotechnology, 18 (2007) 385704.

[105] W. H. Duan, C. M. Wang, Y. Y. Zhang, Calibration of nonlocal scaling effect parameter for free vibration of carbon nanotubes by molecular dynamics, Journal of Applied Physics, 101 (2007) 24305.

[106] A. N. Kounadis, D. Sophianopoulos, The effect of axial inertia on the bending eigenfrequencies of a Timoshenko two-bar frame, Earthquake Engineering and Structural Dynamics, 14 (1986) 429-437.

Table 1. Conditions at both ends based on notations

Conditions	$\eta(x=0)$	$\xi(x=L)$
SS	1	1
CS	2	1
CC	2	2

Table 2. Constitutive boundary conditions

Conditions	Nonlocal strain gradient conditions at (0, L)	Local conditions ($l=\mu=0$) at (0, L)
S	$w=0$ $M=-\left(1+l^2\frac{d^2}{dx^2}\right)M_{cl}+\mu\frac{d}{dx}\left(N_{cl}\frac{dw}{dx}\right)=0$ $M_h=\frac{dM_{cl}}{dx}=0$ $T_{xxz}=-g_{31}h\frac{d^2w}{dx^2}+f_{31}\psi=0$	$w=0$ $M_{cl}=0$ $T_{xxz}=0$
C	$w=0$ $w'=0$ $M\neq 0$ $M_h\neq 0$ $T_{xxz}=0$	$w=0$ $w'=0$ $M_{cl}\neq 0$ $T_{xxz}=0$

* Sub-indexes (*h* and *cl*) are nonlocal and local phases, respectively.

Table 3. Nondimensional natural frequencies of a square nanobeam (First mode, L=10 nm, h=1 nm, ν=0.3, E=1TPa, ρ=2.7kg/dm^3)

L/h	μ	ω_L

		EBT, Navier [99]	EBT, Navier [Present]	EBT, Rayleigh-Ritz, [Present]
5	0	9.7112	9.7112	9.7112
	1	9.2647	9.2647	9.2647
	2	8.8747	8.8747	8.8747
	3	8.5301	8.5301	8.5301
	4	8.2228	8.2228	8.2228
10	0	9.8293	9.8293	9.8293
	1	9.3774	9.3774	9.3774
	2	8.9826	8.9826	8.9826
	3	8.6338	8.6338	8.6338
	4	8.3228	8.3228	8.3228
20	0	9.8595	9.8595	9.8595
	1	9.4062	9.4062	9.4062
	2	9.0102	9.0102	9.0102
	3	8.6604	8.6604	8.6604
	4	8.3483	8.3483	8.3483

Table 4. Ratio of nonlinear to linear cases of frequency for a square macro beam (First mode).

ω_{NL}/ω_L			
Present	[101]	[102]	[103]
1.0874	1.0897	1.0892	1.0892

Table 5. Magneto-mechanical properties of an assumed piezo-flexomagnetic nanotube (PF-NT)

$CoFe_2O_4$
C_{11}=286e9 N/m^2
f_{31}=10^{-10} N/Ampere
q_{31}=580.3 N/Ampere.m
a_{33}=1.57×10^{-4} N/Ampere^2
L=10d, d=1 nm, h=0.34 nm

Table 6. Slenderness ratio vs. axial inertia effect in the nonlinear study of the PF-NT based on several boundary conditions (Ψ=1 *mA*, *l*=1 *nm*, e_0a=0.5 *nm*)

Axial inertia	*L/d*	CC	CS	SS
Presence	5	41.4830	28.1964	16.8231
	10	34.3034	27.5697	18.4081

	20	35.4480	31.4843	22.9379
	30	40.6439	37.1471	28.3744
	40	47.3009	43.7931	34.4555
	5	45.2122	31.0591	18.0210
	10	35.1884	28.3695	18.7697
Absence	20	35.6849	31.7207	23.0533
	30	40.7655	37.2719	28.4381
	40	47.3806	43.8760	34.4992

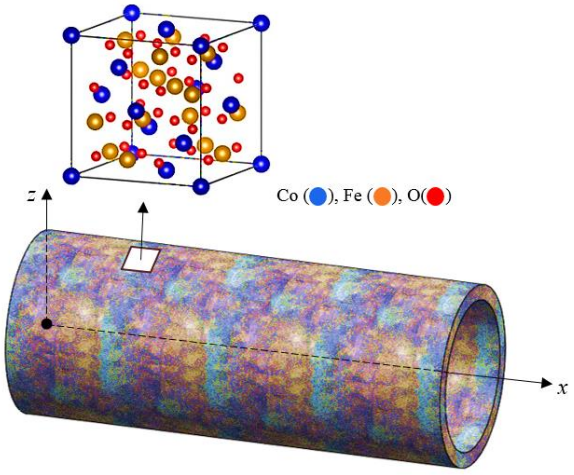

Figure 1. A $CoFe_2O_4$ nanotube

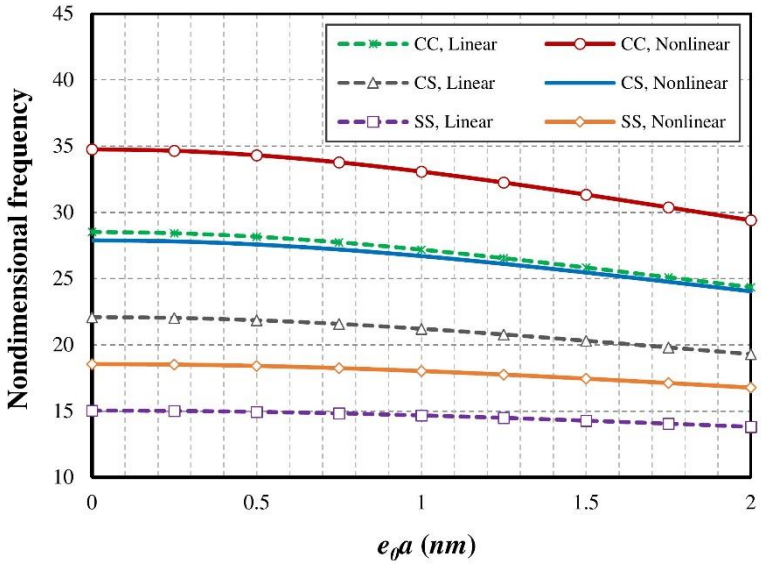

Figure 2. Nonlocal parameter vs. different end conditions for the PF-NT (Ψ=1 *mA*, *l*=1 *nm*)

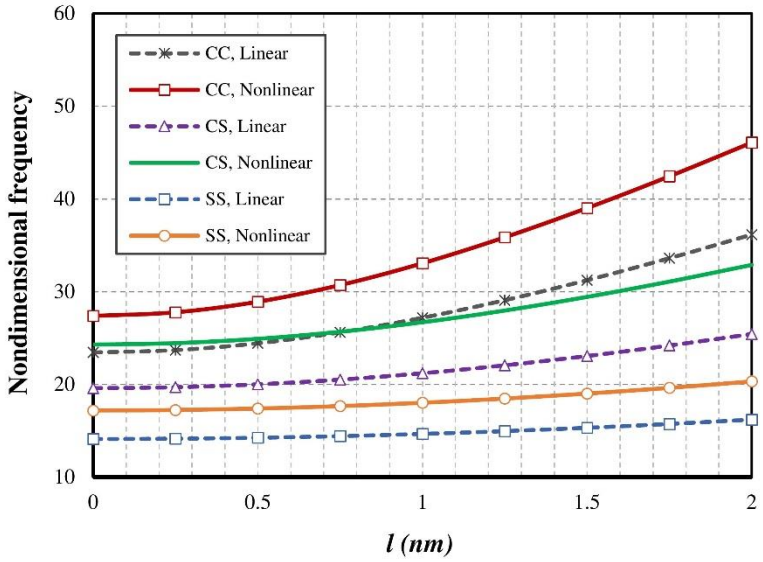

Figure 3. Strain gradient parameter vs. different end conditions for the PF-NT (Ψ=1 *mA*, e_0a=1 nm)

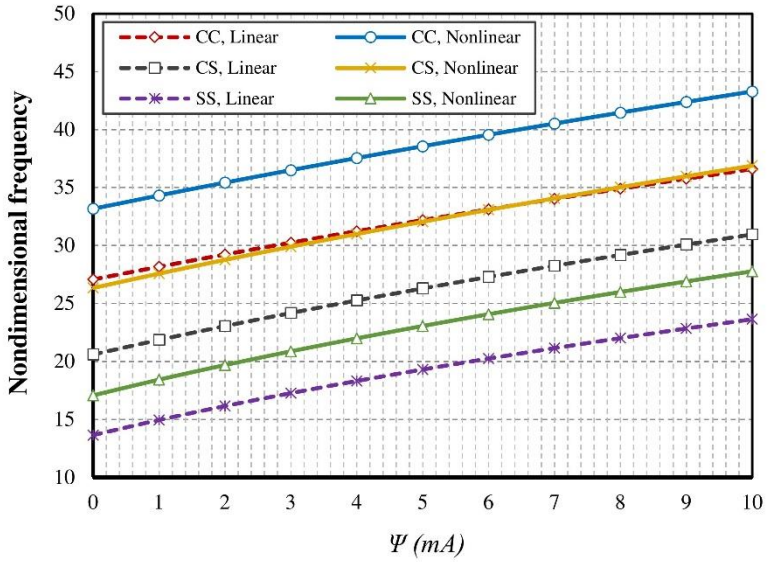

Figure 4. Magnetic potential parameter vs. different end conditions for the PF-NT (l=1 *nm*, e_0a=0.5 *nm*)

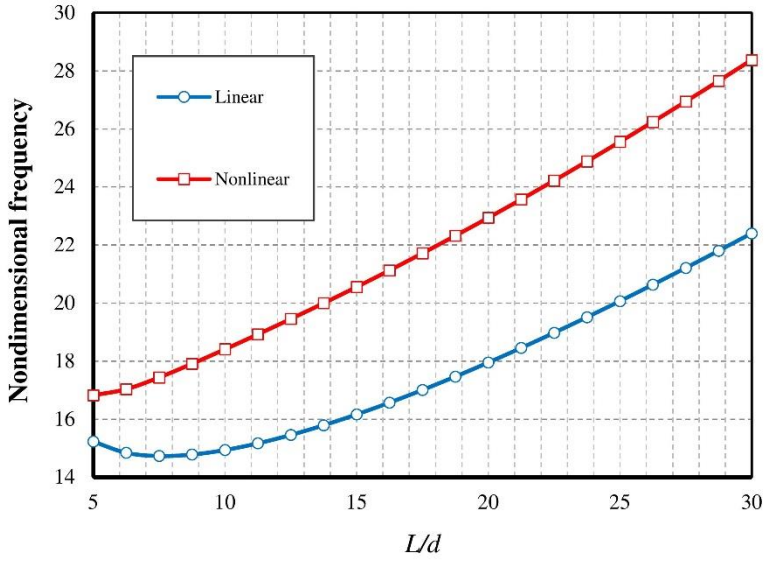

Figure 5. Slenderness ratio vs. linear and nonlinear analyses (Ψ=1 *mA*, *l*=1 *nm*, e_0a=0.5 *nm*, *SS*)

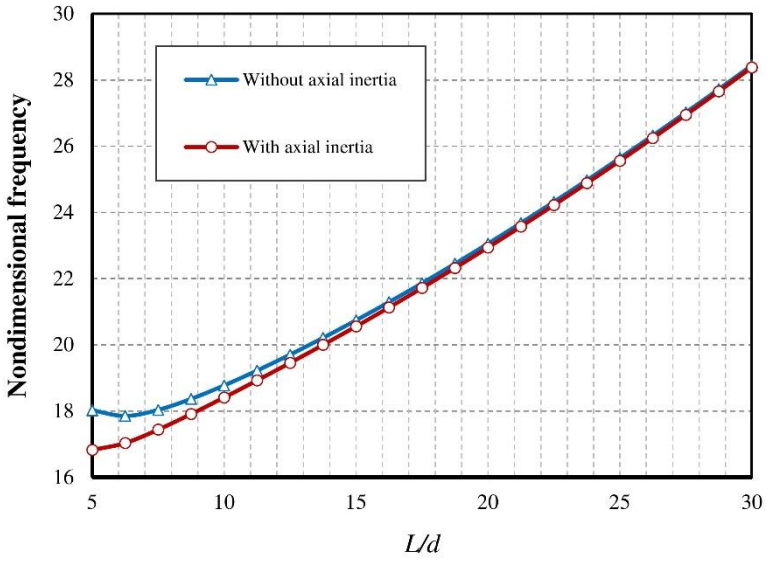

Figure 6. Slenderness ratio vs. the axial inertia effect in the nonlinear case of the PF-NT (Ψ=1 *mA*, *l*=1 *nm*, e_0a=0.5 *nm*, *SS*)

nanomaterials

MDPI

Article

On Nonlinear Bending Study of a Piezo-Flexomagnetic Nanobeam Based on an Analytical-Numerical Solution

Mohammad Malikan [1] and Victor A. Eremeyev [1,2,*]

[1] Department of Mechanics of Materials and Structures, Faculty of Civil and Environmental Engineering, Gdansk University of Technology, 80-233 Gdansk, Poland; mohammad.malikan@pg.edu.pl

[2] Laboratory of Mechanics of Biomaterials, Research and Education Center "Materials", Don State Technical University, Gagarina sq., 1, Rostov on Don 344000, Russia

* Correspondence: victor.eremeev@pg.edu.pl

Received: 19 July 2020; Accepted: 4 September 2020; Published: 6 September 2020

Abstract: Among various magneto-elastic phenomena, flexomagnetic (FM) coupling can be defined as a dependence between strain gradient and magnetic polarization and, contrariwise, elastic strain and magnetic field gradient. This feature is a higher-order one than piezomagnetic, which is the magnetic response to strain. At the nanoscale, where large strain gradients are expected, the FM effect is significant and could be even dominant. In this article, we develop a model of a simultaneously coupled piezomagnetic–flexomagnetic nanosized Euler–Bernoulli beam and solve the corresponding problems. In order to evaluate the FM on the nanoscale, the well-known nonlocal model of strain gradient (NSGT) is implemented, by which the nanosize beam can be transferred into a continuum framework. To access the equations of nonlinear bending, we use the variational formulation. Converting the nonlinear system of differential equations into algebraic ones makes the solution simpler. This is performed by the Galerkin weighted residual method (GWRM) for three conditions of ends, that is to say clamp, free, and pinned (simply supported). Then, the system of nonlinear algebraic equations is solved on the basis of the Newton–Raphson iteration technique (NRT) which brings about numerical values of nonlinear deflections. We discovered that the FM effect causes the reduction in deflections in the piezo-flexomagnetic nanobeam.

Keywords: flexomagnetic; nanobeam; large deflection; NSGT; Galerkin method; Newton–Raphson method

1. Introduction

To study the flexomagnetic (FM) effect and to better identify it, one can use the family close to it, that is, the piezomagnetic effect. In piezomagnetic, simply by compressing or stretching materials, an internal magnetic field is created in them. The piezomagnetic effect and its application can be seen in many materials and structures. However, in addition to these very useful applications, there is an important drawback that this effect can only exist in about 20 crystal structures with a specific symmetrical classification. However, there is no such limit to the FM effect, and materials with wider classes of symmetry can cause such a phenomenon. The flexomagnetic effect can be very strong and effective, so that it may one day be used in nanosensors or nanometer actuators. As a brief explanation of the FM effect, it can be noted that by bending an ionic crystal, the atomic layers are drawn inside it, and it is clear that the outermost layer will have the most tension. This difference in traction in different layers can cause ions to transfer to the crystal so much that they eventually create a magnetic field. In other words, bending some materials creates a magnetic field, a corresponding phenomenon called flexomagnetic effect. The effect of strain gradients shows that the importance of the FM effect

in micro and nano systems is comparable to that of piezomagnetic and even beyond. Additionally, flexomagnetic, unlike piezomagnetic, can be found in a wider class of materials. This means that compared to piezomagnetic, which is invalid and inefficient in materials with central symmetry, there is an FM effect in all biological materials and systems. These traits have led to a growing interest in and research into the flexomagnetic effect in recent years [1,2]. Currently, the role of the flexomagnetic effect in the physics of dielectrics has been investigated in some studies and has shown promising practical applications [3–7]. On the other hand, the difference between theoretical and experimental results shows a limited understanding in this field. This study examines current knowledge of FM in engineering.

The flexomagnetic effect exists in many solid dielectrics, soft membranes, and biological filaments. The flexomagnetic effect is introduced as the effect of size-dependent electromagnetic coupling due to the presence of strain gradients and magnetic fields, and promises many applications in nano-electronic devices (with strong strain gradients). Just as the piezomagnetic effect is expected to have important applications in nano-engines and particles [8–12], so the FM effect can play this role as well. Different fields of science are used to study nanodielectrics by considering the FM effect. These significant parts can be examined from a chemistry and physics point of view, or they can be put under a magnifier in the engineering and industrial aspects. In the engineering aspects, the study of external factors on dielectrics and their mechanical and physical behavioral responses will naturally be the criterion for evaluation. The purpose of this study is to evaluate this aspect in static large deflection analysis of a nano actuator beam. A close look at the history of the study of the mechanical behavior of dielectrics by including the FM effect does not show many studies [13–15]. These studies have generally looked at small deformations (linear strains), which, while important, cannot be the criterion for designing dielectric nanobeams. Definitely, the deformations should be considered as large as possible to obtain a reasonable and reliable safety factor for optimizing these significant nano-electro-magneto-mechanical systems' components.

The present work accounts for the large deflections by adding the nonlinear terms of Lagrangian strain using the von Kármán approach. The constitutive equations are expanded in line with the classical beam theory. It is worth mentioning that the small scale is fulfilled conforming to the second stress and strain gradients. These extra terms should result in two conflict responses, that is softening and hardening in the nanoscale structure based on the literature. We perform the solution of acquired equations, which govern the nonlinear bending of the nanobeam, on the basis of two step solution techniques. The first one is the Galerkin weighted residual method (GWRM) which converts the equations into nonlinear algebraic ones, then the Newton–Raphson technique (NRT), which solves the nonlinear system of algebraic equations and gives the numerical values of displacements into x and z directions. At last, pictorial results are evaluated to show the disagreements and dissimilarities betwixt linear deflection and nonlinear one for the piezo-flexomagnetic nanosize beam.

2. Mathematical Model

Let us consider a piezomagnetic-flexomagnetic nanobeam (PF-NB) with squared cross section of length and thickness L and h; see Figure 1. A uniform vertical static loading acts above the beam. A magnetic potential is joint to the beam to simulate and act as a magnetic field. Moreover, the z-axis is related to the transverse direction, whereas the neutral plane of the beam is coincident with the x-axis.

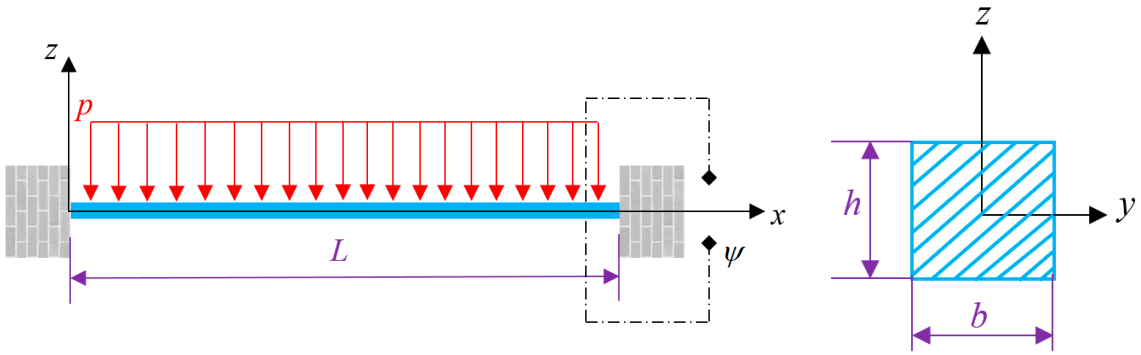

Figure 1. A square ($b = h$) PF-NB clamped at both ends and exposed to a lateral uniform static loading beside an external magnetic potential.

Follow up, the kinematic displacement for each node of the beam is utilized with the aid of the Euler–Bernoulli hypothesis [16,17]. Furthermore, the model is restricted with in-plane deformations. The rectangular displacements correspond with u_1 and u_3, respectively, for axial and transverse directions. However, such displacements for neutral plane are, respectively, regarded with u and w. Thus, one can give accordingly

$$u_1(x\,,z) = u(x) - z\frac{dw(x)}{dx} \tag{1}$$

$$u_3(x,z) = w(x) \tag{2}$$

The Von Kármán assumption tells us that the nonlinear terms related to the u can be excluded from the Lagrangian strain formula because these terms are sufficiently small compared to the other terms [18–24]. The general Lagrangian strain can be mentioned as

$$\varepsilon_{ij} = \frac{1}{2}\left(\frac{\partial u_i}{\partial x_j} + \frac{\partial u_j}{\partial x_i} + \frac{\partial u_k}{\partial x_i}\frac{\partial u_k}{\partial x_j}\right) \tag{3}$$

In regard to this approach, the nonzero nonlinear strain-displacement components can be derived as follows

$$\varepsilon_{xx} = \frac{du}{dx} - z\frac{d^2w}{dx^2} + \frac{1}{2}\left(\frac{dw}{dx}\right)^2 \tag{4}$$

$$\eta_{xxz} = \frac{d\varepsilon_{xx}}{dz} = -\frac{d^2w}{dx^2} \tag{5}$$

where Equations (4) and (5) calculate, respectively, the longitudinal strain and its gradient.

The stress-strain magneto-mechanical coupling relations in the one-dimensional framework can be given owing to [13,14].

$$\sigma_{xx} = C_{11}\varepsilon_{xx} - q_{31}H_z \tag{6}$$

$$\xi_{xxz} = g_{31}\eta_{xxz} - f_{31}H_z \tag{7}$$

$$B_z = a_{33}H_z + q_{31}\varepsilon_{xx} + f_{31}\eta_{xxz} \tag{8}$$

where σ_{xx} is the static stress field component, H_z is the magnetic field component, B_z is the magnetic flux (induction) component, C_{11} is the elastic modulus, f_{31} is the component of the fourth-order flexomagnetic coefficients tensor, a_{33} is the component of the second-order magnetic permeability tensor, q_{31} is the component of the third-order piezomagnetic tensor, g_{31} is the component of the sixth-order gradient elasticity tensor, and ξ_{xxz} is the component of higher-order moment stress tensor.

The variational formulation accurately develops the characteristics relation of PF-NB, thusly

$$\delta U - \delta W = 0 \tag{9}$$

where δ is the symbol of variation, U is the strain energies, and W is created works by outer objects. In such a way, the entire inner energy of the specimen is in the first variation which is equal to zero as well. The strain energy respecting magneto-mechanical composition can be variated just like this (the first variation)

$$\delta U = \int_V (\sigma_{xx}\delta\varepsilon_{xx} + \xi_{xxz}\delta\eta_{xxz} - B_z\delta H_z)dV \tag{10}$$

Equation (10) can be transformed with integration by parts on the basis of the one-dimensional displacement field previously assumed as follows

$$\delta U = \delta\Pi_{U_1}^{Mech} + \delta\Pi_{U_1}^{Mag} + \delta\Pi_{U_2}^{Mech} + \delta\Pi_{U_2}^{Mag} \tag{11}$$

where

$$\delta\Pi_{U_1}^{Mech} = -\int_0^L \left\{ \frac{dN_x}{dx}\delta u + \left[\frac{d^2M_x}{dx^2} + \frac{d}{dx}\left(N_x\frac{dw}{dx}\right) + \frac{d^2T_{xxz}}{dx^2}\right]\delta w \right\} dx \tag{12}$$

$$\delta\Pi_{U_1}^{Mag} = -\int_0^L \int_{-h/2}^{h/2} \frac{dB_z}{dz}\delta\Psi dz dx \tag{13}$$

$$\delta\Pi_{U_2}^{Mech} = \left\{ N_x\delta u - [M_x + T_{xxz}]\frac{d\delta w}{dx} + \left[N_x\frac{dw}{dx} + \frac{dM_x}{dx} + \frac{dT_{xxz}}{dx}\right]\delta w \right\}\Big|_0^L \tag{14}$$

$$\delta\Pi_{U_2}^{Mag} = \int_0^L (B_z\delta\Psi)\Big|_{-h/2}^{h/2} dx \tag{15}$$

where Ψ is the variable of magnetic potential. The resultants of the stress field can be introduced along the following lines

$$N_x = \int_{-h/2}^{h/2} \sigma_{xx} dz \tag{16}$$

$$M_x = \int_{-h/2}^{h/2} \sigma_{xx} z dz \tag{17}$$

$$T_{xxz} = \int_{-h/2}^{h/2} \xi_{xxz} dz \tag{18}$$

In addition, the magnetic potential was introduced through the relation

$$\frac{d\Psi}{dz} = -H_z \tag{19}$$

External forces (axial force as a result of the longitudinal magnetic field and the lateral loading) create work thermodynamically in the particles so that the mathematical relation in the first variation becomes [25].

$$\delta W = \int_0^L \left[N_x^0\left(\frac{d\delta w}{dx}\frac{dw}{dx}\right) + p(x)\delta w\right] dx \tag{20}$$

in which N_x^0 is the in-plane longitudinal axial force, and p is the lateral load per unit length. Taking into account the closed circuit in conjunction with the inverse piezo case, the electrical boundary conditions can be attributed as below

$$\Psi\left(+\frac{h}{2}\right) = \psi \tag{21}$$

$$\Psi\left(-\frac{h}{2}\right) = 0 \tag{22}$$

in which ψ is the external magnetic potential on the upper surface. Making in hand Equations (8), (13), (15), (21) and (22) practicably expresses the magnetic field component and thereupon the magnetic potential function in line with thickness as follows [13,14]

$$\Psi = -\frac{q_{31}}{2a_{33}}\left(z^2 - \frac{h^2}{4}\right)\frac{d^2w}{dx^2} + \frac{\psi}{h}\left(z + \frac{h}{2}\right) \tag{23}$$

$$H_z = z\frac{q_{31}}{a_{33}}\frac{d^2w}{dx^2} - \frac{\psi}{h} \tag{24}$$

On the basis of Equations (23) and (24), Equations (6)–(8) can be developed as

$$\sigma_{xx} = C_{11}\left[\frac{du}{dx} + \frac{1}{2}\left(\frac{dw}{dx}\right)^2\right] - z\left(C_{11} + \frac{q_{31}^2}{a_{33}}\right)\frac{d^2w}{dx^2} + \frac{q_{31}\psi}{h} \tag{25}$$

$$\xi_{xxz} = -\left(g_{31} + \frac{q_{31}f_{31}z}{a_{33}}\right)\frac{d^2w}{dx^2} + \frac{f_{31}\psi}{h} \tag{26}$$

$$B_z = q_{31}\left[\frac{du}{dx} + \frac{1}{2}\left(\frac{dw}{dx}\right)^2\right] - f_{31}\frac{d^2w}{dx^2} - \frac{a_{33}\psi}{h} \tag{27}$$

Subsequently, Equations (16)–(18) can be rewritten in detail as

$$N_x = C_{11}A\left[\frac{du}{dx} + \frac{1}{2}\left(\frac{dw}{dx}\right)^2\right] + q_{31}\psi \tag{28}$$

$$M_x = -I_z\left(C_{11} + \frac{q_{31}^2}{a_{33}}\right)\frac{d^2w}{dx^2} \tag{29}$$

$$T_{xxz} = -g_{31}h\frac{d^2w}{dx^2} + f_{31}\psi \tag{30}$$

in which N_x, M_x, T_{xxz} show the axial, moment, and hyper stress resultants, and $I_z = \int_A z^2 dA$ is the area moment of inertia.

The resultant magnetic axial stress, which is achieved due to the longitudinal magnetic field, based on Equation (28) can be determined as

$$N^{Mag} = q_{31}\psi \tag{31}$$

This force is supposed to act at both ends of the beam, thus

$$N_x^0 = N^{Mag} \tag{32}$$

Eventually, imposing Equation (9), one can write the governing equations in a combination of mechanical and magnetic conditions as

$$\frac{dN_x}{dx} = 0 \tag{33}$$

$$\frac{d^2M_x}{dx^2}+\frac{d^2T_{xxz}}{dx^2}+\left(N_x^0+N_x\right)\frac{d^2w}{dx^2}+\frac{dN_x}{dx}\frac{dw}{dx}-p=0 \tag{34}$$

Due to being the nanobeam a size-dependent particle, the scale-dependent property should be substituted in Equations (33) and (34). In [26], the second strain gradient of Mindlin merged successfully with the nonlocal theory of Eringen. This model (NSGT) was incorporated in a lot of research performed on the nanoparticles in recent years—see e.g., [27–38] and many others—and can be a proper item at the nanoscale.

The model proposed by [26] can be compatible in our case as

$$\left(1-\mu\frac{d^2}{dx^2}\right)\sigma_{xx}^{NonLocal}=\left(1-l^2\frac{d^2}{dx^2}\right)\sigma_{xx}^{Local}$$

or as

$$\left(1-\mu\frac{d^2}{dx^2}\right)\sigma_{xx}^{NonLocal}=\left(1-l^2\frac{d^2}{dx^2}\right)\left\{C_{11}\left[\frac{du}{dx}+\frac{1}{2}\left(\frac{dw}{dx}\right)^2\right]-z\left(C_{11}+\frac{q_{31}^2}{a_{33}}\right)\frac{d^2w}{dx^2}+\frac{q_{31}\psi}{h}\right\} \tag{35}$$

in which $\mu\left(nm^2\right)$ is the nonlocal parameter, and $l(nm)$ is the strain gradient parameter. Thus, $l>0$ establishes a nonzero strain gradient into the model, and $\mu=(e_0a)^2$ is the parameter defining nonlocality. It is germane to note that both scale parameters are dependent on the physics of the model and cannot be material constants [39,40]. This means the parameters are not constant values, something like an elasticity modulus for each material.

To implement the influence of size effects into the equations, Equation (35) is plugged to Equations (28)–(30) as

$$N_x-\mu\frac{d^2N_x}{dx^2}=\left(1-l^2\frac{d^2}{dx^2}\right)\left\{C_{11}A\left[\frac{du}{dx}+\frac{1}{2}\left(\frac{dw}{dx}\right)^2\right]\right\} \tag{36}$$

$$M_x-\mu\frac{d^2M_x}{dx^2}=\left(1-l^2\frac{d^2}{dx^2}\right)\left\{-I_z\left(C_{11}+\frac{q_{31}^2}{a_{33}}\right)\frac{d^2w}{dx^2}\right\} \tag{37}$$

$$T_{xxz}-\mu\frac{d^2T_{xxz}}{dx^2}=\left(1-l^2\frac{d^2}{dx^2}\right)\left\{-g_{31}h\frac{d^2w}{dx^2}+f_{31}\psi\right\} \tag{38}$$

Equations (33) and (34) by means of Equations (36)–(38) can be derived in the framework of displacements, respectively, as series of models.

1.1. Piezo-flexomagnetic nanobeam (PF-NB)—Nonlinear case:

$$C_{11}A\left[\frac{d^2u}{dx^2}+\frac{d^2w}{dx^2}\frac{dw}{dx}-l^2\left(\frac{d^4u}{dx^4}+\frac{d^4w}{dx^4}\frac{dw}{dx}+3\frac{d^3w}{dx^3}\frac{d^2w}{dx^2}\right)\right]=0 \tag{39}$$

$$\begin{gathered}
-g_{31}h\tfrac{d^4w}{dx^4}+q_{31}\psi\tfrac{d^2w}{dx^2}-p-\mu\left(-g_{31}h\tfrac{d^6w}{dx^6}+q_{31}\psi\tfrac{d^4w}{dx^4}-\tfrac{d^2p}{dx^2}\right)\\
-\mu C_{11}A\left[\tfrac{du}{dx}+\tfrac{1}{2}\left(\tfrac{dw}{dx}\right)^2\right]\tfrac{d^4w}{dx^4}+C_{11}A\mu l^2\left[\tfrac{d^3u}{dx^3}+\tfrac{d^3w}{dx^3}\tfrac{dw}{dx}+\left(\tfrac{d^2w}{dx^2}\right)^2\right]\tfrac{d^4w}{dx^4}\\
-\mu C_{11}A\left(\tfrac{d^2u}{dx^2}+\tfrac{dw}{dx}\tfrac{d^2w}{dx^2}\right)\tfrac{d^3w}{dx^3}+C_{11}A\mu l^2\left(\tfrac{d^4u}{dx^4}+3\tfrac{d^3w}{dx^3}\tfrac{d^2w}{dx^2}+\tfrac{dw}{dx}\tfrac{d^4w}{dx^4}\right)\tfrac{d^3w}{dx^3}\\
-\mu C_{11}A\left(\tfrac{d^4u}{dx^4}+\tfrac{dw}{dx}\tfrac{d^4w}{dx^4}+3\tfrac{d^3w}{dx^3}\tfrac{d^2w}{dx^2}\right)\tfrac{dw}{dx}+C_{11}A\left[\tfrac{du}{dx}+\tfrac{1}{2}\left(\tfrac{dw}{dx}\right)^2\right]\tfrac{d^2w}{dx^2}\\
+C_{11}A\mu l^2\left(\tfrac{d^6u}{dx^6}+\tfrac{dw}{dx}\tfrac{d^6w}{dx^6}+5\tfrac{d^5w}{dx^5}\tfrac{d^2w}{dx^2}+10\tfrac{d^4w}{dx^4}\tfrac{d^3w}{dx^3}\right)\tfrac{dw}{dx}\\
-C_{11}Al^2\left[\tfrac{d^3u}{dx^3}+\tfrac{d^3w}{dx^3}\tfrac{dw}{dx}+\left(\tfrac{d^2w}{dx^2}\right)^2\right]\tfrac{d^2w}{dx^2}+C_{11}A\left(\tfrac{d^2u}{dx^2}+\tfrac{dw}{dx}\tfrac{d^2w}{dx^2}\right)\tfrac{dw}{dx}\\
-I_z\left(C_{11}+\tfrac{q_{31}^2}{a_{33}}\right)\left(\tfrac{d^4w}{dx^4}-l^2\tfrac{d^6w}{dx^6}\right)-C_{11}Al^2\left(\tfrac{d^4u}{dx^4}+3\tfrac{d^3w}{dx^3}\tfrac{d^2w}{dx^2}+\tfrac{dw}{dx}\tfrac{d^4w}{dx^4}\right)\tfrac{dw}{dx}=0
\end{gathered} \tag{40}$$

1.2. Piezo-flexomagnetic nanobeam (PF-NB)—Linear case:

$$\begin{array}{l} -g_{31}h\frac{d^4w}{dx^4}+q_{31}\psi\frac{d^2w}{dx^2}-p-\mu\left(-g_{31}h\frac{d^6w}{dx^6}+q_{31}\psi\frac{d^4w}{dx^4}-\frac{d^2p}{dx^2}\right) \\ -I_z\left(C_{11}+\frac{q_{31}^2}{a_{33}}\right)\left(\frac{d^4w}{dx^4}-l^2\frac{d^6w}{dx^6}\right)=0 \end{array} \tag{41}$$

2.1. Piezomagnetic nanobeam (P-NB)—Nonlinear case:

$$C_{11}A\left[\frac{d^2u}{dx^2}+\frac{d^2w}{dx^2}\frac{dw}{dx}-l^2\left(\frac{d^4u}{dx^4}+\frac{d^4w}{dx^4}\frac{dw}{dx}+3\frac{d^3w}{dx^3}\frac{d^2w}{dx^2}\right)\right]=0 \tag{42}$$

$$\begin{array}{l} q_{31}\psi\frac{d^2w}{dx^2}-p-\mu\left(q_{31}\psi\frac{d^4w}{dx^4}-\frac{d^2p}{dx^2}\right)-\mu C_{11}A\left[\frac{du}{dx}+\frac{1}{2}\left(\frac{dw}{dx}\right)^2\right]\frac{d^4w}{dx^4} \\ +C_{11}A\mu l^2\left[\frac{d^3u}{dx^3}+\frac{d^3w}{dx^3}\frac{dw}{dx}+\left(\frac{d^2w}{dx^2}\right)^2\right]\frac{d^4w}{dx^4} \\ -\mu C_{11}A\left(\frac{d^2u}{dx^2}+\frac{dw}{dx}\frac{d^2w}{dx^2}\right)\frac{d^3w}{dx^3}+C_{11}A\mu l^2\left(\frac{d^4u}{dx^4}+3\frac{d^3w}{dx^3}\frac{d^2w}{dx^2}+\frac{dw}{dx}\frac{d^4w}{dx^4}\right)\frac{d^3w}{dx^3} \\ -\mu C_{11}A\left(\frac{d^4u}{dx^4}+\frac{dw}{dx}\frac{d^4w}{dx^4}+3\frac{d^3w}{dx^3}\frac{d^2w}{dx^2}\right)\frac{dw}{dx}+C_{11}A\left[\frac{du}{dx}+\frac{1}{2}\left(\frac{dw}{dx}\right)^2\right]\frac{d^2w}{dx^2} \\ +C_{11}A\mu l^2\left(\frac{d^6u}{dx^6}+\frac{dw}{dx}\frac{d^6w}{dx^6}+5\frac{d^5w}{dx^5}\frac{d^2w}{dx^2}+10\frac{d^4w}{dx^4}\frac{d^3w}{dx^3}\right)\frac{dw}{dx} \\ -C_{11}Al^2\left[\frac{d^3u}{dx^3}+\frac{d^3w}{dx^3}\frac{dw}{dx}+\left(\frac{d^2w}{dx^2}\right)^2\right]\frac{d^2w}{dx^2}+C_{11}A\left(\frac{d^2u}{dx^2}+\frac{dw}{dx}\frac{d^2w}{dx^2}\right)\frac{dw}{dx} \\ -I_z\left(C_{11}+\frac{q_{31}^2}{a_{33}}\right)\left(\frac{d^4w}{dx^4}-l^2\frac{d^6w}{dx^6}\right)-C_{11}Al^2\left(\frac{d^4u}{dx^4}+3\frac{d^3w}{dx^3}\frac{d^2w}{dx^2}+\frac{dw}{dx}\frac{d^4w}{dx^4}\right)\frac{dw}{dx}=0 \end{array} \tag{43}$$

2.2. Piezomagnetic nanobeam (P-NB)—Linear case:

$$q_{31}\psi\frac{d^2w}{dx^2}-p-\mu\left(q_{31}\psi\frac{d^4w}{dx^4}-\frac{d^2p}{dx^2}\right)-I_z\left(C_{11}+\frac{q_{31}^2}{a_{33}}\right)\left(\frac{d^4w}{dx^4}-l^2\frac{d^6w}{dx^6}\right)=0 \tag{44}$$

3.1. Nanobeam (NB)—Nonlinear case:

$$C_{11}A\left[\frac{d^2u}{dx^2}+\frac{d^2w}{dx^2}\frac{dw}{dx}-l^2\left(\frac{d^4u}{dx^4}+\frac{d^4w}{dx^4}\frac{dw}{dx}+3\frac{d^3w}{dx^3}\frac{d^2w}{dx^2}\right)\right]=0 \tag{45}$$

$$\begin{array}{l} -p+\mu\frac{d^2p}{dx^2}-\mu C_{11}A\left[\frac{du}{dx}+\frac{1}{2}\left(\frac{dw}{dx}\right)^2\right]\frac{d^4w}{dx^4} \\ +C_{11}A\mu l^2\left[\frac{d^3u}{dx^3}+\frac{d^3w}{dx^3}\frac{dw}{dx}+\left(\frac{d^2w}{dx^2}\right)^2\right]\frac{d^4w}{dx^4} \\ -\mu C_{11}A\left(\frac{d^2u}{dx^2}+\frac{dw}{dx}\frac{d^2w}{dx^2}\right)\frac{d^3w}{dx^3} \\ +C_{11}A\mu l^2\left(\frac{d^4u}{dx^4}+3\frac{d^3w}{dx^3}\frac{d^2w}{dx^2}+\frac{dw}{dx}\frac{d^4w}{dx^4}\right)\frac{d^3w}{dx^3} \\ -\mu C_{11}A\left(\frac{d^4u}{dx^4}+\frac{dw}{dx}\frac{d^4w}{dx^4}+3\frac{d^3w}{dx^3}\frac{d^2w}{dx^2}\right)\frac{dw}{dx}+C_{11}A\left[\frac{du}{dx}+\frac{1}{2}\left(\frac{dw}{dx}\right)^2\right]\frac{d^2w}{dx^2} \\ +C_{11}A\mu l^2\left(\frac{d^6u}{dx^6}+\frac{dw}{dx}\frac{d^6w}{dx^6}+5\frac{d^5w}{dx^5}\frac{d^2w}{dx^2}+10\frac{d^4w}{dx^4}\frac{d^3w}{dx^3}\right)\frac{dw}{dx} \\ -C_{11}Al^2\left[\frac{d^3u}{dx^3}+\frac{d^3w}{dx^3}\frac{dw}{dx}+\left(\frac{d^2w}{dx^2}\right)^2\right]\frac{d^2w}{dx^2}+C_{11}A\left(\frac{d^2u}{dx^2}+\frac{dw}{dx}\frac{d^2w}{dx^2}\right)\frac{dw}{dx} \\ -I_zC_{11}\left(\frac{d^4w}{dx^4}-l^2\frac{d^6w}{dx^6}\right)-C_{11}Al^2\left(\frac{d^4u}{dx^4}+3\frac{d^3w}{dx^3}\frac{d^2w}{dx^2}+\frac{dw}{dx}\frac{d^4w}{dx^4}\right)\frac{dw}{dx}=0 \end{array} \tag{46}$$

3.2. Nanobeam (NB)—Linear case:

$$-p+\mu\frac{d^2p}{dx^2}-C_{11}I_z\left(\frac{d^4w}{dx^4}-l^2\frac{d^6w}{dx^6}\right)=0 \tag{47}$$

4.1. Classic beam—Nonlinear case:

$$C_{11}A\left(\frac{d^2u}{dx^2}+\frac{d^2w}{dx^2}\frac{dw}{dx}\right)=0 \tag{48}$$

$$-p + C_{11}A\left[\frac{du}{dx} + \frac{1}{2}\left(\frac{dw}{dx}\right)^2\right]\frac{d^2w}{dx^2} + C_{11}A\left(\frac{d^2u}{dx^2} + \frac{dw}{dx}\frac{d^2w}{dx^2}\right)\frac{dw}{dx} - C_{11}I_z\frac{d^4w}{dx^4} = 0 \tag{49}$$

4.2. Classic beam—Linear case:

$$-C_{11}I_z\frac{d^4w}{dx^4} = p \tag{50}$$

In what follows, we consider these cases in more details.

3. Solution Approach

The solution process here has two steps. The first step comes with the Galerkin weighted residual method (GWRM) on the basis of the admissible shape functions which satisfy boundary conditions. The second step is imposing the Newton–Raphson technique (NRT) in order to solve the system of nonlinear algebraic equations originated from GWRM. The following displacements were employed [41].

$$u(x) = \sum_{m=1}^{\infty} U_m \frac{dX_m(x)}{dx} \tag{51}$$

$$w(x) = \sum_{m=1}^{\infty} W_m X_m(x) \tag{52}$$

where U_m and W_m are unknown variables that determine displacements through two axes and should be computed, whereas $X_m(x)$ are shape functions, m is the axial half-wave number, and becomes $m = 1, 2, \ldots \infty$. The allowable shape functions given below satisfy end conditions as [41].

$$\text{S} - \text{S}: \; X_m(x) = \sin\left(\frac{m\pi}{L}x\right) \tag{53}$$

$$\text{C} - \text{C}: \; X_m(x) = \sin^2\left(\frac{m\pi}{L}x\right) \tag{54}$$

$$\text{C} - \text{F}: \; X_m(x) = \sin\left(\frac{m\pi}{4L}x\right)\cos\left(\frac{m\pi}{4L}x\right) \tag{55}$$

in which S, C, and F mark one by one the simply-supported, clamped, and free end conditions. Here, e.g., C-F means a side of the beam is inserted in a clamping fixture and the opposite side is free and hanging.

Based on the Fourier sine series, the transverse load can uniformly behave on the nanobeam as the following form [42,43].

$$p(x) = \sum_{m=1}^{\infty} \frac{4p_0}{m\pi}\sin\left(\frac{m\pi}{L}x\right) \tag{56}$$

in which p_0 is density of the lateral load. Inserting Equations (51), (52), and (56) into Equations (39)–(50), and integrating over the axial domain based on the GWRM approach, one can obtain

$$\int_0^L [\eta(x)Y_m]dx = 0 \tag{57}$$

$$\int_0^L [\xi(x)Z_m]dx = 0 \tag{58}$$

in which η and ξ are the first and second equations, respectively, and Y_m and Z_m show the residuals. Then, with ordering and arranging the aforesaid equations, one can receive the nonlinear algebraic system of two equations and two unknown variables (when considering $m = 1$). To solve such a system,

there are several methods. As long as the NRT converged the results very quickly and accurately, this technique was employed here. A primary guess (U_0 and W_0) was required for results in this approach. We can express the first iteration as [44].

$$U_1 = U_0 - J^{-1} \times A_0 \tag{59}$$

$$W_1 = W_0 - J^{-1} \times A_0 \tag{60}$$

where J denotes the Jacobian matrix 2×2 and A is a vector 2×1.

$$J = \frac{\partial A_0}{\partial x}, \tag{61}$$

$$A_0 = e\begin{pmatrix} U_0 \\ W_0 \end{pmatrix} \tag{62}$$

where e is the governing equations with placing the first guesses. As a matter of fact, Equations (59) and (60) are iterative equations that are

$$U_{n+1} = U_{n+1} - J^{-1} \times A_{n+1}, \tag{63}$$

$$W_{n+1} = W_{n+1} - J^{-1} \times A_{n+1} \tag{64}$$

where n is the number of iterations to receive the convergence. A few iterations are enough to obtain the desired accuracy. It is worth mentioning that the convergence and the expected accuracy were completely dependent on the value of the primary guesses. Consequently, the solution led to numerical values of displacements along axial and transverse axes. To plot the results for large deflections, we needed to obtain the vertical displacement only, and the other will not be drawn.

4. Numerical Results and Discussion

4.1. Results' Validity

Based on performing some comparative studies, the credit of the present results can be checked. In so doing, in Table 1 a pinned–pinned nanobeam under a distributed uniform force is compared with the linear schema. The maximum deflection which occurred at the center of the beam was in a nondimensional state as proposed by [21,45]. A good harmony among the deflections' values is obviously seen from the Table. It is noteworthy that the classical dimensionless deflection is indicated by $e_0a/L = 0$. From the Table, it is found that the nondimensional maximum deflection increased as the value of the nonlocal parameter increased.

Table 1. Dimensionless maximum deflection for a simply-supported nanobeam exposed to transverse uniform loading.

L/h	e_0a/L	EBT, Linear [21]	EBT, Linear [45]	EBT, Linear [Present]
10	0	0.013021	0.013021	0.013021
	0.05	0.013333	0.013333	0.013333
	0.1	0.014271	0.014271	0.014271
	0.15	0.015833	0.015833	0.015833

For an explicit understanding, another comparison is tabulated by Table 2, for which a typical macroscale beam was utilized under both fixed ends. The present results are validated with those of the finite element method (FEM). Both the current and FEM approach are on the basis of linear analysis. As FEM benefits from shear deformations, it gives higher deflections. It is notable in the Table that enlarging the volume of the load resulted in the discrepancy of deflections. The FEM outcomes can be

changeable due to many conditions in its process such as the number of elements, the kind of element, the number of nodes, and the algorithm of meshing, etc.

Table 2. Maximum deflection (mm) for a clamped–clamped macro beam exposed to transverse uniform loading ($E = 210$ GPa, $h = 5$ mm).

L/h	*p* (kN/mm)	EBT, Linear [Present]	FEM, Linear [ABAQUS]
10	0.01	0.0792	0.0824
	0.02	0.1585	0.1648
	0.03	0.2377	0.2472
	0.04	0.3170	0.3297

4.2. Discussion of the Problem

Here, just employing $n = 4$ gave the convergence in numerical results of the Newton–Raphson solving technique. To the best of the authors' knowledge, no paper exists that has studied large deflections of a piezomagnetic nanosize beam with apparent flexomagneticity, unless otherwise stated. Estimations hereon take the necessary properties for a piezomagnetic nanoparticle accorded by Table 3 as [13,14].

Table 3. Engineering necessary features of a piezomagnetic nanobeam with apparent flexomagneticity.

$CoFe_2O_4$
$C_{11} = 286$ GPa
$q_{31} = 580.3$ N/Ampere.m
$a_{33} = 1.57 \times 10^{-4}$ N/Ampere^2
$L = 10\,h$

In light of the lack of sufficient study on FM, we took $f_{31} = 10^{-9}$ N/Ampere, $f_{31} = 10^{-10}$ N/Ampere as [13,14]. These two values were also theoretically obtained based on some simple assumptions and cannot be the exact numeric values of the flexomagnetic parameter of the aforesaid material presented in Table 3.

An NSGT case was chosen to consider nanoscale impacts. In this model, as can be observed by Equation (31), there were two small scale factors. In point of fact, to determine the results of the bending of the nanoparticle, the amounts of these two parameters are vital. Thus, by exploring within the literature, one can find the 0.5 nm $< e_0a <$ 0.8 nm [46], and $0 < e_0a \leq 2$ nm [47,48], unless otherwise stated. The amount of strain gradient parameter was obtained in a similar size to the lattice parameter of the crystalline structure [49]. This factor for the aforementioned material in Table 3 was obtained in an experiment to change between 0.8 and 0.9 nanometers at a set temperature [50]. Hence, the averaged value of the strain gradient parameter is selected as $l = 1$ nm.

4.2.1. Effect of Nonlinearity

To probe the numerical results, we first show the difference between the results of the linear and nonlinear analyses. Figure 2 is provided for the fixed support, Figure 3 is produced for the hinge support, and lastly, Figure 4 is presented for the cantilever nanobeam. It should be noted that all figures in the results section were plotted in both linear and nonlinear modes for the piezomagnetic nanobeam (P-NB), piezomagnetic-flexomagnetic nanobeam (PF-NB), and common nanobeam (NB). Let us come back to Figures 2–4. First, a comparison of the figures shows a much smaller deflection which resulted from the boundary condition of the fix versus the other ones. For this reason, a larger load amplitude was selected to evaluate the results of the fixed–fixed support to better distinguish between linear and nonlinear analyses. In the first figure, as can be seen, the results of the linear analysis were valid as long as the deflection value did not reach 15% of the thickness, i.e., $w < 0.15\,h$. Of course, it is important

to note that according to the second figure and in the boundary condition of the hinge, this value was $w \leq 0.1\ h$ for NB and $w \leq 0.08\ h$ for PF-NB. This means that if the deflections exceed these values, the linear analysis is no longer valid, and we must use nonlinear analysis to examine the nanobeam's deflections. Considering Figure 4 for a more flexible beam with clamped-free end conditions represents that the allowable value for NB was about $w \leq 0.2\ h$ and for PF-NB, about $w \leq 0.1\ h$. It is relevant to state that due to the C-F case, a very small lateral load was chosen because of the high deflection capacity of the nanobeam in free conditions. Comparing the three figures, it is interesting to note that the difference between the results of the linear and nonlinear analyses was greater in, respectively, C-F > S-S > C-C boundary conditions, and the C-F boundary condition was more sensitive. It may be concluded that nanobeams with end conditions with higher degrees of freedom require a more urgent nonlinear analysis. Another result of these diagrams is that the deflections of magnetic nanobeam in both linear and nonlinear analyses were smaller than that of the conventional nanobeam. In addition, the difference between the results of the linear analysis was greater than that of the nonlinear analysis. These results strongly suggest that nonlinear strains must be used for static deflection analysis in materials, unless the loads are selected so that the deflections are within the range obtained for linear analysis. By carefully examining the results in [14], which is based on linear analysis and a thickness of 10 nm, it can be seen that the deflections in some diagrams of this reference (see Figure 3 of the reference) were within the range, and in some others exceeded the obtained range (see Figure 4 of the reference). Therefore, the linear analysis cannot always be valid, and certainly, nonlinear analysis is a matter of need.

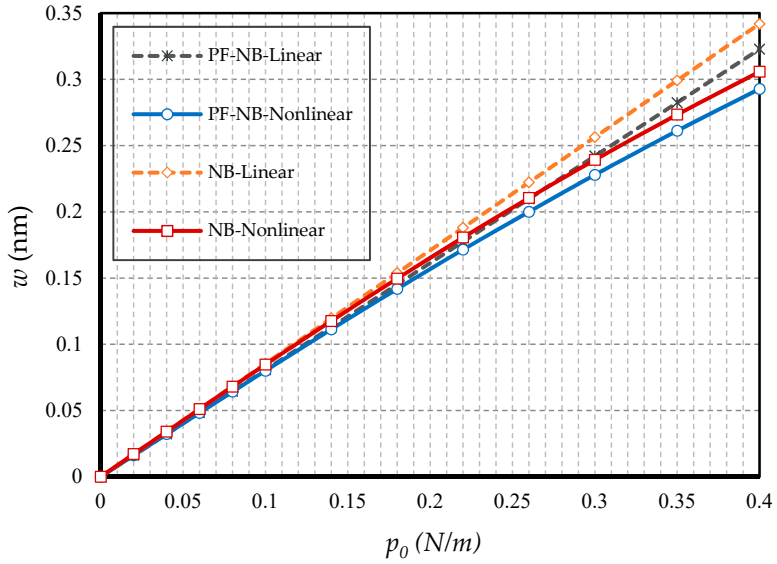

Figure 2. Transverse load vs. different cases of nanobeams (Ψ = 1 mA, l = 1 nm, e_0a = 0.5 nm, C-C).

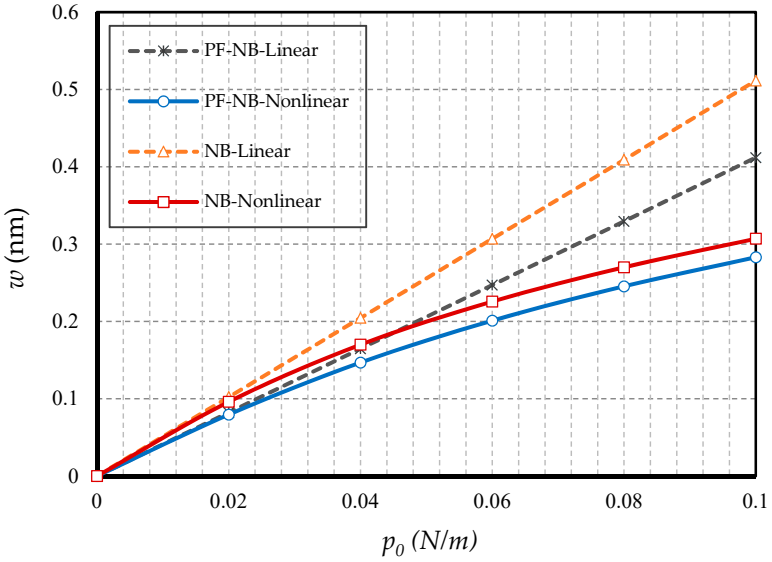

Figure 3. Transverse load vs. different cases of nanobeams (Ψ = 1 mA, l = 1 nm, e_0a = 0.5 nm, S-S).

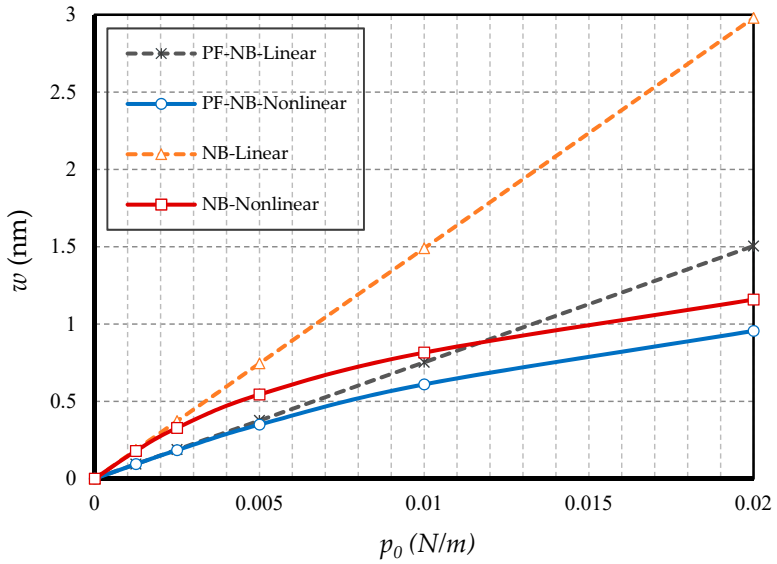

Figure 4. Transverse load vs. different cases of nanobeams (Ψ = 1 mA, l = 1 nm, e_0a = 0.5 nm, C-F).

4.2.2. Effect of Small Scale

In this section, the effect of small-scale parameters is examined, i.e., nonlocal and strain gradient parameters. Figures 5 and 6 show the effect of variations in the value of the nonlocal parameter, respectively, for S-S and C-F, and Figures 7 and 8 exhibit the effect of changes in the value of the strain gradient parameter, respectively, for C-C and S-S. The first and second figure show that as the nonlocal parameters increased, the deflections increased in all four cases examined. As a result, it can be stated that the increase in the nonlocal parameter had a softening effect on the nanobeam material. On the other hand, it is worth noting that as the numerical value of the nonlocal parameter increased, this caused the difference between the linear and nonlinear analyses results. In fact, in the nonlocal analysis of nanobeams, the effect of nonlinear analysis will be greater, and this requires that nonlinear analysis be used to investigate nonlocal deflections. It is important to note that the effect of the nonlocal parameter on the results of magnetic nanobeam was greater than that of the conventional nanobeam. This result is due to the steeper slope of the results of this nanobeam with the increasing nonlocal parameter. It is also interesting to say that the difference between the results of nonlinear and linear

analyses in NB was much more than in PF-NB. From the third and fourth figures, which show the effect of changes in the strain gradient parameter in two different boundary conditions, it is clear that increasing this parameter led to a decrease in deflections of all cases and means that the increase in the strain gradient parameter is a tightening effect inside the material. However, it is important to bear in mind that this tightening effect will be greater in the case of a boundary with lower degrees of freedom. As can be observed, in a nanobeam with a double-sided fixed boundary condition, the slope of the reduction in the deflection's results was much faster than in the case of the boundary conditions of the double-sided hinged. It is also interesting to note that increasing the numerical value of the strain gradient parameter will reduce the difference between the results of linear and nonlinear analyses, and in very large values of this parameter, it can be explicitly stated that nonlinear analysis can be ignored provided that small loads are applied.

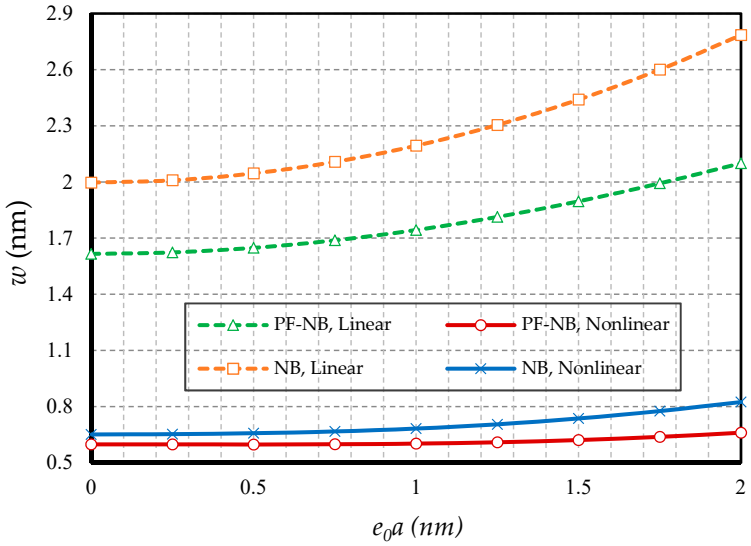

Figure 5. Nonlocal parameter vs. different cases of nanobeams (Ψ = 1 mA, l = 1 nm, p_0 = 0.4 N/m, S-S).

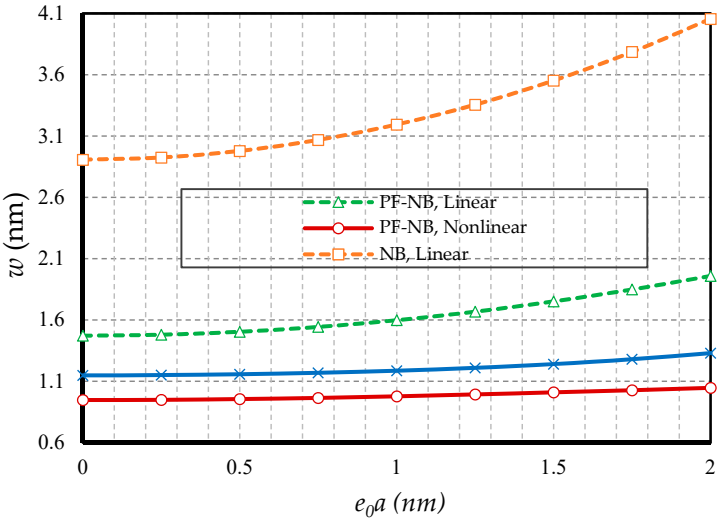

Figure 6. Nonlocal parameter vs. different cases of nanobeams (Ψ = 1 mA, l = 1 nm, p_0 = 0.02 N/m, C-F).

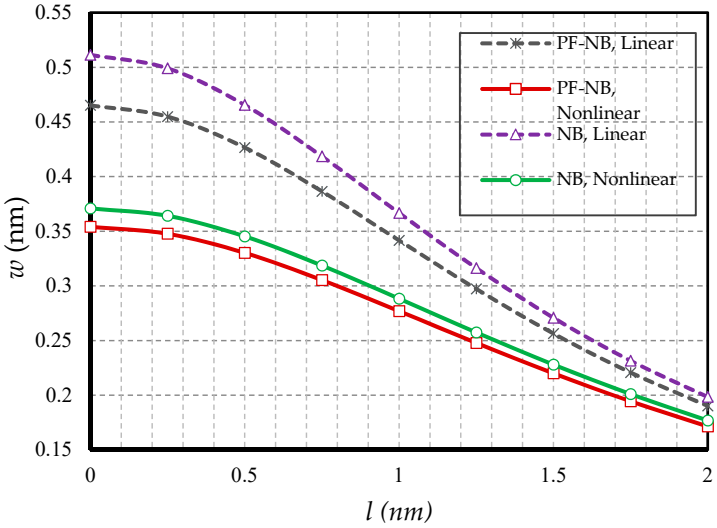

Figure 7. Strain gradient parameter vs. different cases of nanobeams (Ψ = 1 mA, e_0a = 1 nm, p_0 = 0.4 N/m, C-C).

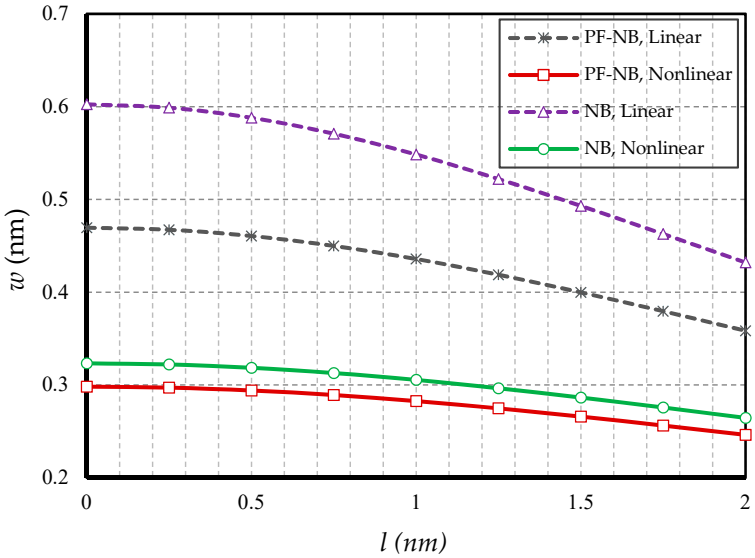

Figure 8. Strain gradient parameter vs. different cases of nanobeams (Ψ = 1 mA, e_0a = 1 nm, p_0 = 0.1 N/m, S-S).

4.2.3. Effect of Magnetic Field

The effect of the external magnetic field was dominant in the mechanical analysis of materials with flexomagnetic capability, while the magnetic effect was inverse. For this purpose, based on Figures 9 and 10, the effect of increasing the magnetic potential in the positive magnetic field is presented in two boundary condition states. Naturally, since the ordinary nanobeam does not have piezomagnetic properties, increasing the magnetic potential will have no effect on this material model. For this reason, the deflections of NB in different values of the external magnetic potential are constant. However, in piezo-flexo nanobeams, with increasing external magnetic potential, the deflections decreased in both linear and nonlinear states in both boundary conditions. Perhaps it can be interpreted that the effect of the magnetic field shrinks the material, and eventually, the material became stiffer and in the case of contraction, most of the deflections became smaller. As can be seen, in the linear analysis case, the difference in results of the conventional and magnetic nanobeams was more visible. In fact, linear analysis showed external effects with a slight exaggeration. Another interesting point is that increasing the potential of external magnetic led to convergence of the results of linear and nonlinear analyses in

the piezo-flexomagnetic nanobeam, but this convergence occurred faster in the boundary condition of the hinge, so much so that in small amounts of external magnetic potential, the results of the linear and nonlinear analyses were perfectly matched to each other. Figure 11 is also displayed to show the impact of a negative magnetic field. The general conclusion that can be drawn from these three figures is that in a positive magnetic field the effect of nonlinear analysis decreases and in contrast in a negative magnetic field the influence of nonlinear analysis will be very prominent.

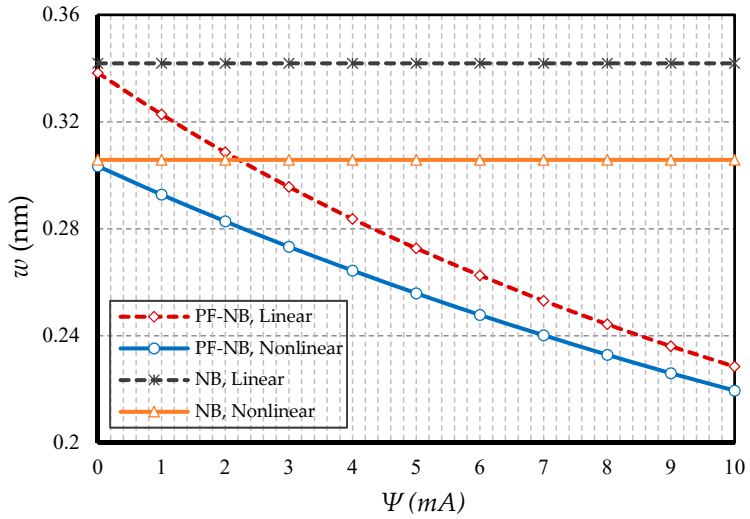

Figure 9. Magnetic potential parameter vs. different cases of nanobeams (l = 1 nm, e_0a = 0.5 nm, p_0 = 0.4 N/m, C-C).

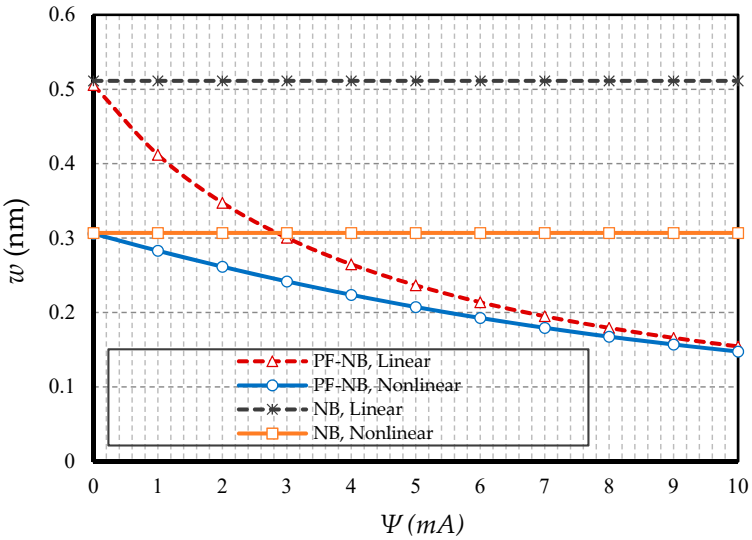

Figure 10. Magnetic potential parameter vs. different cases of nanobeams (l = 1 nm, e_0a = 0.5 nm, p_0 = 0.1 N/m, S-S).

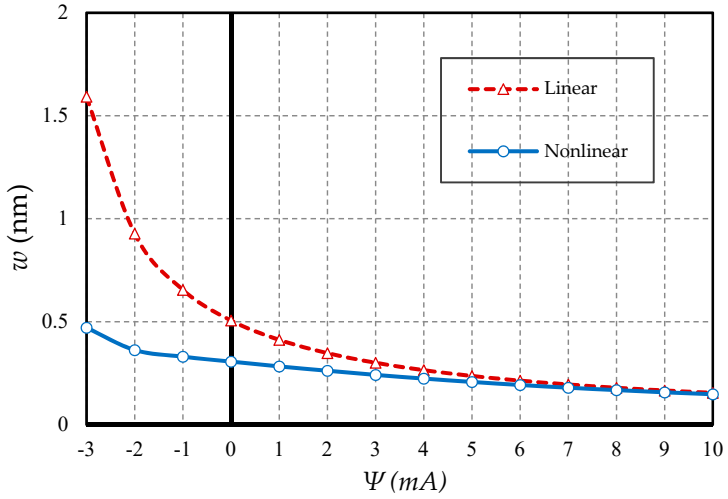

Figure 11. Magnetic potential parameter vs. PF nanobeams (l = 1 nm, e_0a = 0.5 nm, p_0 = 0.1 N/m, S-S).

4.2.4. Effect of Slenderness Ratio

Figures 12 and 13 are drawn by defining the ratio of length to thickness as a slenderness coefficient in the nanobeam. The first figure is reported for the boundary condition of the two heads of fix and the second figure is plotted for the two heads of the hinge. As can be easily seen, increasing the slenderness ratio led to an increase in static deflections in both linear and nonlinear states. Additionally, with increasing this coefficient of the nanobeam, the difference between the results of linear and nonlinear analyses increased significantly. In fact, this suggests that in large quantities of length, the linear analysis presented completely erroneous results. On the other hand, in large quantities of slenderness coefficient, the difference between the results of the magnetic nanobeam and common nanobeam in linear mode were greater than in the nonlinear one, which proves that in large values of length, the linear results showed, with magnification, the mechanical behavior of the magnetic nanobeam versus the conventional nanobeam, and it cannot be true. It should be emphasized that this difference was much greater in the results of the hinge boundary condition even with smaller loads, than in the results of the clamp boundary condition.

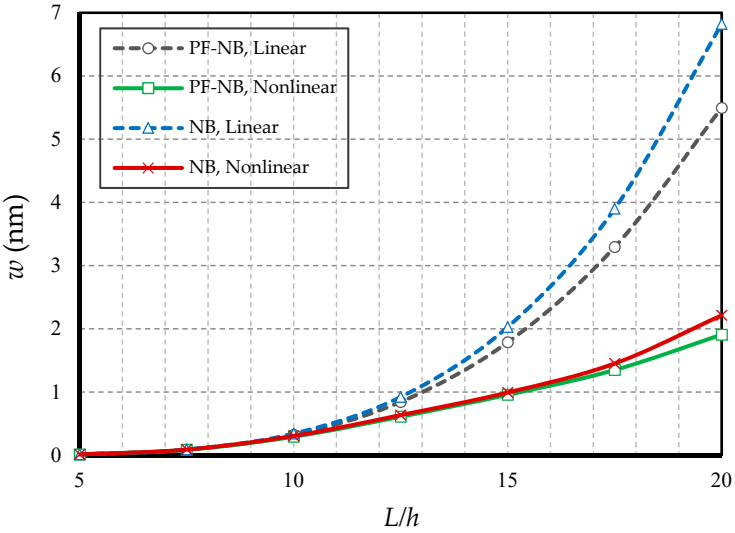

Figure 12. Slenderness ratio vs. different cases of nanobeams (Ψ = 1 mA, l = 1 nm, e_0a = 0.5 nm, p_0 = 0.4 N/m, C-C).

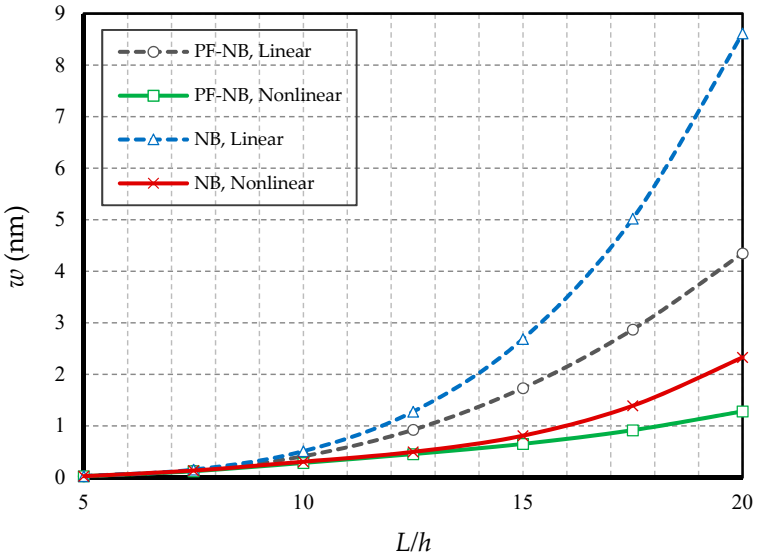

Figure 13. Slenderness ratio vs. different cases of nanobeams (Ψ = 1 mA, l = 1 nm, e_0a = 0.5 nm, p_0 = 0.1 N/m, S-S).

4.2.5. Effect of FM

In this subsection, the aim is to compare the difference in results when the substance has only a piezomagnetic effect when the flexomagnetic effect is added to it. Figure 14 shows the results of the nanobeam with two side clamps; in Figure 15, the nanobeam with two ends of the hinge is presented; finally, Figure 16 shows the cantilever nanobeam. First, as can be seen, the nonlinear analysis reduced the flexomagnetic effect. This result was obtained from the difference between the results of the P-NB and PF-NB in both nonlinear and linear analyses of the figures. On the other hand, as is clear, the results associated with the PF-NB were smaller than those of the P-NB. This finding can be interpreted in such a way that the flexomagnetic effect will lead to more material stiffness, and as a result, the deflections will be smaller while considering this effect. It has to be noted that the slight difference in the results of P-NB versus those of the PF-NB was directly related to the values of the flexomagnetic modulus. According to the references, the value of the parameter was almost based on the assumptions, and due to the novelty, of the discovery of the flexomagnetic effect; the exact values of this parameter have not yet been calculated. For this reason, it is not possible to say why the difference in results between P-NB and PF-NB was high or low. Nevertheless, such a difference was also adequately large on a nanoscale. It should be pointed out that the FM was more remarkable in C-C end conditions. This means that the lower degree of freedom boundary condition increased the impact of FM.

In this study, we end the discussion with Figure 17, in which different values of the flexomagnetic parameter were investigated. To carry out this, the w^* was introduced which was the deflections of the PF-NB divided by the deflections of the P-NB. As seen, there was no appreciable change in deflections originated from FM in lower amounts of the FM parameter. The effect of FM on the P-NB became outstanding for large values of FM, and the assumed value $f_{31} = 10^{-10}$ N/Ampere can affect to some extent the behavior of the PF-NB.

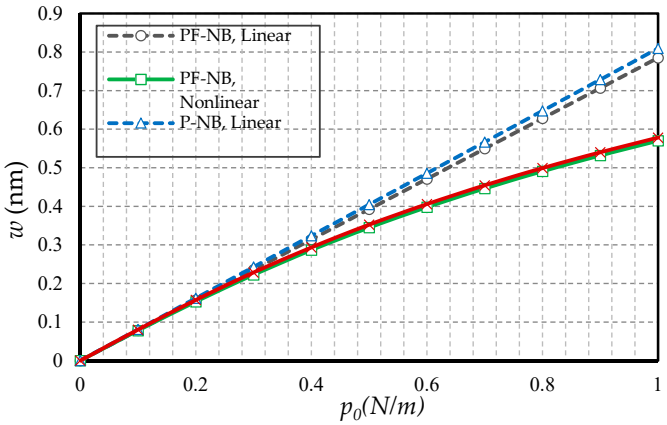

Figure 14. Transverse load vs. deflection for different cases of nanobeams (Ψ = 1 mA, l = 1 nm, e_0a = 0.5 nm, C-C).

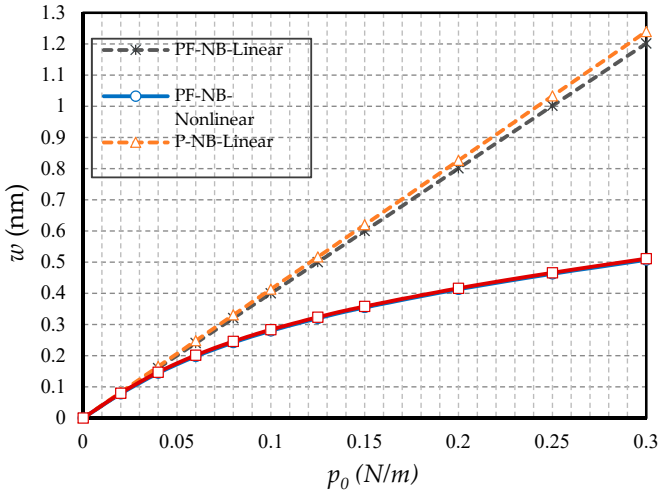

Figure 15. Transverse load vs. deflection for different cases of nanobeams (Ψ = 1 mA, l = 1 nm, e_0a = 0.5 nm, S-S).

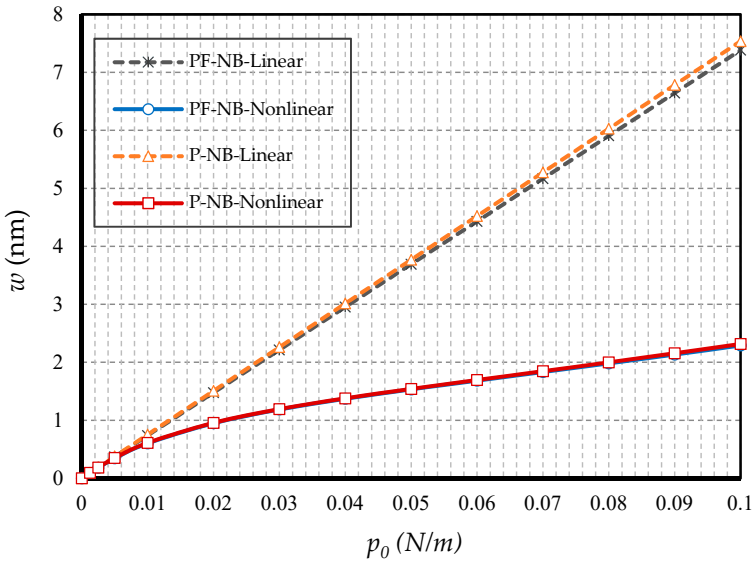

Figure 16. Transverse load vs. deflection for different cases of nanobeams (Ψ = 1 mA, l = 1 nm, e_0a = 0.5 nm, C-F).

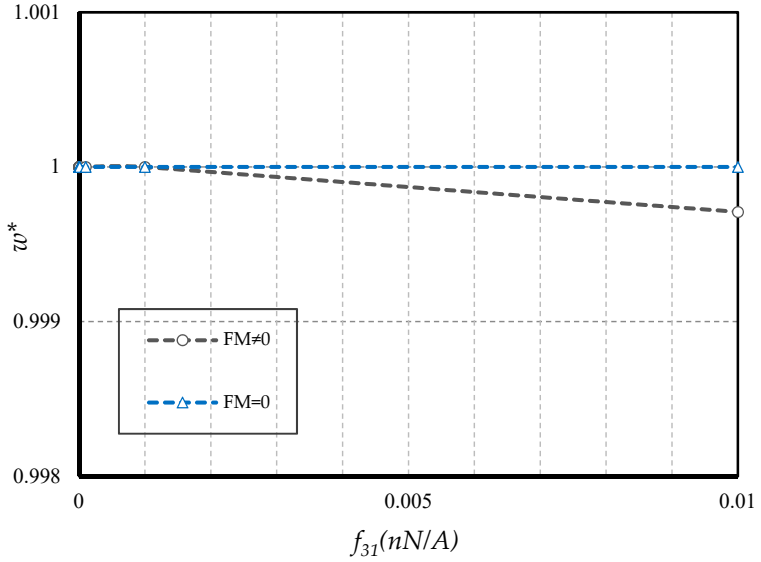

Figure 17. Presence and absence of flexomagnetic modulus for linear bending of a PF-NB (Ψ = 1 mA, l = 1 nm, e_0a = 0.5 nm, p_0 = 0.5 N/m, S-S).

5. Conclusions

Due to the FM influence being new and interesting, we took into account both piezomagnetic and flexomagnetic effects together for a reduced scale thin beam. The geometrical nonlinearity which induces the large deformations was also assessed. Applying the variational formulation derived the favourable governing equations. To capture the consistent nanoscale effect, the NSGT was inserted into the mathematical model. Transmuting the acquired relations based on the NSGT into the displacement relationship gives an eligible equation, which stands to compute large deflections. The translation and shifting of the nonlinear system of ordinary differential equations into the algebraic ones were performed based on the GRWM. The GRWM concerning an analytical flow estimated clamped, simply-supported, and free end conditions. Afterward, the numerical solution regarding NRT was investigated. From the obtained results, one can briefly write

- In hinged–hinged nanobeams, linear deflections for a NB can be used in the range $w \leq 0.1\ h$, and for a PF-NB, about $w \leq 0.08\ h$. This value in a double-fixed NB and PF-NB is in the range $w < 0.15\ h$. However, for a cantilever case in NB, it is $w \leq 0.2\ h$ and in PF-NB, it is $w \leq 0.1\ h$.
- The difference between the nonlinear analysis and the linear one will be more pronounced in the boundary condition with higher degrees of freedom.
- Increasing the numerical value of the nonlocal parameter leads to a softening effect on the material, and in contrast, increasing the numerical value of the strain gradient parameter leads to the appearance of stiffness in the material.
- The effect of nonlinear analysis is greater in large values of nonlocal parameters and small values of strain gradient parameters.
- The effect of nonlinear analysis on a nonlocal study is greater than a local one.
- The effect of nonlinear analysis in the positive magnetic field decreases. However, the opposite is true in the case of a negative magnetic field.
- For nanobeams with very large lengths, linear analysis gives entirely erroneous results even if the values of lateral loads are not large.
- The flexomagnetic effect leads to more material stiffness, and thus reduces the numerical values of deflections in static analysis.
- The less flexible the boundary condition, the higher the flexomagneticity effect.

Author Contributions: Conceptualization, M.M. and V.A.E.; methodology, M.M. and V.A.E.; software, M.M.; validation, M.M.; formal analysis, M.M.; investigation, M.M. and V.A.E.; resources, M.M. and V.A.E.; data curation, M.M. and V.A.E.; writing—original draft preparation, M.M.; writing—review and editing, V.A.E.; visualization, M.M.; supervision, V.A.E.; project administration, V.A.E.; funding acquisition, V.A.E. All authors have read and agreed to the published version of the manuscript.

Funding: This research was funded by the Government of the Russian Federation (contract No. 14.Z50.31.0046).

Conflicts of Interest: The authors declare no conflict of interest.

References

1. Fahrner, W. *Nanotechnology and Nanoelectronics*, 1st ed.; Springer: Berlin, Germany, 2005; p. 269.
2. Kabychenkov, A.F.; Lisovskii, F.V. Flexomagnetic and flexoantiferromagnetic effects in centrosymmetric antiferromagnetic materials. *Tech. Phys.* **2019**, *64*, 980–983. [CrossRef]
3. Eliseev, E.A.; Morozovska, A.N.; Glinchuk, M.D.; Blinc, R. Spontaneous flexoelectric/flexomagnetic effect in nanoferroics. *Phys. Rev. B* **2009**, *79*, 165433. [CrossRef]
4. Lukashev, P.; Sabirianov, R.F. Flexomagnetic effect in frustrated triangular magnetic structures. *Phys. Rev. B* **2010**, *82*, 094417. [CrossRef]
5. Eliseev, E.A.; Morozovska, A.N.; Khist, V.V.; Polinger, V. Effective flexoelectric and flexomagnetic response of ferroics. In *Recent Advances in Topological Ferroics and their Dynamics, Solid State Physics*; Stamps, R.L., Schultheis, H., Eds.; Elsevier: London, UK, 2019; Volume 70, pp. 237–289.
6. Zhang, J.X.; Zeches, R.J.; He, Q.; Chu, Y.H.; Ramesh, R. Nanoscale phase boundaries: A new twist to novel functionalities. *Nanoscale* **2012**, *4*, 6196–6204. [CrossRef] [PubMed]
7. Zhou, H.; Pei, Y.; Fang, D. Magnetic field tunable small-scale mechanical properties of nickel single crystals measured by nanoindentation technique. *Sci. Rep.* **2014**, *4*, 1–6. [CrossRef]
8. Ebrahimi, F.; Barati, M.R. Porosity-dependent vibration analysis of piezo-magnetically actuated heterogeneous nanobeams. *Mech. Syst. Signal. Pr.* **2017**, *93*, 445–459. [CrossRef]
9. Zenkour, A.M.; Arefi, M.; Alshehri, N.A. Size-dependent analysis of a sandwich curved nanobeam integrated with piezomagnetic face-sheets. *Results Phys.* **2017**, *7*, 2172–2182. [CrossRef]
10. Alibeigi, B.; Beni, Y.T. On the size-dependent magneto/electromechanical buckling of nanobeams. *Eur. Phys. J. Plus* **2018**, *133*, 398. [CrossRef]
11. Malikan, M. Electro-mechanical shear buckling of piezoelectric nanoplate using modified couple stress theory based on simplified first order shear deformation theory. *Appl. Math. Model.* **2017**, *48*, 196–207. [CrossRef]
12. Malikan, M.; Krasheninnikov, M.; Eremeyev, V.A. Torsional stability capacity of a nano-composite shell based on a nonlocal strain gradient shell model under a three-dimensional magnetic field. *Int. J. Eng. Sci.* **2020**, *148*, 103210. [CrossRef]
13. Sidhardh, S.; Ray, M.C. Flexomagnetic response of nanostructures. *J. Appl. Phys.* **2018**, *124*, 244101. [CrossRef]
14. Zhang, N.; Zheng, S.; Chen, D. Size-dependent static bending of flexomagnetic nanobeams. *J. Appl. Phys.* **2019**, *126*, 223901. [CrossRef]
15. Malikan, M.; Eremeyev, V.A. Free Vibration of Flexomagnetic Nanostructured Tubes Based on Stress-driven Nonlocal Elasticity. In *Analysis of Shells, Plates, and Beams*, 1st ed.; Altenbach, H., Chinchaladze, N., Kienzler, R., Müller, W.H., Eds.; Springer Nature: Basel, Switzerland, 2020; Volume 134, pp. 215–226.
16. Song, X.; Li, S.-R. Thermal buckling and post-buckling of pinned–fixed Euler–Bernoulli beams on an elastic foundation. *Mech. Res. Commun.* **2007**, *34*, 164–171. [CrossRef]
17. Reddy, J.N. Nonlocal nonlinear formulations for bending of classical and shear deformation theories of beams and plates. *Int. J. Eng. Sci.* **2010**, *48*, 1507–1518. [CrossRef]
18. Fernández-Sáez, J.; Zaera, R.; Loya, J.A.; Reddy, J.N. Bending of Euler–Bernoulli beams using Eringen's integral formulation: A paradox resolved. *Int. J. Eng. Sci.* **2016**, *99*, 107–116. [CrossRef]
19. Feo, L.; Penna, R. On Bending of Bernoulli-Euler Nanobeams for Nonlocal Composite Materials. *Model. Simul. Eng.* **2016**. [CrossRef]
20. Ghannadpour, S. Ritz Method Application to Bending, Buckling and Vibration Analyses of Timoshenko Beams via Nonlocal Elasticity. *J. Appl. Comput. Mech.* **2018**, *4*, 16–26.
21. Demir, C.; Mercan, K.; Numanoglu, H.; Civalek, O. Bending Response of Nanobeams Resting on Elastic Foundation. *J. Appl. Comput. Mech.* **2018**, *4*, 105–114.

22. Jia, N.; Yao, Y.; Yang, Y.; Chen, S. Size effect in the bending of a Timoshenko nanobeam. *Acta Mech.* **2017**, *228*, 2363–2375. [CrossRef]
23. Marotti de Sciarra, F.; Barretta, R. A new nonlocal bending model for Euler–Bernoulli nanobeams. *Mech Res. Commun.* **2014**, *62*, 25–30. [CrossRef]
24. Zenkour, A.M.; Sobhy, M. A simplified shear and normal deformations nonlocal theory for bending of nanobeams in thermal environment. *Phys. E* **2015**, *70*, 121–128. [CrossRef]
25. Yang, L.; Fan, T.; Yang, L.; Han, X.; Chen, Z. Bending of functionally graded nanobeams incorporating surface effects based on Timoshenko beam model. *Theor. Appl. Mech. Lett.* **2017**, *7*, 152–158. [CrossRef]
26. Lim, C.W.; Zhang, G.; Reddy, J.N. A Higher-order nonlocal elasticity and strain gradient theory and Its Applications in wave propagation. *J. Mech. Phys. Solids* **2015**, *78*, 298–313. [CrossRef]
27. Şimşek, M. Some closed-form solutions for static, buckling, free and forced vibration of functionally graded (FG) nanobeams using nonlocal strain gradient theory. *Compos. Struct.* **2019**, *224*, 111041. [CrossRef]
28. Karami, B.; Janghorban, M. On the dynamics of porous nanotubes with variable material properties and variable thickness. *Int. J. Eng. Sci.* **2019**, *136*, 53–66. [CrossRef]
29. Sahmani, S.; Safaei, B. Nonlinear free vibrations of bi-directional functionally graded micro/nano-beams including nonlocal stress and microstructural strain gradient size effects. *Thin Wall. Struct.* **2019**, *140*, 342–356. [CrossRef]
30. Karami, B.; Janghorban, M.; Rabczuk, T. Dynamics of two-dimensional functionally graded tapered Timoshenko nanobeam in thermal environment using nonlocal strain gradient theory. *Compos. Part B-Eng.* **2020**, *182*, 107622. [CrossRef]
31. Malikan, M.; Dimitri, R.; Tornabene, F. Transient response of oscillated carbon nanotubes with an internal and external damping. *Compos. Part B-Eng.* **2019**, *158*, 198–205. [CrossRef]
32. Malikan, M.; Eremeyev, V.A. On the dynamics of a visco-piezo-flexoelectric nanobeam. *Symmetry* **2020**, *12*, 643. [CrossRef]
33. Malikan, M.; Eremeyev, V.A. Post-critical buckling of truncated conical carbon nanotubes considering surface effects embedding in a nonlinear Winkler substrate using the Rayleigh-Ritz method. *Mater. Res. Express* **2020**, *7*, 025005. [CrossRef]
34. Norouzzadeh, A.; Ansari, R.; Rouhi, H. Nonlinear Bending Analysis of Nanobeams Based on the Nonlocal Strain Gradient Model Using an Isogeometric Finite Element Approach. *IJST-T Civ. Eng.* **2019**, *43*, 533–547. [CrossRef]
35. Hashemian, M.; Foroutan, S.; Toghraie, D. Comprehensive beam models for buckling and bending behavior of simple nanobeam based on nonlocal strain gradient theory and surface effects. *Mech. Mater.* **2019**, *139*, 103209. [CrossRef]
36. Malikan, M.; Nguyen, V.B.; Tornabene, F. Damped forced vibration analysis of single-walled carbon nanotubes resting on viscoelastic foundation in thermal environment using nonlocal strain gradient theory. *Eng. Sci. Technol. Int. J.* **2018**, *21*, 778–786. [CrossRef]
37. Ebrahimi, F.; Dabbagh, A.; Tornabene, F.; Civalek, O. Hygro-thermal effects on wave dispersion responses of magnetostrictive sandwich nanoplates. *Adv. Nano Res.* **2019**, *7*, 157–167.
38. She, G.L.; Liu, H.B.; Karami, B. On resonance behavior of porous FG curved nanobeams. *Steel Compos. Struct.* **2020**, *36*, 179–186.
39. Ansari, R.; Sahmani, S.; Arash, B. Nonlocal plate model for free vibrations of single-layered graphene sheets. *Phys. Lett. A* **2010**, *375*, 53–62. [CrossRef]
40. Akbarzadeh Khorshidi, M. The material length scale parameter used in couple stress theories is not a material constant. *Int. J. Eng. Sci.* **2018**, *133*, 15–25. [CrossRef]
41. Malikan, M.; Eremeyev, V.A. A new hyperbolic-polynomial higher-order elasticity theory for mechanics of thick FGM beams with imperfection in the material composition. *Compos. Struct.* **2020**, *249*, 112486. [CrossRef]
42. Berrabah, H.M.; Tounsi, A.; Semmah, A.; Adda Bedia, E.A. Comparison of various refined nonlocal beam theories for bending, vibration and buckling analysis of nanobeams. *Struct. Eng. Mech.* **2013**, *48*, 351–365. [CrossRef]
43. Ansari, R.; Sahmani, S. Bending behavior and buckling of nanobeams including surface stress effects corresponding to different beam theories. *Int. J. Eng. Sci.* **2011**, *49*, 1244–1255. [CrossRef]

44. Dastjerdi, S.; Jabbarzadeh, M. Nonlinear bending analysis of bilayer orthotropic graphene sheets resting on Winkler–Pasternak elastic foundation based on non-local continuum mechanics. *Compos. Part B-Eng.* **2016**, *87*, 161–175. [CrossRef]
45. Reddy, J.N.; Pang, S.D. Nonlocal continuum theories of beams for the analysis of carbon nanotubes. *J. Appl. Phys.* **2008**, *103*, 023511. [CrossRef]
46. Ansari, R.; Sahmani, S.; Rouhi, H. Rayleigh–Ritz axial buckling analysis of single-walled carbon nanotubes with different boundary conditions. *Phys. Lett. A* **2011**, *375*, 1255–1263. [CrossRef]
47. Duan, W.H.; Wang, C.M. Exact solutions for axisymmetric bending of micro/nanoscale circular plates based on nonlocal plate theory. *Nanotechnology* **2007**, *18*, 385704. [CrossRef]
48. Duan, W.H.; Wang, C.M.; Zhang, Y.Y. Calibration of nonlocal scaling effect parameter for free vibration of carbon nanotubes by molecular dynamics. *J. Appl. Phys.* **2007**, *101*, 24305. [CrossRef]
49. Maranganti, R.; Sharma, P. Length scales at which classical elasticity breaks down for various materials. *Phys. Rev. Lett.* **2007**, *98*, 195504. [CrossRef]
50. Stein, C.R.; Bezerra, M.T.S.; Holanda, G.H.A.; André-Filho, J.; Morais, P.C. Structural and magnetic properties of cobalt ferrite nanoparticles synthesized by co-precipitation at increasing temperatures. *AIP Advan.* **2018**, *8*, 056303. [CrossRef]

Postprint for: Malikan, M.; Uglov, N. S.; Eremeyev, V. A. On instabilities and post-buckling of piezomagnetic and flexomagnetic nanostructures. International Journal of Engineering Science. https://doi.org/10.1016/j.ijengsci.2020.103395

On instabilities and post-buckling of piezomagnetic and flexomagnetic nanostructures

Mohammad Malikan[1], Nikolay S. Uglov[2], Victor A. Eremeyev[1,2]*

[1] Department of Mechanics of Materials and Structures,
Gdansk University of Technology, ul. Gabriela Narutowicza 11/12, Gdansk 80-233, Gdansk, Poland,

[2] R.E. Alekseev Nizhny Novgorod Technical University,
Minin St., 24, Nizhny Novgorod 603950, Russia

*Corresponding author:
Email: mohammad.malikan@pg.edu.pl, nikolay-uglov@mail.ru, eremeyev.victor@gmail.com

Abstract

We focus on the mechanical strength of piezomagnetic beam-like nanosize sensors during post-buckling. An effective flexomagnetic property is also taken into account. The modelled sensor is selected to be a Euler-Bernoulli type beam. Long-range interactions between atoms result in a mathematical model based on the nonlocal strain gradient elasticity approach (NSGT). Due to possible large deformations within a post-buckling phenomenon, the resultant equations are essentially nonlinear. We establish the results using an analytical approach, including a variety of boundary conditions. We visualize the effective response of the designed sensor for several key components. It was obtained that the flexomagnetic effect is meaningful for less flexible boundary conditions. Besides, it was found that the failure originated from post-buckling occurs sooner if the numerical amounts of nonlocal parameter and the strain gradient one are respectively so small and exceedingly large.

Keywords: Piezomagnetic beam; Post-buckling; Flexomagneticity; Beam-like sensor; Nonlocal elasticity

Symbols

H_z	Magnetic field component	W	Works done by external objects
η_{xxz}	Gradient of the elastic strain	u_1	Cartesian displacements along x axis
σ_{xx}	Stress component	u_3	Cartesian displacements along z axis
ε_{xx}	Strain component	L	Length of the beam
ξ_{xxz}	Hyper stress	h	Thickness of the beam
B_z	Magnetic flux component	u	Axial displacement of the midplane
C_{11}	Elasticity modulus	w	Transverse displacement of the midplane
M_x	Moment stress resultant	z	Thickness coordinate
T_{xxz}	Hyper stress resultant	q_{31}	Component of the third-order piezomagnetic tensor
U	Strain energy	g_{31}	Component the sixth-order gradient elasticity tensor
δ	Symbol of variations	f_{31}	Fourth order flexomagnetic component
N_x	Axial stress resultant	a_{33}	Component of the second-order magnetic permeability tensor
Ψ	Magnetic potential	N_x^0	Initial total in-plane axial force
I_z	Area moment of inertia	ψ	Initial magnetic potential
μ	Nonlocal parameter (nm^2)	A	Area of cross-section of the beam
l	Strain gradient parameter (nm)	N^p	Post-buckling load
Y	Residue in the solution method		
C_1	A constant		
C_2	Integration constant		

1 Introduction

Post-buckling and collapsing behavior are critical to the design of thin structures (Timoshenko & Gere, 1989, Falzon & Aliabadi, 2008, Amabili, 2008, Stevens et al., 1995, Eltaher et al., 2019). Sensitive and certain industrial parts should sustain maximum loads and should be such as to prevent instability and unwanted buckling to avoid large deformations and collapsing. Post-buckling means the deformation of the structure after the start of buckling (bifurcation point), which helps to better understand the failure resistance of the structure after

the amount of unauthorized and unallowable in-plane loading. The behavior of post-buckling is a nonlinear one that occurs in a very short time. Also, self-contact may occur during post-buckling due to the high deformation amount. The initial onset of buckling is related to the modes obtained from the modal frequency analysis of the structure. After bifurcation point, the structure has become to confront with a new pattern of deformation, that is a large deformation which buckling load at this time refers to failure of structure. Basically, bifurcation buckling cannot imply collapsing in the structure.

Recently the interest grows to electro- and magnetorheological materials including such coupling higher-order phenomena as flexoelectricity and flexomagneticity, see, e.g. (Basutskar, 2019, Ghayesh and Farajpour, 2019, Ghayesh and Farokhi, 2020, Eremeyev et al., 2020, Espinosa-Almeyda et al., 2020, Mawassy et al., 2020) and the references therein. In particular, magnetic nanoparticles (MNPs) have attracted the attention of many researchers due to their exclusive features (Freitas et al., 2007, Justino et al., 2010, Reddy et al., 2012, Xu and Wang, 2012, Agrawal et al., 2014). Numerous applications are expected for MNPs based on fabricating and developing biosensors. Some of these applications can be stated as biology, clinics, foods, and environments sensors. MNPs can be involved in any substances that are excited by an outer magnetic potential, for example transducers. MNPs are classified into two main categories, paramagnetic and ferromagnetic. Their distinguishing feature appears after the removal of the external magnetic field. Thus, there is no magnetic property in paramagnetic particles after removing the outer magnetic field, while the magnetic property is preserved in ferromagnetic materials.

In the group of MNPs and spinel ferrites, cobalt-ferrite magnetic nanostructures (CFMNs) with chemical symbol $CoFe_4O_2$ have highlighted the significant studies and technological applications. The number of published papers on cobalt-ferrite magnetic

nanostructures have been unprecedented during last two decades (Arvand & Hassannezhad, 2014, Theres Baby & Ramaprabhu, 2010; Xin et al., 2013). Of applications of this kind of MNPs are in using electronic devices, optical and magnetic storage in light of its extraordinary features, such as high electromagnetic performance, mechanical hardness, chemical stability, coercivity and high saturation magnetization (Eliseev et al., 2009, Fahrner, 2005, Ju et al., 2008). It should be borne in mind that the CFMNs structure is in the group of ferromagnetic materials. Electromagnetic coupling may influence on the instabilities of such rheological materials, see, e.g., (Broderick et al., 2020, Jalaei and Civalek, 2019, Malikan et al., 2020).

Compared to piezomagneticity (PM), flexomagneticity (FM) is a pervasive property with less restrictive structural symmetry and therefore expands the choice of materials that can be used for sensors and electromechanical actuators (Eliseev et al., 2019, Kabychenkov & Lisovskii, 2019, Lukashev & Sabirianov, 2010, Moosavi et al., 2017, Pereira et al., 2012, Zhang et al., 2012, Zhou et al., 2014). Reduced dimensions would result in larger gradients. This means that the strain difference at a small distance leads to a larger strain gradient. In MNPs technology, the small length scale is discussed, and therefore this type of material will increase the effect of FM, which may even be competitive with PM. This issue is growing rapidly due to the new developments and progresses that have taken place in recent years, especially at the nanoscale.

First, a brief introduction to the first theoretical research on the mechanical response of FM nanostructures is given. Theoretical research performed in the field of FM to elementary papers by Sidhardh & Ray, (2018) and Zhang, Zhang & Chen, (2019). These two early works studied FM in CFMNs within the analysis of static bending deformation. Both research works utilized small deformations and the corresponding domain was assumed as Euler-Bernoulli beam. In these papers, the results were demonstrated on the basis of both direct and converse

magnetization effects. The acting static load imposed on the vertical alignment of the domain was uniformly applied. The superiority of the second research against the former one can be presenting several boundary conditions in the study. However, both research studies didn't show perfectly size-dependent influences. Although the surface effect was examined, the nonlocality as a prominent and well-known impact in nanoscale was not evaluated. Recently, Malikan & Eremeyev, (2020a) explored linear frequency behavior of CFMNs on the basis of Euler-Bernoulli type beam. The stress-driven nonlocal elasticity was substituted in the mathematics formulation in order to survey the size-dependent impacts. Their numerical outcomes affirm the behavior of FM is size-dependent. In a nonlinear investigation, Malikan & Eremeyev, (2020b) inspected nonlinear frequency response of CFMNs containing FM effect. To survey the size-dependent influences, they implemented the well-worked nonlocal strain gradient elasticity theory in the mathematical modeling process. Continuing the reported research performed on CFMNs involving FM, we have tried to analyze the post-stability state of the CFMNs in what follows with FM impact. In accordance with the large deformation which occurs in post-buckling conditions, the nonlinear strains of Lagrangian are mixed with Euler-Bernoulli kinematic field which leads to a local constitutive equation. This equation is changed into a nonlocal post-buckling relationship based on the characteristic equation of the nonlocal strain gradient model. Theoretically, four boundary conditions have been estimated, that is, the beam-like sensor with pivot-pivot, fully fixed, pivot-fixed, and fixed-free ends. The assessment is associated with two cases of the sensor, the first one is considered having only PM property and the second one consists of FM with apparent PM. Besides, two states of buckling are investigated, the bifurcation point and its post-time. Later, by variations in fundamental parameters which are vital factors in designing sensors, we measure their influences on the basis of sketched graphical figures.

The paper is organized as follows; by means of Section 2 we present the mathematical modelling process of the analysis. Thereafter, Section 3 is associated with the solution methodology. Afterwards, Section 4 of the article considers a preliminary validation by reducing the model into a simple one. Later, Section 5 comes to exhibit a parametric study in order to investigate different factors applicable to affect mechanical behavior of the smart sensor. Finally, by assistance of the conclusion section, we briefly survey the present paper.

2 Mathematical statement

2.1 Basic formulation of structures involving PM and FM

In continue with (Kabychenkov & Lisovskii, 2019, Eliseev et al., 2009, Lukashev & Sabirianov, 2010), the elasticity relations which govern the PM-FM structures would be introduced in what follows. The deformations are restricted to the infinitesimal ones on the basis of early isothermal. Thus, vector-values variables can be magnetic field **H** and displacements *u* as follows (**H** is a first-order tensor)

$$\mathbf{u}=\mathbf{u}(\mathbf{x}),\mathbf{H}=\mathbf{H}(\mathbf{x}) \tag{1}$$

in which $\mathbf{x}$ denotes a position vector. The free energy density *U* based on the PM-FM can be written in the below form

$$U=U(\boldsymbol{\varepsilon},\boldsymbol{\eta},\mathbf{H})=-\frac{1}{2}\mathbf{H}\cdot\mathbf{a}\cdot\mathbf{H}+\frac{1}{2}\boldsymbol{\varepsilon}:\mathbf{C}:\boldsymbol{\varepsilon}+\frac{1}{2}\boldsymbol{\eta}\vdots\mathbf{g}\vdots\boldsymbol{\eta}+\boldsymbol{\varepsilon}:\mathbf{r}\vdots\boldsymbol{\eta} \\ -\mathbf{H}\cdot\mathbf{q}:\boldsymbol{\varepsilon}-\mathbf{H}\cdot\mathbf{f}\vdots\boldsymbol{\eta} \tag{2}$$

in which the strain tensor is defined by $\boldsymbol{\varepsilon}$. Moreover, the gradient of the strain tensor can be presented as below

$$\boldsymbol{\varepsilon}=\frac{1}{2}\left(\nabla\mathbf{u}+\nabla\mathbf{u}^{T}\right),\ \boldsymbol{\eta}=\nabla\boldsymbol{\varepsilon} \tag{3}$$

∇ interprets the 3D nabla-operator. Different tensors are introduced by Eq. (2) for material

characterisitcs. Among the mentioned tensors; **f** is the fourth-order flexomagnetic tensor, **C** is the fourth-order elasticity coefficient tensor, the strain and strain-gradient tensors are coupled by **r** that itself is a fifth-order tensor, **g** is the sixth-order gradient elasticity tensor, **a** is the second-order magnetic permeability tensor, **q** is the third-order piezomagnetic tensor, and in addition, "·", ":", and "⋮" define scalar (inner) products in spaces of vectors, second-order and third-order tensors, respectively.

We will now present the relation between **H** through the magnetic potential ψ,

$$\mathbf{H} = -\nabla\psi \tag{4}$$

Static model of flexomagneticity is derived on the basis of principle of virtual work as

$$\delta\Pi = \delta A \tag{5}$$

where $\Pi = \int_V U dV$, and V is the volume of the domain occupying the flexomagnetic structure and δA expresses the work done by outer loads.

To make the process simpler, a simple form is assumed as below

$$\delta A = \int_V \mathbf{F}\cdot\delta\mathbf{u} + \int_{\partial V} \mathbf{t}\cdot\delta\mathbf{u} ds \tag{6}$$

in which **t** and **F** illustrate surface traction and external forces.

On the basis of the standard form of calculus of variations and regarding Eq. (5), one can get

$$\nabla\cdot\left(\boldsymbol{\sigma} - \nabla\cdot\boldsymbol{\xi}\right) + \mathbf{F} = \mathbf{0} \tag{7a}$$

$$\nabla\cdot\mathbf{B} = 0 \tag{7b}$$

where **B** denotes the vector of magnetic induction.

Hence, we introduce the following constitutive equations

$$\boldsymbol{\sigma} = \frac{\partial U}{\partial \boldsymbol{\varepsilon}} \equiv \mathbf{C} : \boldsymbol{\varepsilon} + \mathbf{r} \vdots \boldsymbol{\eta} - \mathbf{H}\cdot\mathbf{q} \tag{8a}$$

$$\xi = \frac{\partial U}{\partial \boldsymbol{\eta}} \equiv \mathbf{g} : \boldsymbol{\eta} + \boldsymbol{\varepsilon} : \mathbf{r} - \mathbf{H} \cdot \mathbf{f} \tag{8b}$$

$$\mathbf{B} = -\frac{\partial U}{\partial \mathbf{H}} = \mathbf{a} \cdot \mathbf{H} + \mathbf{q} : \boldsymbol{\varepsilon} + \mathbf{f} \vdots \boldsymbol{\eta} \tag{8c}$$

In what follows we consuider one-dimensional counterparts of these constitutive relations.

2.2 The PM-FM beam-like sensor model

The presented figures determine the physical conditions of the problem in mathematical definitions. Respectively, Figures 1, 2, and 3, display a fully fixed, fully pivot and cantilever beam-like smart sensor with both ends clamped-clamped, guided-guided and clamped-free. A magnetic field is perpendicularly applied which ensues an extra axial force. An axial mechanical load works on the beam to convey the post-buckling state. Boundary conditions are mathematically conducted on the figures. All the boundary objects are rigid. And the beam is configured in a square shape.

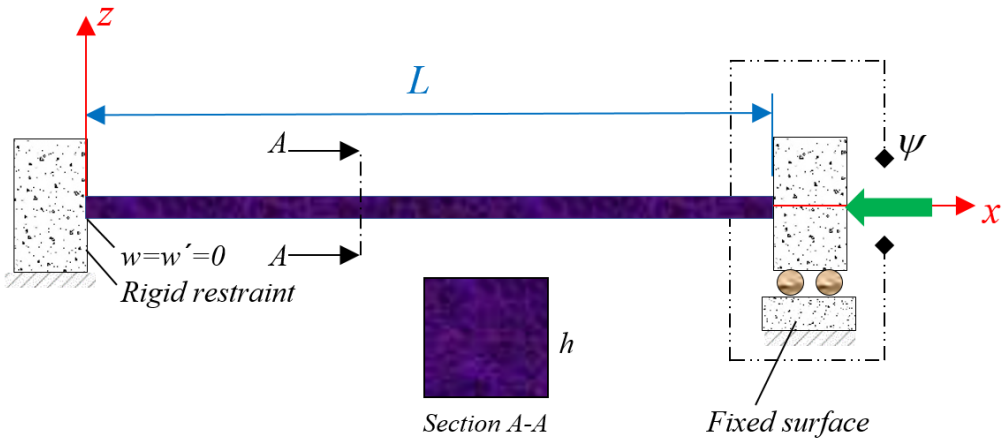

Figure 1. A square beam-like nano sensor containing PM and FM embedded in fully fixed ends

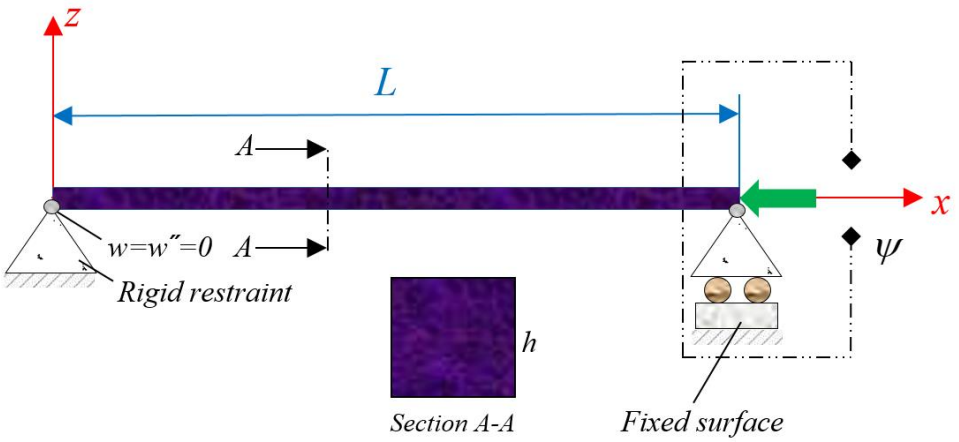

Figure 2. A square beam-like nano sensor containing PM and FM embedded in pivot ends

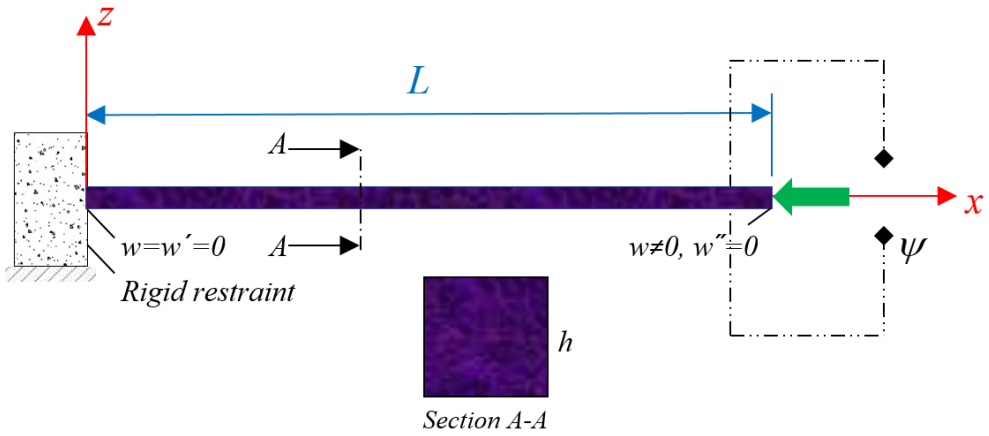

Figure 3. A cantilever square beam-like nano sensor containing PM and FM

It is assumed that the magnetic sensor behaves like a beam structure. Thus, a thin beam approach is carried out as (Hamed et al., 2020, Reddy, 2010, Song & Li, 2007)

$$u_1(x,z) = u(x) - z\frac{dw(x)}{dx} \tag{9}$$

$$u_3(x,z) = w(x) \tag{10}$$

As mentioned before, after buckling and bifurcation point, there would appear the large deformations. Hence, the formulation employs the nonlinear Lagrangian strains as

$$\varepsilon_{xx} = \frac{du}{dx} - z\frac{d^2w}{dx^2} + \frac{1}{2}\left(\frac{dw}{dx}\right)^2 \tag{11}$$

$$\eta_{xxz} = \frac{d\varepsilon_{xx}}{dz} = -\frac{d^2 w}{dx^2} \tag{12}$$

To expand the components of stress, hyper stress, and magnetic induction, one can write (Sidhardh & Ray, 2018, Zhang, Zhang & Chen, 2019).

$$\sigma_{xx} = C_{11}\varepsilon_{xx} - q_{31}H_z \tag{13}$$

$$\xi_{xxz} = g_{31}\eta_{xxz} - f_{31}H_z \tag{14}$$

$$B_z = a_{33}H_z + q_{31}\varepsilon_{xx} + f_{31}\eta_{xxz} \tag{15}$$

To derive the characteristics equation, the following variational energy formula based on the Lagrange functional is defined

$$\delta(U - W) = 0 \tag{16}$$

The entire strain energy of the system is established as

$$\delta U = \int_V \left(\sigma_{xx}\delta\varepsilon_{xx} + \xi_{xxz}\delta\eta_{xxz} - B_z\delta H_z\right)dV \tag{17}$$

By computing the above equation, one can obtain the magnetic and mechanical parts of the strain energy as

$$\delta U = \delta\Pi_{U_1}^{Mech} + \delta\Pi_{U_1}^{Mag} + \delta\Pi_{U_2}^{Mech} + \delta\Pi_{U_2}^{Mag} \tag{18}$$

where

$$\delta\Pi_{U_1}^{Mech} = -\int_0^L \left(\frac{dN_x}{dx}\delta u + \frac{d^2M_x}{dx^2}\delta w + \frac{d}{dx}\left(N_x\frac{dw}{dx}\right)\delta w + \frac{d^2T_{xxz}}{dx^2}\delta w\right)dx \tag{19}$$

$$\delta\Pi_{U_1}^{Mag} = -\int_0^L \int_{-h/2}^{h/2} \frac{dB_z}{dz}\delta\Psi\, dz dx \tag{20}$$

$$\delta\Pi_{U_2}^{Mech} = \left(N_x\delta u - M_x\frac{d\delta w}{dx} - T_{xxz}\frac{d\delta w}{dx} + N_x\frac{dw}{dx}\delta w + \frac{dM_x}{dx}\delta w + \frac{dT_{xxz}}{dx}\delta w\right)\Bigg|_0^L \tag{21}$$

$$\delta\Pi_{U_2}^{Mag} = \int_0^L \left(B_z \delta\Psi\right)\Big|_{-h/2}^{h/2} dx \tag{22}$$

Here we introduced the parameters as follows

$$N_x = \int_{-h/2}^{h/2} \sigma_{xx} dz \tag{23}$$

$$M_x = \int_{-h/2}^{h/2} \sigma_{xx} z dz \tag{24}$$

$$T_{xxz} = \int_{-h/2}^{h/2} \xi_{xxz} dz \tag{25}$$

which specify the resultants of stresses on any element of the beam. The external factors, such as magnetic field and mechanical in-plane force, create the work on the system as (Malikan & Eremeyev, 2020c, d)

$$W = -\frac{1}{2}\int_0^L N_x^0 \left(\frac{dw}{dx}\right)^2 dx \tag{26}$$

$$\delta W = -\int_0^L N_x^0 \left(\frac{d\delta w}{dx}\frac{dw}{dx}\right) dx \tag{27}$$

There is a relation between the component of the magnetic field and the magnetic potential as

$$H_z = -\frac{d\Psi}{dz} \tag{28}$$

Assuming the magnetic potential changes along the thickness of the beam and on the basis of converse effect description and closed circuit of the magnetic field, one can present the electrical boundary conditions as

$$\Psi\left(+\frac{h}{2}\right) = \psi, \ \Psi\left(-\frac{h}{2}\right) = 0 \tag{29}$$

Substituting and combining Eqs. (15), (20), (22), (28) and (29) and simplyfying rigorously, one

can achieve the magnetic potential and the relevance component as (Sidhardh & Ray, 2018, Zhang, Zhang & Chen, 2019)

$$\Psi = -\frac{q_{31}}{2a_{33}}\left(z^2 - \frac{h^2}{4}\right)\frac{d^2w}{dx^2} + \frac{\psi}{h}\left(z + \frac{h}{2}\right) \tag{30}$$

$$H_z = z\frac{q_{31}}{a_{33}}\frac{d^2w}{dx^2} - \frac{\psi}{h} \tag{31}$$

Consequently, by the help of Eqs. (11), (12), (30), and (31), one can re-write Eqs. (13)-(15) as

$$\sigma_{xx} = C_{11}\left[\frac{du}{dx} + \frac{1}{2}\left(\frac{dw}{dx}\right)^2\right] - z\left(C_{11} + \frac{q_{31}^2}{a_{33}}\right)\frac{d^2w}{dx^2} + \frac{q_{31}\psi}{h} \tag{32}$$

$$\xi_{xxz} = -\left(g_{31} + \frac{q_{31}f_{31}z}{a_{33}}\right)\frac{d^2w}{dx^2} + \frac{f_{31}\psi}{h} \tag{33}$$

$$B_z = q_{31}\left[\frac{du}{dx} + \frac{1}{2}\left(\frac{dw}{dx}\right)^2\right] - f_{31}\frac{d^2w}{dx^2} - \frac{a_{33}\psi}{h} \tag{34}$$

Let us write the local resultants of stresses as

$$N_x = C_{11}A\left[\frac{du}{dx} + \frac{1}{2}\left(\frac{dw}{dx}\right)^2\right] + q_{31}\psi \tag{35}$$

$$M_x = -I_z\left(C_{11} + \frac{q_{31}^2}{a_{33}}\right)\frac{d^2w}{dx^2} \tag{36}$$

$$T_{xxz} = -g_{31}h\frac{d^2w}{dx^2} + f_{31}\psi \tag{37}$$

Eq. (35) plays the role of axial stress resultant which consisted of both mechanical and magnetic terms. Therefore, the magnetic part can be provided as

$$N^{Mag} = q_{31}\psi \tag{38}$$

Then, the total axial loading can be noted as below

$$N_x^0 = N^p + N^{Mag} \tag{39}$$

Ultimately the bond of all formulation will lead to local nonlinear equilibrium equations as follows

$$\frac{dN_x}{dx}=0 \tag{40}$$

$$\frac{d^2M_x}{dx^2}+\frac{d^2T_{xxz}}{dx^2}+\frac{d}{dx}\left(N_x\frac{dw}{dx}\right)+N_x^0\frac{d^2w}{dx^2}=0 \tag{41}$$

Size-dependent properties should be established into the mathematical model in order to address nanoscale influences. The size-dependent model is not here restricted to the nonlocal interactions of atoms, but it also considers the higher strain gradients in a constitutive postulate as follows (Lim, Zhang & Reddy, 2015)

$$\left(1-\mu\frac{d^2}{dx^2}\right)\sigma_{xx}^{NonLocal}=\left(1-l^2\frac{d^2}{dx^2}\right)\sigma_{xx}^{Local} \tag{42}$$

where $\mu=(e_0a)^2$. For applications of nonlocal approach to beam models we refer also to (Barretta and de Sciarra, 2019, Barreta et al., 2020).

By developing Eq. (42) for the axial stress of present problem (Eq. (42)), one can see

$$\left(1-\mu\frac{d^2}{dx^2}\right)\sigma_{xx}^{NonLocal}=\left(1-l^2\frac{d^2}{dx^2}\right)\left\{C_{11}\left[\frac{du}{dx}+\frac{1}{2}\left(\frac{dw}{dx}\right)^2\right]-z\left(C_{11}+\frac{q_{31}^2}{a_{33}}\right)\frac{d^2w}{dx^2}+\frac{q_{31}\psi}{h}\right\} \tag{43}$$

By integrating rigorously from both parts of Eq. (43) based on the dz and using Eqs. (23-25), one can express

$$N_x-\mu\frac{d^2N_x}{dx^2}=C_{11}A\left(1-l^2\frac{d^2}{dx^2}\right)\left\{\left[\frac{du}{dx}+\frac{1}{2}\left(\frac{dw}{dx}\right)^2\right]+q_{31}\psi\right\} \tag{44}$$

$$M_x-\mu\frac{d^2M_x}{dx^2}=-I_z\left(C_{11}+\frac{q_{31}^2}{a_{33}}\right)\left(1-l^2\frac{d^2}{dx^2}\right)\left\{\frac{d^2w}{dx^2}\right\} \tag{45}$$

$$T_{xxz}-\mu\frac{d^2T_{xxz}}{dx^2}=\left(1-l^2\frac{d^2}{dx^2}\right)\left\{-g_{31}h\frac{d^2w}{dx^2}+f_{31}\psi\right\} \tag{46}$$

By re-writing Eq. (41) based on the first term and plugging it in Eq. (45), one can have (Karami

& Janghorban, 2019, Karami et al., 2020, Karami & Janghorban, 2020, Eyvazian et al., 2020, Li & Hu, 2017, Malikan et al., 2019, Malikan et al., 2020, Malikan et al., 2018, Sahmani & Safaei, 2019, Ebrahimi et al., 2019)

$$M_x = -\mu\left(\frac{d^2T_{xxz}}{dx^2}+\frac{d}{dx}\left(N_x\frac{dw}{dx}\right)+N_x^0\frac{d^2w}{dx^2}\right)-I_z\left(C_{11}+\frac{q_{31}^2}{a_{33}}\right)\left(\frac{d^2w}{dx^2}-l^2\frac{d^4w}{dx^4}\right) \tag{47}$$

Since there are two unknown variables (u and w) in the equations, it would result in difficulties to solve the equations as far as there is a third unknown, which is post-critical buckling load (N^p). Therefore, let us write the u based on the w as

$$N_x = C_{11}A\left[\frac{du}{dx}+\frac{1}{2}\left(\frac{dw}{dx}\right)^2\right]=C_1 \tag{48}$$

Writing Eq. (48) based on the u and integrating gives

$$u=-\frac{1}{2}\int_0^L\left(\frac{dw}{dx}\right)^2dx+\frac{C_1}{C_{11}A}x+C_2 \tag{49}$$

Imposing the initial conditions as $u(0)=u(L)=0$, one can obtain

$$N_x=\frac{C_{11}A}{2L}\int_0^L\left(\frac{dw}{dx}\right)^2dx \tag{50}$$

Thereafter, based on the Eqs. (39), (41), (47), and (50), the model of the problem can be formulated mathematically as a single integro-differential equation

$$\begin{aligned}
&-g_{31}h\frac{d^4w}{dx^4}+\left(N^p+q_{31}\psi\right)\frac{d^2w}{dx^2}-\mu\left(-g_{31}h\frac{d^6w}{dx^6}+\left(N^p+q_{31}\psi\right)\frac{d^4w}{dx^4}\right)\\
&-\mu\left[\frac{C_{11}A}{2L}\int_0^L\left(\frac{dw}{dx}\right)^2dx\right]\frac{d^4w}{dx^4}-\mu\frac{d}{dx}\left[\frac{C_{11}A}{2L}\int_0^L\left(\frac{dw}{dx}\right)^2dx\right]\frac{d^3w}{dx^3}\\
&-\mu\frac{d^2}{dx^2}\left[\frac{C_{11}A}{2L}\int_0^L\left(\frac{dw}{dx}\right)^2dx\right]\frac{d^2w}{dx^2}-\mu\frac{d^3}{dx^3}\left[\frac{C_{11}A}{2L}\int_0^L\left(\frac{dw}{dx}\right)^2dx\right]\frac{dw}{dx}\\
&+\left[\frac{C_{11}A}{2L}\int_0^L\left(\frac{dw}{dx}\right)^2dx\right]\frac{d^2w}{dx^2}+\frac{d}{dx}\left[\frac{C_{11}A}{2L}\int_0^L\left(\frac{dw}{dx}\right)^2dx\right]\frac{dw}{dx}\\
&-I_z\left(C_{11}+\frac{q_{31}^2}{a_{33}}\right)\left(\frac{d^4w}{dx^4}-l^2\frac{d^6w}{dx^6}\right)=0
\end{aligned} \tag{51}$$

3 Solution approach

In this section, the aim is to solve the appropriate boundary conditions along with the nonlinear governing equation (Eq. (51)). Some admissible shape functions are described by which several end conditions are satisfied. The procedure is entirely analytical. However, as far as the boundary conditions seem to be homogeneous, the present analytical solution sounds like an exact solving method (Malikan & Eremeyev, 2020e).

$$w(x) = W \cdot X(x) \tag{52}$$

where the deflection resulted from post-buckling conditions is dedicated symbolically by *W*. The permissible shape functions appeared in the following can satisfy quite different end conditions (Malikan & Eremeyev, 2020e, Gunda, 2014). The notations are respectively allocated for guided or pivot (S), fixed or clamped (C) and free (F) border conditions (BCs) as follows

$$\text{SS: } X(x) = \sin\left(\frac{\pi}{L}x\right) \tag{53}$$

$$\text{CC: } X(x) = \sin^2\left(\frac{\pi}{L}x\right) \tag{54}$$

$$\text{CS: } \begin{array}{c} X(x) = \delta_1\left(\sin(k_1 x) - \mathrm{k}_1 L cos(k_1 x) + k_1 L\left(1-(x/L)\right)\right) \\ \delta_1 = 0.1709382933,\ \mathrm{k}_1 = 1.4318\pi/L \end{array} \tag{55}$$

$$\text{CF: } X(x) = \sin\left(\frac{\pi}{4L}x\right)\cos\left(\frac{\pi}{4L}x\right) \tag{56}$$

where for example CF accounts a side with free and another one with fully fixture conditions. Incorporating Eq. (51) with Eq. (52) and integrating over the length of the beam, one attains

$$\left(K_L + K_{NL} - N^p K_G\right) X = 0 \tag{57}$$

After some algebra, one obtains the nonlinear algebraic equation that by computing the N^p, that presents post-buckling loads for the magnetic beam-like sensor considering FM. The coefficients in Eq. (57) can be expanded as below

$$K_L = \int_0^L \left[\lambda_1(x) \cdot Y \right] dx \tag{58}$$

$$K_{NL} = \int_0^L \left[\lambda_2(x) \cdot Y \right] dx \tag{59}$$

$$K_G = \int_0^L \left[\lambda_3(x) \cdot Y \right] dx \tag{60}$$

in which Y illustrates a residue, λ_1 to λ_3 are as follows:

$$\begin{aligned} \lambda_1(x) &= -g_{31} h \frac{d^4 w}{dx^4} + q_{31} \psi \frac{d^2 w}{dx^2} - \mu \left(-g_{31} h \frac{d^6 w}{dx^6} + q_{31} \psi \frac{d^4 w}{dx^4} \right) \\ &- I_z \left(C_{11} + \frac{q_{31}^2}{a_{33}} \right) \left(\frac{d^4 w}{dx^4} - l^2 \frac{d^6 w}{dx^6} \right) \end{aligned} \tag{61}$$

$$\begin{aligned} \lambda_2(x) &= -\mu \left[\frac{C_{11} A}{2L} \int_0^L \left(\frac{dw}{dx} \right)^2 dx \right] \frac{d^4 w}{dx^4} - \mu \frac{d}{dx} \left[\frac{C_{11} A}{2L} \int_0^L \left(\frac{dw}{dx} \right)^2 dx \right] \frac{d^3 w}{dx^3} \\ &- \mu \frac{d^2}{dx^2} \left[\frac{C_{11} A}{2L} \int_0^L \left(\frac{dw}{dx} \right)^2 dx \right] \frac{d^2 w}{dx^2} - \mu \frac{d^3}{dx^3} \left[\frac{C_{11} A}{2L} \int_0^L \left(\frac{dw}{dx} \right)^2 dx \right] \frac{dw}{dx} \\ &+ \left[\frac{C_{11} A}{2L} \int_0^L \left(\frac{dw}{dx} \right)^2 dx \right] \frac{d^2 w}{dx^2} + \frac{d}{dx} \left[\frac{C_{11} A}{2L} \int_0^L \left(\frac{dw}{dx} \right)^2 dx \right] \frac{dw}{dx} = 0 \end{aligned} \tag{62}$$

$$\lambda_3(x) = \frac{d^2 w}{dx^2} - \mu \frac{d^4 w}{dx^4} \tag{63}$$

If we assume $K_{NL} = 0$, the bifurcation buckling will result.

4 Validity

To begin the discussion and results of the present study, a results comparison is required to verify the analytical solution's efficiency and accuracy. This is performed regarding Tables 1 to 4 (Wang et al., 2006, Pradhan & Reddy, 2011). In the existing data, bifurcation buckling of a common squared section nanoscale beam was investigated on the basis of the following elasticity properties; E=1TPa, υ= 0.19, the exact solution method (Wang et al., 2006) and differential transformed solution method (DTM) (Pradhan & Reddy, 2011). Both references benefited from the Euler-Bernoulli beam. All the boundary conditions examined in the present paper are validated. A reasonable agreement is observed between the present solution and those reported in (Wang et al., 2006, Pradhan & Reddy, 2011).

Table 1. For a SS beam.

	P_{Cr} (nN)								
	μ=0 nm^2			μ=1 nm^2			μ=4 nm^2		
L (nm)	(Wang et al., 2006)	(Pradhan & Reddy, 2011)	Present	(Wang et al., 2006)	(Pradhan & Reddy, 2011)	Present	(Wang et al., 2006)	(Pradhan & Reddy, 2011)	Present
10	4.8447	4.8447	4.84473	4.4095	4.4095	4.40953	3.4735	3.4735	3.47346
12	3.3644	3.3644	3.36439	3.1486	3.1486	3.14859	2.6405	2.6405	2.64049
14	2.4718	2.4718	2.47180	2.3533	2.3533	2.35330	2.0574	2.0574	2.05739
16	1.8925	1.8925	1.89247	1.8222	1.8222	1.82222	1.6396	1.6396	1.63962
18	1.4953	1.4953	1.49529	1.4511	1.4511	1.45109	1.3329	1.3329	1.33288
20	1.2112	1.2112	1.21118	1.182	1.182	1.18201	1.1024	1.1024	1.10238

Table 2. For a CS beam.

	P_{Cr} (nN)								
	μ=0 nm^2			μ=1 nm^2			μ=2 nm^2		
L (nm)	(Wang et al., 2006)	(Pradhan & Reddy, 2011)	Present	(Wang et al., 2006)	(Pradhan & Reddy, 2011)	Present	(Wang et al., 2006)	(Pradhan & Reddy, 2011)	Present
10	9.887	9.887	9.91111	8.2295	8.2295	8.24614	7.048	7.048	7.06015
12	6.886	6.886	6.88271	6.0235	6.0235	6.03631	5.3651	5.3651	5.37530
14	5.044	5.044	5.05668	4.5744	4.5744	4.58441	4.1844	4.1844	4.19285
16	3.8621	3.8621	3.87152	3.5804	3.5804	3.58849	3.337	3.337	3.34403
18	3.0516	3.0516	3.05898	2.873	2.873	2.87954	2.7141	2.7141	2.71998
20	2.4718	2.4718	2.47777	2.3533	2.3533	2.35871	2.2456	2.2456	2.25057

Table 3. For a CC beam.

	P_{Cr} (nN)								
	μ=0 nm^2			μ=1 nm^2			μ=2 nm^2		
L (nm)	(Wang et al., 2006)	(Pradhan & Reddy, 2011)	Present	(Wang et al., 2006)	(Pradhan & Reddy, 2011)	Present	(Wang et al., 2006)	(Pradhan & Reddy, 2011)	Present
10	19.379	19.379	19.37895	13.8939	13.8939	13.89386	10.828	10.828	10.8288
12	13.458	13.458	13.45760	10.652	10.652	10.56197	8.6917	8.6917	8.69178
14	9.877	9.877	9.88721	8.2296	8.2296	8.22960	7.0479	7.0479	7.04799
16	7.4699	7.4699	7.56990	6.5585	6.5585	6.55849	5.7854	5.7854	5.78550
18	5.9811	5.9811	5.98115	5.3375	5.3375	5.33153	4.8091	4.8091	4.80918
20	4.8447	4.8447	4.84473	4.4095	4.4095	4.40953	4.046	4.046	4.04607

Table 4. For a CF beam.

	P_{Cr} (nN)								
	μ=0 nm^2			μ=1 nm^2			μ=2 nm^2		
L (nm)	(Wang et al., 2006)	(Pradhan & Reddy, 2011)	Present	(Wang et al., 2006)	(Pradhan & Reddy, 2011)	Present	(Wang et al., 2006)	(Pradhan & Reddy, 2011)	Present
10	1.2112	1.2112	1.21118	1.1820	1.1820	1.18201	1.1542	1.1542	1.15422
12	0.8411	0.8411	0.84109	0.8269	0.8269	0.82693	0.8132	0.8132	0.81323
14	0.6179	0.6179	0.61795	0.6103	0.6103	0.61026	0.6027	0.6027	0.60277
16	0.4731	0.4731	0.47311	0.4686	0.4686	0.46860	0.4641	0.4641	0.46417
18	0.3738	0.3738	0.37382	0.3710	0.3710	0.37099	0.3682	0.3682	0.36821
20	0.3028	0.3028	0.30279	0.3009	0.3009	0.30094	0.2991	0.2991	0.29910

5 Discussion and results

After the preliminary comparison, the nonlinear buckling and post-buckling behaviors of a CFMN comprising FM in a parametric study based on some examples are calculated. It is well-established that a CFMN structure gives perceptibly FM effect in a nanosize (Sidhardh & Ray, 2018, Zhang, Zhang & Chen, 2019, Malikan & Eremeyev, 2020a, b). Accordingly, the properties of CFMNs in the framework of magnetic and mechanics are available as (Pan et al. 2003, Pan et al., 2005, Senthil et al., 2018)

Table 5. Magneto-mechanical properties for CFMN beam-like nanosize sensors.

$CoFe_2O_4$
C_{11}=286e9 N/m^2
f_{31}=10^{-9} N/Ampere
q_{31}=580.3 N/Ampere.m
a_{33}=1.57×10^{-4} N/Ampere^2

5.1 Size-dependent effects

Due to the existence of two variable parameters in NSGT, their exact amounts are momentous. However, with regard to the literature (Ansari et al., 2010, Akbarzadeh Khorshidi, 2018), their values are dependent on several cases and there cannot be a constant value for each one in association with every nanomaterial.

Figures 4 and 5 focus on the effect of size-dependent parameters on the buckling and post-buckling behaviors of the nanobeam. In the first figure, by assuming the nonlocal parameter to be constant, we evaluate the changes in the strain gradient parameter. All four cases of boundary conditions mentioned before are presented in these figures. It is important to note that the buckling's results obtained linearly are represented by the index (L) and the post-buckling results obtained by nonlinear analysis are displayed by the index (NL). This is true for all diagrams. Moreover, CBL in all diagrams means critical load whether from buckling or post-buckling. The first point that we get to a superficial look at Figure 4 is that the strain gradient parameter has the greatest impact on the beam with the boundary condition of the two sides completely clamped. Interestingly, this effect decreases with an increase in the degree of freedom of border conditions. If we pay attention to Figure 4, this result is quite clear in the behavior of the curves. Thus, the changes in the strain gradient parameter, for example, have completely differentiated the slope of the beam's results with the fully fixed boundary conditions. Another important point that can be obtained by looking more closely at this figure is that by increasing the values of the strain gradient parameter, the buckling and post-buckling results of each boundary condition are converging. This theorem can be interpreted as meaning that at very large values of the strain gradient parameter, the distance between the occurrence of buckling and the failure of the material will be smaller. Therefore, large values of this parameter indicate faster failure of the material. On the other hand, with a brief overview of

Figure 5, other points can be extracted. In this figure, in contrast to Figure 4, we assume the strain gradient parameter is constant and examine the changes in the nonlocal parameter. It is quite clear from Figure 5 that increasing the values of the nonlocal parameter decreases the results. However, this decreasing trend in the results of buckling analysis is more regular and with a certain harmony. Also, the severity in the decrease of the results, which is as a result of increasing the nonlocal parameter, in the buckling results is more than the post-buckling ones. In a point of fact, it can be said that the effect of the nonlocal parameter decreases after buckling. Another interesting result is that with increasing the nonlocal parameter, the distance between the curves related to the buckling and post-buckling results increases. Therefore, it can be stated that if the value of the nonlocal parameter is large, it indicates that the material fails later after buckling. As a final point obtained from Figures 4 and 5, it can be stated that the cantilever beam behind the buckle will be extremely weak compared to the other cases. This result can be understood by comparing the difference between the curves of the cantilever beam in the two states of buckling and post-buckling with other boundary conditions.

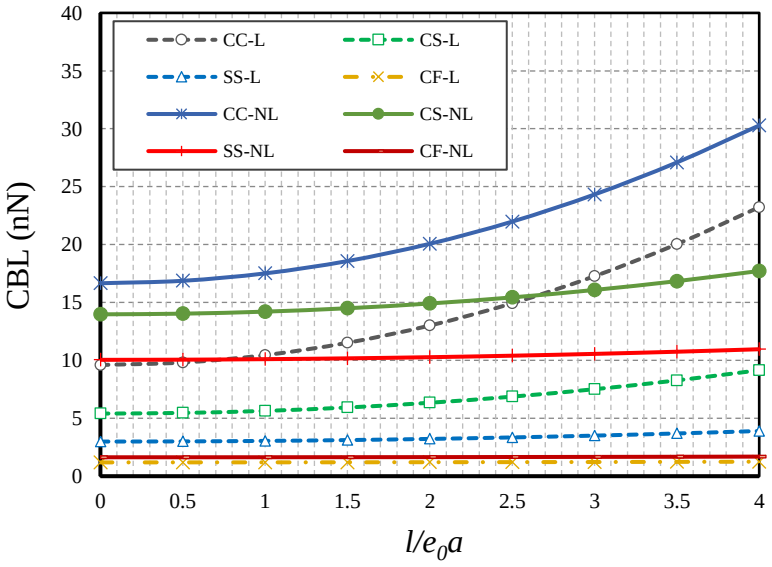

Fig. 4. Size-dependent parameters vs. CBL for different cases of BCs (Ψ=1 mA, e_0a=0.5 nm, L=10h)

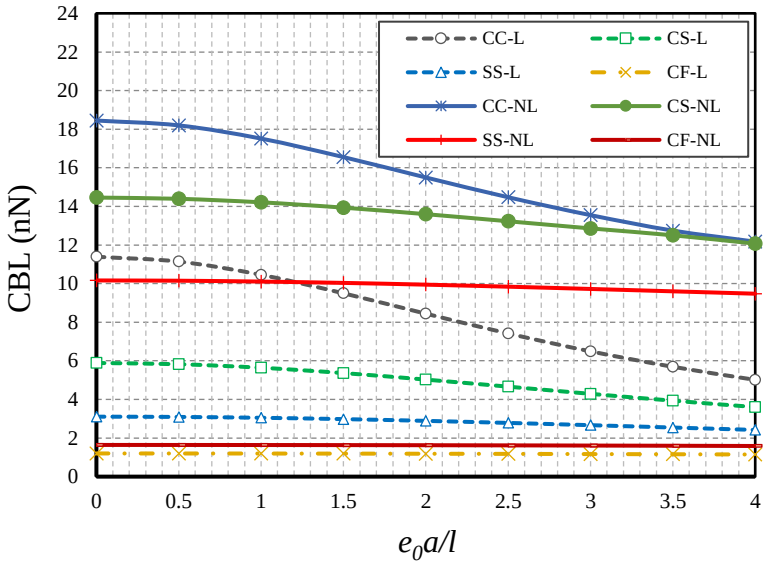

Fig. 5. Size-dependent parameters vs. CBL for different cases of BCs (Ψ=1 mA, l=0.5 nm, L=10h)

5.2 Magnetic field effect

Assuming that a magnetic field surrounds the sensor, changes, and increases or even decreases the magnitude of the magnetic potential can be very important and have a significant impact on the mechanical behavior of the sensor. Hence, we would like to examine this effect with the help of Figure 6. The magnitude of the magnetic potential is considered from negative 2 to positive 2 to include both positive and negative external fields. First, it is interesting to know that increasing the numerical value of the external potential leads to an increase in the stiffness of the material and ultimately its greater stability. As can be seen from the curves, the increasing slope of the results is linear. In addition, the distances between the post-buckling results' curves are longer than the buckling-related curves. This means that the boundary condition becomes more important in the post-buckling mode. On the other hand, the cantilever beam goes into buckling and post-buckling in negative values of external potential with a tensile axial force,

which of course other cases will experience, but later than the cantilever beam with a larger negative potential.

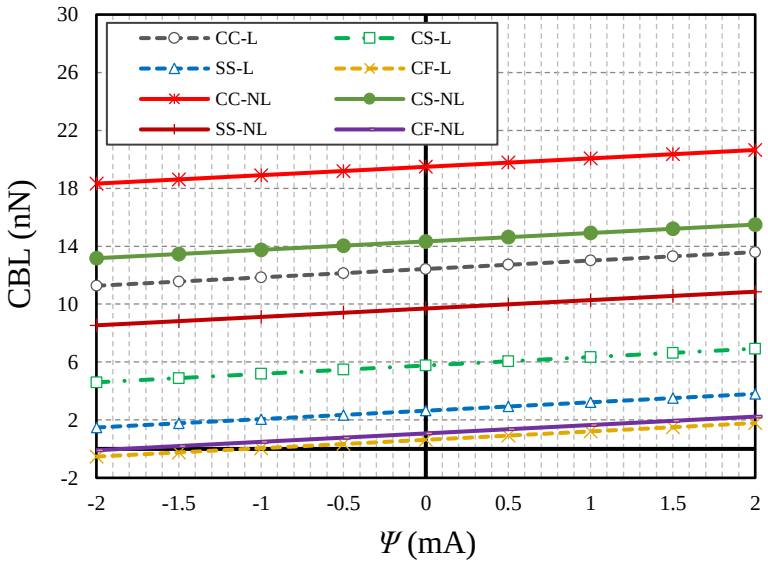

Fig. 6. Magnetic potential vs. CBL for different cases of BCs (l=1 nm, e_0a=0.5 nm, L=10h)

5.3 Slenderness ratio effect

The amount of narrowing of structures in buckling has always been a vital issue in their design. The ratio of length to thickness (slenderness ratio) in the design of beams and plates is a serious parameter for their stability. We will evaluate this for the nanosensor under study using Figures 7 and 8. Figure 7 is plotted for the two boundary conditions CC and SS and Figure 8 is drawn for the two boundary conditions CS and CF. As can be seen from both figures, with increasing the slenderness coefficient of the beam, the results of buckling and post-buckling tend to each other. This means that in beams with long lengths and small thicknesses, the post-buckling state and failure occur in a very short time after buckling. It can even be said that in very long beams, buckling and post-buckling occur together. But if the slenderness coefficient of the beam is low, and it is better to say that if the length of the beam is not long, the material will fail after bifurcation buckling after a certain time, and this is better for the structure. Therefore,

in beam-like sensors with long lengths, designers should think of measures to prevent material failure with the occurrence of buckling.

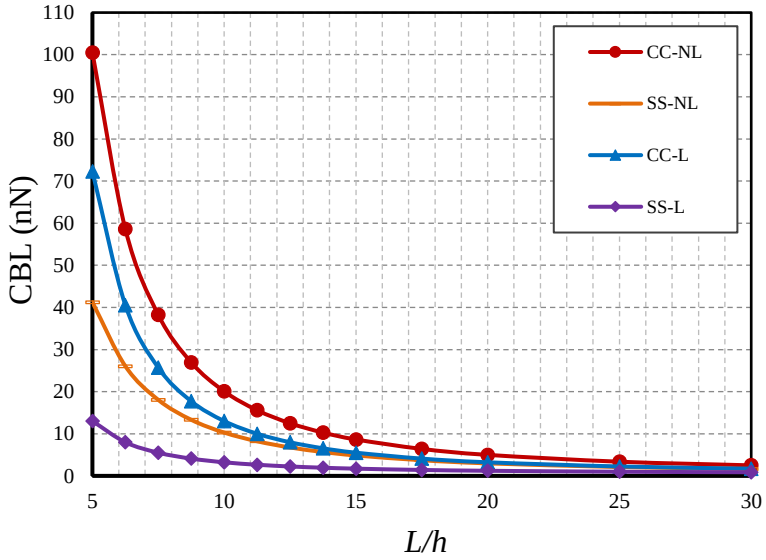

Fig. 7. Slenderness ratio vs. CBL for different BCs (Ψ=1 mA, e_0a=0.5 nm, l=1 nm)

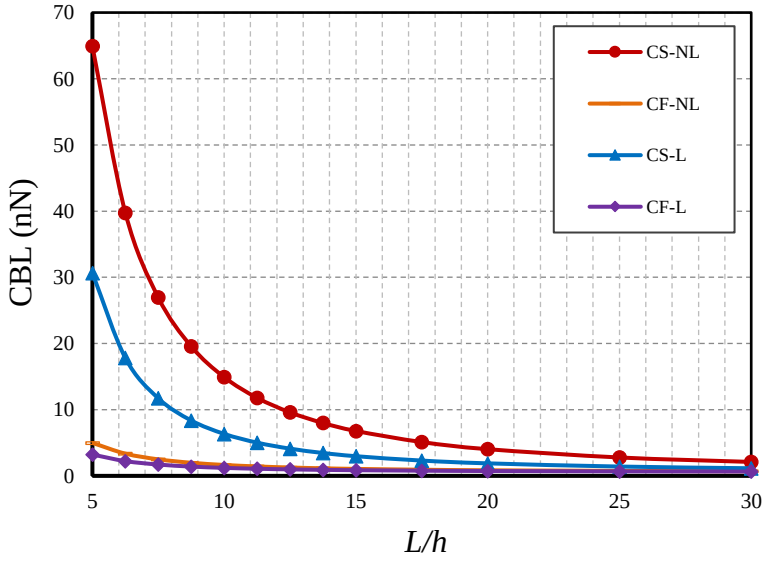

Fig. 8. Slenderness ratio vs. CBL for different BCs (Ψ=1 mA, e_0a=0.5 nm, l=1 nm)

5.4 Flexomagneticity (FM) effect

The study of the effect of FM in post-buckling conditions is the main goal of this research. For this purpose, Figures 9 to 12 are drawn. In Figure 9 and the horizontal axis of the diagram, we examine the changes in the nonlocal parameter while the beam is embedded in the two boundary conditions CC and SS. The beam is modeled in two modes without FM effect (PM sensor) and considering this effect (PFM sensor). The same factors, however, are presented for the two boundary conditions CF and CS in Figure 10. Figures 11 and 12 are similar to Figures 9 and 10, but with the difference that the horizontal axis of the diagrams shows the changes in magnetic potential. At the first glance, it can be seen that the flexomagnetic effect is noticeable when the boundary conditions are fully fixed in at least one of the two ends of the beam. It can be seen from the figures that in the CC and CS boundary conditions, the greatest effect can be obtained from the FM influence. On the other hand, the results of buckling and post-buckling load in PFM mode are larger, which indicates that the FM effect in the positive magnetic field leads to greater stability of the material.

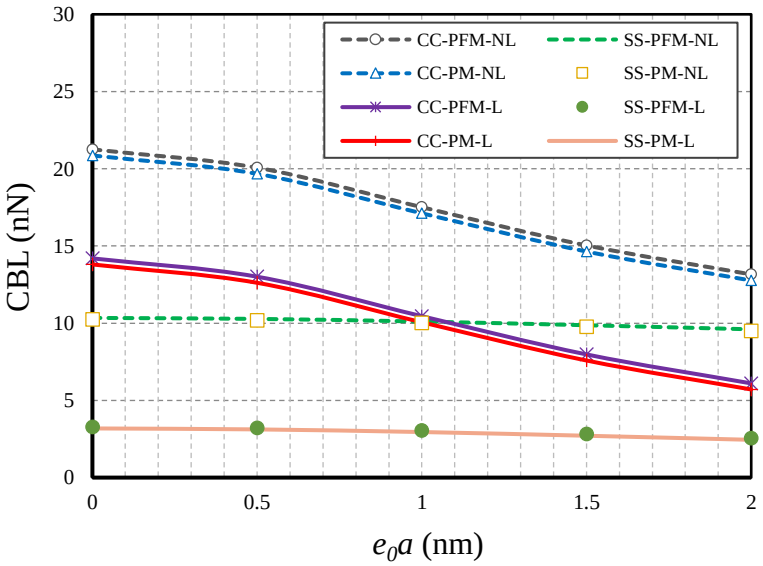

Fig. 9. Nonlocal parameter vs. CBL for different cases of BCs (Ψ=1 mA, l=0.5 nm, L=10h)

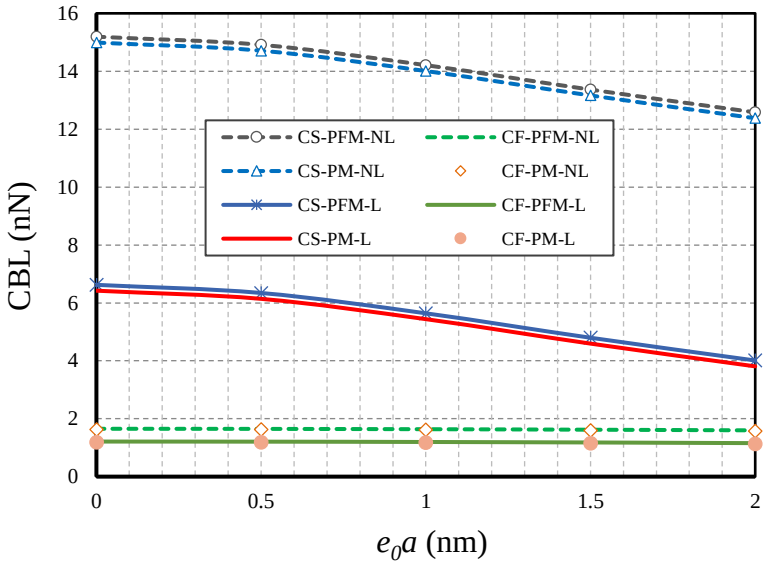

Fig. 10. Nonlocal parameter vs. CBL for different cases of BCs (Ψ=1 mA, l=0.5 nm, L=10h)

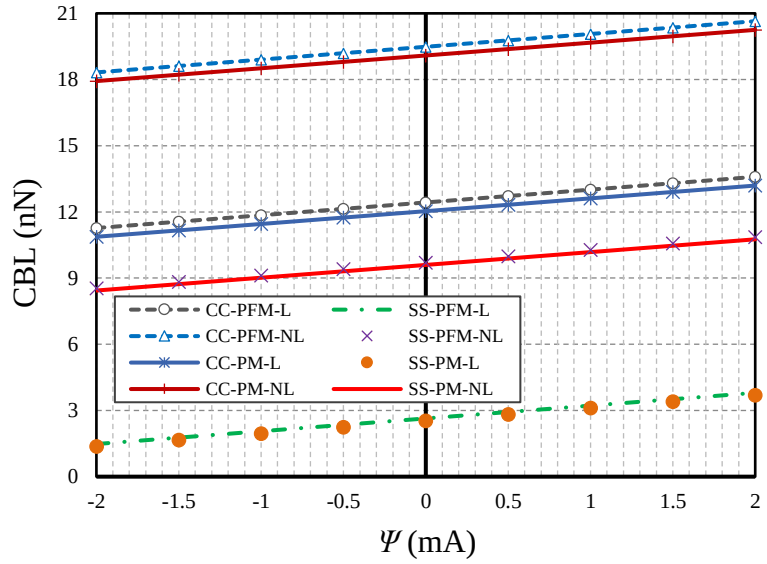

Fig. 11. Magnetic potential vs. CBL for different cases of BCs (l=1 nm, e_0a=0.5 nm, L=10h)

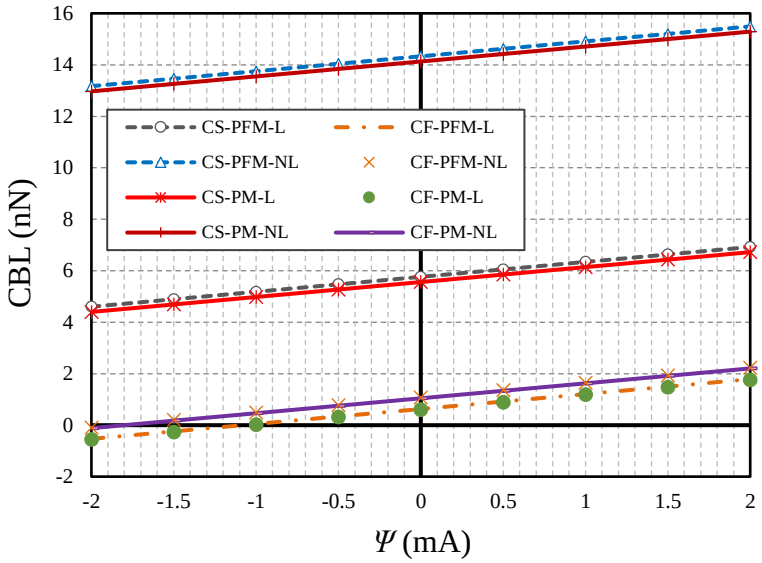

Fig. 12. Magnetic potential vs. CBL for different cases of BCs (l=1 nm, e_0a=0.5 nm, L=10h)

6 Conclusions

Both bifurcation buckling and post-buckling phenomena for cobalt-ferrite magnetic nanostructures (CFMNs) were discussed in this paper while the magnetic nanoparticle (MNP) accommodated flexomagneticity (FM) influence. The mathematical model was derived according to the Euler-Bernoulli beam, nonlinear Lagrangian-von Kármán strains and nonlocal approach of strain gradient elasticity (NSGT). The buckling and post-buckling were analytically studied for changes in size-dependent parameters, slenderness ratio, magnetic field in the presence and absence of the FM when the ends conditions of the beam-like nanosensor were differed. This research work concluded that:

- The post-buckling and failure resulted from it, would happen sooner for nanostructures whilst the values of strain gradient and the nonlocal parameters are respectively very large and negligible.

- In post-buckling, both small scale parameters affect remarkably results of boundary conditions with lower degrees of freedom.
- In so-called lengthy sensors, critical buckling and post-buckling loads can occur simultaneously. This means, exactly at the time of critical buckling the structure will fail.
- The boundary condition with lower degrees of freedom makes the flexomagnetic effect more pronounced.

Acknowledgements

V.A.E. and N.S.U. acknowledge the support by grant 14.Z50.31.0036 awarded to R. E. Alekseev Nizhny Novgorod Technical University by Department of Education and Science of the Russian Federation.

References

Agrawal, S., Paknikar, K., & Bodas, D. (2014). Development of immunosensor using magnetic nanoparticles and circular microchannels in PDMS. *Microelectronic Engineering*, *115*, 66-69.

Akbarzadeh Khorshidi, M. (2018). The material length scale parameter used in couple stress theories is not a material constant. *International Journal of Engineering Science*, *133*, 15-25.

Amabili, M. (2008). Nonlinear vibrations and stability of shells and plates. Cambridge University Press.

Ansari, R., Sahmani, S., & Arash, B. (2010). Nonlocal plate model for free vibrations of single-layered graphene sheets. *Physics Letters A*, *375*, 53-62.

Arvand, M., & Hassannezhad, M. (2014). Magnetic core–shell Fe_3O_4@SiO_2/MWCNT nanocomposite modified carbon paste electrode for amplified electrochemical sensing of uric acid. *Materials Science and Engineering*: *C*, *36*, 160-167.

Barretta, R., Čanađija, M., de Sciarra, F.M. (2020). On thermomechanics of multilayered beams. *International Journal of Engineering Science*, 155, 103364.

Barretta, R., de Sciarra, F.M. (2019) Variational nonlocal gradient elasticity for nano-beams. *International Journal of Engineering Science*, 143,.73-91.

Basutkar, R., (2019). Analytical modelling of a nanoscale series-connected bimorph piezoelectric energy harvester incorporating the flexoelectric effect. *International Journal of Engineering Science*, 139,.42-61.

Broderick, H.C., Righi, M., Destrade, M., Ogden, R.W. (2020). Stability analysis of charge-controlled soft dielectric plates. *International Journal of Engineering Science*, 151, 103280

Ebrahimi, F., Dabbagh, A., Tornabene, F., & Civalek, O. (2019). Hygro-thermal effects on wave dispersion responses of magnetostrictive sandwich nanoplates. *Advanced Nano Research, 7*, 157-167.

Eliseev, E. A., Morozovska, A. N., Glinchuk, M. D., & Blinc, R. (2009). Spontaneous flexoelectric/flexomagnetic effect in nanoferroics. *Physical Review B, 79*, 165433.

Eliseev, E. A., Morozovska, A. N., Khist, V. V., & Polinger, V. (2019). effective flexoelectric and flexomagnetic response of ferroics, In Recent Advances in Topological Ferroics and their Dynamics, Solid State Physics; Stamps, R. L., Schultheis, H.; Elsevier, Netherlands, *70*, 237-289.

Eltaher, M. A., Mohamed, N., Mohamed, S., & Seddek, L. F. (2019). Postbuckling of Curved Carbon Nanotubes Using Energy Equivalent Model. *Journal of Nano Research, 57*, 136-157.

Eremeyev, V.A., Ganghoffer, J.F., Konopińska-Zmysłowska, V., Uglov, N.S. (2020). Flexoelectricity and apparent piezoelectricity of a pantographic micro-bar. *International Journal of Engineering Science*, 149, 103213.

Espinosa-Almeyda, Y., Camacho-Montes, H., Otero, J.A., Rodríguez-Ramos, R., López-Realpozo, J.C., Guinovart-Díaz, R. and Sabina, F.J. (2020) Interphase effect on the effective magneto-electro-elastic properties for three-phase fiber-reinforced composites by a semi-analytical approach. *International Journal of Engineering Science*, 154, 103310.

Eyvazian, A., Shahsavari, D., & Karami, B. (2020). On the dynamic of graphene reinforced nanocomposite cylindrical shells subjected to a moving harmonic load. *International Journal of Engineering Science*, *154*, Article 103339.

Fahrner, W. (2005). Nanotechnology and Nanoelectronics. 1st ed.; Springer, Germany, 269.

Falzon, B. G., & Aliabadi, M. H. (2008). Buckling and Postbuckling Structures: Experimental, Analytical and Numerical Studies. Imperial College London, UK.

Freitas, P. P., Ferreira, R., Cardoso, S., & Cardoso, F. (2007). Magnetoresistive sensors. *Journal of Physics: Condensed Matter*, *19*, 165221.

Ghayesh, M.H., Farajpour, A. (2019). A review on the mechanics of functionally graded nanoscale and microscale structures. *International Journal of Engineering Science*, 137, 8-36.

Ghayesh, M.H., Farokhi, H. (2020) Nonlinear broadband performance of energy harvesters. *International Journal of Engineering Science*, 147, 103202

Gunda, J. B. (2014). Thermal post-buckling & large amplitude free vibration analysis of Timoshenko beams: Simple closed-form solutions. Applied Mathematical Modelling, 38, 4548–4558.

Hamed, M.A., Mohamed, N.A. & Eltaher, M.A. (2020). Stability buckling and bending of nanobeams including cutouts. *Engineering with Computers*, https://doi.org/10.1007/s00366-020-01063-2

Jalaei, M.H., Civalek, Ö. (2019). On dynamic instability of magnetically embedded viscoelastic porous FG nanobeam. *International Journal of Engineering Science*, 143, 14-32.

Ju, Y.-W., Park, J.-H., Jung, H.-R., Cho, S.-J., & Lee, W.-J. (2008). Fabrication and characterization of cobalt ferrite ($CoFe_2O_4$) nanofibers by electrospinning. *Materials Science and Engineering: B*, *147*, 7-12.

Justino, C. I. L., Rocha-Santos, T. A., Duarte, A. C., & Rocha-Santos, T. A. (2010). Review of analytical figures of merit of sensors and biosensors in clinical applications. *TrAC Trends*

in Analytical Chemistry, *29*, 1172-1183.

Kabychenkov, A. F., & Lisovskii, F. V. (2019). Flexomagnetic and flexoantiferromagnetic effects in centrosymmetric antiferromagnetic materials. *Technical Physics*, *64*, 980-983.

Karami, B., & Janghorban, M. (2019). On the dynamics of porous nanotubes with variable material properties and variable thickness. *International Journal of Engineering Science*, *136*, 53-66.

Karami, B., & Janghorban, M. (2020). On the mechanics of functionally graded nanoshells. *International Journal of Engineering Science*, *153*, Article 103309.

Karami, B., Janghorban, M., & Rabczuk, T. (2020). Dynamics of two-dimensional functionally graded tapered Timoshenko nanobeam in thermal environment using nonlocal strain gradient theory. *Composites Part B-Engineering*, *182*, 107622.

Li, L., Hu, Y. (2017). Post-buckling analysis of functionally graded nanobeams incorporating nonlocal stress and microstructure-dependent strain gradient effects. *International Journal of Mechanical Sciences*, *120*, 159-170.

Lim, C. W., Zhang, G., & Reddy, J. N. (2015). A Higher-order nonlocal elasticity and strain gradient theory and Its Applications in wave propagation. *Journal of the Mechanics and Physics of Solids*, *78*, 298-313.

Lukashev, P., & Sabirianov, R. F. (2010). Flexomagnetic effect in frustrated triangular magnetic structures. *Physical Review B*, *82*, 094417.

Moosavi, S., Zakaria, S., Chia, C. H., Gan, S., Azahari, N. A., & Kaco, H. (2017). Hydrothermal synthesis, magnetic properties and characterization of $CoFe_2O_4$ nanocrystals. *Ceramics International*, *43*, 7889-7894

Malikan, M., & Eremeyev, V. A. (2020a). Free Vibration of Flexomagnetic Nanostructured Tubes Based on Stress-driven Nonlocal Elasticity. In Analysis of Shells, Plates, and Beams, 1st ed.; Springer Nature, Switzerland, *134*, 215-226.

Malikan, M., & Eremeyev, V. A. (2020b). On the geometrically nonlinear vibration of a piezo-

flexomagnetic nanotube. *Mathematical Methods in the Applied Sciences*, https://doi.org/10.1002/mma.6758

Malikan, M., & Eremeyev, V. A. (2020c). On the dynamics of a visco-piezo-flexoelectric nanobeam. *Symmetry*, *12*, 643. doi: 10.3390/sym12040643

Malikan, M., & Eremeyev, V. A. (2020d). Post-critical buckling of truncated conical carbon nanotubes considering surface effects embedding in a nonlinear Winkler substrate using the Rayleigh-Ritz method. *Materials Research Express*, *7*, 025005.

Malikan, M., & Eremeyev, V. A. (2020e). A new hyperbolic-polynomial higher-order elasticity theory for mechanics of thick FGM beams with imperfection in the material composition. *Composite Structures*, *249*, 112486.

Malikan, M., Dimitri, R., & Tornabene, F. (2019). Transient response of oscillated carbon nanotubes with an internal and external damping. *Composites Part B-Engineering*, *158*, 198-205.

Malikan, M., Krasheninnikov, M., & Eremeyev, V. A. (2020). Torsional stability capacity of a nano-composite shell based on a nonlocal strain gradient shell model under a three-dimensional magnetic field. *International Journal of Engineering Science*, *148*, Article 103210.

Malikan, M., Nguyen, V. B., & Tornabene, F. (2018). Damped forced vibration analysis of single-walled carbon nanotubes resting on viscoelastic foundation in thermal environment using nonlocal strain gradient theory. *Engineering Science and Technology, an International Journal*, *21*, 778-786.

Mawassy, N., Reda, H., Ganghoffer, J.-F., Eremeyev, V.A., Lakiss, H. (2020). A variational approach of homogenization of piezoelectric composites towards piezoelectric and flexoelectric effective media. *International Journal of Engineering Science* (submitted)

Pereira, C., Pereira, A. M., Fernandes, C., Rocha, M., Mendes, R., Fernández-García, M. P., Guedes, A., Tavares, P. B., Grenèche, J.-M., Araújo, J. P., & Freire, C. (2012). Superparamagnetic MFe_2O_4 (M = Fe, Co, Mn) Nanoparticles: Tuning the Particle Size and

Magnetic Properties through a Novel One-Step Coprecipitation Route. *Chemistry of Materials, 24*, 1496-1504.

Pan, E., & Han, F. (2005). Exact solution for functionally graded and layered magneto-electro-elastic plates. *International Journal of Engineering Science, 43*, 321-339.

Pan, E., & Heyliger, P. R. (2003). Exact solutions for magneto-electro-elastic laminates in cylindrical bending. *International Journal of Solids and Structures, 40*, 6859-6876.

Pradhan, S. C., & Reddy, G. K. (2011). Buckling analysis of single walled carbon nanotube on Winkler foundation using nonlocal elasticity theory and DTM. *Computational Materials Science, 50*, 1052-1056.

Reddy, J. N. (2010). Nonlocal nonlinear formulations for bending of classical and shear deformation theories of beams and plates. *International Journal of Engineering Science, 48*, 1507-1518.

Reddy, L. H., Arias, J. L., Nicolas, J., & Couvreur, P. (2012). Magnetic Nanoparticles: Design and Characterization, Toxicity and Biocompatibility, Pharmaceutical and Biomedical Applications. *Chemistry of Materials, 112*, 5818-5878.

Sahmani, S., & Safaei, B. (2019). Nonlinear free vibrations of bi-directional functionally graded micro/nano-beams including nonlocal stress and microstructural strain gradient size effects. *Thin-Walled Structures, 140*, 342-356.

Senthil, V. P., Gajendiran, J., Gokul Raj, S., Shanmugavel, T., Ramesh Kumar, G., & Parthasaradhi Reddy, C. (2018). Study of structural and magnetic properties of cobalt ferrite (CoFe2O4) nanostructures. *Chemical Physics Letters, 695*, 19-23.

Sidhardh, S., & Ray, M. C. (2018). Flexomagnetic response of nanostructures. *Journal of Applied Physics, 124*, 244101.

Song, X., & Li, S.-R. (2007). Thermal buckling and post-buckling of pinned–fixed Euler–Bernoulli beams on an elastic foundation. *Mechanics Research Communications, 34*, 164–171.

Stevens, K. A., Ricci, R., Davies, G. A. O. (1995). Buckling and postbuckling of composite structures. *Composites*, *26*, 189-199.

Theres Baby, T., & Ramaprabhu, S. (2010). SiO_2 coated Fe_3O_4 magnetic nanoparticle dispersed multiwalled carbon nanotubes based amperometric glucose biosensor. *Talanta*, *80*, 2016-2022.

Timoshenko, S. P., & Gere, J. M. (1989). Theory of elastic stability. 2nd edition. Mineola: Dover.

Wang, C. M., Zhang, Y. Y., Sudha Ramesh, S., & Kitipornchai, S. (2006). Buckling analysis of micro- and nano-rods/tubes based on nonlocal Timoshenko beam theory. *Journal of Physics D: Applied Physics*, *39*, 3904.

Xu, Y., & Wang, E. (2012). Electrochemical biosensors based on magnetic micro/nano particles. *Electrochimica Acta*, *84*, 62-73.

Xin, Y., Fu-bing, X., Hong-wei, L., Feng, W., Di-zhao, C., Zhao-yang, W. (2013). A novel H_2O_2 biosensor based on Fe_3O_4–Au magnetic nanoparticles coated horseradish peroxidase and graphene sheets–Nafion film modified screen-printed carbon electrode. *Electrochimica Acta*, *109*, 750-755.

Zhang, J. X., Zeches, R. J., He, Q., Chu, Y. H., & Ramesh, R. (2012). Nanoscale phase boundaries: a new twist to novel functionalities. *Nanoscale*, *4*, 6196-6204.

Zhang, N., Zheng, Sh., & Chen, D. (2019). Size-dependent static bending of flexomagnetic nanobeams. *Journal of Applied Physics*, *126*, 223901.

Zhou, H., Pei, Y., & Fang, D. (2014). Magnetic field tunable small-scale mechanical properties of nickel single crystals measured by nanoindentation technique. *Scientific Reports*, *4*, 1-6.

symmetry

MDPI

Article

Effect of Axial Porosities on Flexomagnetic Response of In-Plane Compressed Piezomagnetic Nanobeams

Mohammad Malikan [1], Victor A. Eremeyev [1,2,3] and Krzysztof Kamil Żur [4,*]

[1] Department of Mechanics of Materials and Structures, Faculty of Civil and Environmental Engineering, Gdansk University of Technology, 80-233 Gdansk, Poland; mohammad.malikan@pg.edu.pl (M.M.); victor.eremeev@pg.edu.pl (V.A.E.)

[2] Laboratory of Mechanics of Biomaterials, Research and Education Center "Materials", Don State Technical University, Gagarina sq. 1, 344000 Rostov on Don, Russia

[3] Department of Civil and Environmental Engineering and Architecture (DICAAR), University of Cagliari, Via Marengo 2, 09123 Cagliari, Italy

[4] Faculty of Mechanical Engineering, Bialystok University of Technology, 15-351 Bialystok, Poland

* Correspondence: k.zur@pb.edu.pl

Received: 29 October 2020; Accepted: 23 November 2020; Published: 24 November 2020

Abstract: We investigated the stability of an axially loaded Euler–Bernoulli porous nanobeam considering the flexomagnetic material properties. The flexomagneticity relates to the magnetization with strain gradients. Here we assume both piezomagnetic and flexomagnetic phenomena are coupled simultaneously with elastic relations in an inverse magnetization. Similar to flexoelectricity, the flexomagneticity is a size-dependent property. Therefore, its effect is more pronounced at small scales. We merge the stability equation with a nonlocal model of the strain gradient elasticity. The Navier sinusoidal transverse deflection is employed to attain the critical buckling load. Furthermore, different types of axial symmetric and asymmetric porosity distributions are studied. It was revealed that regardless of the high magnetic field, one can realize the flexomagnetic effect at a small scale. We demonstrate as well that for the larger thicknesses a difference between responses of piezomagnetic and piezo-flexomagnetic nanobeams would not be significant.

Keywords: flexomagneticity; stability analysis; Euler–Bernoulli beam; porous nanobeam

1. Introduction

Flexomagneticity arises through elastic strain gradient or magnetic field gradient during electric magnetization in the magneto-elastic coupling in smart structures and actuators [1–3]. Such an effect should be significant in nano electro-mechanical systems (NEMS) and other smart sensors and actuators. Similar to this influence, viz. flexoelectricity for centrosymmetric and non-centrosymmetric structures has been estimated widely [4–19]. However, the flexomagneticity effect has been less known. Although the structure and physics of a flexomagneticity phenomenon are very complicated, it has economic implications. Physically, it may be difficult to interpret, but the basic idea satisfactorily shows the importance of flexomagneticity.

In discussing a mechanical response of nanomaterials with magneto-mechanical coupling, the importance of piezomagneticity has been profoundly evaluated by scholars in the contemporary decade [20–39]. However, fewer studies are available regarding flexomagneticity [40–45]. In the available literature, Sidhardh and Ray [40] worked on the bending response of a thin cantilever nanobeam with flexomagnetic property. They discussed both direct and reverse impacts of magneto-elastic coupling with the presence of the surface elasticity. Zhang et al. [41] conducted the importance

of flexomagneticity for a nanoscale size-dependent Euler-Bernoulli beam exposed to transverse static loading. To present the size-dependent mechanical behavior of the structure, they utilized the surface elasticity. Both direct and converse flexomagnetic influences were investigated when the nano-sized beam was kept in ends with fixed, pivot, and free edge conditions. One of their momentous achievements was the conclusion that the flexomagneticity is a scale-dependent property of materials. Recently, Malikan and Eremeyev [42] investigated vibrating nanobeams by taking into account the piezomagnetic, particularly flexomagnetic, properties. The free vibration frequencies were evaluated by linear assumptions of strain and the impact of size-dependency was inspected on the basis of a new nonlocal elasticity theory. The size-dependent behavior of the flexomagnetic effect was affirmed by their results. In another effort, Malikan and Eremeyev [43] explored the flexomagnetic response of a smart nanobeam in a vibrational condition based on large frequency modes. The small scale response of the nanoscale beam was searched by imposing a nonlocal strain gradient elasticity approach into the constitutive equations. Besides these, Malikan and Eremeyev [44] performed research on non-linear static bending of smart nanoscale beams while the material included a remarkable flexomagnetic response. The computational model was solved by coupling between an analytical and numerical solution method. The new finding demonstrated that the presence of the flexomagnetic feature leads to diminishing the deflections. More recently, Malikan et al. [45] examined post-buckling stability of a nanoparticle in which both flexomagnetic and piezomagnetic properties were included. The calculations extracted new findings that are helpful for magnetic nanosensors applications.

To the best of our knowledge, the flexomagnetic studies on the mechanical response of nanostructures referred to above represent the majority of cases in the literature, unless otherwise stated. In these references, the models are restricted to piezomagnetic nanobeams under some mechanical analyses. The present research attempts to demonstrate the flexomagnetic property for the stability problem of a nano-sized beam, while it includes a material imperfection with intentional nonlocality and size-dependent characteristics according to the nonlocal strain gradient constitutive equation. The structural and material imperfection is estimated in the framework of different types of porosities. The nonlocal influences that can affect the flexomagnetic response of the Euler–Bernoulli nanoscale beam are addressed in this paper. A sinusoidal transverse deflection is assumed when applying the Navier approach to beam flexure. Terminally, the nanobeam is considered for variations of key parameters based on the three cases, i.e., a simple nanobeam, piezomagnetic nanobeam, and piezo-flexomagnetic nanobeam.

2. Formulation of the Problem

2.1. Constitutive Relations for Piezo-Flexomagnetic Solids

Pursuing [1–3], we briefly introduce constitutive relations for flexomagnetic material. In the following, we assume infinitesimal deformations under isothermal conditions. Therefore, the variables are the displacements u and the magnetic field is H as below

$$u = u(x),\ H{=}H(x). \tag{1}$$

where x is a position vector, and H is a tensor of first-order. Within the flexomagneticity, the free energy density function U has the form

$$\begin{aligned} U = U(\varepsilon,\eta,H) = &-\frac{1}{2}H\cdot a\cdot H+\frac{1}{2}\varepsilon : C : \varepsilon+\frac{1}{2}\eta\vdots g\vdots\eta+\varepsilon : r\vdots\eta \\ &-H\cdot q : \varepsilon - H\cdot f\vdots\eta \end{aligned}. \tag{2}$$

where ε is the strain tensor and its gradient is

$$\varepsilon = \frac{1}{2}\left(\nabla u+\nabla u^{T}\right),\ \eta = \nabla\varepsilon\,. \tag{3}$$

where ∇ is the 3D nabla-operator in a general case. We introduced to Equation (2) several tensors of material parameters. q is the third-order piezomagnetic tensor, a is the second-order magnetic

permeability tensor, g is the sixth-order gradient elasticity tensor, C is the fourth-order elasticity coefficient tensor, f is the fourth-order flexomagnetic tensor, and the strain and strain-gradient tensors are coupled by r, which itself is a fifth-order tensor. Moreover, "·", ":", and "⋮" stand for scalar (inner) products in spaces of vectors, second-order and third-order tensors, respectively.

In the following, we express H through the magnetic potential ψ [40,41],

$$H = -\nabla\psi\,. \tag{4}$$

The governing equations of the static flexomagneticity can be derived using the virtual work principle as

$$\delta\Pi = \delta A. \tag{5}$$

in which $\Pi = \int_V U dV$, where V is the volume of domain that occupies the flexomagnetic solid and δA is the work of external loads.

For simplicity, we assume the simple form of

$$\delta A = \int_V F\cdot\delta u + \int_{\partial V} t\cdot\delta u ds\,. \tag{6}$$

where F and t are external mass forces and surface traction.

Using the standard calculus of variations from Equation (5) we get

$$\nabla\cdot\left(\sigma - \nabla\cdot\xi\right) + F = 0\,, \tag{7a}$$

$$\nabla\cdot B = 0. \tag{7b}$$

in which B is the magnetic induction vector. The following constitutive equations are introduced

$$\sigma = \frac{\partial U}{\partial\varepsilon} \equiv C:\varepsilon + r\vdots\eta - H\cdot q\,, \tag{8a}$$

$$\xi = \frac{\partial U}{\partial\eta} \equiv g:\eta + \varepsilon:r - H\cdot f\,, \tag{8b}$$

$$B = -\frac{\partial U}{\partial H} = a\cdot H + q:\varepsilon + f\vdots\eta\,. \tag{8c}$$

2.2. The Piezo-Flexomagnetic Beam Model

The piezo-flexomagnetic nanobeam studied in this research is exhibited in Figure 1. In the figure, length and height of the beam are denoted by L and h, respectively.

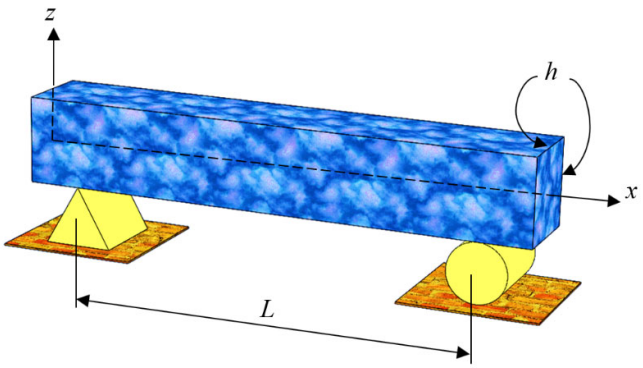

Figure 1. Geometry and description of a continuum nanobeam as a square actuator installed on simple end conditions.

The constitutive equations (Equation (8)) can be re-written for a beam incorporating the flexomagnetic property as [40,41]

$$\sigma_{xx} = C_{11}^{p}\varepsilon_{xx} - q_{31}H_z, \tag{9}$$

$$\xi_{xxz} = g_{31}\eta_{xxz} - f_{31}H_z, \tag{10}$$

$$B_z = a_{33}H_z + q_{31}\varepsilon_{xx} + f_{31}\eta_{xxz}. \tag{11}$$

in which η_{xxz} and ε_{xx} are the gradient of the axial elastic strain and the strain itself, $C_{11} = C_{1111}$ is the elastic modulus, σ_{xx} is the axial stress, $f_{31} = f_{3311}$ denotes the component of the fourth-order flexomagnetic coefficients tensor, a_{33} represents the component of the second-order magnetic permeability tensor, $q_{31} = q_{311}$ depicts the component of the third-order piezomagnetic tensor, ξ_{xxz} is the component of the higher-order hyper stress tensor and is an induction of coverse flexomagnetic effect, B_z and H_z exhibit the magnetic flux and the component of magnetic field, respectively, and $g_{31} = g_{311311}$ illustrates the influence of the sixth-order gradient elasticity tensor. It is worth mentioning that the piezomagnetic tensor would be non-zero for non-centrosymmetric ferroics only, but the flexomagnetic tensor would be non-zero for both centrosymmetric and non-centrosymmetric materials.

The displacement field with respect to the Euler–Bernoulli beam is available as [46–48]

$$\begin{aligned} u_1(x,z) &= u(x) - z\frac{dw(x)}{dx}, \\ u_3(x,z) &= w(x). \end{aligned} \tag{12}$$

where u_i (i = 1,3) represent the points' displacements in direction of x and z, u and w are the axial and transverse displacements of the mid-plan, respectively, see Figure 1. To show the thickness coordinate, the z parameter is used.

Due to the linear problem studied in this research, the linear Lagrangian strain can be employed as

$$\varepsilon_{ij} = \frac{1}{2}\left(\frac{\partial u_i}{\partial x_j} + \frac{\partial u_j}{\partial x_i}\right). \tag{13}$$

The components of the transverse strain and the strain gradient can be presented on the basis of substituting Equation (12) into Equation (13) as below

$$\begin{aligned} \varepsilon_{xx} &= \frac{du}{dx} - z\frac{d^2w}{dx^2}, \\ \eta_{xxz} &= \frac{d\varepsilon_{xx}}{dz} = -\frac{d^2w}{dx^2}, \\ \eta_{xxx} &= \frac{d\varepsilon_{xx}}{dx} = -z\frac{d^3w}{dx^3}. \end{aligned} \tag{14}$$

As the η_{xxx} is small compared to the η_{xxz}, it can be ignored. With respect to the Lagrange's principle, we have

$$\delta\int\left(\Pi_W + \Pi_U\right) = 0. \tag{15}$$

in which Π_W and Π_U depict the performed work by outer loads, and the total internal strain energy (magnetic potential energy and mechanical strain energy). The total strain energy by means of Equation (14) can be demonstrated as

$$\delta\Pi_U = \int_V\left(\sigma_{xx}\delta\varepsilon_{xx} + \xi_{xxz}\delta\eta_{xxz} - B_z\delta H_z\right)dV. \tag{16}$$

One can obtain the governing equation and non-classical boundary conditions as below

$$\delta\Pi_{U_1}^{Mech} = -\int_0^L \left(\frac{dN_x}{dx}\delta u + \frac{d^2M_x}{dx^2}\delta w + \frac{d^2T_{xxz}}{dx^2}\delta w \right) dx\,, \tag{17a}$$

$$\delta\Pi_{U_2}^{Mag} = -\int_0^L \int_{-h/2}^{h/2} \frac{dB_z}{dz}\delta\Psi dz dx\,, \tag{17b}$$

$$\delta\Pi_{U_1}^{Mech} = \left(N_x\delta u - M_x\frac{d\delta w}{dx} - T_{xxz}\frac{d\delta w}{dx} + \frac{dM_x}{dx}\delta w + \frac{dT_{xxz}}{dx}\delta w \right)\Big|_0^L\,, \tag{18a}$$

$$\delta\Pi_{U_2}^{Mag} = \int_0^L \left(B_z\delta\Psi \right)\Big|_{-h/2}^{h/2} dx\,. \tag{18b}$$

in which

$$N_x = \int_{-h/2}^{h/2} \sigma_{xx} dz\,, \tag{19}$$

$$M_x = \int_{-h/2}^{h/2} \sigma_{xx} z dz\,, \tag{20}$$

$$T_{xxz} = \int_{-h/2}^{h/2} \xi_{xxz} dz\,. \tag{21}$$

The performed work by external factors can be expressed as below [49,50]

$$\Pi_W = \frac{1}{2}\int_0^L N_x^0 \left(\frac{dw}{dx} \right)^2 dx\,. \tag{22}$$

Its first variational form is

$$\delta\Pi_W = \int_0^L N_x^0 \left(\frac{d\delta w}{dx}\frac{dw}{dx} \right) dx \tag{23}$$

in which N_x^0 shows the axial membrane load.

Hereafter, the magnetic field's transverse component can be expressed as

$$H_z + \frac{d\Psi}{dz} = 0\,. \tag{24}$$

Assuming the condition of a closed circuit as well as the inverse piezomagnetic effect, one gives the magnetic boundary conditions as

$$\Psi\left(+\frac{h}{2} \right) = \psi\,, \tag{25a}$$

$$\Psi\left(-\frac{h}{2} \right) = 0\,. \tag{25b}$$

where ψ determines the external magnetic potential applied to the upper surface of the beam. With mixing Equations (11), (17b), (18b), (24) and (25), one can derive the magnetic polarization and magnetic field as [40,41]

$$\Psi = -\frac{q_{31}}{2a_{33}}\left(z^2 - \frac{h^2}{4} \right)\frac{d^2w}{dx^2} + \frac{\psi}{h}\left(z + \frac{h}{2} \right), \tag{26}$$

$$H_z = z\frac{q_{31}}{a_{33}}\frac{d^2w}{dx^2} - \frac{\psi}{h}\,. \tag{27}$$

The nanoscale atomic interactions can be projected in a continuum space by means of the nonlocal strain gradient elasticity theory (NSGT) given as [51]

$$\left(1-\mu\frac{d^2}{dx^2}\right)\sigma_{xx}^{NL}=\left(1-l^2\frac{d^2}{dx^2}\right)\sigma_{xx}^{L}. \tag{28}$$

In order to allocate the influence of nonlocality, namely stiffness-softening, the nonlocal parameter μ (unit: square nanometers $=(nm)^2$) is employed. Note that $\mu(nm)^2=(e_0a)^2$, in which e_0 and a are two small scale factors that determine the nonlocal parameter. Furthermore, in order to set the effect of the size deduction, namely stiffness-hardening, the $l(nm)$ parameter is used, which is named as the strain gradient length scale parameter. It is to be noted that [52,53] confirmed the fact that the aforesaid small scale factors are not material constants and can be varied by respecting a variety of conditions. Additionally, the *NL* and *L* indexes respectively express the nonlocal and the local components of stress.

Thus, inserting Equations (26)–(28) into Equations (9)–(11), it is possible to present the stress field component, the higher-order moment stress tensor component, and magnetic induction component in the NSGT form as

$$\left(1-\mu\frac{d^2}{dx^2}\right)\sigma_{xx}=\left(1-l^2\frac{d^2}{dx^2}\right)\left[C_{11}^{p}\frac{du}{dx}-z\left(C_{11}^{p}+\frac{q_{31}^2}{a_{33}}\right)\frac{d^2w}{dx^2}+\frac{q_{31}\psi}{h}\right], \tag{29}$$

$$\left(1-\mu\frac{d^2}{dx^2}\right)\xi_{xxz}=\left(1-l^2\frac{d^2}{dx^2}\right)\left[-\left(g_{31}+\frac{q_{31}f_{31}z}{a_{33}}\right)\frac{d^2w}{dx^2}+\frac{f_{31}\psi}{h}\right], \tag{30}$$

$$\left(1-\mu\frac{d^2}{dx^2}\right)B_z=\left(1-l^2\frac{d^2}{dx^2}\right)\left(-f_{31}\frac{d^2w}{dx^2}-\frac{a_{33}\psi}{h}\right). \tag{31}$$

Hence, on the basis of Equations (29)–(31), Equations (19)–(21) can be expanded as [54–61]

$$\left(1-\mu\frac{d^2}{dx^2}\right)N_x=\left(1-l^2\frac{d^2}{dx^2}\right)\left(C_{11}^{p}h\frac{du}{dx}+q_{31}\psi\right), \tag{32}$$

$$\left(1-\mu\frac{d^2}{dx^2}\right)M_x=\left(1-l^2\frac{d^2}{dx^2}\right)\left(-I_z\left(C_{11}^{p}+\frac{q_{31}^2}{a_{33}}\right)\frac{d^2w}{dx^2}\right), \tag{33}$$

$$\left(1-\mu\frac{d^2}{dx^2}\right)T_{xxz}=\left(1-l^2\frac{d^2}{dx^2}\right)\left(-g_{31}h\frac{d^2w}{dx^2}+f_{31}\psi\right). \tag{34}$$

in which $I_z=\int_A z^2dA$ is the moment of inertia.

Due to inevitable variations in the manufacturing processes, the presence of some porosity in nanobeams is unavoidable. Inclusion of this imperfection into mechanical analysis of the piezomagnetic-flexomagnetic nano-sized beam is performed as [62]

$$C_{11}^{p}=C_{11}\left(\frac{1.21-\alpha\lambda(x)}{1.21}\right)^{2.3} \tag{35}$$

where α denotes the porosity coefficient. Axial porosities are defined mathematically and analytically in Table 1 [62].

Table 1. Axial porosity distribution patterns.

Porosity Type	$\lambda(x)$	Ranges of α
"O" type distribution	$\eta_1^2 \sin\left(\frac{\pi}{L}x\right)$	$0 \le \alpha < 0.344$
"$\overline{\text{O}}$" type distribution	$\eta_2^2\left[1-\sin\left(\frac{\pi}{L}x\right)\right]$	$0 \le \alpha < 0.112$
"X" type distribution	$\eta_1\eta_2 \sin\left(\frac{\pi}{L}x\right)$	$0 \le \alpha < 0.197$
"$\overline{\text{X}}$" type distribution	$\eta_1\eta_2\left[1-\sin\left(\frac{\pi}{L}x\right)\right]$	$0 \le \alpha < 0.197$
Uniform type distribution	1	$0 \le \alpha < 0.85$
$\eta_1 = \frac{\pi}{2},\ \eta_2 = \frac{\pi}{\pi-2}$		

On the basis of Equations (17a) and (23), and replacing into Equation (15), one can derive the local governing relations as below

$$\frac{dN_x}{dx} = 0\,, \tag{36}$$

$$\frac{d^2M_x}{dx^2} + \frac{d^2T_{xxz}}{dx^2} + N_x^0\frac{d^2w}{dx^2} = 0\,. \tag{37}$$

Equations (36) and (37) are decoupled and thus, Equation (37) gives the stability equation in order to have values of critical buckling loads.

Thus, we should transfer the local stability equation (Equation (37)) to a size-dependent relation. In so doing, inserting Equation (37) into Equation (33), one gets

$$M_x = -\mu\left(\frac{d^2T_{xxz}}{dx^2} + N_x^0\frac{d^2w}{dx^2}\right) - I_z\left(C_{11}^p + \frac{q_{31}^2}{a_{33}}\right)\left(1-l^2\frac{d^2}{dx^2}\right)\frac{d^2w}{dx^2}\,. \tag{38}$$

Then, Equation (37) can be re-derived by mixing Equation (38) and Equation (34) as follows

$$\left(1-\mu\frac{d^2}{dx^2}\right)\left(B\frac{d^4w}{dx^4} + N_x^0\frac{d^2w}{dx^2}\right) + D\left(1-l^2\frac{d^2}{dx^2}\right)\frac{d^4w}{dx^4} = 0\,. \tag{39}$$

in which $B = -g_{31}h$, and $D = -I_z\left(C_{11}^p + \frac{q_{31}^2}{a_{33}}\right)$.

Here, it is required to define the pre-buckling compression as membrane loads as

$$N_x^0 = N^{Mech} + N^{Mag}\,. \tag{40}$$

where N^{Mech} and N^{Mag} are the axial membrane magnetic and mechanical loads assumed as follows:

$$N^{Mech} = -P_{cr}\,, \tag{41a}$$

$$N^{Mag} = -q_{31}\psi\,. \tag{41b}$$

3. Solution of the Problem

Regarding the analytical closed-form solution, we apply the following transverse deflection equation

$$w(x) = \sum_{m=1}^{\infty} X_m(x) \quad . \tag{42}$$

in which X_m is an allowable function satisfying the boundary conditions of simply-simply supported (S-S) for two ends.

The dedicated kinematic and nonlocal strain gradient constitutive boundary conditions for the S-S nanobeam are expressed by Table 2 [63–66]

Table 2. Constitutive boundary conditions for S-S.

Nonlocal Strain Gradient Conditions at (0, *L*)	**Local Conditions ($l = \mu = 0$) at (0, *L*)**
$w = 0$	$w = 0$
$M_{nl} = \left(1 + l^2 \frac{d^2}{dx^2}\right) M_l + \mu \frac{d}{dx}\left(\frac{d^2 T_{xxz}}{dx^2} + N_x^0 \frac{d^2 w}{dx^2}\right) = 0$ *	$M_l = -D \frac{d^2 w}{dx^2} = 0$ *
$T_{xxz} = B \frac{d^2 w}{dx^2} + f_{31} \psi = 0$	$T_{xxz} = B \frac{d^2 w}{dx^2} + f_{31} \psi = 0$

* Sub-indexes (*nl* and *l*) are nonlocal and local phases, respectively.

The pointed conditions in Table 2 may be satisfied by the admissible function given below [57]

$$X_m(x) = \sin(\alpha_m x). \tag{43}$$

in which $\alpha_m = \frac{m\pi}{L}$.

Substituting Equation (42) into Equation (39), the closed-form size-dependent buckling relation for the piezo-flexomagnetic nanobeam becomes

$$P_{cr} = \int_0^L \frac{-\left(B\mu + l^2 D\right)\alpha_m^6 + \left(B - q_{31}\psi\mu + D\right)\alpha_m^4 + q_{31}\psi\alpha_m^2}{\mu\alpha_m^4 - \alpha_m^2} Y_m \, dx \, . \tag{44}$$

in which Y_m is a residue. It is important to bear in mind that all of the results of the present work are given for $m = 1$.

4. Numerical Results

4.1. Validation of Results

The literature survey clearly and obviously showed that the static bifurcation buckling of a piezo-flexomagnetic nanobeam has not been studied thus far. Therefore, the only path to validate correctness of the formulation is neglecting piezomagneticity, flexomagneticity, and the strain gradient model to compare the results with a nano-sized circular beam [67,68]. Both parts of the literature employed a classical beam, however, ref. [67] used the differential transform solution method and ref. [68] used an explicit solution method. As can be shown from Table 3, our results are entirely matched with the literature.

Table 3. Critical loads' validation with literature (E = 1 TPa, ν = 0.19, d = 1 nm).

L (nm)	P_{Cr} (nN)								
	μ = 0 nm²			μ = 1 nm²			μ = 4 nm²		
	[67]	[68]	Present	[67]	[68]	Present	[67]	[68]	Present
10	4.8447	4.8447	4.8447	4.4095	4.4095	4.4095	3.4735	3.4735	3.4735
12	3.3644	3.3644	3.3644	3.1486	3.1486	3.1486	2.6405	2.6405	2.6405
14	2.4718	2.4718	2.4718	2.3533	2.3533	2.3533	2.0574	2.0574	2.0574
16	1.8925	1.8925	1.8925	1.8222	1.8222	1.8222	1.6396	1.6396	1.6396
18	1.4953	1.4953	1.4953	1.4511	1.4511	1.4511	1.3329	1.3329	1.3329
20	1.2112	1.2112	1.2112	1.182	1.182	1.182	1.1024	1.1024	1.1024

4.2. Stability Analysis

Investigating the flexomagneticity effect on the stability of a nanostructure is the main goal of this work. Table 4 presents applied material properties [40,41]. To take a rational amount for the nonlocal parameter, 0.5 nm < e_0a < 0.8 nm [69], and 0 < e_0a ≤ 2 nm [70,71], are utilized.

Table 4. Material parameters of the piezo-flexomagnetic nanobeam.

$CoFe_2O_4$
C_{11} = 286 GPa
q_{31} = 580.3 N/A.m
a_{33} = 1.57 × 10^{-4} N/A^2
(A = Ampere)

Given Figure 2a, the nonlocal coefficient variations are plotted for four nanobeam states. That is, first, we have just the usual nanobeam by eliminating magnetic effects; the latter is a state where we merely have the piezomagnetic effect and finally the third and fourth states are when we have both the piezo- and flexomagnetic effects but with two different values of flexomagnetic property. As is clear from the figure, increasing the numerical value of the nonlocal parameter reduces the critical loads in all four states. Thereby, one of the important results of this graph is that when we consider a positive magnetic field and we have the piezomagnetic as well as flexomagnetic effect, the nanobeam has greater stability against the axial membrane forces. Furthermore, while purely having the piezomagnetic effect, the least stability is observed for the magneto-mechanical nanobeams. Further investigation is needed and is shown by the next figures. On the other hand, Figure 2b shows a comparison of both piezomagnetic and piezo-flexomagnetic nanoscale beams while the strain gradient parameter is the changeable factor of the horizontal axis of the figure. As it is clarified by Figure 2b, it is noteworthy to say that increasing the strain gradient parameter results in a decrease in difference between the results of the piezo-flexomagnetic nanobeam with the piezomagnetic nanobeam. It is worth underlining that this proximity pertains to the flexomagnetic feature. This means that the increase of the value of the length scale parameter leads to a stiffening effect; therefore, by increasing the values of this parameter, the critical load's results tend to each other in magnetic beams. It can be argued that the length scale parameter makes the flexomagnetic effect ineffective. Eventually, if the length scale parameter is a large numerical value, it can be stated that the flexomagnetic effect is nothing and all the magnetic nanobeams will respond similarly.

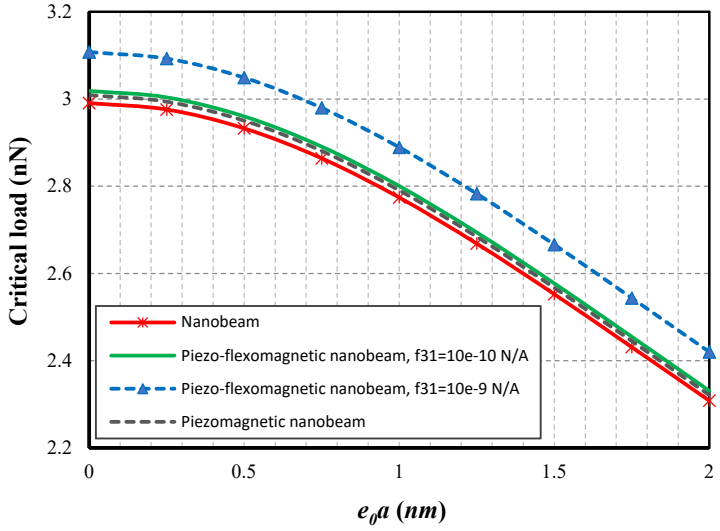

(**a**)

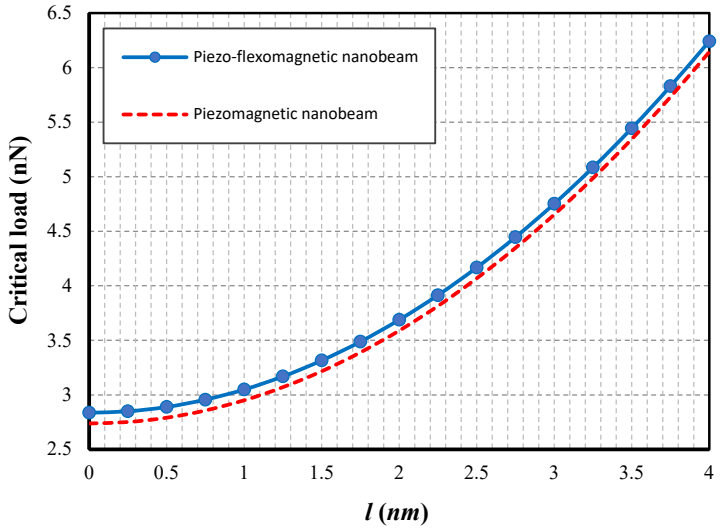

(**b**)

Figure 2. (**a**) Nonlocal parameter vs. four cases of non-porous nanobeams (l = 0.5 nm, L = 10 h, ψ = 1 mA). (**b**) The length scale strain gradient parameter vs. different cases of non-porous nanobeams (e_0a = 0.5 nm, L = 10 h, ψ = 1 mA).

In Figure 3, we investigate the effects of given patterns of the porosities for two cases of the nano-sized magnetic beam, the first one with the flexomagnetic property (PFM) and the later one ignoring this physical feature. We observed in the previous figure that in attending the positive magnetic field, if the piezomagnetic nanobeam has a flexomagnetic property (piezo-flexomagnetic), it is the most stable case in terms of magneto-mechanical nanobeams. It can now be seen from this figure that for all PFM cases, the further in-plane resistance can be observed. Hence, one can prove that this effect makes material stiffer. Furthermore, increase of the value of the porosity parameter (α) leads to reduction of material stability in all cases. However, this decline is more noticeable for $\overline{\mathrm{X}}$ and $\overline{\mathrm{O}}$ porosities and insignificant for O and X samples. It is also notable that in terms of $\overline{\mathrm{X}}$ and $\overline{\mathrm{O}}$ porosity types, an increase of value of the porosity parameter leads to more gaps between PFM and PM. This means that these kinds of porosities make the flexomagnetic property more important.

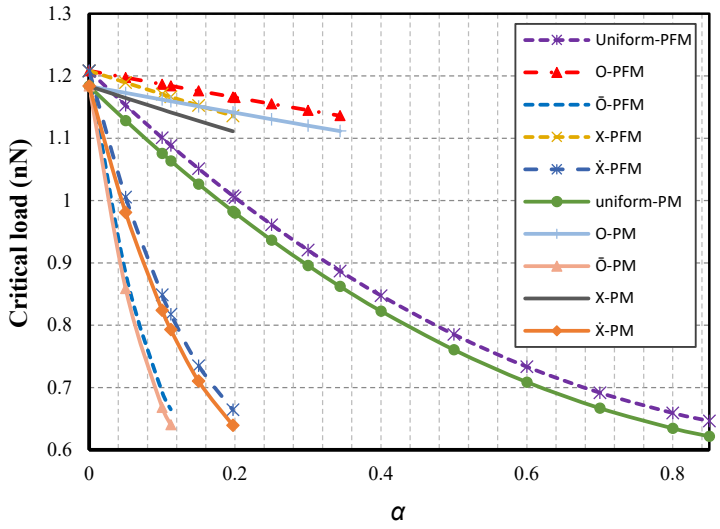

Figure 3. Types of porosity vs. two cases of nanobeams (e_0a = 0.5 nm, l = 1 nm, L = 20 h, ψ = 1 mA).

Figure 4 is presented correspondingly to reveal the incremental variations of the external magnetic potential. In this figure, as in the previous ones, the nanobeam is investigated in different cases. As can be seen, the increased magnetization potential leads to greater stability of the magnetic nanobeams. Of importance in the diagram is the magnetic nanobeams containing lesser critical loads than the conventional nanobeam. As a matter of fact, the in-plane static stability for such beams in negative amounts of magnetic potential is smaller than that of the conventional nanobeam. This downward/upward trend is linear in the form of a steep slope, indicating that in very strong positive magnetic fields, the piezomagnetic effects and, especially the flexomagnetic ones, will be more and more pronounced. However, these effects are also significant and undeniable in a weak magnetic environment.

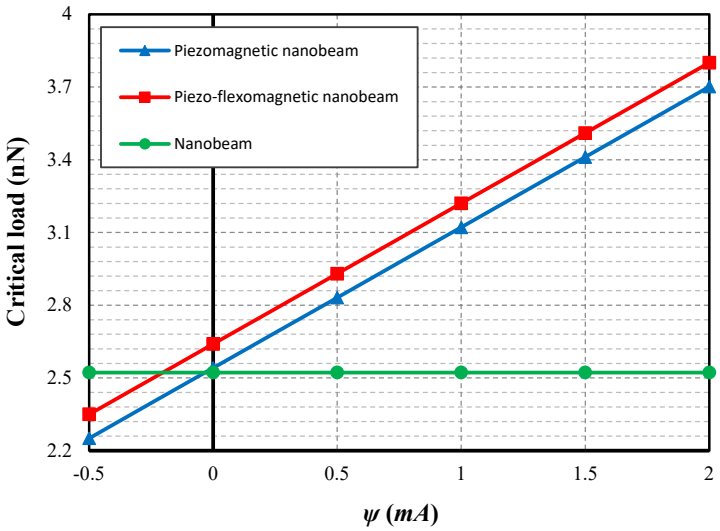

Figure 4. Magnetic potential vs. two cases of non-porous nanobeams (e_0a = 0.5 nm, l = 1 nm, L = 10 h).

Figure 5 displays the aforementioned states of nanobeams concerning changes in their thicknesses. It can be inferred from the figure that at very small thicknesses, and also positive magnetic potential, the flexomagnetic property plays a vital role in in-plane stability. With the thickening of the nanobeams, the difference between the results of the piezomagnetic and piezo-

flexomagnetic nanobeams decreases. Thereupon, for larger thicknesses, the flexomagnetic effect seems to be unimportant.

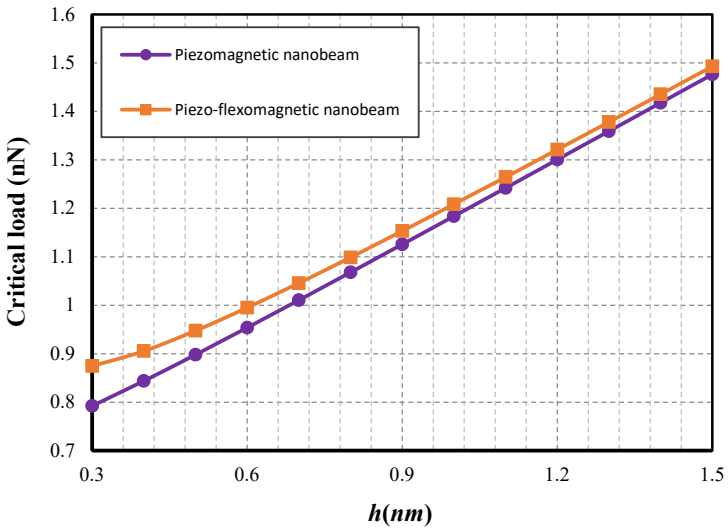

Figure 5. Thickness vs. two cases of non-porous nanobeams (e_{0a} = 0.5 nm, l = 1 nm, ψ = 1 mA, L = 20 h).

5. Conclusions

This study presented the stability capacity of a porous nanobeam involving piezomagnetic as well as flexomagnetic impacts. To date, it is known that the mechanism of action of nanostructures is based on two principles of hardening and softening. This research applied these actions to a piezo-flexomagnetic nanobeam. Substituting Lagrangian, and nonlocal theory of strain gradient elasticity, the stability relation of the piezo-flexomagnetic nanobeam was gained. Thereafter, the Navier method gave a closed-form solution to reach numerical amounts of the in-plane static stability.

The flexomagnetic effect as a complex physical phenomenon into the magneto-mechanical coupling is known as a size-dependent property that was also here affected by small-scale parameters. Furthermore, the variations of thickness of the nanobeam affected the flexomagneticity, and this property is further noticeable for lower thicknesses of nanobeams. Moreover, comparing a piezomagnetic nanobeam with a piezo-flexomagnetic one showed that this feature presents more stable material. In addition, based on our observations, it was proved that despite the flexomagnetic effect being important in the lowest positive external magnetic potentials, if the potential is sufficiently large, the capacity of static stability for piezo-flexomagnetic nanobeams will be enhanced markedly. Another significant point obtained in this research work was the influence of porosity on the flexomagnetic response of the piezomagnetic nano-sized beam. The results showed that in some patterns of porosity, this imperfection can affect the flexomagnetic behavior of the material.

Author Contributions: Conceptualization, M.M., V.A.E. and K.K.Ż; methodology, M.M., V.A.E. and K.K.Ż; software, M.M.; validation, M.M.; formal analysis, M.M.; investigation, M.M. and V.A.E.; resources, M.M., V.A.E. and K.K.Ż; data curation, M.M., V.A.E. and K.K.Ż; writing—original draft preparation, M.M.; writing—review and editing, V.A.E. and K.K.Ż.; visualization, M.M.; supervision, V.A.E.; project administration, V.A.E; funding acquisition, V.A.E. and K.K.Ż. All authors have read and agreed to the published version of the manuscript.

Funding: This research received no external funding.

Acknowledgments: V.A.E. acknowledges the support of the Government of the Russian Federation (contract No. 14.Z50.31.0046). K.K.Ż. acknowledges the support of the Ministry of Science and Higher Education of Poland (project No. W/WM-IIM/3/2020).

Conflicts of Interest: The authors declare no conflict of interest. The authors declare that they have no known competing financial interests or personal relationships that could have appeared to influence the work reported in this paper.

References

1. Kabychenkov, A.F.; Lisovskii, F.V. Flexomagnetic and Flexoantiferromagnetic Effects in Centrosymmetric Antiferromagnetic Materials. *Tech. Phys.* **2019**, *64*, 980–983, doi:10.1134/s1063784219070144.
2. Eliseev, E.A.; Morozovska, A.N.; Glinchuk, M.D.; Blinc, R. Spontaneous flexoelectric/flexomagnetic effect in nanoferroics. *Phys. Rev. B* **2009**, *79*, 165433, doi:10.1103/physrevb.79.165433.
3. Lukashev, P.; Sabirianov, R.F. Flexomagnetic effect in frustrated triangular magnetic structures. *Phys. Rev. B* **2010**, *82*, 094417, doi:10.1103/physrevb.82.094417.
4. Ma, W. Flexoelectricity: Strain gradient effects in ferroelectrics. *Phys. Scr.* **2007**, *T129*, 180–183, doi:10.1088/0031-8949/2007/t129/041.
5. Lee, D.; Yoon, A.; Jang, S.Y.; Yoon, J.-G.; Chung, J.-S.; Kim, M.; Scott, J.F.; Noh, T.W. Giant Flexoelectric Effect in Ferroelectric Epitaxial Thin Films. *Phys. Rev. Lett.* **2011**, *107*, 057602, doi:10.1103/physrevlett.107.057602.
6. Nguyen, T.D.; Mao, S.; Yeh, Y.-W.; Purohit, P.K.; McAlpine, M.C. Nanoscale Flexoelectricity. *Adv. Mater.* **2013**, *25*, 946–974, doi:10.1002/adma.201203852.
7. Zubko, P.; Catalan, G.; Tagantsev, A.K. Flexoelectric Effect in Solids. *Annu. Rev. Mater. Res.* **2013**, *43*, 387–421, doi:10.1146/annurev-matsci-071312-121634.
8. Yudin, P.V.; Tagantsev, A.K. Fundamentals of flexoelectricity in solids. *Nanotechnology* **2013**, *24*, 432001, doi:10.1088/0957-4484/24/43/432001.
9. Jiang, X.; Huang, W.; Zhang, S.; Tagantsev, A.K. Flexoelectric nano-generators: Materials, structures and devices. *Nano Energy* **2013**, *2*, 1079–1092.
10. Yurkov, A.S.; Tagantsev, A.K. Strong surface effect on direct bulk flexoelectric response in solids. *Appl. Phys. Lett.* **2016**, *108*, 022904, doi:10.1063/1.4939975.
11. Wang, B.; Gu, Y.; Zhang, S.; Chen, L.-Q. Flexoelectricity in solids: Progress, challenges, and perspectives. *Prog. Mater. Sci.* **2019**, *106*, 100570, doi:10.1016/j.pmatsci.2019.05.003.
12. Cross, L.E. Flexoelectric effects: Charge separation in insulating solids subjected to elastic strain gradients. *J. Mater. Sci.* **2006**, *41*, 53–63, doi:10.1007/s10853-005-5916-6.
13. Ma, W.; Cross, L.E. Observation of the flexoelectric effect in relaxor Pb(Mg1/3Nb2/3)O3 ceramics. *Appl. Phys. Lett.* **2001**, *78*, 2920–2921, doi:10.1063/1.1356444.
14. Ma, W.; Cross, L.E. Flexoelectricity of barium titanate. *Appl. Phys. Lett.* **2006**, *88*, 232902, doi:10.1063/1.2211309.
15. Zubko, P.; Catalan, G.; Buckley, A.; Welche, P.R.L.; Scott, J.F. Strain-gradient-induced polarization in SrTiO3 single crystals. *Phys. Rev. Lett.* **2007**, *99*, 167601.
16. Eremeyev, V.A.; Ganghoffer, J.-F.; Konopińska-Zmysłowska, V.; Uglov, N.S. Flexoelectricity and apparent piezoelectricity of a pantographic micro-bar. *Int. J. Eng. Sci.* **2020**, *149*, 103213, doi:10.1016/j.ijengsci.2020.103213.
17. Samani, M.S.E.; Beni, Y.T. Size dependent thermo-mechanical buckling of the flexoelectric nanobeam. *Mater. Res. Express* **2018**, *5*, 085018, doi:10.1088/2053-1591/aad2ca.
18. Malikan, M.; Eremeyev, V.A. On the Dynamics of a Visco–Piezo–Flexoelectric Nanobeam. *Symmetry* **2020**, *12*, 643, doi:10.3390/sym12040643.
19. Singhal, A.; Sedighi, H.M.; Ebrahimi, F.; Kuznetsova, I. Comparative study of the flexoelectricity effect with a highly/weakly interface in distinct piezoelectric materials (PZT-2, PZT-4, PZT-5H, LiNbO3, BaTiO3). *Waves Random Complex Media* **2019**, 1–19, doi:10.1080/17455030.2019.1699676.
20. Chen, W.; Yan, Z.; Wang, L. On mechanics of functionally graded hard-magnetic soft beams. *Int. J. Eng. Sci.* **2020**, *157*, 103391, doi:10.1016/j.ijengsci.2020.103391.
21. Ke, L.-L.; Wang, Y.-S. Free vibration of size-dependent magneto-electro-elastic nanobeams based on the nonlocal theory. *Phys. E Low-Dimens. Syst. Nanostruct.* **2014**, *63*, 52–61, doi:10.1016/j.physe.2014.05.002.
22. Ping, T. Nonlinear free vibration analysis of nanobeams under magnetic field based on nonlocal elasticity theory. *J. Vibroeng.* **2016**, *18*, 1912–1919, doi:10.21595/jve.2015.16751.

23. Baghani, M.; Mohammadi, M.; Farajpour, A. Dynamic and Stability Analysis of the Rotating Nanobeam in a Nonuniform Magnetic Field Considering the Surface Energy. *Int. J. Appl. Mech.* **2016**, *8*, 1650048, doi:10.1142/s1758825116500484.
24. Ebrahimi, F.; Barati, M.R. Porosity-dependent vibration analysis of piezo-magnetically actuated heterogeneous nanobeams. *Mech. Syst. Signal Process.* **2017**, *93*, 445–459, doi:10.1016/j.ymssp.2017.02.021.
25. Zenkour, A.M.; Arefi, M.; AlShehri, N.A. Size-dependent analysis of a sandwich curved nanobeam integrated with piezomagnetic face-sheets. *Results Phys.* **2017**, *7*, 2172–2182, doi:10.1016/j.rinp.2017.06.032.
26. Sun, X.-P.; Hong, Y.-Z.; Dai, H.; Wang, L. Nonlinear frequency analysis of buckled nanobeams in the presence of longitudinal magnetic field. *Acta Mech. Solida Sin.* **2017**, *30*, 465–473, doi:10.1016/j.camss.2017.08.002.
27. Arefi, M.; Zenkour, A.M. Transient sinusoidal shear deformation formulation of a size-dependent three-layer piezo-magnetic curved nanobeam. *Acta Mech.* **2017**, *228*, 3657–3674, doi:10.1007/s00707-017-1892-6.
28. Liu, H.; Yang, J. Vibration of FG magneto-electro-viscoelastic porous nanobeams on visco-Pasternak foundation. *Compos. Part B Eng.* **2018**, *155*, 244–256, doi:10.1016/j.compositesb.2018.08.042.
29. Karami, B.; Shahsavari, D.; Li, L. Hygrothermal wave propagation in viscoelastic graphene under in-plane magnetic field based on nonlocal strain gradient theory. *Phys. E Low-Dimens. Syst. Nanostructures* **2018**, *97*, 317–327, doi:10.1016/j.physe.2017.11.020.
30. Arefi, M.; Arani, A.H.S. Higher order shear deformation bending results of a magnetoelectrothermoelastic functionally graded nanobeam in thermal, mechanical, electrical, and magnetic environments. *Mech. Based Des. Struct. Mach.* **2018**, *46*, 669–692, doi:10.1080/15397734.2018.1434002.
31. Alibeigi, B.; Beni, Y.T. On the size-dependent magneto/electromechanical buckling of nanobeams. *Eur. Phys. J. Plus* **2018**, *133*, 398, doi:10.1140/epjp/i2018-12208-6.
32. Azrar, A.; Ben Said, M.; Azrar, L.; Aljinaidi, A. Dynamic instability analysis of magneto-electro-elastic beams with uncertain parameters under static and parametric electric and magnetic fields. *Compos. Struct.* **2019**, *226*, 111185, doi:10.1016/j.compstruct.2019.111185.
33. Zhen, Y.-X.; Wen, S.-L.; Tang, Y. Free vibration analysis of viscoelastic nanotubes under longitudinal magnetic field based on nonlocal strain gradient Timoshenko beam model. *Phys. E: Low-Dimens. Syst. Nanostructures* **2019**, *105*, 116–124, doi:10.1016/j.physe.2018.09.005.
34. Arefi, M.; Kiani, M.; Civalek, Ö. 3-D magneto-electro-thermal analysis of layered nanoplate including porous core nanoplate and piezomagnetic face-sheets. *Appl. Phys. A* **2020**, *126*, 76, doi:10.1007/s00339-019-3241-1.
35. Mirjavadi, S.S.; Forsat, M.; Nikookar, M.; Barati, M.R.; Hamouda, A. Nonlinear forced vibrations of sandwich smart nanobeams with two-phase piezo-magnetic face sheets. *Eur. Phys. J. Plus* **2019**, *134*, 508, doi:10.1140/epjp/i2019-12806-8.
36. Mirjavadi, S.S.; Forsat, M.; Barati, M.R.; Abdella, G.M.; Hamouda, A.M.S.; Afshari, B.M.; Rabby, S. Post-buckling analysis of piezo-magnetic nanobeams with geometrical imperfection and different piezoelectric contents. *Microsyst. Technol.* **2019**, *25*, 3477–3488, doi:10.1007/s00542-018-4241-3.
37. Jalaei, M.; CivalekÖ. On dynamic instability of magnetically embedded viscoelastic porous FG nanobeam. *Int. J. Eng. Sci.* **2019**, *143*, 14–32, doi:10.1016/j.ijengsci.2019.06.013.
38. Ghane, M.; Saidi, A.R.; Bahaadini, R. Vibration of fluid-conveying nanotubes subjected to magnetic field based on the thin-walled Timoshenko beam theory. *Appl. Math. Model.* **2020**, *80*, 65–83, doi:10.1016/j.apm.2019.11.034.
39. Żur, K.; Arefi, M.; Kim, J.; Reddy, J. Free vibration and buckling analyses of magneto-electro-elastic FGM nanoplates based on nonlocal modified higher-order sinusoidal shear deformation theory. *Compos. Part B Eng.* **2020**, *182*, 107601, doi:10.1016/j.compositesb.2019.107601.
40. Sidhardh, S.; Ray, M. Flexomagnetic response of nanostructures. *J. Appl. Phys.* **2018**, *124*, 244101, doi:10.1063/1.5060672.
41. Zhang, N.; Zheng, S.; Chen, D. Size-dependent static bending of flexomagnetic nanobeams. *J. Appl. Phys.* **2019**, *126*, 223901, doi:10.1063/1.5128940.
42. Malikan, M.; Eremeyev, V.A. Free Vibration of Flexomagnetic Nanostructured Tubes Based on Stress-driven Nonlocal Elasticity. In *Engineering Design Applications*; Springer Science and Business Media LLC.: Berlin/Heidelberg, Germany, 2020; Volume 134, pp. 215–226.
43. Malikan, M.; Eremeyev, V.A. On the geometrically nonlinear vibration of a piezo-flexomagnetic nanotube. *Math. Methods Appl. Sci.* **2020**, doi:10.1002/mma.6758.

44. Malikan, M.; Eremeyev, V.A. On Nonlinear Bending Study of a Piezo-Flexomagnetic Nanobeam Based on an Analytical-Numerical Solution. *Nanomaterials* **2020**, *10*, 1762, doi:10.3390/nano10091762.
45. Malikan, M.; Uglov, N.S.; Eremeyev, V.A. On instabilities and post-buckling of piezomagnetic and flexomagnetic nanostructures. *Int. J. Eng. Sci.* **2020**, *157*, 103395, doi:10.1016/j.ijengsci.2020.103395.
46. Song, X.; Li, S.-R. Thermal buckling and post-buckling of pinned–fixed Euler-Bernoulli beams on an elastic foundation. *Mech. Res. Commun.* **2007**, *34*, 164–171, doi:10.1016/j.mechrescom.2006.06.006.
47. Reddy, J. Nonlocal nonlinear formulations for bending of classical and shear deformation theories of beams and plates. *Int. J. Eng. Sci.* **2010**, *48*, 1507–1518, doi:10.1016/j.ijengsci.2010.09.020.
48. Barretta, R.; Feo, L.; Luciano, R.; De Sciarra, F.M. Variational formulations for functionally graded nonlocal Bernoulli-Euler nanobeams. *Compos. Struct.* **2015**, *129*, 80–89, doi:10.1016/j.compstruct.2015.03.033.
49. Akgöz, B.; Civalek, Ö. Buckling analysis of functionally graded microbeams based on the strain gradient theory. *Acta Mech.* **2013**, *224*, 2185–2201, doi:10.1007/s00707-013-0883-5.
50. Sarparast, H.; Ebrahimi-Mamaghani, A.; Safarpour, M.; Ouakad, H.M.; Dimitri, R.; Tornabene, F. Nonlocal study of the vibration and stability response of small-scale axially moving supported beams on viscoelastic-Pasternak foundation in a hygro-thermal environment. *Math. Methods Appl. Sci.* **2020**, doi:10.1002/mma.6859.
51. Lim, C.; Zhang, G.; Reddy, J. A higher-order nonlocal elasticity and strain gradient theory and its applications in wave propagation. *J. Mech. Phys. Solids* **2015**, *78*, 298–313, doi:10.1016/j.jmps.2015.02.001.
52. Ansari, R.; Sahmani, S.; Arash, B. Nonlocal plate model for free vibrations of single-layered graphene sheets. *Phys. Lett. A* **2010**, *375*, 53–62, doi:10.1016/j.physleta.2010.10.028.
53. Khorshidi, M.A. The material length scale parameter used in couple stress theories is not a material constant. *Int. J. Eng. Sci.* **2018**, *133*, 15–25, doi:10.1016/j.ijengsci.2018.08.005.
54. She, G.L. Wave propagation of FG polymer composite nanoplates reinforced with GNPs. *Steel Compos. Struct.* **2020**, *37*, 27–35.
55. She, G.L.; Liu, H.B.; Karami, B. On resonance behavior of porous FG curved nanobeams. *Steel Compos. Struct.* **2020**, *36*, 179–186.
56. Malikan, M.; Dimitri, R.; Tornabene, F. Transient response of oscillated carbon nanotubes with an internal and external damping. *Compos. Part B Eng.* **2019**, *158*, 198–205, doi:10.1016/j.compositesb.2018.09.092.
57. Malikan, M.; Krasheninnikov, M.; Eremeyev, V.A. Torsional stability capacity of a nano-composite shell based on a nonlocal strain gradient shell model under a three-dimensional magnetic field. *Int. J. Eng. Sci.* **2020**, *148*, 103210, doi:10.1016/j.ijengsci.2019.103210.
58. Malikan, M. On the plastic buckling of curved carbon nanotubes. *Theor. Appl. Mech. Lett.* **2020**, *10*, 46–56, doi:10.1016/j.taml.2020.01.004.
59. Malikan, M.; Eremeyev, V.A. Post-critical buckling of truncated conical carbon nanotubes considering surface effects embedding in a nonlinear Winkler substrate using the Rayleigh-Ritz method. *Mater. Res. Express* **2020**, *7*, 025005, doi:10.1088/2053-1591/ab691c.
60. Karami, B.; Janghorban, M.; Rabczuk, T. Dynamics of two-dimensional functionally graded tapered Timoshenko nanobeam in thermal environment using nonlocal strain gradient theory. *Compos. Part B Eng.* **2020**, *182*, 107622, doi:10.1016/j.compositesb.2019.107622.
61. Apuzzo, A.; Barretta, R.; Faghidian, S.A.; Luciano, R.; De Sciarra, F.M. Nonlocal strain gradient exact solutions for functionally graded inflected nano-beams. *Compos. Part B Eng.* **2019**, *164*, 667–674, doi:10.1016/j.compositesb.2018.12.112.
62. Tang, H.; Li, L.; Hu, Y. Buckling analysis of two-directionally porous beam. *Aerosp. Sci. Technol.* **2018**, *78*, 471–479, doi:10.1016/j.ast.2018.04.045.
63. Barretta, R.; De Sciarra, F.M. Constitutive boundary conditions for nonlocal strain gradient elastic nano-beams. *Int. J. Eng. Sci.* **2018**, *130*, 187–198, doi:10.1016/j.ijengsci.2018.05.009.
64. Barretta, R.; De Sciarra, F.M. Variational nonlocal gradient elasticity for nano-beams. *Int. J. Eng. Sci.* **2019**, *143*, 73–91, doi:10.1016/j.ijengsci.2019.06.016.
65. De Sciarra, F.M.; Barretta, R. A new nonlocal bending model for Euler-Bernoulli nanobeams. *Mech. Res. Commun.* **2014**, *62*, 25–30, doi:10.1016/j.mechrescom.2014.08.004.
66. Romano, G.; Barretta, R.; Diaco, M.; De Sciarra, F.M. Constitutive boundary conditions and paradoxes in nonlocal elastic nanobeams. *Int. J. Mech. Sci.* **2017**, *121*, 151–156, doi:10.1016/j.ijmecsci.2016.10.036.

67. Pradhan, S.; Reddy, G. Buckling analysis of single walled carbon nanotube on Winkler foundation using nonlocal elasticity theory and DTM. *Comput. Mater. Sci.* **2011**, *50*, 1052–1056, doi:10.1016/j.commatsci.2010.11.001.
68. Wang, C.M.; Zhang, Y.Y.; Ramesh, S.S.; Kitipornchai, S. Buckling analysis of micro- and nano-rods/tubes based on nonlocal Timoshenko beam theory. *J. Phys. D Appl. Phys.* **2006**, *39*, 3904–3909, doi:10.1088/0022-3727/39/17/029.
69. Ansari, R.; Sahmani, S.; Rouhi, H. Rayleigh-Ritz axial buckling analysis of single-walled carbon nanotubes with different boundary conditions. *Phys. Lett. A* **2011**, *375*, 1255–1263, doi:10.1016/j.physleta.2011.01.046.
70. Duan, W.H.; Wang, C.M. Exact solutions for axisymmetric bending of micro/nanoscale circular plates based on nonlocal plate theory. *Nanotechnology* **2007**, *18*, 385704, doi:10.1088/0957-4484/18/38/385704.
71. Duan, W.H.; Wang, C.M.; Zhang, Y.Y. Calibration of nonlocal scaling effect parameter for free vibration of carbon nanotubes by molecular dynamics. *J. Appl. Phys.* **2007**, *101*, 024305, doi:10.1063/1.2423140.

Postprint for: Malikan M., Wiczenbach T., Eremeyev V. A. On thermal stability of piezo-flexomagnetic microbeams considering different temperature distributions. Continuum Mechanics and Thermodynamics. https://doi.org/10.1007/s00161-021-00971-y

On thermal stability of piezo-flexomagnetic microbeams considering different temperature distributions

Mohammad Malikan[1], Tomasz Wiczenbach[1], Victor A. Eremeyev[1,2,3]*

[1] Department of Mechanics of Materials and Structures, Gdansk University of Technology, 80-233 Gdansk, Poland

[2] Research and Education Center "Materials" Don State Technical University, Gagarina sq., 1, 344000 Rostov on Don, Russia

[3] DICAAR, Università degli Studi di Cagliari, Via Marengo, 2, 09123, Cagliari, Italy

*Corresponding author:
Email: victor.eremeev@pg.edu.pl, eremeyev.victor@gmail.com

Abstract

By relying on the Euler-Bernoulli beam model and energy variational formula, we indicate critical temperature causes in the buckling of piezo-flexomagnetic microscale beams. The corresponding size-dependent approach is underlying as a second strain gradient theory. Small deformations of elastic solids are assessed and the mathematical discussion is linear. With regardless of the pyromagnetic effects, the thermal loading of the thermal environment is varied in three states along with the thickness, which is linear, uniform, and nonlinear

forms. We then establish the results by developing consistent shape functions which independently evaluate boundary conditions. Next, we analytically develop and explore the effective properties of the studied beam with regard to vital factors. It was achieved that piezomagnetic-flexomagnetic microbeams are more affected by the thermal environment while the thermal loading is nonlinearly distributed across the thickness, particularly when the boundaries involve simple supports.

Keywords: Piezo-flexomagnetic microbeam; Critical temperature; Strain gradient theory; Analytical solution

Symbols

H_z	Magnetic field component
η_{xxz}	Gradient of the elastic strain
σ_{xx}	Stress component
ε_{xx}	Strain component
ξ_{xxz}	Hyper stress
B_z	Magnetic flux component
C_{11}	Elasticity modulus
M_x	Moment stress resultant
T_{xxz}	Hyper stress resultant
U	Strain energy
δ	Symbol of variations
N_x	Axial stress resultant
Ψ	Magnetic potential
I_z	Area moment of inertia
l	Microscale parameter
α	Thermal expansion coefficient
ΔT	Temperature variations
T_0	Environment temperature
T_f	Critical temperature
W	Works done by external objects
u_1	Cartesian displacements along x axis
u_3	Cartesian displacements along z axis
L	Length of the beam
h	Thickness of the beam
u	Axial displacement of the midplane
w	Transverse displacement of the midplane
z	Thickness coordinate
q_{31}	Component of the third-order piezomagnetic tensor
g_{31}	Component the sixth-order gradient elasticity tensor
f_{31}	Component of fourth-order flexomagnetic
a_{33}	Component of the second-order magnetic permeability tensor
N_x^0	Initial total in-plane axial force
ψ	Initial Magnetic potential
A	Area of cross-section of the beam
Y	Residue in the solution method
m	Mode number

1 Introduction

Many mechanical structures are used in environments with high-temperature differences. It causes significant temperature changes, stresses, and deformations. Applying heat load in some structures is inevitable, and in others it is accidental. Some structures are subjected to thermal loads frequently during the working period. The effect of heat on the structure and performance of structures such as spacecraft, nuclear reactors, and heat exchangers are examples of this type of heat loading. On the other hand, a thermal load may be accidentally applied to a structure. An example of this is the fire in urban and industrial buildings and facilities. Regardless of the effects of heat load, the design of a structure will not be a complete and safe design. An important group of structures among the applicable structures is the beam, which in many cases form a large part of the structure of a composite structure. In cases where the mechanical structure is composed of lean elements, e.g. beams, one of the major problems caused by rising temperature is the occurrence of thermal buckling [1].

As solid phase support, magnetic microparticles (MMP) promise a lot of significant advances in experimental works. New technology emerged by which magnetic separation can occur during magnetism. Different molecules can be isolated or absorbed by these particles in many applications such as magnetic cell separation, ribonucleic acid (RNA) purification, etc. [2-4]. One of the biotic and useful applications of MMPs is targeting cancer cell qua these particles can separate cells from human blood. But timeless usages are waiting to be found.

Today, due to the widespread advances in engineering sciences, the need for optimizations resulting from small scale technology is felt more and more. Micro-sensors are highly improved, high-performance materials that are just one example of applications in the micro-industry. Devices display properties such as temperature, pressure, traction, or current output the desired parameter. Magnetic micro-sensors, on the other hand, detect changes or disturbances in the magnetic field and then, based on that, extract the required information

such as direction, presence, rotation angle, or potential [5-10].

Apart from the piezomagneticity, magnetic micro-sensors and generally magnetic particles can have another physical property, which is flexomagneticity. The difference is that flexomagnetic is a pervasive effect on all materials with any symmetry, the discovery of which dates back to the current decade. Flexomagneticity is the coupling between the polarization and the strain gradient, but piezomagneticity is the coupling between the polarization and the strain itself [11-18]. The small scale theme is the main debate in MMPs technology, which shows the more effective role of flexomagneticity. In light of the new progress and developments which emerge these years, particularly at a small scale, the flexomagneticity debate is increasing quickly.

Based on the research background performed on the mechanics of piezomagnetic-flexomagnetic structures, theoretical research can be found. These studies were preliminarily begun by Sidhardh and Ray [19] and Zhang et al. [20]. In these introductory works, they showed studies on piezomagnetic-flexomagnetic nanostructures by investigating bending properties. The deformations were assumed as the small and linear analysis was taken into consideration. Both published research employed Euler-Bernoulli displacement kinematic field to model the structure as a thin beam. Magnetization influences were regarding both reverse and direct impacts. The acted static loading was vertically and uniformly imposed throughout the length of the beam. The first research examined cantilever beams, however the second one demonstrated premier study by evaluating several end conditions. The shortcoming of both works is a lack of considering size-dependent effects. Though they simply inspected only surface effect and nonlocal or microstructural influences were not figured out. Newly, Malikan and Eremeyev [21] carried out piezomagnetic-flexomagnetic Euler-Bernoulli small scale beams exposed in a vibrational mode. The linear frequency

analysis was done whilst the size-dependent impacts were explored according to the stress-driven nonlocal elasticity approach. Based on their results, it was affirmed that the flexomagnetic feature is size-dependent. Another research on piezomagnetic-flexomagnetic small size structures has been performed by Malikan and Eremeyev [22] in which they studied nonlinear frequencies of the structure. They fulfilled size-dependent influences on the basis of the nonlocal strain gradient elasticity model. In addition to these, Malikan and Eremeyev [23] studied large deflections of piezo-flexomagnetic nano size beams using two step analytical-numerical solution techniques. They discovered that analysis of nonlinear bending properties of a piezo-flexomagnetic nanobeam is seriously required to design nano-electro-mechanical systems (NEMS) based piezomagnetic-flexomagnetic properties. They demonstrated many new results of which we can refer to reducing the deflections as a result of flexomagnetic effect. Malikan et al. [24] continued the studies on magnetic nanoparticles involving both piezomagnetic and flexomagnetic features. The new study investigated post-buckling response of the structures which led to some new results and achievements in the field of smart nanosensors.

To extend the accomplished works on piezomagnetic-flexomagnetic structures, this research attempts to estimate temperature impacts on these structures. In doing so, this article investigates a microscale piezomagnetic-flexomagnetic beam-shaped sensor and peruses the size-dependent influences pursuant to a strain gradient model. The elastic strains are supposed to be linear and the kinematic displacement components are due to Euler-Bernoulli thin beam. Two boundary conditions are mathematically represented, namely clamped and simple supports. Then, the assessments are continued with changes in associated factors which are effective in designing the magnetic sensor and the results are exhibited graphically by several figures.

2 Theoretical Modeling

Let us discuss the applied model in more details. In Figures 1 and 2, the microscale beams are shown which are installed into clamped-clamped and simple-simple supported, respectively. The cross-section of the beams is geometrically square. The beam is placed in a magnetic field which acts vertically. Thermal environment is also taken into account and affects the beam in direction with the thickness only.

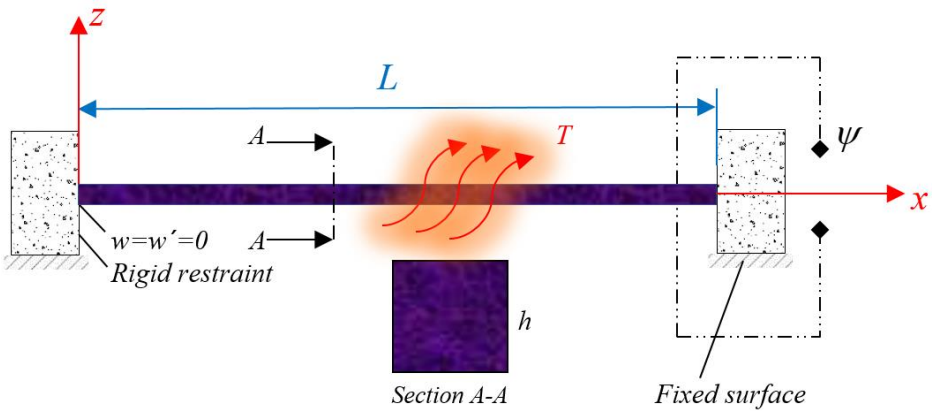

Figure 1. A square microbeam containing PM and FM embedded in fully fixed ends

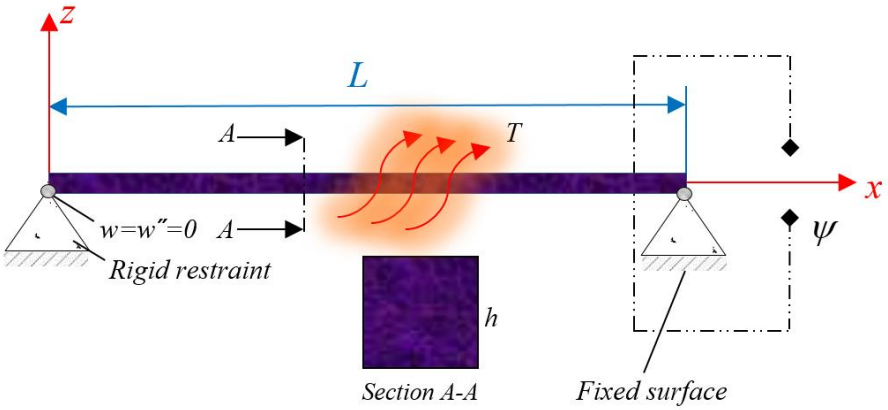

Figure 2. A square microbeam containing PM and FM embedded in pivot ends

To carry out the problem, the beam is considered to act as the Euler-Bernoulli beam hypothesis as [25, 26]

$$u_1(x,z) = u(x) - z\frac{dw(x)}{dx} \tag{1}$$

$$u_3(x,z) = w(x) \tag{2}$$

where we introduced axial displacement $u(x)$ and deflection $w(x)$ as functions of x coordinate, see Figures. 1 and 2.

The compatible components of strain-displacement relations have the following form

$$\varepsilon_{xx} = \frac{du}{dx} - z\frac{d^2w}{dx^2} \tag{3}$$

$$\eta_{xxz} = \frac{d\varepsilon_{xx}}{dz} = -\frac{d^2w}{dx^2} \tag{4}$$

The nonzero stress σ_{xx} and hyper stress ξ_{xxz} components alongside magnetic induction can be expanded as [19, 20]

$$\sigma_{xx} = C_{11}\varepsilon_{xx} - \alpha C_{11}\Delta T - q_{31}H_z \tag{5}$$

$$\xi_{xxz} = g_{31}\eta_{xxz} - f_{31}H_z \tag{6}$$

$$B_z = a_{33}H_z + q_{31}\varepsilon_{xx} + f_{31}\eta_{xxz} \tag{7}$$

where C_{11} is an elastic modulus, α is a coefficient of thermal expansion, ΔT is the temperature change across the cross-section of the beam, H_z is the vertical component of the magnetic field, q_{31} is a piezomagnetic modulus, g_{31} is a higher order elastic modulus, f_{31} is a flexomagnetic modulus responsible for coupling between magnetic flux B_z and strain gradient η_{xxz}, and a_{33} is a magnetic permeability.

The characteristics equation can be derived on the basis of a virtual displacement in the system according to first variation in total energy relationship as below

$$\delta U - \delta W = 0 \tag{8}$$

where δU is the first variation of the energy functional and δW is the work of external actions.

To establish the strain energy in the global form, one can write

$$\delta U = \int_V \left(\sigma_{xx} \delta \varepsilon_{xx} + \xi_{xxz} \delta \eta_{xxz} - B_z \delta H_z \right) dV \tag{9}$$

Thus, based on Eqs. (5-7), Eq. (9) can be calculated by integrating part by part as follows

$$\delta U = \delta \Pi_{U_1}^{Mech} + \delta \Pi_{U_1}^{Mag} + \delta \Pi_{U_2}^{Mech} + \delta \Pi_{U_2}^{Mag} \tag{10}$$

where

$$\delta \Pi_{U_1}^{Mech} = -\int_0^L \left[\frac{dN_x}{dx} \delta u + \left(\frac{d^2 M_x}{dx^2} + \frac{d^2 T_{xxz}}{dx^2} \right) \delta w \right] dx \tag{11}$$

$$\delta \Pi_{U_1}^{Mag} = -\int_0^L \int_{-h/2}^{h/2} \frac{dB_z}{dz} \delta \Psi \, dz dx \tag{12}$$

$$\delta \Pi_{U_2}^{Mech} = \left(N_x \delta u - M_x \frac{d\delta w}{dx} - T_{xxz} \frac{d\delta w}{dx} + \frac{dM_x}{dx} \delta w + \frac{dT_{xxz}}{dx} \delta w \right) \Bigg|_0^L \tag{13}$$

$$\delta \Pi_{U_2}^{Mag} = \int_0^L \left(B_z \delta \Psi \right) \Big|_{-h/2}^{h/2} dx \tag{14}$$

where the associated parameters would be

$$N_x = \int_{-h/2}^{h/2} \sigma_{xx} dz \tag{15}$$

$$M_x = \int_{-h/2}^{h/2} \sigma_{xx} z dz \tag{16}$$

$$T_{xxz} = \int_{-h/2}^{h/2} \xi_{xxz} dz \tag{17}$$

which are axial, moment and hyper stress resultants on beam elements.

The virtual work as results of axial magnetic field and thermal environment can be

expressed as [27, 28]

$$W = -\frac{1}{2}\int_0^L N_x^0 \left(\frac{dw}{dx}\right)^2 dx \tag{18}$$

$$\delta W = -\int_0^L N_x^0 \left(\frac{d\delta w}{dx}\frac{dw}{dx}\right) dx \tag{19}$$

We are allowed to write the relationship between magnetic potential and the magnetic component as

$$H_z = -\frac{d\Psi}{dz} \tag{20}$$

Let us assume the magnetic field varies linearly in direction with thickness, hence

$$\Psi\left(+\frac{h}{2}\right) = \psi,\ \Psi\left(-\frac{h}{2}\right) = 0 \tag{21}$$

where the closed circuit beside reverse effect of the field is investigated. Plugging Eqs. (7), (12), (20) and (21) and some simplifications gives [19, 20]

$$\Psi = -\frac{q_{31}}{2a_{33}}\left(z^2 - \frac{h^2}{4}\right)\frac{d^2w}{dx^2} + \frac{\psi}{h}\left(z + \frac{h}{2}\right) \tag{22}$$

$$H_z = z\frac{q_{31}}{a_{33}}\frac{d^2w}{dx^2} - \frac{\psi}{h} \tag{23}$$

To apear Eqs. (5-7) in detail, we can take the help of Eqs. (3), (4), (22) and (23), thus

$$\sigma_{xx} = -z\left(C_{11} + \frac{q_{31}^2}{a_{33}}\right)\frac{d^2w}{dx^2} + \frac{q_{31}\psi}{h} - \sigma^T \tag{24}$$

$$\xi_{xxz} = -\left(g_{31} + \frac{q_{31}f_{31}z}{a_{33}}\right)\frac{d^2w}{dx^2} + \frac{f_{31}\psi}{h} \tag{25}$$

$$B_z = -f_{31}\frac{d^2w}{dx^2} - \frac{a_{33}\psi}{h} \tag{26}$$

We now express the stress and hyper stress resultants as

$$N_x = C_{11} A \frac{du}{dx} + N^{Mag} - N^T \tag{27}$$

$$M_x = -I_z \left(C_{11} + \frac{q_{31}^2}{a_{33}} \right) \frac{d^2 w}{dx^2} - M^T \tag{28}$$

$$T_{xxz} = -g_{31} h \frac{d^2 w}{dx^2} + f_{31} \psi \tag{29}$$

To attach the microstructural property into the model of problem, the second strain gradient of Mindlin will be implemented [29, 30]. It is crucial to note that the couple stress models [31-37] are unable to be embedded into the energy formulation while the problem is flexoelectric or flexomagnetic ones. This is due to this fact that both magnetic and couple stress terms in the energy formulation mathematically act similar to each other and the couple stress term would be pointless. Therefore, the second strain gradient is employed which is not directly placed in the energy formulation. The second strain gradient relationship can be expressed as below

$$\sigma_{ij} = C_{ijkl} \left(1 \pm l^2 \frac{d^2}{dx^2} \right) \varepsilon_{kl} \tag{30}$$

The model showed by Eq. (30) can be utilized into two parts, a model with negative sign and another one with positive sign. The positive sign makes the model destabilizing [37, 38], but the negative sign produces a stable model.

The stress resultants in the form of second strain gradient model can be written as follows

$$N_x = \left(1 - l^2 \frac{d^2}{dx^2} \right) \left\{ C_{11} A \frac{du}{dx} \right\} - N^{Mag} - N^T \tag{31}$$

$$M_x = \left(1 - l^2 \frac{d^2}{dx^2} \right) \left\{ -I_z \left(C_{11} + \frac{q_{31}^2}{a_{33}} \right) \frac{d^2 w}{dx^2} \right\} - M^T \tag{32}$$

$$T_{xxz}=\left(1-l^2\frac{d^2}{dx^2}\right)\left\{-g_{31}h\frac{d^2w}{dx^2}+f_{31}\psi\right\} \tag{33}$$

As stated by the Lorentz' law, the transverse magnetic field can generate a longitudinal mechanical force. Therefore,

$$N^{Mag}=q_{31}\psi \tag{34}$$

Assuming the variations of temperature in line with thickness of the beam, the below relation can be presented [39, 40]

$$\Delta T(z)=\left(\frac{z+h/2}{h}\right)^{\varphi}T, \quad -h/2\le z\le h/2, \quad 0\le\varphi\le\infty \tag{35}$$

in which T is the temperature variation as

$$T=T_f-T_0 \tag{36}$$

The temperature variation along the thickness has here three forms (Figure 3) defined in the following

$$\varphi\begin{cases}=0:Uniform\\=1:Linear\\>1:Nonlinear\end{cases} \tag{37}$$

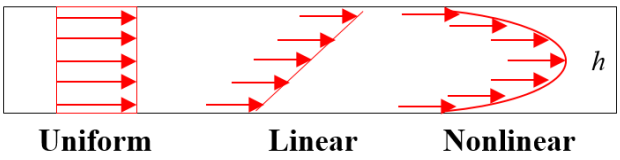

Figure 3. Thermal loading across the thickness

The temperature can cause a thermal load axially applied on the beam as below

$$N^T=\frac{\alpha C_{11}}{1-\nu}\int_{-h/2}^{h/2}\Delta T(z)\,dz \tag{38}$$

$$M^T=\frac{\alpha C_{11}}{1-\nu}\int_{-h/2}^{h/2}\Delta T(z)\,z\,dz \tag{39}$$

Afterwards, the total longitudinal and moment forces performed on the system can be briefly shown as

$$N_x^0 = N^{Mag} + N^T \tag{40}$$

$$M_x = M^{Mech} + M^T \tag{41}$$

which the axial resultant is divided into magnetic and thermal parts. Moreover, the moment stress resultant is sectioned into two parts, that is mechanical and thermal ones.

Taking into account Eqs. (11), (13), and (19) and embedding all in Eq. (8) result in the local governing equations as follows

$$\frac{dN_x}{dx} = 0 \tag{42}$$

$$\frac{d^2M_x}{dx^2} + \frac{d^2T_{xxz}}{dx^2} + N_x^0 \frac{d^2w}{dx^2} = 0 \tag{43}$$

Writing Eqs. (42) and (43) on the basis of Eqs. (31-33), (40) and (41) leads to two independent equations which in order to solve the values of critical temperature, the second equation is required and sufficient as

$$D\left(l^2 \frac{d^6w}{dx^6} - \frac{d^4w}{dx^4} \right) + \left(N^{Mag} + \beta T \right) \frac{d^2w}{dx^2} = 0 \tag{44}$$

in which

$$D = \left[I_z \left(C_{11} + \frac{q_{31}^2}{a_{33}} \right) + g_{31} h \right],$$

$$\beta = \frac{\alpha C_{11} h}{(1-\nu)(1+\varphi)}$$

3 Solution approach

This section develops analytical solution methods for the present problem investigating two boundary conditions. Clamped and simply supported end conditions are satisfied here based on the two different admissible functions describing mathematically the physical conditions of these supports. A totally analytical process is demonstrated [41, 42]. Hence,

$$w(x) = W \cdot X(x) \tag{45}$$

The admissible function indices in Eq. (45) needed in the process is given as follows [41, 43].

$$\text{SS: } X(x) = \sin\left(\frac{\pi}{L}x\right) \tag{46}$$

$$\text{CC: } X(x) = \sin^2\left(\frac{\pi}{L}x\right) \tag{47}$$

The associated notations denote respectively for simply-supported (S), and clamped (C) boundary conditions.

Substituting Eq. (45) into Eq. (44) and integrating over the longitudinal domain will lead to

$$\left(K_1 + TK_2\right)X = 0 \tag{48}$$

Some manipulating and arranging give the linear algebraic equation in which there can be critical temperature as the unknown parameter which requires to be determined. The coefficients in Eq. (48) can be expressed as follows

$$K_1 = \int_0^L \left[\lambda_1(x) \cdot Y(x)\right] dx \tag{49}$$

$$K_2 = \int_0^L \left[\lambda_2(x) \cdot Y(x)\right] dx \tag{50}$$

in which

$$\lambda_1 = D\left(l^2 \frac{d^6 w}{dx^6} - \frac{d^4 w}{dx^4}\right) + N^{Mag} \frac{d^2 w}{dx^2},$$

$$\lambda_2 = \beta \frac{d^2 w}{dx^2}$$

Consequently, let us manipulate and simplify the equation based on the critical temperature load and admissible functions as

$$T = \frac{D\left(l^2 \int_0^L \left(\frac{d^6 X(x)}{dx^6} \cdot Y(x) \right) dx - \int_0^L \left(\frac{d^4 X(x)}{dx^4} \cdot Y(x) \right) dx \right) + N^{Mag} \int_0^L \left(\frac{d^2 X(x)}{dx^2} \cdot Y(x) \right) dx}{\beta \int_0^L \left(\frac{d^2 X(x)}{dx^2} \cdot Y(x) \right) dx} \tag{51}$$

One cane write the thermal analytical buckling formula for CC as:

$$T = \frac{N^{Mag} L^4 + 4DL^2 \pi^2 m^2 + 16Dl^2 \pi^4 m^4}{\beta L^4} \tag{52}$$

And also for SS as:

$$T = \frac{N^{Mag} L^4 + DL^2 \pi^2 m^2 + Dl^2 \pi^4 m^4}{\beta L^4} \tag{53}$$

4 Solution validity

Results' discussion shall be begun with a validation example in order to find the solution process accuracy. To do this, [44, 45] are utilized leading to tabulated results in Tables 1 and 2. It should be noted that this comparison section is prepared for mechanical elastic buckling of a square macroscale Euler-Bernoulli beam for which the elastic properties E=1TPa, υ= 0.19 are put. It is also worthy to note that [44] applied an exact solution method and [45] exerted the numerical differential transformed technique. We try to valid both end conditions used in this article. Accordingly, we can observe a very good agreement and accordance among the tabulated results.

Table 1. For a SS beam.

L / h	[44]	[45]	Present
10	4.8447	4.8447	4.84473
12	3.3644	3.3644	3.36439
14	2.4718	2.4718	2.47180
16	1.8925	1.8925	1.89247
18	1.4953	1.4953	1.49529
20	1.2112	1.2112	1.21118

Table 2. For a CC beam.

L / h	[44]	[45]	Present
10	19.379	19.379	19.37895
12	13.458	13.458	13.45760
14	9.877	9.877	9.88721
16	7.4699	7.4699	7.56990
18	5.9811	5.9811	5.98115
20	4.8447	4.8447	4.84473

5 Discussion and results

The preparatory validation confirmed that the present analytical procedure can be transferred into further problems. Thereupon, we are here focusing on the temperature by which the piezomagnetic-flexomagnetic microscale beam buckles. At first, the structural specifications involving elasticity and magnetic features shall be identified to get to the main problem. Such the properties can be seen by Table 3 which were picked up from [46-48]

Table 3. Magneto-mechanical features of a microscale ferromagnetic sensor

$CoFe_2O_4$
C_{11}=286 GPa, ν=0.32
f_{31}=10^{-9} N/Ampere
α=11.80×10^{-6} 1/K (room temperature)

q_{31}=580.3 N/Ampere.m

a_{33}=157×10^{-6} N/Ampere^2

5.1 Microstructural effect

It was shown by literature and experimental works that when a particle size diminishes, the stiffness of the material can be strongly affected, which this influence causes in enhancing the stiffness [49]. In order to consider this effect here, Figures 4a and 4b are drawn for simple and clamp supports, respectively. It is worth noting that the notations NL, L, and U are dedicated to nonlinear, linear, and uniform thermal loading distribution (TD) along the thickness. Furthermore, all the nonlinear results in this paper are extracted for second order nonlinearity expression. As expected, when the beam goes in micro size, the stiffness value becomes up leading to further resistance and stability of the MMP against temperature. Depending on the type of thermal loading, the intensity of this additive trend is different. For the nonlinear variation of temperature, it can be observed that the increasing slope is steeper. However, this case for uniform variation is smoother. It should be pointed out that the microscale parameter has affected the thermal loading so that the increase of the parameter increments the difference in the results of three cases. Thus, it can be concluded that the type of thermal loading for a microscale beam is more significant than a macroscale one. It is obvious that the beam has the highest stability against the nonlinear case of temperature variation and the lowest stability to the uniform temperature variation. A comparison of the results of both ends supports brings us to this conclusion that the type of thermal loading at less flexible end conditions is further important. This is obtained due to the more difference between the three cases results at CC. Moreover, it is apparent that the clamped end support is more resistant than the simple one, and further thermal stability is seen for CC. It should be remembered that all results in this paper

are presented for the first mode number.

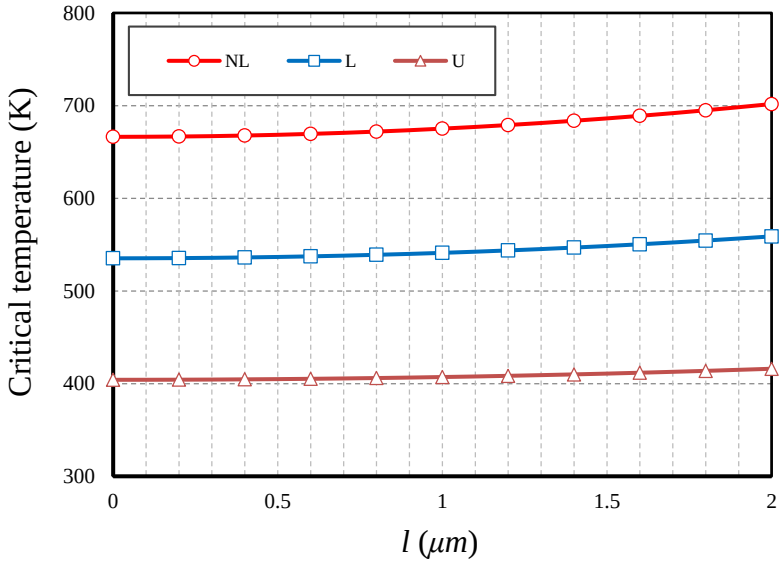

Fig. 4a. Microscale parameter vs. critical temperature for different cases of TD (Ψ=0.1A, L/h=20, SS)

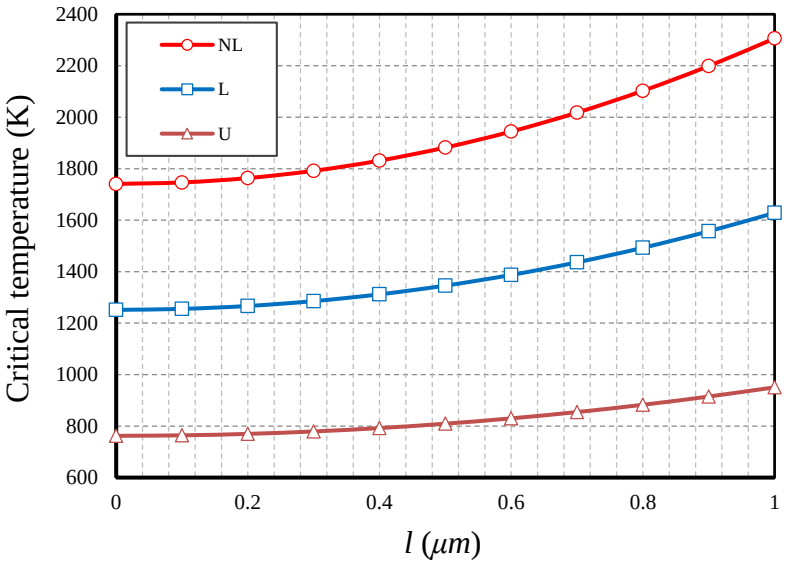

Fig. 4b. Microscale parameter vs. critical temperature for different cases of TD (Ψ=0.1A, L/h=20, CC)

5.2 Magnetic field effect

There are various reports on the effect of the magnetic field on micro and nanoscale smart

materials. But this study will, for the first time, investigate a microbeam in a magnetic field considering both the effects of piezomagnetic and flexomagnetic by the aid of Figures 5a and 5b. To examine the magnetic potential, we inspect the reverse effect of the magnetic field, from the external potential of zero to the potential value of one Ampere. In this section, similar to the previous section, two figures are presented for the boundary condition of simple and clamped, respectively, based on the three modes of thermal loading. By looking at both figures, we can see that the magnetic potential has a significant impact on the results of the critical buckling temperature, and this effect leads to an increase in the amount of stability of the material against thermal load when the potential is high. Interestingly, this incremental effect is not with the same slope in the three thermal loading items for both boundary conditions, and for the nonlinear thermal loading distribution, the results increase with a steeper slope.

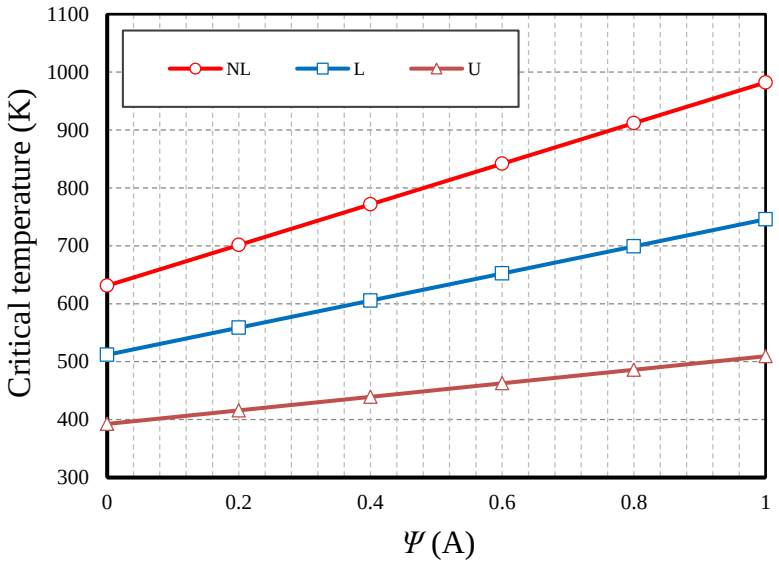

Fig. 5a. Magnetic parameter vs. critical temperature for different cases of TD (l=0.1 μm, L/h=20, SS)

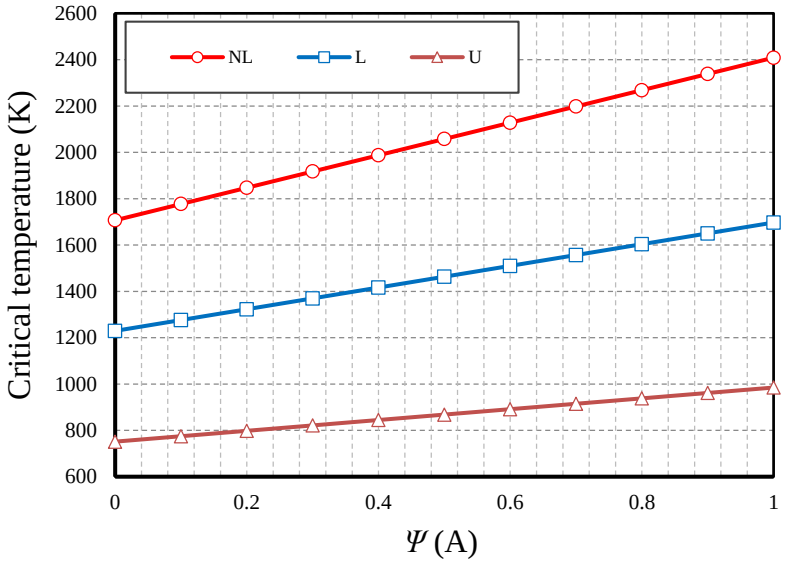

Fig. 5b. Magnetic parameter vs. critical temperature for different cases of TD (l=0.1 μm, L/h=20, CC)

5.3 Slenderness ratio effect

One of the necessary and influential parameters for designing beams and columns in mechanical engineering is the slenderness ratio of the beam. As a rule, this coefficient can also play an essential role in the design of beam-shaped micro sensors. Therefore, in this section, by presenting numerical results based on two Figures 6a and 6b, we will underestimate this coefficient in the current problem. The figures are for simple and clamped boundary conditions, respectively. All three cases of thermal loading are also considered in these two figures. It should be noted that the range of slenderness ratio variations is considered between 10 to 25, which is the range of a relatively thick to a thin beam. As can be seen, the greater the ratio of length to thickness of the beam, the lower the thermal stability of the micro sensor. This decrease in stability occurs in clamped boundary conditions with a steeper slope, which indicates that the beam with this boundary condition is more sensitive to the value of the slenderness coefficient. It can also be seen from the two figures that the larger the slenderness

ratio, the less important the type of thermal loading. This result is obtained due to reducing the difference between the results of the three thermal loading states by increasing the slenderness coefficient.

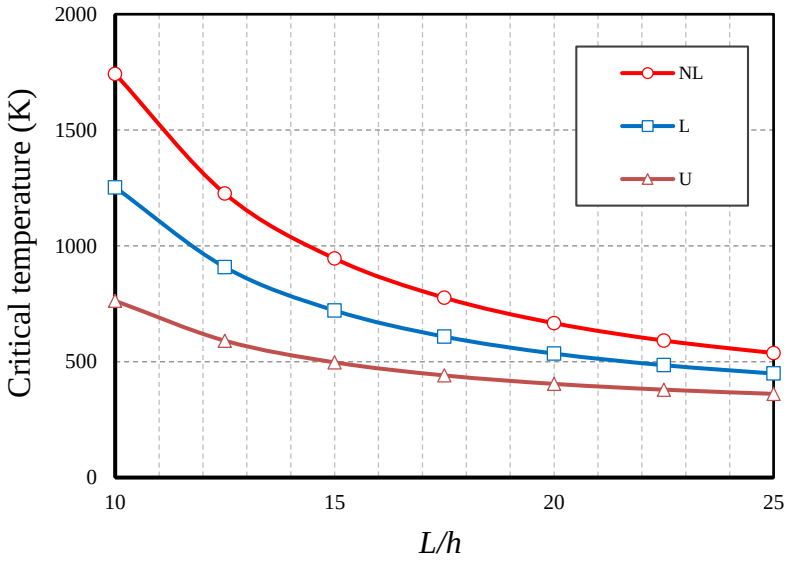

Fig. 6a. Slenderness ratio vs. critical temperature for different cases of TD (Ψ=0.1A, l=0.1 μm, SS)

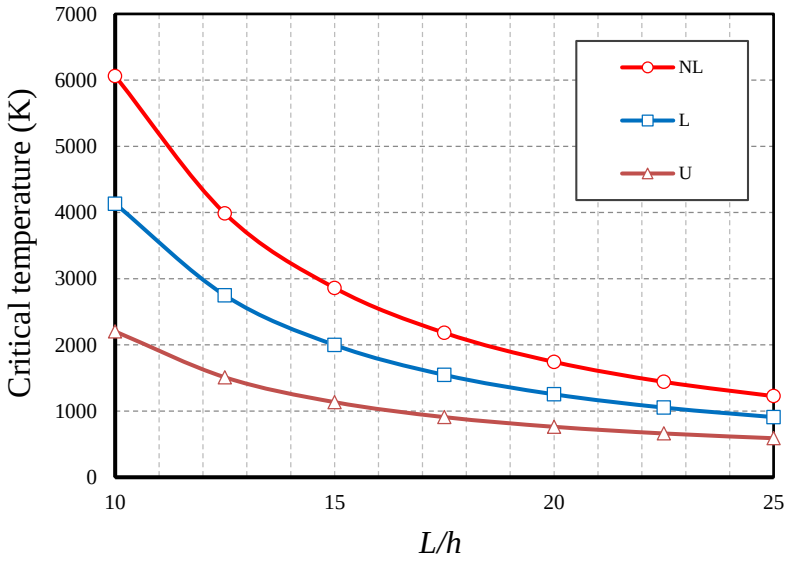

Fig. 6b. Slenderness ratio vs. critical temperature for different cases of TD (Ψ=0.1A, l=0.1 μm, CC)

5.4 Piezomagnetic-flexomagnetic effects

Comparing the mechanical behavior of a piezomagnetic-flexomagnetic microbeam (PFM) with an ordinary and normal microbeam (MB) can be interesting. In order to address this issue, this section was prepared, based on which four figures are presented. Figures 7a and 7b are prepared with micro parameter changes in the horizontal axis for the two boundary conditions of simple and clamp, respectively. However, the two Figures 8a and 8b are drawn by considering the changes of the magnetic potential in the horizontal axis and for the two boundary conditions of simple and clamp, respectively. The results for all three thermal loading cases were prepared separately for both smart and ordinary microbeams. From Figures 7a and 7b, it is quite clear that the biggest difference between the results of a smart beam with a normal beam is when the thermal loading is nonlinear in the direction of thickness and the smallest difference is related to the uniform thermal loading. This difference is more evident in the results of the two beams for the simple boundary condition. The examination of Figures 8a and 8b also proves this. From these two figures, it can be concluded that the higher the amount of external magnetic potential, the more important the smart beam will be, which can be understood from the increase in the difference between the results of the two beams with increasing the magnetic potential.

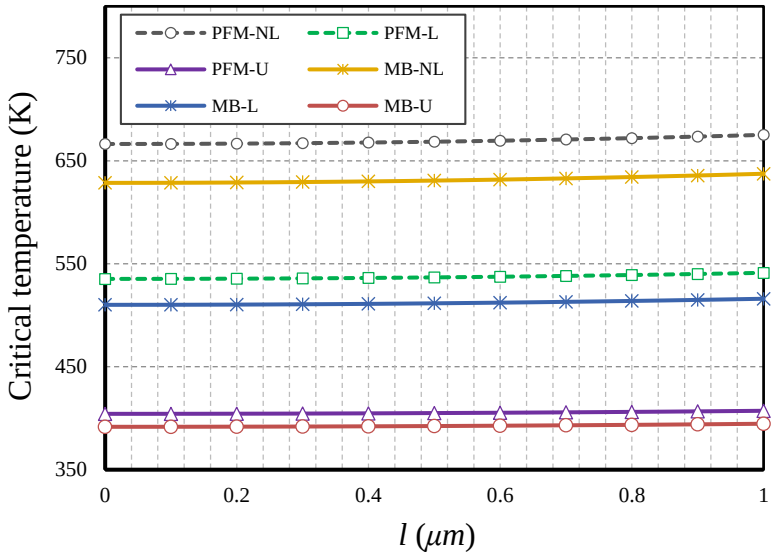

Fig. 7a. Microscale parameter vs. critical temperature for PFM effect (Ψ=0.1A, L/h=20, SS)

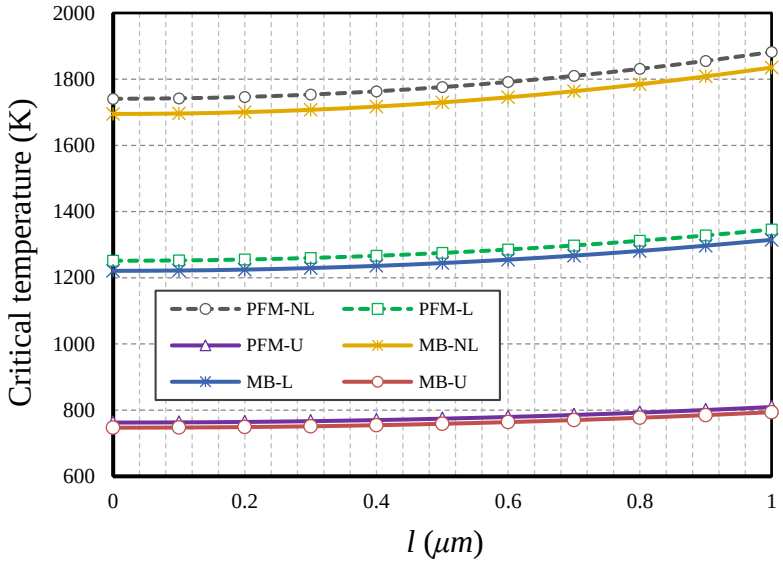

Fig. 7b. Microscale parameter vs. critical temperature for PFM effect (Ψ=0.1A, L/h=20, CC)

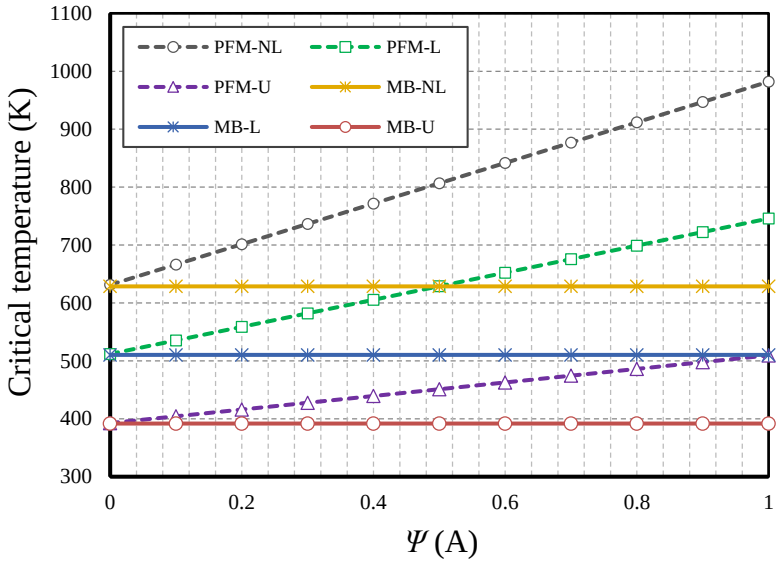

Fig. 8a. Magnetic parameter vs. critical temperature for PFM effect (l=0.1 μm, L/h=20, SS)

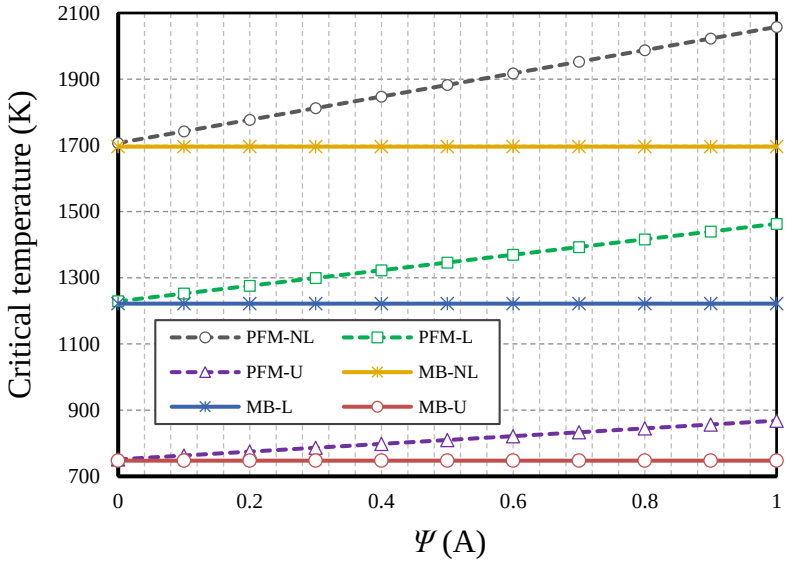

Fig. 8b. Magnetic parameter vs. critical temperature for PFM effect (l=0.1 μm, L/h=20, CC)

6 Conclusions

Herein we reported a distinct investigation on piezomagnetic-flexomagnetic micro size beam-shaped sensors on the basis of thin beam theory. In regard to the strain gradient theory, the microstructural effect was studied. The microbeam physical structure was defined based on magnetic micro particles. The constitutive equation, which is dominant on the problem, was

obtained by linear Lagrangian strain and the critical temperature was computed for clamped and simple end supports. The distribution of thermal loading in line with thickness was in linear, uniform, and nonlinear states. Influences of essential parameters were probed and some vital points were concluded, organized here as,

- The topmost thermal stability of microbeam is in the nonlinear case of thermal loading distribution and the lowermost for the uniform one.
- The higher the magnetic potential, the greater the critical temperature of buckling.
- The type of thermal loading distribution at CC boundary conditions is further significant than the SS one.
- For lengthy beam-shaped micro sensors, the effect of type of thermal loading distribution is insignificant.
- The importance of piezomagnetic-flexomagnetic properties is further while the thermal loading distribution is nonlinear.

Acknowledgements

V.A.E acknowledges the support of the Government of the Russian Federation (contract No. 14.Z50.31.0046).

References

[1] M. Mohammadabadi, A. R. Daneshmehr, M. Homayounfard, Size-dependent thermal buckling analysis of micro composite laminated beams using modified couple stress theory, International Journal of Engineering Science, 92 (2015) 47-62.

[2] O. Olsvik, T. Popovic, E. Skjerve, K. S. Cudjoe, E. Hornes, J. Ugelstad, M. Uhlén, Magnetic separation techniques in diagnostic microbiology, Clinical Microbiology Reviews,

7 (1994) 43-54.

[3] S. Berensmeier, Magnetic particles for the separation and purification of nucleic acids, Applied Microbiology and Biotechnology, 73 (2006) 495–504.

[4] M. Franzreb, M. Siemann-Herzberg, T. J. Hobley, O. R. T. Thomas, Protein purification using magnetic adsorbent particles, Applied Microbiology and Biotechnology, 70 (2006) 505-516.

[5] P. P. Freitas, R. Ferreira, S. Cardoso and F. Cardoso, Magnetoresistive sensors, Journal of Physics: Condensed Matter, 19 (2007) 165221.

[6] C. I. L. Justino, T. A. Rocha-Santos, A. C. Duarte, T. A. Rocha-Santos, Review of analytical figures of merit of sensors and biosensors in clinical applications, TrAC Trends in Analytical Chemistry, 29 (2010) 1172-1183.

[7] L. Chen, T. Wang, J. Tong, Application of derivatized magnetic materials to the separation and the preconcentration of pollutants in water samples, TrAC Trends in Analytical Chemistry, 30 (2011) 1095-1108.

[8] Y. Xu, E. Wang, Electrochemical biosensors based on magnetic micro/nano particles, Electrochimica Acta, 84 (2012) 62-73.

[9] M. Iranifam, Analytical applications of chemiluminescence-detection systems assisted by magnetic microparticles and nanoparticles, TrAC Trends in Analytical Chemistry, 51 (2013) 51-70.

[10] W. Fahrner, Nanotechnology and Nanoelectronics, 1st ed.; Springer, Germany, 2005; pp. 269.

[11] P. Lukashev, R. F. Sabirianov, Flexomagnetic effect in frustrated triangular magnetic structures, Physical Review B, 82 (2010) 094417.

[12] C. Pereira, A. M. Pereira, C. Fernandes, M. Rocha, R. Mendes, M. P. Fernández-García, A. Guedes, P. B. Tavares, J.-M. Grenèche, J. P. Araújo, and C. Freire, Superparamagnetic MFe_2O_4 (M = Fe, Co, Mn) Nanoparticles: Tuning the Particle Size and Magnetic Properties

through a Novel One-Step Coprecipitation Route, Chemistry of Materials, 24 (2012) 1496-1504.

[13] J. X. Zhang, R. J. Zeches, Q. He, Y. H. Chu, R. Ramesh, Nanoscale phase boundaries: a new twist to novel functionalities, Nanoscale, 4 (2012) 6196-6204.

[14] H. Zhou, Y. Pei, D. Fang, Magnetic field tunable small-scale mechanical properties of nickel single crystals measured by nanoindentation technique, Scientific Reports, 4 (2014) 1-6.

[15] S. Moosavi, S. Zakaria, C. H. Chia, S. Gan, N. A. Azahari, H. Kaco, Hydrothermal synthesis, magnetic properties and characterization of $CoFe_2O_4$ nanocrystals, Ceramics International, 43 (2017) 7889-7894

[16] E. A. Eliseev, A. N. Morozovska, V. V. Khist, V. Polinger, effective flexoelectric and flexomagnetic response of ferroics, In Recent Advances in Topological Ferroics and their Dynamics, Solid State Physics; Stamps, R. L., Schultheis, H.; Elsevier, Netherlands, 2019; Volume 70, pp. 237-289.

[17] A. F. Kabychenkov, F. V. Lisovskii, Flexomagnetic and flexoantiferromagnetic effects in centrosymmetric antiferromagnetic materials, Technical Physics, 64 (2019) 980-983.

[18] E. A. Eliseev, A. N. Morozovska, M. D. Glinchuk, R. Blinc, Spontaneous flexoelectric/flexomagnetic effect in nanoferroics, Physical Review B, 79 (2009) 165433.

[19] S. Sidhardh, M. C. Ray, Flexomagnetic response of nanostructures, Journal of Applied Physics, 124 (2018) 244101.

[20] N. Zhang, Sh. Zheng, D. Chen, Size-dependent static bending of flexomagnetic nanobeams, Journal of Applied Physics, 126 (2019) 223901.

[21] M. Malikan, V. A. Eremeyev, Free Vibration of Flexomagnetic Nanostructured Tubes Based on Stress-driven Nonlocal Elasticity. In Analysis of Shells, Plates, and Beams, 1st ed.; Altenbach, H., Chinchaladze, N., Kienzler R., Müller, W. H., Eds.; Springer Nature, Switzerland, 2020; Volume 134, pp. 215-226.

[22] M. Malikan, V. A. Eremeyev, On the geometrically nonlinear vibration of a piezo-flexomagnetic nanotube, Mathematical Methods in the Applied Sciences, (2020). https://doi.org/10.1002/mma.6758

[23] M. Malikan, V. A. Eremeyev, On nonlinear bending study of a piezo-flexomagnetic nanobeam based on an analytical-numerical solution, Nanomaterials, 10 (2020) 1-22. https://doi.org/10.3390/nano10091762

[24] M. Malikan, Nikolay S. Uglov, V. A. Eremeyev, On instabilities and post-buckling of piezomagnetic and flexomagnetic nanostructures, International Journal of Engineering Science, 157 (2020) Article no 103395.

[25] X. Song, S.-R. Li, Thermal buckling and post-buckling of pinned–fixed Euler–Bernoulli beams on an elastic foundation, Mechanics Research Communications, 34 (2007) 164–171.

[26] J. N. Reddy, Nonlocal nonlinear formulations for bending of classical and shear deformation theories of beams and plates, International Journal of Engineering Science, 48 (2010) 1507-1518.

[27] M. Malikan, V. A. Eremeyev, On the dynamics of a visco-piezo-flexoelectric nanobeam, Symmetry, 12 (2020) 643. doi: 10.3390/sym12040643

[28] M. Malikan, V. A. Eremeyev, Post-critical buckling of truncated conical carbon nanotubes considering surface effects embedding in a nonlinear Winkler substrate using the Rayleigh-Ritz method, Materials Research Express, 7 (2020) 025005.

[29] R. D. Mindlin, Second gradient of train and surface-tension in linear elasticity, International Journal of Solids and Strucutres, 1 (1965) 417-438.

[30] R. D. Mindlin, N. N. Eshel, On first strain-gradient theories in linear elasticity, International Journal of Solids and Strucutres, 4 (1968) 109-124.

[31] M. Akbarzadeh Khorshidi, The material length scale parameter used in couple stress theories is not a material constant, International Journal of Engineering Science, 133 (2018) 15-25.

[32] M. Malikan, Electro-mechanical shear buckling of piezoelectric nanoplate using modified couple stress theory based on simplified first order shear deformation theory, Applied Mathematical Modelling, 48 (2017) 196-207.

[33] A. Skrzat, V. A. Eremeyev, On the effective properties of foams in the framework of the couple stress theory, Continuum Mechanics and Thermodynamics. (2020). https://doi.org/10.1007/s00161-020-00880-6

[34] R. D. Mindlin, Micro-structure in linear elasticity, Archive for Rational Mechanics and Analysis, 16 (1964) 51-78.

[35] R. A. Toupin, Elastic materials with couple stresses, Archive for Rational Mechanics and Analysis, 11 (1962) 385-414.

[36] R. A. Toupin, Theories of elasticity with couple-stress, Archive for Rational Mechanics and Analysis, 17 (1964) 85-112.

[37] M. Rubin, P. Rosenau, O. Gottlieb, Continuum model of dispersion caused by an inherent material characteristic length, Journal of Applied physics, 77 (1995) 4054-4063.

[38] A. V. Metrikine, H. Askes, One-dimensional dynamically consistent gradient elasticity models derived from a discrete microstructures. Part 1: Generic formulation, European journal of mechanics – A/Solids., 21 (2002) 555-572.

[39] N. Radić, D. Jeremić, Thermal buckling of double-layered graphene sheets embedded in an elastic medium with various boundary conditions using a nonlocal new first-order shear deformation theory, Composites Part B: Engineering, 97 (2016) 201-215.

[40] A. M. Zenkour, M. Sobhy, Nonlocal elasticity theory for thermal buckling of nanoplates lying on Winkler–Pasternak elastic substrate medium, Physica E: Low-dimensional Systems and Nanostructures, 53 (2013) 251-259.

[41] M. Malikan, V. A. Eremeyev, A new hyperbolic-polynomial higher-order elasticity theory for mechanics of thick FGM beams with imperfection in the material composition, Composite Structures, 249 (2020) 112486.

[42] G. L. She, H. B. Liu, B. Karami, On resonance behavior of porous FG curved nanobeams, Steel and Composite Structures, 36 (2020) 179–186.

[43] J. B. Gunda, Thermal post-buckling & large amplitude free vibration analysis of Timoshenko beams: Simple closed-form solutions, Applied Mathematical Modelling, 38 (2014) 4548–4558.

[44] C. M. Wang, Y. Y. Zhang, S. Sudha Ramesh, S. Kitipornchai, Buckling analysis of micro- and nano-rods/tubes based on nonlocal Timoshenko beam theory, Journal of Physics D: Applied Physics, 39 (2006) 3904.

[45] S.C. Pradhan, G.K. Reddy, Buckling analysis of single walled carbon nanotube on Winkler foundation using nonlocal elasticity theory and DTM, Computational Materials Science, 50 (2011) 1052-1056.

[46] E. Pan, P. R. Heyliger, Exact solutions for magneto-electro-elastic laminates in cylindrical bending, International Journal of Solids and Structures, 40 (2003) 6859-6876.

[47] E. Pan, F. Han, Exact solution for functionally graded and layered magneto-electro-elastic plates, International Journal of Engineering Science, 43 (2005) 321-339.

[48] V. P. Senthil, J. Gajendiran, S. Gokul Raj, T. Shanmugavel, G. Ramesh Kumar, C. Parthasaradhi Reddy, Study of structural and magnetic properties of cobalt ferrite (CoFe2O4) nanostructures, Chemical Physics Letters, 695 (2018) 19-23.

[49] H. M. Ma, X.-L. Gao, J. N. Reddy, A microstructure-dependent Timoshenko beam model based on a modified couple stress theory, Journal of the Mechanics and Physics of Solids, 56 (2008) 3379-3391.

Postprint for: Malikan, M, Eremeyev, VA. Flexomagnetic response of buckled piezomagnetic composite nanoplates. Composite Structures. https://doi.org/10.1016/j.compstruct.2021.113932

Flexomagnetic response of buckled piezomagnetic composite nanoplates

Mohammad Malikan[1], Victor A. Eremeyev[1,2,3]*

[1] Department of Mechanics of Materials and Structures, Gdansk University of Technology,80-233 Gdansk, Poland,

[2] Research and Education Center "Materials" Don State Technical University, Gagarina sq., 1, 344000 Rostov on Don, Russia,

[3] DICAAR, Università degli Studi di Cagliari, Via Marengo, 2, 09123, Cagliari, Italy

*Corresponding author:
Email: victor.eremeev@pg.edu.pl, eremeyev.victor@gmail.com

Abstract

In this paper, the equation governing the buckling of a magnetic composite plate under the influence of an in-plane one-dimensional magnetic field, assuming the concept of flexomagnetic and considering the resulting flexural force and moment, is investigated for the first time by different analytical boundary conditions. To determine the equation governing the stability of the plate, the nonlocal strain gradient theory has been used by taking into account the classical plate theory. The axial magnetic force, which is originated from the magnetic field, is investigated. After extracting the governing differential equation, the critical

buckling load is obtained for different support conditions. The effect of nonlocal parameter, sheet aspect ratio and the effect of one-dimensional magnetic field on critical load are discussed. It was earned that if the nanoplate is rectangular so that the value of aspect ratio is less than one, the flexomagnetic response will be more noticeable.

Keywords: Composite plate; Flexomagnetic; Critical buckling load; Nonlocal strain gradient theory; Analytical solution

Symbols

H_x, H_y, H_z Magnetic field components
η_{xxz} Gradient of the axial strain
η_{yyz} Gradient of the lateral strain
σ_{xx} Axial stress component
σ_{yy} Lateral stress component
σ_{xy} Shear stress component
ε_{xx} Axial strain component
ε_{yy} Lateral strain component
ε_{xy} Shear strain component
ξ_{xxz} Hyper axial stress
ξ_{yyz} Hyper lateral stress
B_z Transverse magnetic flux component
U Strain energy
δ Symbol of variation
Ψ Magnetic potential
m Mode number
μ Nonlocal parameter
a Length of the plate
b Width of the plate
h Thickness of the plate
W Work done by external factors
u_1 Cartesian displacement along x axis
u_2 Cartesian displacement along y axis
u_3 Cartesian displacement along z axis
u Displacement of the midplane along x
v Displacement of the midplane along y
w Transverse displacement of the midplane
x, y, z Length, width, and thickness coordinates
$\bar{q}_{31}, \bar{q}_{15}$ Components of the third-order piezomagnetic tensor
g_{14}, g_{15} Components the sixth-order gradient elasticity tensor
f_{14}, f_{15} Components of fourth-order flexomagnetic
$\bar{d}_{11}, \bar{d}_{33}$ Components of the second-order magnetic permeability tensor
N_{xx}^0, N_{yy}^0, N_{xy}^0 Initial total in-plane axial force
ψ Initial Magnetic potential
X_m, Y_n Residues in the solution method
$\bar{C}_{11}, \bar{C}_{22}, \bar{C}_{12}, \bar{C}_{44}, \bar{C}_{66}$ Elasticity constants
l Length scale strain gradient parameter
T_{xxz}, T_{yyz} Hyper stress resultants
N_{xx}, N_{yy}, N_{xy} Axial stress resultants
M_{xx}, M_{yy}, M_{xy} Moment stress resultants

1 Introduction

The main characteristic of magneto-electro-elastic materials is the magneto-electric effect. This effect makes mechanical, electrical, and magnetic energies convertible to each other. Like the piezoelectric layers, magneto-elastic layers can be used to control the structure. Because, magneto-electro-elastic materials have the ability to convert energy between three electric, mechanical, and magnetic fields, these materials have direct applications in sensors and actuators, vibration control in structures, and so on. Their magneto-electro-elastic correlation occurs through stress-strain relationships. The difference is that the magneto-elastic layers can be controlled remotely by applying a magnetic field to the mechanical response of the structure.

Magnetic nanosheets (MNSs) are classified into small size particles handled by the aid of a magnetic field. These elements regularly include magnetic parts in the macro scale, for instance, cobalt, nickel, iron, and their mixtures. MNSs are commonly in the range of 5-500 nanometers in thickness or diameter. Many MNSs have recently been studied due to their marvelous potential features. Optical filters, catalysts consisting of nanoparticles, and semiconductors can be a few examples of using MNSs [1-6].

In response to mechanical impact, the magnetization and/or polarization can physically appear into materials as a result of flexo-effect. It is worth to underline that polarization leads to piezoelectric [7-15] or flexoelectric [16-31] effects and magnetization results in piezomagnetic [32-40] and flexomagnetic [41-47] impacts. The piezoelectric and piezomagnetic properties resulted from the elastic strain, but the flexoelectric and flexomagnetic come from the gradient of elastic strain. In a general definition, elastic stress gradient induces magnetization in centrosymmetric magnetic materials that this concept is described as the direct flexomagnetic effect which may be exhibited in a linear behavior. Reversely, the flexomagnetic effect occurs when the magnetic field gradient induces

magnetization in the material. The difference between piezomagnetic and flexomagnetic is not limited to the aforementioned content. Piezoelectric or piezomagnetic properties can appear in non-centrosymmetric crystallines only; however, flexomagneticity can exist in centrosymmetric structures but those without time inversion. The well-studied flexoelectricity is entirely similar to the flexomagneticity in this definition.

According to existing studies, it is observed that the flexomagnetic effect in two-dimensional media and for piezomagnetic sheets has never been studied. Not long ago, Sidhardh and Ray [41] and Zhang et al. [42] developed early studies on the flexomagnetic model of piezomagnetic nanosized one-dimensional (1D) beams. These researches presented a flexomagnetic model described by the Euler-Bernoulli thin beam approach evaluating bending properties of the material. They have applied small deformations based on the linear strains of Lagrangian. They have captured both direct and converse magnetization in regard to the one-dimensional magnetic field. To bend the beam, a uniform static force was loaded on the beam length. The load acted transversely. [41] investigated a beam with one end free and another one clamped so-called cantilever. Moreover, [42] considered several boundary conditions and showed a good evaluation in this regard. Both references include a deficiency in inspecting size and nonlocal effects. In fact, they did not figure out the effects of stress nonlocality that is significant in nanoscale. However, they have used surface effects to analyze size influences. Further growth of flexomagneticity returns to [43-47] in which the size-dependency behavior of flexomagneticity was confirmed fully. Malikan and Eremeyev [43] continued [41, 42] studies but with implementing stress-driven nonlocal elasticity while imposing the vibrational environment for the Euler-Bernoulli beam. Their formulation was performed based on the linear strains and their results were carried out by different diagrams. In another research, Malikan and Eremeyev [44] extended [43] for nonlinear natural

frequencies of a flexomagnetic model that existed in a piezomagnetic nanosized beam. In this work, the small-scale effect was fulfilled according to the nonlocal strain gradient elasticity approach. Besides the mentioned researches, in a benchmark study, Malikan and Eremeyev [45] investigated the static nonlinear bending of a piezomagnetic small size beam with the inclusion of flexomagneticity. They have combined Newton-Raphson iterative solution technique with the analytical Galerkin weighted residual method to calculate values of large deflections. Their brilliant results certified that the nonlinear bending analysis is severely applicable for the flexomagnetic response of a micro/nano-electromechanical system. Their conclusions acknowledged that the existence of flexomagnetic will lead to decreasing the deflections. Malikan et al. [46] kept up their studies in the category of flexomagneticity. This new research involved the response of post-buckling of a nanobeam containing both piezomagnetic and flexomagnetic features. Malikan et al. [47] studied the influence of porosities in several manners on an axially pressurized piezomagnetic nanoscale beam incorporating flexomagnetic effect. They have confirmed that some kinds of porosity can affect the material behavior of the flexomagnetic model.

In this research and in continuation of studies on the flexomagnetic effect, the biaxial buckling of a nanosized smart piezomagnetic composite sheet consisting of flexomagnetic property in the isotropic state has been investigated for the first time. The classical plate theory, linear magneto-elastic stress-strain law, and the nonlocal strain gradient theory have been used to calculate the biaxial stability of the nanosheet. The characteristic equation was derived using Hamilton's principle and Lagrangian strain considering von Kármán hypothesis. To make the numerical outputs further certain, our results are compared with the available molecular dynamics simulations in a simple case. Numerical results are presented analytically and graphically using the solution of the Galerkin integral method. Attempts have

been made to include two boundary conditions, clamped and simply-supported, in the evaluations.

2 The Problem Modeling

As shown in Figure 1, consider a piezomagnetic nanoplate with *a*, *b*, and *h* as its length, width, and thickness, respectively. The magneto-elastic material features are dedicated to this sheet. The plate is affected by the magnetic potential resulted from the one-dimensional magnetic field. The plate is supposed to be square/rectangular.

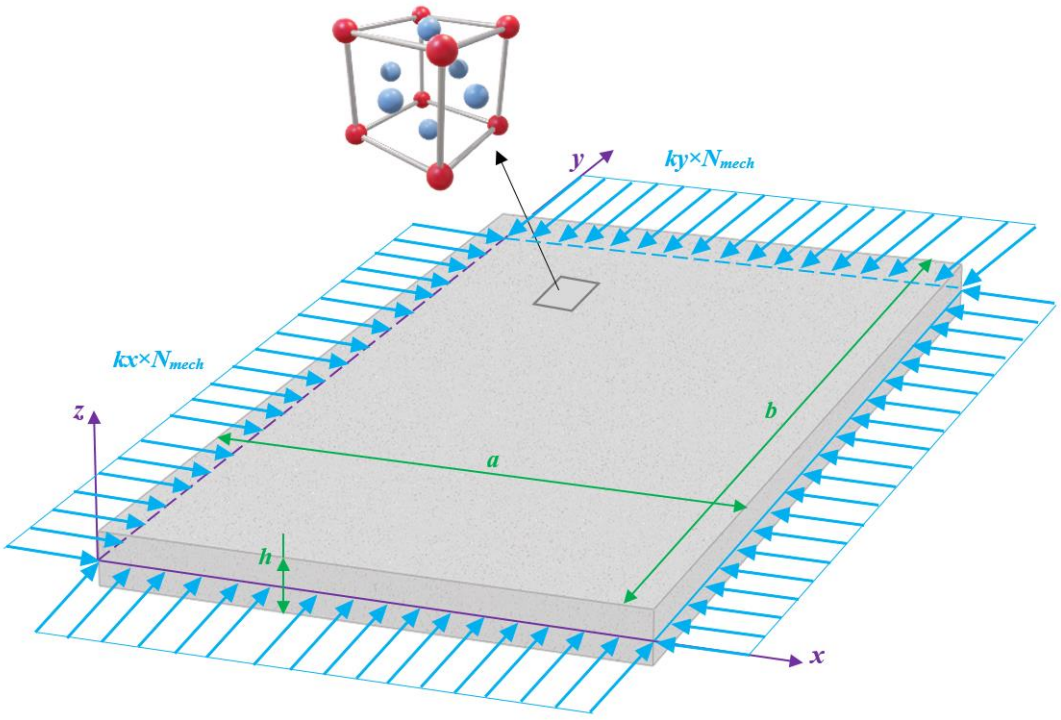

Figure 1. A square/non-square PM nanoscale plate compressed biaxially involving FM

The physical condition of the nanoplate is mathematically designed based on the classical plate theory. This is carried out as follows [48]

$$u_1(x,y,z) = u(x,y) - z\frac{\partial w(x,y)}{\partial x} \tag{1}$$

$$u_2(x,y,z) = v(x,y) - z\frac{\partial w(x,y)}{\partial y} \tag{2}$$

$$u_3(x,y,z) = w(x,y) \tag{3}$$

Using the equations of motion of the nanosheet according to the classical theory, and relations (1-3), the linear forms of strain-displacement equations are obtained in terms of non-zero displacement derivatives as follows

$$\varepsilon_{xx} = \frac{\partial u}{\partial x} - z\frac{\partial^2 w}{\partial x^2} \tag{4}$$

$$\varepsilon_{yy} = \frac{\partial v}{\partial y} - z\frac{\partial^2 w}{\partial y^2} \tag{5}$$

$$\varepsilon_{xy} = \frac{\partial u}{\partial y} + \frac{\partial v}{\partial x} - 2z\frac{\partial^2 w}{\partial x \partial y} \tag{6}$$

$$\eta_{xxz} = \frac{\partial \varepsilon_{xx}}{\partial z} = -\frac{\partial^2 w}{\partial x^2} \tag{7}$$

$$\eta_{yyz} = \frac{\partial \varepsilon_{yy}}{\partial z} = -\frac{\partial^2 w}{\partial y^2} \tag{8}$$

The constitutive relations that couple magneto-elastic properties can be expressed by tensor calculus as follows [41, 42]

$$\sigma_{ij} = C_{ijkl}\varepsilon_{kl} - q_{kij}H_k \tag{9}$$

$$\xi_{ijk} = g_{ij}\eta_{ijk} - f_{ij}H_k \tag{10}$$

$$B_i = q_{ikl}\varepsilon_{kl} + d_{ij}H_k + f_{ij}\eta_{ijk} \tag{11}$$

The Lagrangian variational principle can help find the equilibrium equations in the following

$$\delta U - \delta W = 0 \tag{12}$$

It is assumed that the magnetic field exists only in line with the transverse axis.

Therefore, the global form of the strain energy including magneto-elastic effects can be established as follows

$$\delta U = \int_V \left(\sigma_{xx}\delta\varepsilon_{xx} + \sigma_{yy}\delta\varepsilon_{yy} + +\sigma_{xy}\delta\varepsilon_{xy} + \xi_{xxz}\delta\eta_{xxz} + \xi_{yyz}\delta\eta_{yyz} - B_z\delta H_z \right) dV \tag{13}$$

Thus, as per the infinitesimal deformations, the integration by parts gives

$$\delta U = \delta\Pi_{U_1}^{Mech} + \delta\Pi_{U_1}^{Mag} + \delta\Pi_{U_2}^{Mech} + \delta\Pi_{U_2}^{Mag} \tag{14}$$

where

$$\delta\Pi_{U_1}^{Mech} = -\int_0^b \int_0^a \left[\begin{array}{l} \dfrac{\partial N_{xx}}{\partial x}\delta u + \dfrac{\partial N_{yy}}{\partial y}\delta v + \dfrac{\partial N_{xy}}{\partial x}\delta v + \dfrac{\partial N_{xy}}{\partial y}\delta u \\ + \left(\dfrac{\partial^2 M_{xx}}{\partial x^2} + \dfrac{\partial^2 M_{yy}}{\partial y^2} + 2\dfrac{\partial^2 M_{xy}}{\partial x \partial y} + \dfrac{\partial^2 T_{xxz}}{\partial x^2} + \dfrac{\partial^2 T_{yyz}}{\partial y^2} \right)\delta w \end{array} \right] dxdy \tag{15}$$

$$\delta\Pi_{U_1}^{Mag} = -\int_0^b \int_0^a \int_{-h/2}^{h/2} \frac{\partial B_z}{\partial z}\delta\Psi dz dx dy \tag{16}$$

$$\begin{array}{l} \delta\Pi_{U_2}^{Mech} = \left(\begin{array}{l} N_{xx}\delta u + N_{xy}\delta v - M_{xx}\dfrac{\partial \delta w}{\partial x} - \\ T_{xxz}\dfrac{\partial \delta w}{\partial x} + \dfrac{\partial M_{xx}}{\partial x}\delta w + \dfrac{\partial T_{xxz}}{\partial x}\delta w \end{array} \right)\Bigg|_0^a + \\ \left(\begin{array}{l} N_{yy}\delta v + N_{xy}\delta u - M_{yy}\dfrac{\partial \delta w}{\partial y} - \\ T_{yyz}\dfrac{\partial \delta w}{\partial y} + \dfrac{\partial M_{yy}}{\partial y}\delta w + \dfrac{\partial T_{yyz}}{\partial y}\delta w \end{array} \right)\Bigg|_0^b + 2M_{xy}\delta w\Big|_0^a\Big|_0^b \end{array} \tag{17}$$

$$\delta\Pi_{U_2}^{Mag} = \int_0^b \int_0^a \left(B_z\delta\Psi \right)\Big|_{-h/2}^{h/2} dxdy \tag{18}$$

The resultants of the biaxial in-plane forces, moment, and hyper stresses can be calculated by the below equations,

$$\left\{N_{xx}, N_{yy}, N_{xy}\right\} = \int_{-h/2}^{h/2} \left\{\sigma_{xx}, \sigma_{yy}, \sigma_{xy}\right\} dz \tag{19}$$

$$\left\{M_{xx}, M_{yy}, M_{xy}\right\} = \int_{-h/2}^{h/2} \left\{\sigma_{xx}, \sigma_{yy},, \sigma_{xy}\right\} z dz \tag{20}$$

$$\left\{T_{xxz}, T_{yyz}\right\} = \int_{-h/2}^{h/2} \left\{\xi_{xxz}, \xi_{yyz}\right\} dz \tag{21}$$

Due to the existence of outer loads, there would be thermodynamics work performed on the system. To determine it, we have,

$$W = -\frac{1}{2}\int_0^b \int_0^a \left\{ N_{xx}^0 \left(\frac{\partial w}{\partial x}\right)^2 + N_{yy}^0 \left(\frac{\partial w}{\partial y}\right)^2 + N_{xy}^0 \left(\frac{\partial^2 w}{\partial xy}\right)^2 \right\} dxdy \tag{22}$$

in which N_{xy}^0 shows shear in-plane force and is eliminated in this work. Hence,

$$\delta W = -\int_0^b \int_0^a \left\{ N_{xx}^0 \left(\frac{\partial w}{\partial x}\frac{\partial \delta w}{\partial x}\right) + N_{yy}^0 \left(\frac{\partial w}{\partial y}\frac{\partial \delta w}{\partial y}\right) \right\} dxdy \tag{23}$$

Let us rewrite the constitutive equation of the piezomagnetic nanoplate as follows,

$$\begin{Bmatrix} \sigma_{xx} \\ \sigma_{yy} \\ \tau_{xz} \\ \tau_{yz} \\ \tau_{xy} \end{Bmatrix} = \begin{bmatrix} \overline{C}_{11} & \overline{C}_{12} & 0 & 0 & 0 \\ \overline{C}_{12} & \overline{C}_{22} & 0 & 0 & 0 \\ 0 & 0 & \overline{C}_{44} & 0 & 0 \\ 0 & 0 & 0 & \overline{C}_{44} & 0 \\ 0 & 0 & 0 & 0 & \overline{C}_{66} \end{bmatrix} \begin{Bmatrix} \varepsilon_{xx} \\ \varepsilon_{yy} \\ \varepsilon_{xz} \\ \varepsilon_{yz} \\ \varepsilon_{xy} \end{Bmatrix} - \begin{bmatrix} 0 & 0 & \overline{q}_{31} \\ 0 & 0 & \overline{q}_{31} \\ \overline{q}_{15} & 0 & 0 \\ 0 & \overline{q}_{15} & 0 \\ 0 & 0 & 0 \end{bmatrix} \begin{Bmatrix} H_x \\ H_y \\ H_z \end{Bmatrix} \tag{24}$$

where

$$\tau_{xz} = \tau_{yz} = 0$$

In Eq. (24), the elastic and piezomagnetic properties of the nanoplate can be obtained using the following relations,

$$\begin{Bmatrix} \overline{C}_{11} \\ \overline{C}_{12} \\ \overline{C}_{44} \\ \overline{C}_{66} \end{Bmatrix} = \begin{Bmatrix} C_{11} - \dfrac{C_{13}^2}{C_{33}} \\ C_{12} - \dfrac{C_{13}^2}{C_{33}} \\ C_{44} \\ C_{66} \end{Bmatrix} \tag{25}$$

$$\begin{Bmatrix} \overline{q}_{31} \\ \overline{q}_{15} \end{Bmatrix} = \begin{Bmatrix} q_{31} - \dfrac{C_{13} q_{33}}{C_{33}} \\ q_{15} \end{Bmatrix} \tag{26}$$

And the constitutive equation of the flexomagneticity effect can be written as follows,

$$\begin{Bmatrix} \xi_{xxz} \\ \xi_{yyz} \\ \xi_{xzz} \\ \xi_{yzz} \\ \xi_{xyz} \end{Bmatrix} = \begin{bmatrix} 0 & 0 & g_{15} & 0 & 0 \\ 0 & 0 & 0 & g_{15} & 0 \\ g_{14} & g_{14} & 0 & 0 & 0 \end{bmatrix} \begin{Bmatrix} \eta_{xxz} \\ \eta_{yyz} \\ \eta_{xzz} \\ \eta_{yzz} \\ \eta_{xyz} \end{Bmatrix} - \begin{bmatrix} 0 & 0 & f_{14} \\ 0 & 0 & f_{14} \\ f_{15} & 0 & 0 \\ 0 & f_{15} & 0 \\ 0 & 0 & 0 \end{bmatrix} \begin{Bmatrix} H_x \\ H_y \\ H_z \end{Bmatrix} \tag{27}$$

in which

$$\eta_{xzz} = \eta_{yzz} = \eta_{xyz} = 0$$

$$\begin{Bmatrix} B_x \\ B_y \\ B_z \end{Bmatrix} = \begin{bmatrix} \overline{d}_{11} & 0 & 0 \\ 0 & \overline{d}_{11} & 0 \\ 0 & 0 & \overline{d}_{33} \end{bmatrix} \begin{Bmatrix} H_x \\ H_y \\ H_z \end{Bmatrix} + \begin{bmatrix} 0 & 0 & \overline{q}_{15} & 0 & 0 \\ 0 & 0 & 0 & \overline{q}_{15} & 0 \\ \overline{q}_{31} & \overline{q}_{31} & 0 & 0 & 0 \end{bmatrix} \begin{Bmatrix} \varepsilon_{xx} \\ \varepsilon_{yy} \\ \varepsilon_{xz} \\ \varepsilon_{yz} \\ \varepsilon_{xy} \end{Bmatrix} + \tag{28}$$

$$\begin{bmatrix} 0 & 0 & f_{15} & 0 & 0 \\ 0 & 0 & 0 & f_{15} & 0 \\ f_{14} & f_{14} & 0 & 0 & 0 \end{bmatrix} \begin{Bmatrix} \eta_{xxz} \\ \eta_{yyz} \\ \eta_{xzz} \\ \eta_{yzz} \\ \eta_{xyz} \end{Bmatrix}$$

in which

$$\varepsilon_{yz} = \varepsilon_{xz} = \eta_{xzz} = \eta_{yzz} = \eta_{xyz} = 0$$

$$\begin{Bmatrix} \bar{d}_{11} \\ \bar{d}_{33} \end{Bmatrix} = \begin{Bmatrix} d_{11} \\ d_{33} + \dfrac{q_{33}^2}{C_{33}} \end{Bmatrix} \tag{29}$$

The magnetic potential-component relationship can be expanded as follows,

$$H_k = \begin{Bmatrix} H_x \\ H_y \\ H_z \end{Bmatrix} = \begin{Bmatrix} -\dfrac{\partial \Psi}{\partial x} \\ -\dfrac{\partial \Psi}{\partial y} \\ -\dfrac{\partial \Psi}{\partial z} \end{Bmatrix} \tag{30}$$

To prescribe the electrical boundary conditions, one gets

$$\Psi\left(+\frac{h}{2}\right) = \psi, \ \Psi\left(-\frac{h}{2}\right) = 0 \tag{31}$$

The theoretical 1D magnetic field is supplemented by some mathematical efforts among Eqs. (18), (28), (30) and (31) as follows

$$\Psi = -\frac{\bar{q}_{31}}{2\bar{d}_{33}}\left(z^2 - \frac{h^2}{4}\right)\left(\frac{\partial^2 w}{\partial x^2} + \frac{\partial^2 w}{\partial y^2}\right) + \frac{\psi}{h}\left(z + \frac{h}{2}\right) \tag{32}$$

and then

$$H_z = z\frac{\bar{q}_{31}}{\bar{d}_{33}}\left(\frac{\partial^2 w}{\partial x^2} + \frac{\partial^2 w}{\partial y^2}\right) - \frac{\psi}{h} \tag{33}$$

Now it is possible to expand the stress field components, hyper stresses, and magnetic flux as follows

$$\begin{Bmatrix} \sigma_{xx} \\ \sigma_{yy} \\ \tau_{xy} \end{Bmatrix} = \begin{Bmatrix} \bar{C}_{11}\left(\dfrac{\partial u}{\partial x} - z\dfrac{\partial^2 w}{\partial x^2}\right) + \bar{C}_{12}\left(\dfrac{\partial v}{\partial y} - z\dfrac{\partial^2 w}{\partial y^2}\right) - \bar{q}_{31}\left(z\dfrac{\bar{q}_{31}}{\bar{d}_{33}}\left(\dfrac{\partial^2 w}{\partial x^2} + \dfrac{\partial^2 w}{\partial y^2}\right) - \dfrac{\psi}{h}\right) \\ \bar{C}_{12}\left(\dfrac{\partial u}{\partial x} - z\dfrac{\partial^2 w}{\partial x^2}\right) + \bar{C}_{22}\left(\dfrac{\partial v}{\partial y} - z\dfrac{\partial^2 w}{\partial y^2}\right) - \bar{q}_{31}\left(z\dfrac{\bar{q}_{31}}{\bar{d}_{33}}\left(\dfrac{\partial^2 w}{\partial x^2} + \dfrac{\partial^2 w}{\partial y^2}\right) - \dfrac{\psi}{h}\right) \\ \bar{C}_{66}\left(\dfrac{\partial u}{\partial y} + \dfrac{\partial v}{\partial x} - 2z\dfrac{\partial^2 w}{\partial x \partial y}\right) \end{Bmatrix} \tag{34}$$

$$\begin{Bmatrix}\xi_{xxz}\\ \xi_{yyz}\end{Bmatrix}=\begin{Bmatrix}-g_{14}\left(\dfrac{\partial^2 w}{\partial x^2}+\dfrac{\partial^2 w}{\partial y^2}\right)-f_{14}\left[z\dfrac{\bar{q}_{31}}{\bar{d}_{33}}\left(\dfrac{\partial^2 w}{\partial x^2}+\dfrac{\partial^2 w}{\partial y^2}\right)-\dfrac{\psi}{h}\right]\\ -g_{14}\left(\dfrac{\partial^2 w}{\partial x^2}+\dfrac{\partial^2 w}{\partial y^2}\right)-f_{14}\left[z\dfrac{\bar{q}_{31}}{\bar{d}_{33}}\left(\dfrac{\partial^2 w}{\partial x^2}+\dfrac{\partial^2 w}{\partial y^2}\right)-\dfrac{\psi}{h}\right]\end{Bmatrix} \tag{35}$$

$$B_z=\bar{d}_{33}\left[z\frac{\bar{q}_{31}}{\bar{d}_{33}}\left(\frac{\partial^2 w}{\partial x^2}+\frac{\partial^2 w}{\partial y^2}\right)-\frac{\psi}{h}\right]+\bar{q}_{31}\left(\frac{\partial u}{\partial x}-z\frac{\partial^2 w}{\partial x^2}+\frac{\partial v}{\partial y}-z\frac{\partial^2 w}{\partial y^2}\right)$$
$$-f_{14}\left(\frac{\partial^2 w}{\partial x^2}+\frac{\partial^2 w}{\partial y^2}\right) \tag{36}$$

Making the use of Eqs. (34-36), Eqs. (19-21) are re-written as follows

$$\begin{Bmatrix}N_{xx}\\ N_{yy}\\ N_{xy}\end{Bmatrix}=\begin{Bmatrix}A_{11}\dfrac{\partial u}{\partial x}+A_{12}\dfrac{\partial v}{\partial y}+\bar{q}_{31}\psi\\ A_{12}\dfrac{\partial u}{\partial x}+A_{22}\dfrac{\partial v}{\partial y}+\bar{q}_{31}\psi\\ A_{66}\left(\dfrac{\partial u}{\partial y}+\dfrac{\partial v}{\partial x}\right)\end{Bmatrix} \tag{37}$$

$$\begin{Bmatrix}M_{xx}\\ M_{yy}\\ M_{xy}\end{Bmatrix}=-\begin{Bmatrix}D_{11}\dfrac{\partial^2 w}{\partial x^2}+D_{12}\dfrac{\partial^2 w}{\partial y^2}\\ D_{12}\dfrac{\partial^2 w}{\partial x^2}+D_{22}\dfrac{\partial^2 w}{\partial y^2}\\ 2D_{66}\dfrac{\partial^2 w}{\partial x\partial y}\end{Bmatrix} \tag{38}$$

$$\begin{Bmatrix}T_{xxz}\\ T_{yyz}\end{Bmatrix}=\begin{Bmatrix}-g_{14}h\left(\dfrac{\partial^2 w}{\partial x^2}+\dfrac{\partial^2 w}{\partial y^2}\right)+f_{14}\psi\\ -g_{14}h\left(\dfrac{\partial^2 w}{\partial x^2}+\dfrac{\partial^2 w}{\partial y^2}\right)+f_{14}\psi\end{Bmatrix} \tag{39}$$

where

$$A_{ij}=\int_{-h/2}^{h/2}\bar{C}_{ij}dz\quad(i,j=1,2,4,6) \tag{40}$$

$$D_{ij} = \int_{-h/2}^{h/2} \left(\overline{C}_{ij} + \frac{\overline{-2}}{\overline{a}_{33}} \right) z^2 dz \quad (i, j = 1,2) \tag{41}$$

$$D_{66} = \int_{-h/2}^{h/2} \overline{C}_{66} z^2 dz \tag{42}$$

$$H_{14} = \int_{-h/2}^{h/2} g_{14} dz \tag{43}$$

Let us collect the terms in Eqs. (15) and (16) related to the governing equations, hence,

$$\frac{\partial N_{xx}}{\partial x} + \frac{\partial N_{xy}}{\partial y} = 0 \tag{44}$$

$$\frac{\partial N_{yy}}{\partial y} + \frac{\partial N_{xy}}{\partial x} = 0 \tag{45}$$

$$\frac{\partial^2 M_{xx}}{\partial x^2} + \frac{\partial^2 M_{yy}}{\partial y^2} + 2\frac{\partial^2 M_{xy}}{\partial x \partial y} + \frac{\partial^2 T_{xxz}}{\partial x^2} + \frac{\partial^2 T_{yyz}}{\partial y^2} + N_{xx}^0 \frac{\partial^2 w}{\partial x^2} + N_{yy}^0 \frac{\partial^2 w}{\partial y^2} = 0 \tag{46}$$

In the above equation, there are general biaxial compressive loads divided into two parts, mechanical and magnetic ones as follows,

$$N_{xx}^0 = k_x \times N^{Mech} + N^{Mag} \tag{47}$$

$$N_{yy}^0 = k_y \times N^{Mech} + N^{Mag} \tag{48}$$

Conforming to the Lorentz' law, one can write

$$N^{Mag} = q_{31} \psi \tag{49}$$

In mechanics, there are two general solutions to determine the strength behavior of nanostructures: 1- Laboratory methods and 2- Mathematical modeling. Since nanodimensional laboratory methods are expensive and have their own difficulties; Therefore, three main methods of mathematical modeling are considered, which are: a- Atomic modeling, b- Combined molecular and mechanical modeling, and c- Modeling based on continuum

mechanics. In terms of time constraints and the maximum number of atoms in the simulation, the first two methods are more expensive compared to modeling based on continuum mechanics, and also the unique relationships and formulations of the two methods are more complex. Therefore, this indicates that continuum mechanics can be used as a suitable solution to study physical phenomena in the field of nanotechnology.

One of the most important issues in the field of continuum mechanics is the discussion of the effects of size and its effect on the mechanical behavior of different materials. These effects will have a predominant impact on the mechanical behavior of matter when the particle size becomes very small, and theories based on classical continuum mechanics are unable to take such effects into account. This is especially evident in atomic space where the size of structures is not very large compared to the intra-atomic properties of materials. In fact, the effects of size occur due to the interaction of two scales of internal characteristic length such as distance between particles and external characteristic length such as crack length. One of the generalized theories of continuum mechanics that study such a phenomenon is the theory of nonlocal elasticity of the strain gradient [49].

$$\left\{1-\mu\left(\frac{\partial^2}{\partial x^2}+\frac{\partial^2}{\partial y^2}\right)\right\}\sigma_{ij}=C_{ijkl}\left\{1-l^2\left(\frac{\partial^2}{\partial x^2}+\frac{\partial^2}{\partial y^2}\right)\right\}\varepsilon_{kl} \tag{50}$$

In the absence of thickness effect ($\partial/\partial z$) on Eq. (50), Eqs. (37-39) shall be rewritten in terms of Eq. (50) as [50-55],

$$\left\{1-\mu\left(\frac{\partial^2}{\partial x^2}+\frac{\partial^2}{\partial y^2}\right)\right\}\begin{Bmatrix}N_{xx}\\N_{yy}\\N_{xy}\end{Bmatrix}=\left\{1-l^2\left(\frac{\partial^2}{\partial x^2}+\frac{\partial^2}{\partial y^2}\right)\right\}\begin{Bmatrix}A_{11}\dfrac{\partial u}{\partial x}+A_{12}\dfrac{\partial v}{\partial y}+\bar{q}_{31}\psi\\A_{12}\dfrac{\partial u}{\partial x}+A_{22}\dfrac{\partial v}{\partial y}+\bar{q}_{31}\psi\\A_{66}\left(\dfrac{\partial u}{\partial y}+\dfrac{\partial v}{\partial x}\right)\end{Bmatrix} \tag{51}$$

$$\left\{1-\mu\left(\frac{\partial^2}{\partial x^2}+\frac{\partial^2}{\partial y^2}\right)\right\}\begin{Bmatrix}M_{xx}\\M_{yy}\\M_{xy}\end{Bmatrix}=-\left\{1-l^2\left(\frac{\partial^2}{\partial x^2}+\frac{\partial^2}{\partial y^2}\right)\right\}\begin{Bmatrix}D_{11}\dfrac{\partial^2 w}{\partial x^2}+D_{12}\dfrac{\partial^2 w}{\partial y^2}\\D_{12}\dfrac{\partial^2 w}{\partial x^2}+D_{22}\dfrac{\partial^2 w}{\partial y^2}\\2D_{66}\dfrac{\partial^2 w}{\partial x\partial y}\end{Bmatrix} \tag{52}$$

$$\left\{1-\mu\left(\frac{\partial^2}{\partial x^2}+\frac{\partial^2}{\partial y^2}\right)\right\}\begin{Bmatrix}T_{xxz}\\T_{yyz}\end{Bmatrix}=\left\{1-l^2\left(\frac{\partial^2}{\partial x^2}+\frac{\partial^2}{\partial y^2}\right)\right\}\begin{Bmatrix}-H_{14}\left(\dfrac{\partial^2 w}{\partial x^2}+\dfrac{\partial^2 w}{\partial y^2}\right)+f_{14}\psi\\-H_{14}\left(\dfrac{\partial^2 w}{\partial x^2}+\dfrac{\partial^2 w}{\partial y^2}\right)+f_{14}\psi\end{Bmatrix} \tag{53}$$

If we compare the *x*-*y* in-plane magnetic field and deformations with those in line with thickness, then the in-plane derivatives can be eliminated. Thus, by means of Eqs. (46) and (51-53), the characteristic equation of buckling of the PM nanocomposite plate representing FM, can be simplified as follows,

$$\begin{aligned}&-\left(D_{11}+H_{14}+\mu N_{xx}^0\right)\frac{\partial^4 w}{\partial x^4}-\left[2D_{12}+4D_{66}+2H_{14}+\mu\left(N_{xx}^0+N_{yy}^0\right)\right]\\&\times\frac{\partial^4 w}{\partial x^2\partial y^2}-\left(D_{22}+H_{14}+\mu N_{yy}^0\right)\frac{\partial^4 w}{\partial y^4}+N_{xx}^0\frac{\partial^2 w}{\partial x^2}+N_{yy}^0\frac{\partial^2 w}{\partial y^2}+\\&l^2\left\{\begin{bmatrix}\left(D_{11}+H_{14}\right)\dfrac{\partial^6 w}{\partial x^6}+\left(D_{11}+2D_{12}+4D_{66}+3H_{14}\right)\dfrac{\partial^6 w}{\partial x^4\partial y^2}\end{bmatrix}\right.\\&\left.+\left(D_{22}+2D_{12}+4D_{66}+3H_{14}\right)\frac{\partial^6 w}{\partial x^2\partial y^4}+\left(D_{22}+H_{14}\right)\frac{\partial^6 w}{\partial y^6}\right\}=0\end{aligned} \tag{54}$$

3 Solving approach

3.1 Analytical process

The solution of Eq. (54) gives the numerical values of critical buckling loads for the PM-FM nanocomposite plate. This section supplements an analytical process in conjunction with the

two analytical boundary/edge conditions that are simply supported and clamped. The essential and natural edge conditions can be mentioned as follows,

Simply-supported (S):

$$w\,(0, y) = w\,(a, y) = 0 \tag{55a}$$

$$w\,(x, 0) = w\,(x, b) = 0 \tag{55b}$$

$$M_x\,(x, 0) = M_x\,(x, b) = 0 \tag{56a}$$

$$M_y\,(0, y) = M_y\,(a, y) = 0 \tag{56b}$$

Clamped (C):

$$w\,(0, y) = w\,(a, y) = 0 \tag{57a}$$

$$w\,(x, 0) = w\,(x, b) = 0 \tag{57b}$$

The closed-form approximate function is devoted to applying the analytical solution as follows,

$$w = \sum_{m=1}^{\infty}\sum_{n=1}^{\infty} W_{mn} X_m(x) Y_n(y) \tag{58}$$

The natural and essential conditions mentioned by Eqs. (55-57) can be satisfied by the next equation in which the admissible functions are demonstrated by Table 1 [33, 56],

$$\int_0^a \int_0^b \left(w \times X_m(x) Y_n(y)\right) dy dx \tag{59}$$

Table 1. Simply-supported and clamped analytical boundary conditions for plates

Analytical edge conditions						
Notation	$x=0$	$y=0$	$x=a$	$y=b$	$X_m(x)$	$Y_n(y)$
SSSS	S	S	S	S	$\sin\left(\frac{\pi}{a}x\right)$	$\sin\left(\frac{\pi}{b}y\right)$

CCCC	C	C	C	C	$\sin^2\left(\frac{\pi}{a}x\right)$	$\sin^2\left(\frac{\pi}{b}y\right)$

3.2 Solution validity

To validate the proposed model, the isotropic nanosheet without piezo-flexomagnetic properties is considered and its critical load is shown and tabulated in Table 2 for the values provided for the simple boundary conditions and various values of length and width. The solution method is tested through molecular dynamics [57] and a good agreement can be seen. E=1TPa, υ=0.3, h=0.34 nm, μ=1.85nm^2, l=0, β=a/b=1, k_1=1, k_2=1, SSSS [57]

Table 2. A fully simply-supported nanoplate compressed biaxially

Critical buckling load ($Pa.m$)		
Present (CPT)	MD [57]	a=b
1.1570	1.0837	4.99
0.6979	0.6536	8.080
0.4658	0.4331	10.77
0.2829	0.2609	14.65
0.1874	0.1714	18.51
0.1325	0.1191	22.35
0.0981	0.0889	26.22
0.0756	0.0691	30.04
0.0601	0.0554	33.85
0.0484	0.0449	37.81

4 Discussion and results

In this section, the importance of the flexomagnetic property will be evaluated in detail by changing important and key parameters, and we will find the conditions during which this effect manifests itself most. First, the magneto-elastic properties of the sheet are presented in Table 3 [33, 41, 42]. Variable parameters are expressed below each figure.

Table 3. Magneto-elastic constants for the proposed PM-FM $CoFe_2O_4$ nanoplate

C_{11}= C_{22}=226GPa, C_{12}=125GPa, C_{13}=124GPa,
C_{33}=216GPa, C_{44}=44.2GPa, C_{66}=50.5GPa,
f_{31}=10^{-9} N/A
q_{31}=290.1 N/A.m, q_{33}=349.9 N/A.m
d_{33}=83.5×10^{-6} N/A^2

The most important problem in terms of micro/nanoscale discussions is nothing but determining the amount of nonlocal and strain gradient length scale (SGLS) parameters. Some researchers found that these factors shall not have constant values and are dependent on several objects [58, 59]. In the case of SGLS, [59] indicated that geometrical sizes, particularly thickness has strongly affected the value of SGLS. However, in the matter of values of the nonlocal parameter, the effective factors influenced it, can be the type of boundary conditions. On that account, in this part, we realize the values of SGLS concerning the thickness of the plate and the values of the nonlocal parameter with reference to the previous works between 0-2 nm.

More importantly, in most figures, the behavior of the plate in the uniaxial compression mode is compared to that of the two-axis. The sheet will have an isotropic behavior and therefore no difference in the square state if the axial load of the uniaxial axis is longitudinal or lateral. Abbreviated terms such as PFM and PM define the sheet with piezomagnetic-flexomagnetic and piezomagnetic properties, respectively. Magnetic potential values are obtained in milli-Amperes, which in turn indicates the greater importance of the magnetic field at the nanoscale. The β parameter has also been used to determine the length to width ratio (aspect ratio).

Figures 2a and 2b show how changes in the SGLS will affect the flexomagnetic properties of the sheet. The first argument that the appearance of the two figures shows can be

the greater difference between PM and PFM results in uniaxial buckling. This means that if the magnetic sheet is subjected to in-plane loading of buckling in only one direction, its flexomagnetic property will be greater. As it turns out, the increasing slope of the critical load results from increasing the SGLS parameter for the CCCC boundary conditions is greater than the SSSS ones. This excess is also more obtained for uniaxial buckling. On the other hand, comparing the results of the two boundary conditions proves that the flexomagnetic effect is greater for the CCCC quadrilateral plate than the SSSS one. The last conclusion from these figures can be the impact of SGLS on the flexomagnetic response of the nanoplate. When l/h=0 which means we eliminate the SGLS, the PFM/PM result for the uniaxial case would be 1.069 and for l/h=1, it would be 1.070. These differences confirm that the larger the SGLS parameter values, the bit more emphasize the flexomagnetic property.

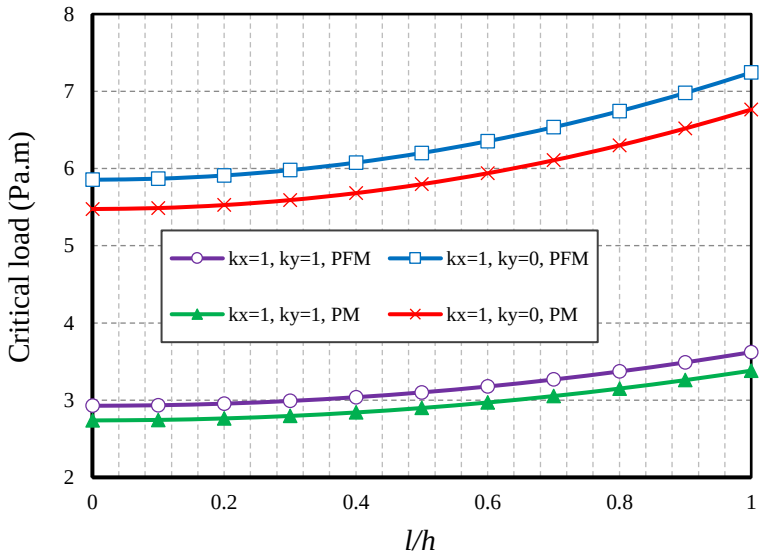

Fig. 2a. SGLS parameter vs. critical load of buckling (ψ=1mA, e_0a=1nm, β=1, b/h=15, CCCC)

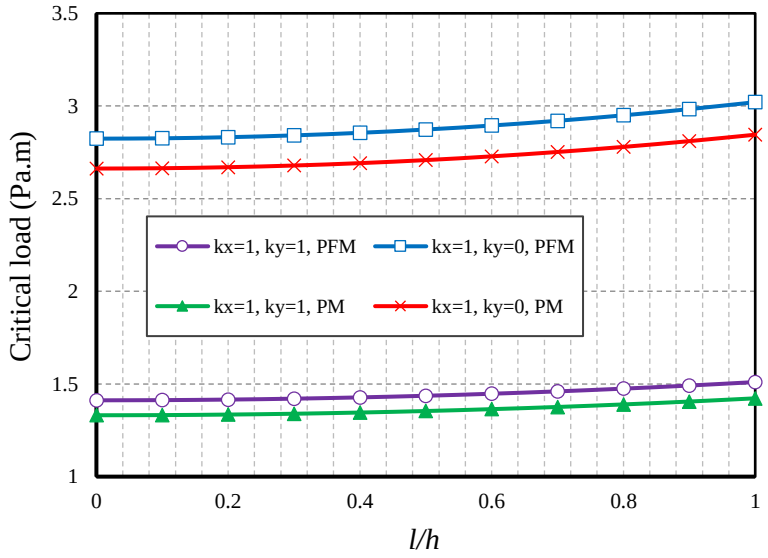

Fig. 2b. SGLS parameter vs. critical load of buckling (ψ=1mA, e_0a=1nm, β=1, b/h=15, SSSS)

After examining Figures 2a and 2b and obtaining some important results, with the help of Figures 3a and 3b we will investigate the effect of changes in the nonlocal parameter. The effect of this parameter, as has been proved many times, is a reducing effect on the stiffness of the material, and therefore increasing it here will lead to reducing the critical load. According to these two figures, we can say that if the numerical value of the nonlocal parameter is large, in both uniaxial and biaxial buckling, we will see the results of the PM and PFM approach to each other. As a result, it can be stated that nonlocality will have a considerable effect on flexomagnetic behavior. However, unlike the SGLS parameter, which has a positive effect on the flexomagnetic behavior of the sheet, the nonlocal parameter will have a negative effect and leads to less importance of this magneto-elastic property of the material.

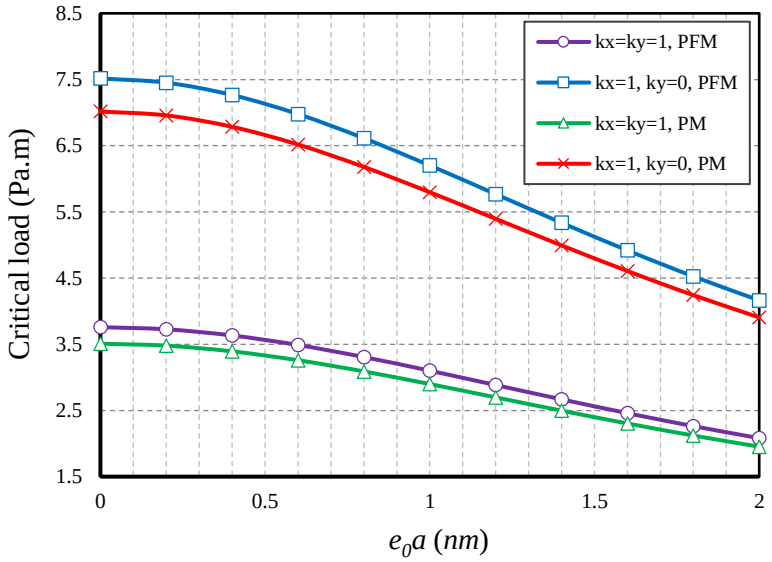

Fig. 3a. Nonlocal parameter vs. critical load of buckling in two states of magnetic (ψ=1mA, l=0.5h, b/h=15, β=1, CCCC)

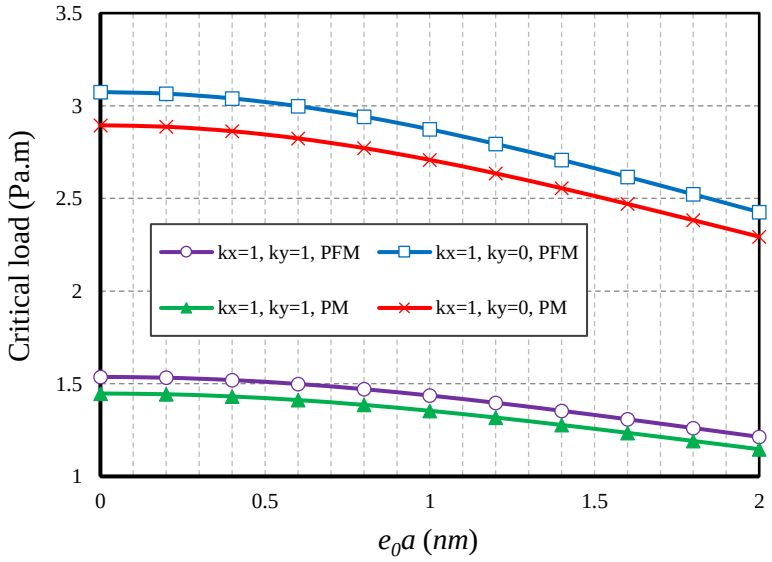

Fig. 3b. Nonlocal parameter vs. critical load of buckling in two states of magnetic (ψ=1mA, l=0.5h, b/h=15, β=1, SSSS)

Although the effect of the magnetic potential will be more predictable due to the application of a linear magnetic field, its study is not without merit. Figures 4a and 4b deal with this issue. By observing these two diagrams, it can be seen that if the sheet is subjected to

uniaxial buckling, it will be more affected by the magnetic field. In general, increasing the numerical values of the magnetic potential will increase the stiffness of the material, but this is more the case in uniaxial buckling than in the biaxial one. The interesting thing about these two figures is that if the potential of the magnetic field is negative, the critical load of the PM plate will be greater than that of the PFM sheet. As a result, the positive or negative potential of the magnetic field indicates that the PM or PFM material is stiffer.

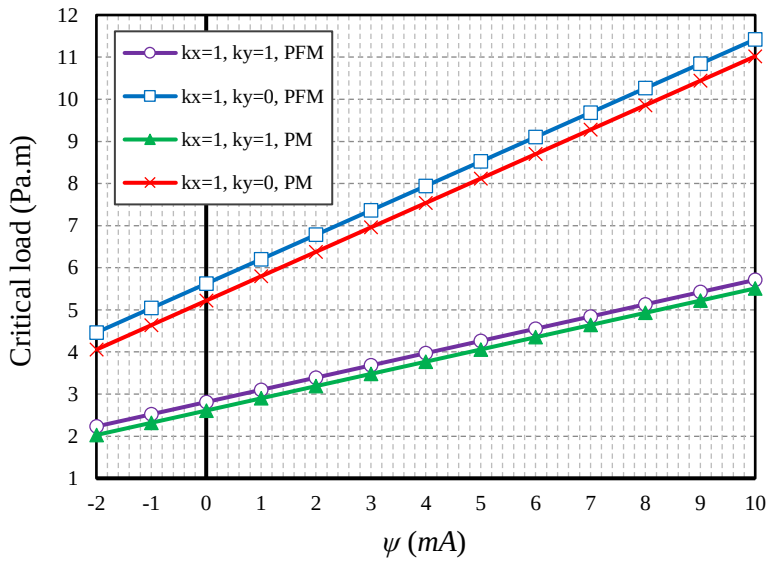

Fig. 4a. Magnetic potential vs. critical load of buckling in two states of magnetic (e_0a=1nm, l=0.5h, b/h=15, β=1, CCCC)

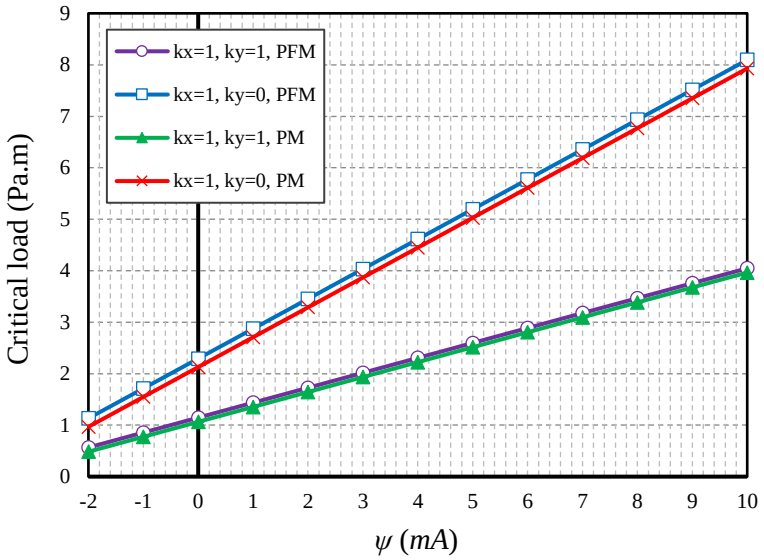

Fig. 4b. Magnetic potential vs. critical load of buckling in two states of magnetic (e_0a=1nm, l=0.5h, b/h=15, β=1, SSSS)

In the continuation of the discussion and results, we would like to examine the rectangularity of the sheet and its effect on the flexomagnetic response of the material. According to Figures 5a and 5b, we see that increasing the β coefficient leads to a reduction of the critical load and the overall stiffness of the material, which is true in both boundary conditions. But the most important result that can be found from these two figures is that in the case of a rectangular nanoplate, if the values of β are greater than 1, the results of PM are closer to the results of PFM, and this will increase with more amount of β. Rectangular nanosheets with a large value of β coefficient will not have a significant flexomagnetic effect. However, if the value of aspect ratio is less than 1, although the sheet is rectangular, the difference between the results of the PM plate and the PFM one is remarkable.

Figures 6a and 6b are plotted to examine the results of Figures 5a and 5b for uniaxial buckling. It is interesting that when the critical buckling load is applied uniaxially on the sheet, before β=1, the critical load has a decreasing behavior, but after β=1, the critical load results

will have an increasing trend. Perhaps the physical reason is that because the uniaxial critical load is applied along the x-axis, and since β greater than 1 means that the longitudinal dimension of the nanoplate is larger, then increasing the value of aspect ratio will increase the critical load.

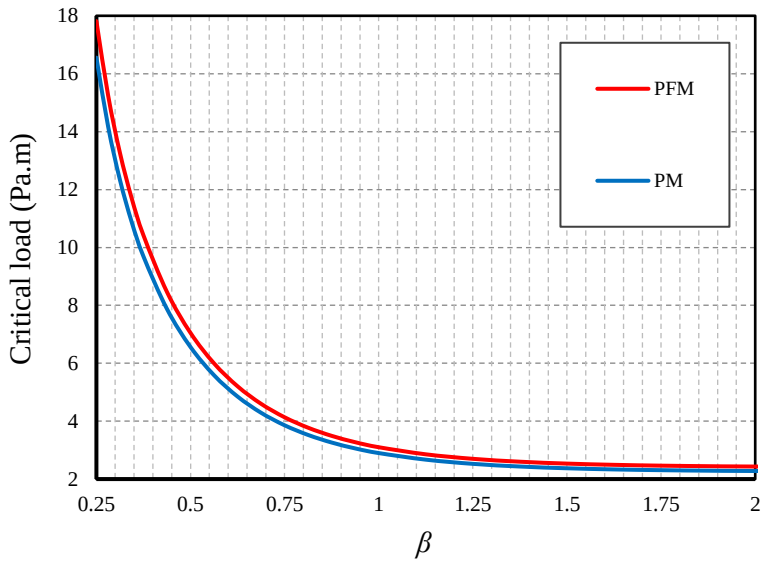

Fig. 5a. Aspect ratio vs. critical load of biaxial buckling in two states of magnetic (ψ=1mA, l=0.5h, e_0a=1nm, b/h=15, CCCC)

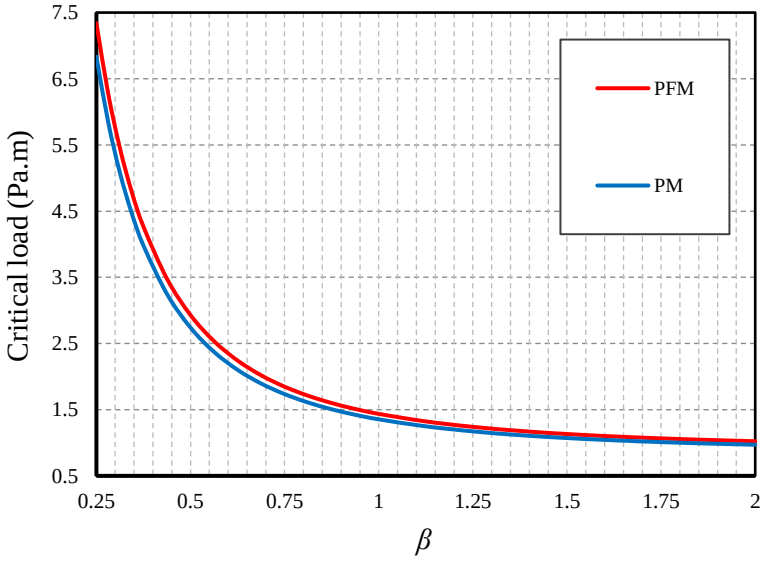

Fig. 5b. Aspect ratio vs. critical load of biaxial buckling in two states of magnetic (ψ=1mA, l=0.5h, e_0a=1nm, b/h=15, SSSS)

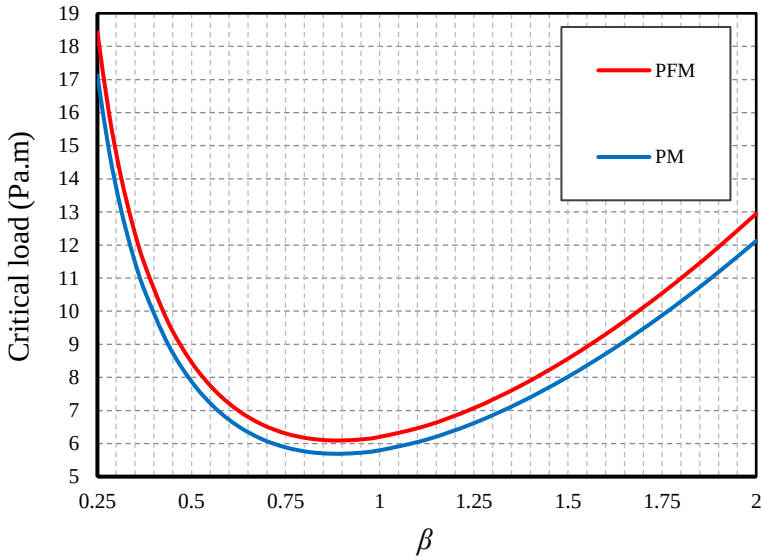

Fig. 6a. Aspect ratio vs. critical load of uniaxial buckling in two states of magnetic (ψ=1mA, l=0.5h, e_0a=1nm, b/h=15, k_x=1, k_y=0, CCCC)

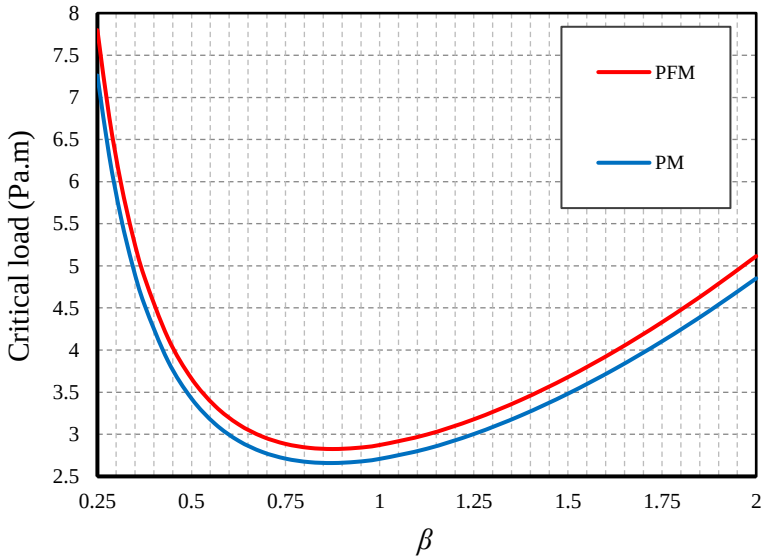

Fig. 6b. Aspect ratio vs. critical load of uniaxial buckling in two states of magnetic (ψ=1mA, l=0.5h, e_0a=1nm, b/h=15, k_x=1, k_y=0, SSSS)

5 Conclusions

A biaxial buckling analysis-based mathematical modeling was depicted for converse flexomagnetic influence on a piezomagnetic nanoparticle composition of cobalt and ferrite.

The equation of motion was obtained based on the classical plate theory and plane strain assumptions. And after the analytical solution of the equation, the analytical relation was obtained for the first mode of the buckling load of this sheet based on the clamped and simply-supported edge conditions. A MATLAB code was written to calculate the 2D domain flexomagneticity response. The following results are obtained by providing some examples and due to varying in values of fundamental parameters:

- The uniaxial buckling makes the flexomagnetic response of the nanoplate more notable.
- For the case of uniaxial buckling, the magnetic field has affected further the critical buckling load.
- In terms of biaxial buckling, while $\beta<1$, the flexomagnetic response is more obvious in contrast to $\beta>1$.
- Under uniaxial loading, whenever the nanoplate is rectangular and $\beta<1$, an increase of aspect ratio leads to softening and this is vice versa for rectangular nanoplate with $\beta>1$.

Data availability

The raw/processed data required to reproduce these findings cannot be shared at this time as the data also forms part of an ongoing study.

Acknowledgements

V.A.E acknowledges the support of the Government of the Russian Federation (contract No. 14.Z50.31.0046).

References

[1] A. H. Lu, W. Schmidt, N. Matoussevitch, H. Bönnemann, B. Spliethoff, B. Tesche, E.

Bill, W. Kiefer, F. Schüth, Nanoengineering of a Magnetically Separable Hydrogenation, Catalyst, Angewandte Chemie International, 43 (2004) 4303–4306.

[2] A. K. Gupta, M. Gupta, Synthesis and surface engineering of iron oxide nanoparticles for biomedical applications, Biomaterials, 26 (2005) 3995–4021.

[3] S. Mornet, S. Vasseur, F. Grasset, P. Verveka, G. Goglio, A. Demourgues, J. Portier, E. Pollert, E. Duguet, Magnetic nanoparticle design for medical applications, Progress in Solid State Chemistry, 34 (2006) 237-247.

[4] B. Gleich, J. Weizenecker, Tomographic imaging using the nonlinear response of magnetic particles, Nature, 435 (2005) 1214–1217.

[5] J. Philip, T. J. Kumar, P. Kalyanasundaram, B. Raj, Tunable Optical Filter, Measurement Science & Technology, 14 (2003) 1289–1294.

[6] C. Wang, M. Ge, J. Z. Jiang, Magnetic behavior of SnO2 nanosheets at room temperature, Applied Physics Letters, 97 (2010) 042510.

[7] Ch. Sun, J. Shi, X. Wang, Fundamental study of mechanical energy harvesting using piezoelectric nanostructures, Journal of Applied Physics, 108 (2010) 034309.

[8] X.-Q. Fang, J.-X. Liu, V. Gupta, Fundamental formulations and recent achievements in piezoelectric nano-structures: a review, Nanoscale, 5 (2013) 1716-1726.

[9] A. A. Girchenko, V. A. Eremeyev, N. F. Morozov, Modeling of spiral nanofilms with piezoelectric properties, Physical Mesomechanics, 14 (2011) 10-15.

[10] V. A. Eremeev, A.V. Nasedkin, Natural vibrations of nanodimensional piezoelectric

bodies with contact-type boundary conditions, Mechanics of Solids, 50 (2015) 495–507.

[11] J. Chróścielewski, R. Schmidt, V. A. Eremeyev, Nonlinear finite element modeling of vibration control of plane rod-type structural members with integrated piezoelectric patches, Continuum Mechanics and Thermodynamics, 31 (2019) 147–188.

[12] M. Malikan, Electro-mechanical shear buckling of piezoelectric nanoplate using modified couple stress theory based on simplified first order shear deformation theory, Applied Mathematical Modelling, 48 (2017) 196-207.

[13] M. Malikan, Temperature influences on shear stability of a nanosize plate with piezoelectricity effect, Multidiscipline Modeling in Materials and Structures, 14 (2018) 122-142.

[14] M. Malikan, Electro-thermal buckling of elastically supported double-layered piezoelectric nanoplates affected by an external electric voltage, Multidiscipline Modeling in Materials and Structures, 15 (2019) 50-78.

[15] H. M Sedighi, M. Malikan, A. Valipour, K. Kamil Żur, Nonlocal vibration of carbon/boron-nitride nano-hetero-structure in thermal and magnetic fields by means of nonlinear finite element method, Journal of Computational Design and Engineering, 7 (2020) 591–602.

[16] A. S. Yurkov, A. K. Tagantsev, Strong surface effect on direct bulk flexoelectric response in solids, Applied Physics Letters, 108 (2016) 022904.

[17] B. Wang, Y. Gu, S. Zhang, L.-Q. Chen, Flexoelectricity in solids: Progress, challenges, and perspectives, Progress in Materials Science, 106 (2019) 100570.

[18] L. Cross, Flexoelectric effects: charge separation in insulating solids subjected to elastic strain gradients, Journal of Materials Science, 41 (2006) 53–63.

[19] W. Ma, L. E. Cross, Observation of the flexoelectric effect in relaxor Pb ($Mg_{1/3}Nb_{2/3}$)O_3 ceramics, Applied Physics Letters,78 (2001) 2920–21.

[20] W. Ma, L. E. Cross, Flexoelectricity of barium titanate, Applied Physics Letters, 88 (2006) 232902.

[21] P. Zubko, G. Catalan, A. Buckley, P. R. L. Welche, J. F. Scott, Strain-gradient-induced polarization in SrTiO3 single crystals, Physical Review Letters, 99 (2007) 167601.

[22] V. A. Eremeyev, J.-F. Ganghoffer, V. Konopinska-Zmysłowska, N. S. Uglov, Flexoelectricity and apparent piezoelectricity of a pantographic micro-bar, International Journal of Engineering Science, 149 (2020) 103213.

[23] M. Esmaeili, Y. Tadi Beni, Vibration and Buckling Analysis of Functionally Graded Flexoelectric Smart Beam, Journal of Applied and Computational Mechanics, 5 (2019) 900-917. doi: 10.22055/jacm.2019.27857.1439

[24] M. Malikan, V. A. Eremeyev, On the Dynamics of a Visco–Piezo–Flexoelectric Nanobeam, Symmetry, 12 (2020) 643. https://doi.org/10.3390/sym12040643

[25] W. Ma, Flexoelectricity: strain gradient effects in ferroelectrics, Physica Scripta, T129 (2007) 180-183.

[26] D. Lee, A. Yoon, S. Y. Jang, J.-G. Yoon, J.-S. Chung, M. Kim, J. F. Scott, and T. W. Noh, Giant Flexoelectric Effect in Ferroelectric Epitaxial Thin Films, Physical Review Letters, 107 (2011) 057602.

[27] T. D. Nguyen, S. Mao, Y.-W. Yeh, P. K. Purohit, M. C. McAlpine, Nanoscale Flexoelectricity, Advanced Materials, 25 (2013) 946-974.

[28] P. Zubko, G. Catalan, A. K. Tagantsev, Flexoelectric Effect in Solids, Annual Review of Materials Research, 43 (2013) 387-421.

[29] P. V. Yudin, A. K. Tagantsev, Fundamentals of flexoelectricity in solids, Nanotechnology, 24 (2013) 432001.

[30] P. Zubko, G. Catalan, A. K. Tagantsev, Flexoelectric Effect in Solids, Annual Review of Materials Research, 43 (2013) 387–421.

[31] P. V. Yudin, A. K. Tagantsev, Fundamentals of flexoelectricity in solids, Nanotechnology, 24 (2013) 432001.

[32] M. Malikan, V. B. Nguyen, F. Tornabene, Electromagnetic forced vibrations of composite nanoplates using nonlocal strain gradient theory, Materials Research Express, 5 (2018) 075031.

[33] M. Malikan, V. B. Nguyen, Buckling analysis of piezo-magnetoelectric nanoplates in hygrothermal environment based on a novel one variable plate theory combining with higher-order nonlocal strain gradient theory, Physica E: Low-dimensional Systems and Nanostructures, 102 (2018) 8-28.

[34] M. Malikan, V. B. Nguyen, F. Tornabene, Damped forced vibration analysis of single-walled carbon nanotubes resting on viscoelastic foundation in thermal environment using nonlocal strain gradient theory, Engineering Science and Technology, an International Journal, 21 (2018) 778–786.

[35] M. Malikan, M. Krasheninnikov, V. A. Eremeyev, Torsional stability capacity of a nano-composite shell based on a nonlocal strain gradient shell model under a three-dimensional magnetic field, International Journal of Engineering Science, 148 (2020) 103210.

[36] P. Lukashev, R. F. Sabirianov, Flexomagnetic effect in frustrated triangular magnetic structures, Physical Review B, 82 (2010) 094417.

[37] E. A. Eliseev, A. N. Morozovska, V. V. Khist, V. Polinger, effective flexoelectric and flexomagnetic response of ferroics, In Recent Advances in Topological Ferroics and their Dynamics, Solid State Physics; Stamps, R. L., Schultheis, H.; Elsevier, Netherlands, 2019; Volume 70, pp. 237-289.

[38] A. F. Kabychenkov, F. V. Lisovskii, Flexomagnetic and flexoantiferromagnetic effects in centrosymmetric antiferromagnetic materials, Technical Physics, 64 (2019) 980-983.

[39] E. A. Eliseev, A. N. Morozovska, M. D. Glinchuk, R. Blinc, Spontaneous flexoelectric/flexomagnetic effect in nanoferroics, Physical Review B, 79 (2009) 165433.

[40] W. Fahrner, Nanotechnology and Nanoelectronics, 1st ed.; Springer, Germany, 2005; pp. 269.

[41] S. Sidhardh, M. C. Ray, Flexomagnetic response of nanostructures, Journal of Applied Physics, 124 (2018) 244101.

[42] N. Zhang, Sh. Zheng, D. Chen, Size-dependent static bending of flexomagnetic nanobeams, Journal of Applied Physics, 126 (2019) 223901.

[43] M. Malikan, V. A. Eremeyev, Free Vibration of Flexomagnetic Nanostructured Tubes Based on Stress-driven Nonlocal Elasticity. In Analysis of Shells, Plates, and Beams, 1st ed.; Altenbach, H., Chinchaladze, N., Kienzler R., Müller, W. H., Eds.; Springer Nature, Switzerland, 2020; Volume 134, pp. 215-226.

[44] M. Malikan, V. A. Eremeyev, On the geometrically nonlinear vibration of a piezo-flexomagnetic nanotube, Mathematical Methods in the Applied Sciences, (2020). https://doi.org/10.1002/mma.6758

[45] M. Malikan, V. A. Eremeyev, On nonlinear bending study of a piezo-flexomagnetic nanobeam based on an analytical-numerical solution, Nanomaterials, 10 (2020) 1-22. https://doi.org/10.3390/nano10091762

[46] M. Malikan, Nikolay S. Uglov, V. A. Eremeyev, On instabilities and post-buckling of piezomagnetic and flexomagnetic nanostructures, International Journal of Engineering Science, 157 (2020) Article no 103395.

[47] M. Malikan, V. A. Eremeyev, K. K. Żur, Effect of Axial Porosities on Flexomagnetic Response of In-Plane Compressed Piezomagnetic Nanobeams, Symmetry, 12 (2020) 1935.

[48] J. N. Reddy, Nonlocal nonlinear formulations for bending of classical and shear deformation theories of beams and plates, International Journal of Engineering Science, 48 (2010) 1507-1518.

[49] C. W. Lim, G. Zhang, J. N. Reddy, A Higher-order nonlocal elasticity and strain gradient theory and Its Applications in wave propagation, Journal of the Mechanics and Physics of Solids, 78 (2015) 298-313.

[50] G. L. She, H. B. Liu, B. Karami, On resonance behavior of porous FG curved nanobeams, Steel and Composite Structures, 36 (2020) 179–186.

[51] B. Karami, D. Shahsavari, M. Janghorban, L. Li, On the resonance of functionally graded nanoplates using bi-Helmholtz nonlocal strain gradient theory, International Journal of Engineering Science, 144 (2019) 103143.

[52] S. Esfahani, S. Esmaeilzade Khadem, A. Ebrahimi Mamaghani, Nonlinear vibration analysis of an electrostatic functionally graded nano-resonator with surface effects based on nonlocal strain gradient theory, International Journal of Mechanical Sciences, 151 (2019) 508-522.

[53] X. Xu, B. Karami, M. Janghorban, On the dynamics of nanoshells, International Journal

of Engineering Science, 158 (2021) 103431.

[54] M. Malikan, On the plastic buckling of curved carbon nanotubes, Theoretical and Applied Mechanics Letters, 10 (2020) 46-56.

[55] H. Sarparast, A. Ebrahimi-Mamaghani, M. Safarpour, H. M. Ouakad, R. Dimitri, F. Tornabene, Nonlocal study of the vibration and stability response of small-scale axially moving supported beams on viscoelastic-Pasternak foundation in a hygro-thermal environment, Mathematical Methods in the Applied Sciences, (2020). https://doi.org/10.1002/mma.6859

[56] M. Malikan, V. A. Eremeyev, A new hyperbolic-polynomial higher-order elasticity theory for mechanics of thick FGM beams with imperfection in the material composition, Composite Structures, 249 (2020) 112486.

[57] R. Ansari, S. Sahmani, Prediction of biaxial buckling behavior of single-layered graphene sheets based on nonlocal plate models and molecular dynamics simulations, Applied Mathematical Modelling, 37 (2013) 7338–7351.

[58] R. Ansari, S. Sahmani, B. Arash, Nonlocal plate model for free vibrations of single-layered graphene sheets, Physics Letters A, 375 (2010) 53-62.

[59] M. Akbarzadeh Khorshidi, The material length scale parameter used in couple stress theories is not a material constant, International Journal of Engineering Science, 133 (2018) 15-25.

Postprint for: Malikan, M, Eremeyev, VA. Effect of surface on the flexomagnetic response of ferroic composite nanostructures; nonlinear bending analysis. Composite Structures.
https://doi.org/10.1016/j.compstruct.2021.114179

Effect of surface on the flexomagnetic response of ferroic composite nanostructures; nonlinear bending analysis

Mohammad Malikan[1], Victor A. Eremeyev[1,2,3]*

[1] Department of Mechanics of Materials and Structures, Gdansk University of Technology, 80-233 Gdansk, Poland

[2] Research and Education Center "Materials" Don State Technical University, Gagarina sq., 1, 344000 Rostov on Don, Russia

[3] DICAAR, Università degli Studi di Cagliari, Via Marengo, 2, 09123, Cagliari, Italy

*Corresponding author:
Email: victor.eremeev@pg.edu.pl, eremeyev.victor@gmail.com

Abstract

Our analysis incorporates the geometrically nonlinear bending of the Euler-Bernoulli ferromagnetic nanobeam accounting for a size-dependent model through assuming surface effects. In the framework of the flexomagnetic phenomenon, the large deflections are investigated referring to von-Kármán nonlinearity. Employing the nonlocal effects of stress coupled to the gradient of strain generates a scale-dependent Hookean stress-strain scheme related to the small scale. Taking into account the supports of the nanobeam in two cases,

that is, totally fixed and hinged, the deformations are predicted. A constant static lateral load is postulated uniformly along the length of the beam, which forces the deformation. As the analysis is based on the one-dimensional media, the electrodes are embedded so that they give off a transverse magnetic field creating a longitudinal force. The newly developed mathematical model is computed by means of the differential quadrature method together with the Newton-Raphson technique. The computational section discusses and reveals the numerical results in detail for the characteristics and parameters involved in the design of beam-like magnetic nanosensors. As shown later, the conducted research presents that there is a strong linkage between the surface effect and the flexomagneticity behavior of the bulk.

Keywords: Flexomagnetic; Euler-Bernoulli beam; Surface effects; Nonlinear bending; Nonlocal strain gradient theory; Differential quadrature method

List of symbols

σ_{xx}	Stress component	u	Axial displacement of the midplane
ε_{xx}	Strain component	w	Transverse displacement of the midplane
C_{11}	Elasticity modulus	q_{31}	Component of the third-order *piezomagnetic* tensor
ν	Poisson's ratio	g_{31}	Component of the sixth-order gradient elasticity tensor
m	Mode number	f_{31}	Component of fourth-order flexomagnetic tensor
z	Thickness coordinate	a_{33}	Component of the second-order *magnetic permeability* tensor
I_z	Area moment of inertia	N^{Mag}	In-plane axial magnetic force
L	Length of the beam	A	Area of cross-section of the beam
ψ	Magnetic potential		
b	Width of the beam		
h	Thickness of the beam		

1 Introduction

Flexomagnetic coupling is between magnetic polarization and strain gradient or reversely,

elastic strain and magnetic field gradient. The perception of the flexomagnetic effect dates back to not-so-distant years, which can be a pervasive influence for all structures including symmetrical and nonsymmetrical crystals. However, studies of flexomagneticity in solids are rare in bulk samples due to the small amount of this effect. With the development of nanoscale technology, interest in flexomagnetic has renewed; because the large strain gradient is often manifested at the nanoscale, which leads to a strong flexomagnetic effect. One of the attractive applications of piezomagnetic is the extraction of energy from the mechanical vibrations of the environment in order to power micro-and nanodevices. However, piezomagnetic is limited to specific materials and is strongly influenced by temperature, which does not exist in flexomagnetic. This feature can be considered as a higher-order effect than piezomagneticity. The gradient size effect shows that the importance of the flexomagnetic effect in micro-and nanosystems is comparable to piezomagnetic and even beyond. In addition, flexomagnetic, unlike piezomagnetic, is found in any material with any symmetry. This means that compared to piezomagneticity, which is inefficient and invalid in materials with central symmetry, the effects of flexomagnetic are present in all biological materials and systems. These features have led to a growing interest and research in flexomagnetic in the last decade. As expected, in the future the effect of piezomagnetic on nanomotors and nano memory has important applications, the flexomagnetic effect may also play such an important role in the construction of these devices [1-9].

As a brief physical explanation of this effect, it can be mentioned that by bending a crystal, the atomic layers are stretched inside it, and it is clear that the outermost layer will have the most tension. A magnetic field can be created into the crystal due to movement of ions as a result of tension differences between the different layers. In other words, bending some materials creates a magnetic field, which is called flexomagnetism.

The effect of flexomagnetic in nanoscale should be considered and evaluated in light of several reasons, including [1-9]: a- Flexomagneticity is a pervasive property of any structural symmetry compared to piezomagnetic, and therefore expands the choice of materials that can be used for sensors and electro-magneto-mechanical actuators. b- Reduced dimensions lead to a larger strain gradient, meaning that the strain difference at smaller distances results in the larger strain gradient. The small scale is introduced in nanotechnology and therefore leads to an increase in the effect of flexomagnetism, which at the nanoscale can compete with piezomagnetism. c- A number of experiments have reported strong flexomagnetic coupling constants that are several times higher than theoretical estimates.

Utterly different properties can be revealed for body surfaces from those dedicated to the interior [10] on account of unalike environmental conditions. At very small sizes, the importance of surface property can be pivotally considerable owing to the high surface-to-volume ratio. In spite of the significance of surface effects at the mesoscale, it can be responsible as a size-dependent property. Gurtin and Murdoch [11, 12] posed a mathematical schema in terms of a continuum elasticity framework involving effects of the surface, where the surface was assumed as a virtual layer with zero thickness concerning a mathematical layer, in which the membrane has dissimilar material features and characteristics and underlying the layer as an entirely bonding with the bulk.

By an exact look at the literature, the extensity can be found in studies of surface effects phenomena with electro-magneto-elastic coupling [13-18]. However, study of the flexomagnetic effect does exist in none of them, and the need to examine it is quite obvious which merits an investigation between surface effect and flexomagneticity. Furthermore, mathematical studies on the impact of flexomagneticity on micro/nanostructures have been extended slowly hitherto [19-26]. Despite the attention to this issue in recent years,

flexomagnetism has still many questions, ambiguities, and unresolved issues. According to the literature, it was found and confirmed that the surface effects can strongly and directly affect the electro-magneto-elastic coupling in an electro-elastic nanomaterial. For this reason, we were persuaded to theoretically consider the surface effect on the flexomagneticity as a higher-order coupling effect in ferrite nanostructures. In this research, while re-introducing the flexomagnetic effect and the relations governing its static bending, theoretical discussions on the subject are presented considering the effect of the surface layer. Specifically, a theoretical explanation of the effect of the surface layer on the flexomagnetic effect is given and the reason for its importance in nanoscale systems is stated. Noted that the effects of surface residual stress are eliminated in this paper and the surface energy alone has been investigated. After explaining the physical model of the theory, the governing relations are solved using the numerical method of differential quadrature and specifically the Newton-Raphson method. Finally, the potential effects of the surface layer on the flexomagnetic effect are stated.

2 Mathematical Model

Regarding Fig. 1, the magnetic nanomaterial specimen in the form of a rectangular nanobeam with initial length L and height/thickness h is schematically discussed in an orthogonal coordinate system. The left-most end of the beam is postulated as the location of the rectangular coordinate system. Two flexible electrodes are covered and attached to the top and bottom transversal surfaces of the beam, which are connected to an ampere meter. These electrodes produce a lateral magnetic field.

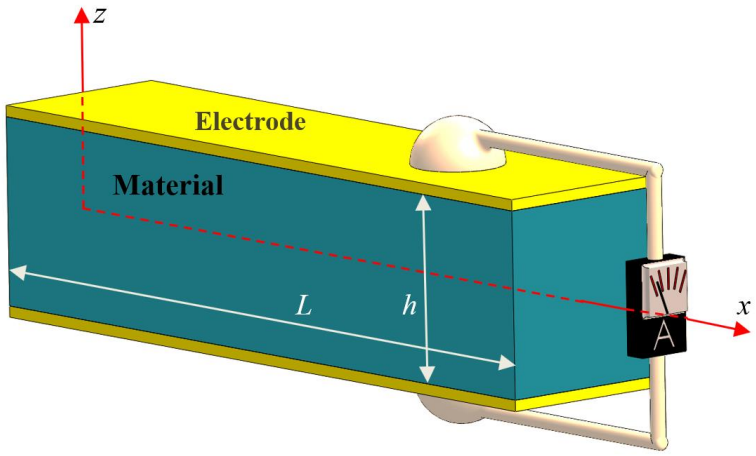

Fig. 1. A square magnetic material specimen connected to a magnetic system

The nonlocal strain gradient size-dependent model [27-36] has advantages in contrast to the Eringen's nonlocal elasticity theory [37-40] and coupled stress/strain gradient approaches [41-47] which contain one length scale factor only. Thus, the nonlinear nonlocal strain gradient static elasticity bending model of flexoferroic beam-like magnetic nanomaterial involving flexomagnetic effect is made available by use of [48]

$$C_{11}A\left[\frac{d^2u}{dx^2}+\frac{d^2w}{dx^2}\frac{dw}{dx}-l^2\left(\frac{d^4u}{dx^4}+\frac{d^4w}{dx^4}\frac{dw}{dx}+3\frac{d^3w}{dx^3}\frac{d^2w}{dx^2}\right)\right]=0 \tag{1}$$

$$-g_{31}h\frac{d^4w}{dx^4}+q_{31}\psi\frac{d^2w}{dx^2}-p-\mu\left(-g_{31}h\frac{d^6w}{dx^6}+q_{31}\psi\frac{d^4w}{dx^4}-\frac{d^2p}{dx^2}\right)$$
$$-\mu C_{11}A\left[\frac{du}{dx}+\frac{1}{2}\left(\frac{dw}{dx}\right)^2\right]\frac{d^4w}{dx^4}+C_{11}A\mu l^2\left[\frac{d^3u}{dx^3}+\frac{d^3w}{dx^3}\frac{dw}{dx}+\left(\frac{d^2w}{dx^2}\right)^2\right]\frac{d^4w}{dx^4}$$
$$-\mu C_{11}A\left(\frac{d^2u}{dx^2}+\frac{dw}{dx}\frac{d^2w}{dx^2}\right)\frac{d^3w}{dx^3}+C_{11}A\mu l^2\left(\frac{d^4u}{dx^4}+3\frac{d^3w}{dx^3}\frac{d^2w}{dx^2}+\frac{dw}{dx}\frac{d^4w}{dx^4}\right)\frac{d^3w}{dx^3}$$
$$-\mu C_{11}A\left(\frac{d^4u}{dx^4}+\frac{dw}{dx}\frac{d^4w}{dx^4}+3\frac{d^3w}{dx^3}\frac{d^2w}{dx^2}\right)\frac{dw}{dx}+C_{11}A\left[\frac{du}{dx}+\frac{1}{2}\left(\frac{dw}{dx}\right)^2\right]\frac{d^2w}{dx^2}$$
$$+C_{11}A\mu l^2\left(\frac{d^6u}{dx^6}+\frac{dw}{dx}\frac{d^6w}{dx^6}+5\frac{d^5w}{dx^5}\frac{d^2w}{dx^2}+10\frac{d^4w}{dx^4}\frac{d^3w}{dx^3}\right)\frac{dw}{dx}$$
$$-C_{11}Al^2\left[\frac{d^3u}{dx^3}+\frac{d^3w}{dx^3}\frac{dw}{dx}+\left(\frac{d^2w}{dx^2}\right)^2\right]\frac{d^2w}{dx^2}+C_{11}A\left(\frac{d^2u}{dx^2}+\frac{dw}{dx}\frac{d^2w}{dx^2}\right)\frac{dw}{dx}$$
$$-I_z\left(C_{11}+\frac{q_{31}^2}{a_{33}}\right)\left(\frac{d^4w}{dx^4}-l^2\frac{d^6w}{dx^6}\right)-C_{11}Al^2\left(\frac{d^4u}{dx^4}+3\frac{d^3w}{dx^3}\frac{d^2w}{dx^2}+\frac{dw}{dx}\frac{d^4w}{dx^4}\right)\frac{dw}{dx}=0 \tag{2}$$

Along with the longitudinal direction, the surface effect is important. This issue can be mathematically modeled by the following one-dimenional relation [49],

$$\sigma^S=C_{11}^S\varepsilon_{11}^S \tag{3}$$

in which C_{11}^S denotes the surface elasticity modulus which the value may be found either based on experiments or atomic simulations [50, 51]. Noted that, in this paper, the upper index *S* introduces constants relate to the surface layer.

The effective axial and flexural rigidities showed by Eq. (3) can be calculated as [52-56],

$$C_{11}^*I_z^*=C_{11}\frac{bh^3}{12}+C_{11}^S\left(\frac{bh^2}{2}+\frac{h^3}{6}\right) \tag{4}$$

Moreover, the effective magnetic properties can be written as follows,

$$f_{11}^{*} = f_{11} + f_{11}^{S} \tag{5}$$

$$q_{31}^{*} = q_{31} + q_{31}^{S} \tag{6}$$

$$a_{33}^{*} = a_{33} + a_{33}^{S} \tag{7}$$

Accounts for the surface effect, the governing differential equations which define the large deflections of the magnetic beam-like nanomaterial can be conducted as,

$$C_{11}^{*}A^{*}\left[\frac{d^2u}{dx^2}+\frac{d^2w}{dx^2}\frac{dw}{dx}-l^2\left(\frac{d^4u}{dx^4}+\frac{d^4w}{dx^4}\frac{dw}{dx}+3\frac{d^3w}{dx^3}\frac{d^2w}{dx^2}\right)\right]=0 \tag{8}$$

$$\begin{aligned}
&-g_{31}^{*}h\frac{d^4w}{dx^4}+q_{31}^{*}\psi\frac{d^2w}{dx^2}-p-\mu\left(-g_{31}^{*}h\frac{d^6w}{dx^6}+q_{31}^{*}\psi\frac{d^4w}{dx^4}-\frac{d^2p}{dx^2}\right)\\
&-\mu C_{11}^{*}A^{*}\left[\frac{du}{dx}+\frac{1}{2}\left(\frac{dw}{dx}\right)^2\right]\frac{d^4w}{dx^4}+C_{11}^{*}A^{*}\mu l^2\left[\frac{d^3u}{dx^3}+\frac{d^3w}{dx^3}\frac{dw}{dx}+\left(\frac{d^2w}{dx^2}\right)^2\right]\frac{d^4w}{dx^4}\\
&-\mu C_{11}^{*}A^{*}\left(\frac{d^2u}{dx^2}+\frac{dw}{dx}\frac{d^2w}{dx^2}\right)\frac{d^3w}{dx^3}+C_{11}^{*}A^{*}\mu l^2\left(\frac{d^4u}{dx^4}+3\frac{d^3w}{dx^3}\frac{d^2w}{dx^2}+\frac{dw}{dx}\frac{d^4w}{dx^4}\right)\frac{d^3w}{dx^3}\\
&-\mu C_{11}^{*}A^{*}\left(\frac{d^4u}{dx^4}+\frac{dw}{dx}\frac{d^4w}{dx^4}+3\frac{d^3w}{dx^3}\frac{d^2w}{dx^2}\right)\frac{dw}{dx}+C_{11}^{*}A^{*}\left[\frac{du}{dx}+\frac{1}{2}\left(\frac{dw}{dx}\right)^2\right]\frac{d^2w}{dx^2}\\
&+C_{11}^{*}A^{*}\mu l^2\left(\frac{d^6u}{dx^6}+\frac{dw}{dx}\frac{d^6w}{dx^6}+5\frac{d^5w}{dx^5}\frac{d^2w}{dx^2}+10\frac{d^4w}{dx^4}\frac{d^3w}{dx^3}\right)\frac{dw}{dx}-C_{11}^{*}A^{*}l^2\times\\
&\left[\frac{d^3u}{dx^3}+\frac{d^3w}{dx^3}\frac{dw}{dx}+\left(\frac{d^2w}{dx^2}\right)^2\right]\frac{d^2w}{dx^2}+C_{11}^{*}A^{*}\left(\frac{d^2u}{dx^2}+\frac{dw}{dx}\frac{d^2w}{dx^2}\right)\frac{dw}{dx}-I_z^{*}\left(C_{11}^{*}+\frac{q_{31}^{*2}}{a_{33}^{*}}\right)\\
&\times\left(\frac{d^4w}{dx^4}-l^2\frac{d^6w}{dx^6}\right)-C_{11}^{*}A^{*}l^2\left(\frac{d^4u}{dx^4}+3\frac{d^3w}{dx^3}\frac{d^2w}{dx^2}+\frac{dw}{dx}\frac{d^4w}{dx^4}\right)\frac{dw}{dx}=0
\end{aligned} \tag{9}$$

3 Solution of equations

Let us apply a superb, accurate, and convenient numerical solution method, namely, the differential quadrature method (DQM), to transfer the nonlinear differential equations

displayed by Eqs. (8, 9) into algebraic ones to advance the solution [57-66]. In comparison with other numerical techniques employed to solve complicated differential equations, such as finite difference, finite element, and dynamic relaxation, the differential quadrature technique provides low computational cost and simple procedure.

For a one-dimensional problem, the first-order derivative of variables is carried out as

$$\frac{du}{dx}\left(x_i\right)=\sum_{k=1}^{N}a_{ik}^{x}U\left(x_k\right),\quad i=1,2,...,N \tag{10a}$$

$$\frac{dw}{dx}\left(x_i\right)=\sum_{k=1}^{N}a_{ik}^{x}W\left(x_k\right),\quad i=1,2,...,N \tag{10b}$$

where the number of grid points along the axial direction is depicted by N. Moreover, a^{x} is expressed as follows,

$$\begin{cases} a_{ij}^{x}=\dfrac{R\left(x_i\right)}{\left(x_i-x_j\right)R\left(x_j\right)} & \text{for } i\neq j \\ a_{ii}^{x}=-\displaystyle\sum_{j=1,\neq i}^{N}a_{ij}^{x}, & i,j=1,2,...,N \end{cases} \tag{11}$$

in which

$$R\left(x_i\right)=\prod_{j=1,\neq i}^{N}\left(x_i-x_j\right) \tag{12}$$

In addition, higher-order derivatives can be written as

$$\frac{d^{(n)}u}{dx^{(n)}}\left(x_i\right)=\sum_{k=1}^{N}C_{ik}^{(n)}U\left(x_k\right) \tag{13a}$$

$$\frac{d^{(n)}w}{dx^{(n)}}\left(x_i\right)=\sum_{k=1}^{N}C_{ik}^{(n)}W\left(x_k\right) \tag{13b}$$

where $C^{(n)}$ shows a weighting equation which can be defined as follows,

$$C^{(1)} = a^x \tag{14}$$

$$\begin{cases} C_{ij}^{(n)} = n\left[a_{ij}^x C_{ii}^{(n-1)} - \dfrac{C_{ij}^{(n-1)}}{x_i - x_j} \right] & \text{for } i \neq j \\ C_{ii}^{(n)} = -\sum\limits_{j=1,\neq i}^{N} C_{ij}^{(n)}, \quad i, j = 1,2,...,N \end{cases} \tag{15}$$

Another issue that needs to be mentioned is how to mesh the beam. Different methods have been proposed for distributing nodes in the mesh network. The simplest type of meshing is the uniform distribution of nodes on the surface of the beam with equal distances. This type of meshing, although simple, is often less accurate (Fig. 2a). A high efficient mesh point can be obtained by embedding Chebyshev– Gauss–Lobatto relation as (Fig. 2b),

$$x_i = \frac{L}{2}\left(1 - \cos\left(\frac{i-1}{N-1}\pi\right)\right) \;\; ; \;\; i = 1,2,...,N \tag{16}$$

In fact, this type of meshing leads to more stability of the equations and the speed of convergence of the results.

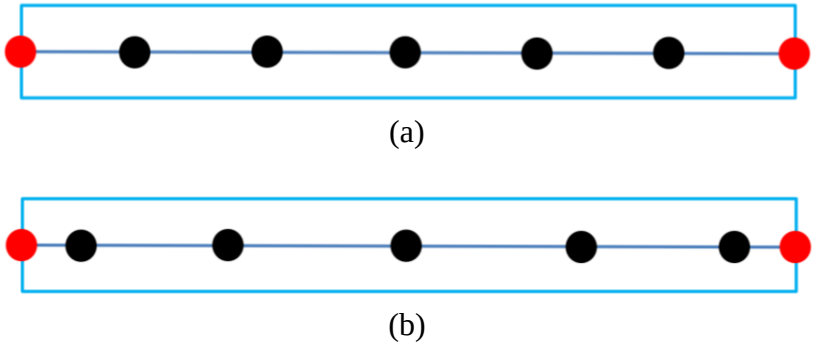

(a)

(b)

Fig. 2a. Uniform points distribution, **2b.** Chebyshev– Gauss–Lobatto points distribution (assume N=7 grid points for the beam, the red points relate to the boundary conditions)

Implementation of the DQM presents Eqs. (8, 9) in the following scheme,

$$C_{11}^{*}A^{*}\left[\sum_{k=1}^{N}C_{ik}^{(2)}U\left(x_k\right)+\sum_{k=1}^{N}C_{ik}^{(2)}W\left(x_k\right)\times\sum_{k=1}^{N}C_{ik}^{(1)}W\left(x_k\right)-l^2\times\left(\sum_{k=1}^{N}C_{ik}^{(4)}U\left(x_k\right)\right.\right.$$
$$\left.\left.+\sum_{k=1}^{N}C_{ik}^{(4)}W\left(x_k\right)\times\sum_{k=1}^{N}C_{ik}^{(1)}W\left(x_k\right)+3\times\sum_{k=1}^{N}C_{ik}^{(3)}W\left(x_k\right)\times\sum_{k=1}^{N}C_{ik}^{(2)}W\left(x_k\right)\right)\right]=0 \tag{17}$$

$$-g_{31}^{*}h\sum_{k=1}^{N}C_{ik}^{(4)}W\left(x_k\right)+q_{31}^{*}\psi\sum_{k=1}^{N}C_{ik}^{(2)}W\left(x_k\right)-p-\mu\left(-g_{31}^{*}h\sum_{k=1}^{N}C_{ik}^{(6)}W\left(x_k\right)+q_{31}^{*}\psi\sum_{k=1}^{N}C_{ik}^{(4)}W\left(x_k\right)\right)+$$
$$\mu\frac{d^2p}{dx^2}-\mu C_{11}^{*}A^{*}\left[\sum_{k=1}^{N}C_{ik}^{(1)}U\left(x_k\right)+\frac{1}{2}\left(\sum_{k=1}^{N}C_{ik}^{(1)}W\left(x_k\right)\right)^2\right]\times\sum_{k=1}^{N}C_{ik}^{(4)}W\left(x_k\right)+C_{11}^{*}A^{*}\mu l^2\left[\sum_{k=1}^{N}C_{ik}^{(3)}U\left(x_k\right)\right.$$
$$\left.+\sum_{k=1}^{N}C_{ik}^{(3)}W\left(x_k\right)\times\sum_{k=1}^{N}C_{ik}^{(1)}W\left(x_k\right)+\left(\sum_{k=1}^{N}C_{ik}^{(2)}W\left(x_k\right)\right)^2\right]\times\sum_{k=1}^{N}C_{ik}^{(4)}W\left(x_k\right)-\mu C_{11}^{*}A^{*}\left(\sum_{k=1}^{N}C_{ik}^{(2)}U\left(x_k\right)+\right.$$
$$\left.\sum_{k=1}^{N}C_{ik}^{(1)}W\left(x_k\right)\times\sum_{k=1}^{N}C_{ik}^{(2)}W\left(x_k\right)\right)\times\sum_{k=1}^{N}C_{ik}^{(3)}W\left(x_k\right)+C_{11}^{*}A^{*}\mu l^2\left(\sum_{k=1}^{N}C_{ik}^{(4)}U\left(x_k\right)+3\sum_{k=1}^{N}C_{ik}^{(3)}W\left(x_k\right)\times\right.$$
$$\left.\sum_{k=1}^{N}C_{ik}^{(2)}W\left(x_k\right)+\sum_{k=1}^{N}C_{ik}^{(1)}W\left(x_k\right)\times\sum_{k=1}^{N}C_{ik}^{(4)}W\left(x_k\right)\right)\times\sum_{k=1}^{N}C_{ik}^{(3)}W\left(x_k\right)-\mu C_{11}^{*}A^{*}\left(\sum_{k=1}^{N}C_{ik}^{(4)}U\left(x_k\right)+\right.$$
$$\left.\sum_{k=1}^{N}C_{ik}^{(1)}W\left(x_k\right)\times\sum_{k=1}^{N}C_{ik}^{(4)}W\left(x_k\right)+3\times\sum_{k=1}^{N}C_{ik}^{(3)}W\left(x_k\right)\times\sum_{k=1}^{N}C_{ik}^{(2)}W\left(x_k\right)\right)\times\sum_{k=1}^{N}C_{ik}^{(1)}W\left(x_k\right)+C_{11}^{*}A^{*}\times$$
$$\left[\sum_{k=1}^{N}C_{ik}^{(1)}U\left(x_k\right)+\frac{1}{2}\left(\sum_{k=1}^{N}C_{ik}^{(1)}W\left(x_k\right)\right)^2\right]\times\sum_{k=1}^{N}C_{ik}^{(2)}W\left(x_k\right)+C_{11}^{*}A^{*}\mu l^2\left(\sum_{k=1}^{N}C_{ik}^{(6)}U\left(x_k\right)+\sum_{k=1}^{N}C_{ik}^{(1)}W\left(x_k\right)\right.$$
$$\left.\times\sum_{k=1}^{N}C_{ik}^{(6)}W\left(x_k\right)+5\times\sum_{k=1}^{N}C_{ik}^{(5)}W\left(x_k\right)\times\sum_{k=1}^{N}C_{ik}^{(2)}W\left(x_k\right)+10\times\sum_{k=1}^{N}C_{ik}^{(4)}W\left(x_k\right)\times\sum_{k=1}^{N}C_{ik}^{(3)}W\left(x_k\right)\right)$$
$$\times\sum_{k=1}^{N}C_{ik}^{(1)}W\left(x_k\right)-C_{11}^{*}A^{*}l^2\times\left[\sum_{k=1}^{N}C_{ik}^{(3)}U\left(x_k\right)+\sum_{k=1}^{N}C_{ik}^{(3)}W\left(x_k\right)\times\sum_{k=1}^{N}C_{ik}^{(1)}W\left(x_k\right)+\left(\sum_{k=1}^{N}C_{ik}^{(2)}W\left(x_k\right)\right)^2\right]$$
$$\times\sum_{k=1}^{N}C_{ik}^{(2)}W\left(x_k\right)+C_{11}^{*}A^{*}\times\left(\sum_{k=1}^{N}C_{ik}^{(2)}U\left(x_k\right)+\sum_{k=1}^{N}C_{ik}^{(1)}W\left(x_k\right)\times\sum_{k=1}^{N}C_{ik}^{(2)}W\left(x_k\right)\right)\times\sum_{k=1}^{N}C_{ik}^{(1)}W\left(x_k\right)$$
$$-I_z^{*}\left(C_{11}^{*}+\frac{q_{31}^{*2}}{a_{33}^{*}}\right)\left(\sum_{k=1}^{N}C_{ik}^{(4)}W\left(x_k\right)-l^2\times\sum_{k=1}^{N}C_{ik}^{(6)}W\left(x_k\right)\right)-C_{11}^{*}A^{*}l^2\left(\sum_{k=1}^{N}C_{ik}^{(4)}U\left(x_k\right)+\sum_{k=1}^{N}C_{ik}^{(3)}W\left(x_k\right)\right.$$
$$\left.\times\sum_{k=1}^{N}C_{ik}^{(2)}W\left(x_k\right)+\sum_{k=1}^{N}C_{ik}^{(1)}W\left(x_k\right)\times\sum_{k=1}^{N}C_{ik}^{(4)}W\left(x_k\right)\right)\times\sum_{k=1}^{N}C_{ik}^{(1)}W\left(x_k\right)=0 \tag{18}$$

To complete the formulation, Eqs. (17, 18) are merged with the boundary conditions. These end conditions are exerted as follows,

Clamped (C): $U = W = 0 \quad : \quad x = 0, L$

Simply-supported (S): $U = W = M_x = 0 \quad : \quad x = 0, L$

Then, by inserting the introduced end conditions in Eqs. (17, 18), nonlinear algebraic matrix equations can be obtained.

The accuracy and convergence rate of the Newton-Raphson technique is quite high, leading to performing it on the current problem [67, 68]. In this approach, there should be primary guesses (U_0 and W_0) whose amounts directly regulate the convergence rate. The first loop can be written as [48]

$$\left[U_1\right] = \left[U_0\right] - \left[J^{-1}\right] \times \left\{A\right\} \tag{19}$$

$$\left[W_1\right] = \left[W_0\right] - \left[J^{-1}\right] \times \left\{A\right\} \tag{20}$$

in which *A* exhibits a vector, *J* shows Jacobian in the framework of a matrix.

$$J\left(i, j\right) = \frac{\partial e_i}{\partial x} \tag{21}$$

$$\left\{A\right\} = e_i \left(\begin{matrix} \left[U_0\right] \\ \left[W_0\right] \end{matrix} \right) \tag{22}$$

in which *e* is dedicated for equilibrium equations on the basis of the first guesses. In a point of fact, Eqs. (19, 20) should be in an iterative form as

$$\left[U_{n+1}\right] = \left[U_n\right] - \left[J^{-1}\right] \times \left[A\right] \tag{23}$$

$$\left[W_{n+1}\right] = \left[W_n\right] - \left[J^{-1}\right] \times \left[A\right] \tag{24}$$

in which the iteration number n determines the convergence speed. The desired accuracy can be obtained based on a few iterations. As a consequence, Eqs. (23, 24) result in values of deformations along the x and z axes in which the deflections are related to the transverse deformations.

4 Solution method validation

The method used to solve the nonlinear equations should be checked prior to the parametric study in order to assess its efficiency. Based on Tables 1 and 2, some results are tabulated which are reported from a finite element commercial software (FECS) and present study for linear and nonlinear deflections of an isotropic local beam alongside simple and clamped supports. It is borne to keep it in mind that the convergence rate of the present solution method is N=9. To achieve large deflections, the chosen load is much bigger than that of the first comparison. The validation criterion is the length-to-thickness ratio, which is selected in a range from a thick beam up to a thin one.

The observation of these two tabulated examples says that in the case of large deflections the agreement is further passable particularly in terms of thinner beams. Of course, it should be logical as the present work used thin beam theory without involving shear deformations and, on the other side, FECS has the advantage of using shear deformations. More importantly, FECS considers large displacements in three axes, but the present formulation examines nonlinearity in the transverse axis respecting the von-Kármán theorem. Furthermore, the present mathematical model is based on the one-dimensional analysis; however, FECS is regarding three-dimensional problems. Regardless of these, FECS's outcomes vary due to lots of options in the solution, such as type of element, number of elements, and size. Consequently, a full matching among the results is not reasonable and the difference percentages (

$Diff\% = \frac{|FECS - DQM|}{DQM} \times 100$) can be desirable.

Table 1. Providing small deflections for a square macro beam (E=210GPa, p=100N/m, CC).

L/h	Linear deflections (mm)		
	FECS	Present (DQM)	Diff%
5	0.000272	0.000198	37.37%
10	0.001648	0.001585	3.97%
15	0.005243	0.005348	1.96%
20	0.012173	0.012680	3.99%
25	0.023553	0.024765	4.89%
30	0.040499	0.042790	5.35%
35	0.064131	0.067956	5.62%
40	0.095561	0.101440	5.79%
45	0.135907	0.144432	5.90%
50	0.186285	0.198126	5.97%

Table 2. Providing large deflections for a square macro beam (E=210GPa, p=0.5kN/m, CC).

L/h	Nonlinear deflections (mm)		
	FECS	Present (DQM)	Diff%
5	0.001362	0.000990	37.57%
10	0.008242	0.007924	4.01%
15	0.026218	0.026744	1.96%
20	0.060869	0.063371	3.94%
25	0.117767	0.123616	4.73%
30	0.202465	0.212890	4.89%
35	0.320469	0.335536	4.49%
40	0.477106	0.493667	3.35%
45	0.677421	0.685871	1.23%
50	0.925881	0.906756	2.10%

5 Practical examples

The most fundamental concept in terms of nanoscale problems consists of establishing nanosize effects by formulating between continuum mechanics and nonlocal and also strain gradient approaches proposed theoretically. The concept of nonlocality expands and indicates interaction between atoms based on Eringen's postulations. It is discussed that stress at a point/atom under consideration relates not only to strain at that point but all atoms' strains in that media. This is mathematically meaningful by the Laplace operator which computes an average of a quantity in a planar domain. In addition to this, one can measure the large strain gradient of atoms by the use of well-known strain gradient elasticity models given by literature. These properties arrive from the bulk of a nanostructure. Another effective factor implies a nanostructure can behave differently against a macroscale and that this operator can be the effects of the exterior surface. Of course, surface effects happen on a macroscale though, this is eminent and more explicit on a small scale because of the large ratio of surface to volume. As a matter of fact, [10-12] showed that the surface of materials reacts differently from bulk.

The focus of this section is to surface effects on the flexomagnetic behavior of the cobalt iron oxide as a ferromagnetic material with the structural properties assigned in Table 3 [69-72] and three categories, that is, a piezo-flexomagnetic (PFM) actuator, piezomagnetic (PM) and an ordinary nanobeam (NB).

Table 3. Employed structural properties

Bulk ($CoFe_2O_4$)	Surface layer
C_{11}=286GPa	C_{11}^S=35.3 N/m
f_{31}=10^{-9} N/A	f_{31}^S=10^{-9} N/A
q_{31}=580.3 N/A.m	q_{31}^S=3.4 N/A.m
a_{33}=1.57×10^{-4} N/A^2	a_{33}^S=1.4×10^{-4} H/m

In the first study of the correlation between flexomagnetic and surface effects, Figs. 3a and 3b are drawn with changes in nonlocal and strain gradient length scale (SGLS) coefficients. The

aim here is that the surface layer affects the flexomagnetic behavior at smaller or larger values of these two small-scale parameters. In the first figure, which relies on the nonlocal parameter, it can be clearly seen that as we move towards the selection of larger values for the nonlocal parameter, the nonlocal parameter is effective in highlighting the flexomagnetic effect and it can increase the flexomagnetic response of the material even in the attendance of the surface effect. This result cannot be seen in Fig. 3b, and in fact, the boundary conditions have a direct effect on this achievement. Since the purpose of this study is to investigate the relationship between surface effect and flexomagnetic response, we will not interpret the results of the surface layer on the mechanics of the nanostructure. For example, the effect of the surface layer has led to a reduction in deflections and, as a result, greater stiffness of the material, which has been thoroughly discussed in the research background. Other results considered according to these two figures show a growth in the flexomagnetic effect while the surface effect is not examined. This is because, as mentioned before, the effect of the surface leads to the stiffness of the material and as a result, deduces the deflections. As the deflections decrease, the flexomagnetic effect will be less important. In fact, if the nanostructure under study has inestimable surface effects, the flexomagnetic effect on that material will be larger.

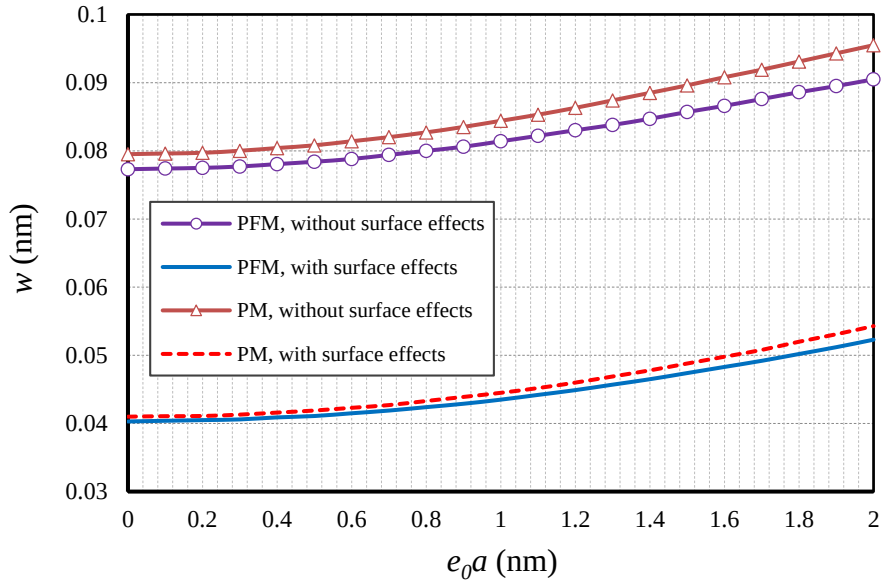

Fig. 3a. Nonlocal parameter vs. deflections for beams with and without surface effects (Ψ=1 mA, m=1, L/h=10, p_0=0.1 N/m, l=1 nm, CC)

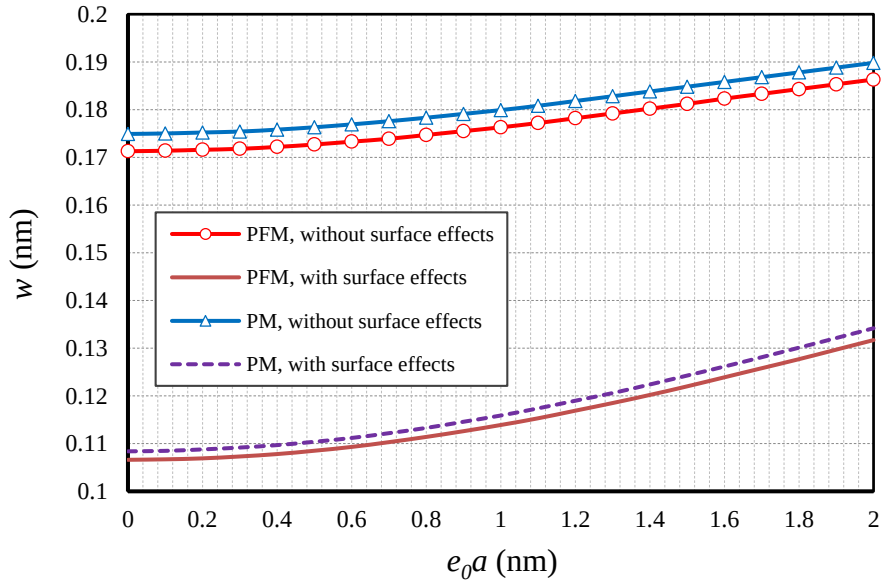

Fig. 3b. Nonlocal parameter vs. deflections for beams with and without surface effects (Ψ=1 mA, m=1, L/h=10, p_0=0.05 N/m, l=1 nm, SS)

In this section, by presenting Figs. 4a and 4b, there will be a similar study of Figs. 3a and 3b, with the difference that here the changes of the SGLS are evaluated. Since in the previous figures we have come to the conclusion that in larger values of the nonlocal parameter, despite

the surface effect, the flexomagnetic effect becomes more dominant. This was because increasing the nonlocal parameter reduced the stiffness of the material, resulting in a larger strain gradient. Since the behavior of SGLS parameter is the opposite of the nonlocal parameter, it means that its enhancement leads to an increase in the stiffness of the material and, as a rule, the flexomagnetic effect should be underestimated, which is simply shown in Fig. 4a. However, it cannot be found in Fig. 4b.

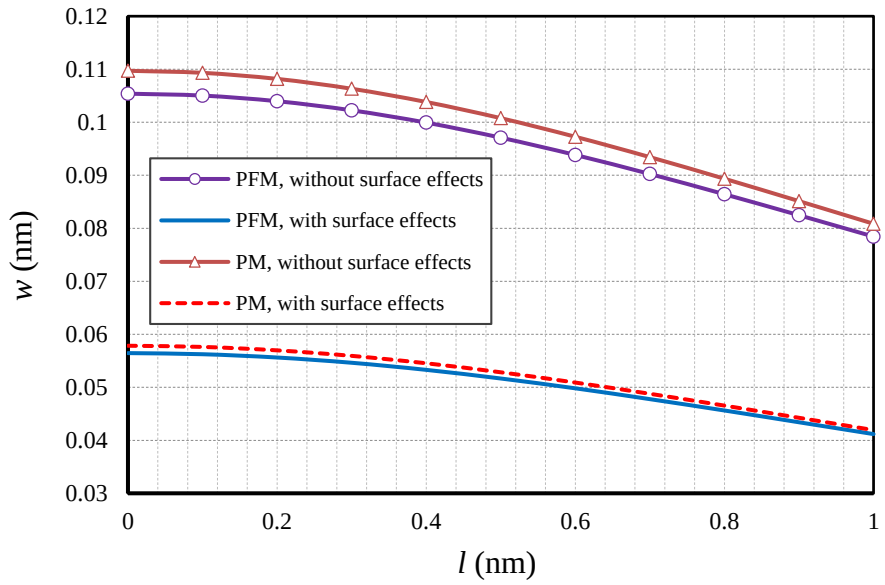

Fig. 4a. Nonlocal parameter vs. deflections for beams with and without surface effects (Ψ=1 mA, m=1, L/h=10, p_0=0.1 N/m, e_0a=0.5 nm, CC)

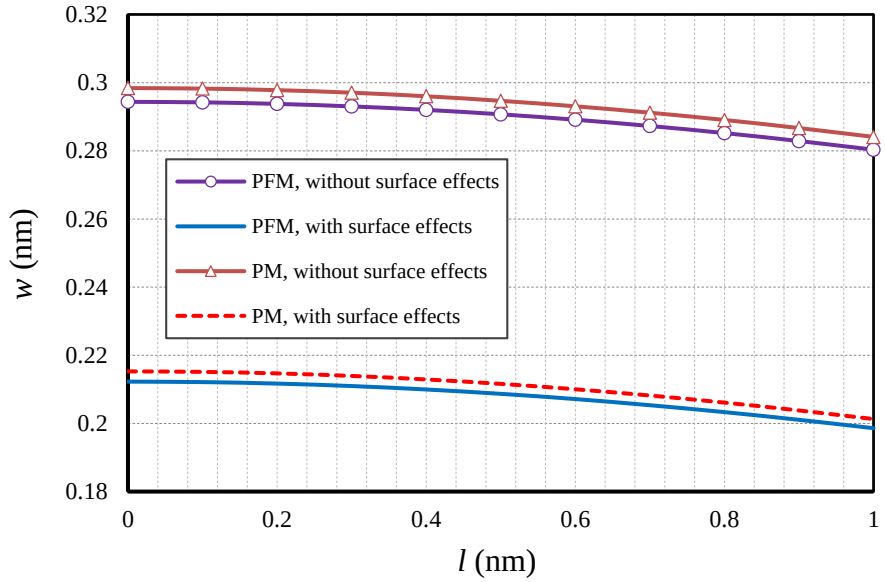

Fig. 4b. Nonlocal parameter vs. deflections for beams with and without surface effects (Ψ=1 mA, m=1, L/h=10, p_0=0.05 N/m, e_0a=0.5 nm, SS)

By preparing Figs. 5a and 5b, we consider the changes in transverse static load to find the effect of these changes on the connection between the surface layer and the flexomagnetic effect. As can be vividly seen, in the range of larger nonlinear deflections, the surface effect is more outstanding in particular when the loading is becoming greater in size. In the first figure, the difference between the results when the surface effect is examined compared with when it is omitted, the results are greater than those in the second figure. In fact, the first plot, which is prepared for the boundary condition of two clamped edges, shows that the larger the transverse load, the more substantial the surface effect, as well as its relationship to the flexomagnetic effect. However, if the two ends of the nanobeam use the hinge boundary condition, the differences will not increase significantly despite the larger static loads.

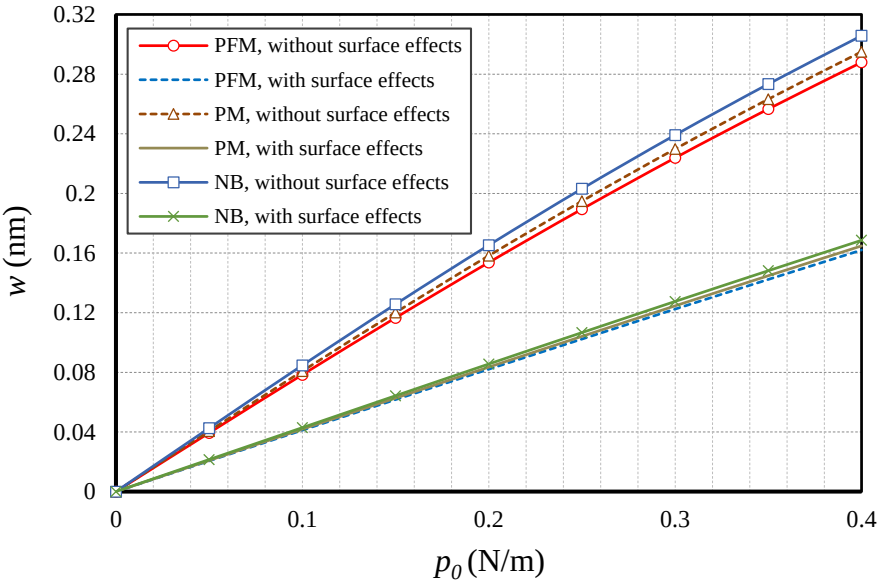

Fig. 5a. Static load vs. deflections for beams with and without surface effects (Ψ=1 mA, m=1, L/h=10, l=1 nm, e_0a=0.5 nm, CC)

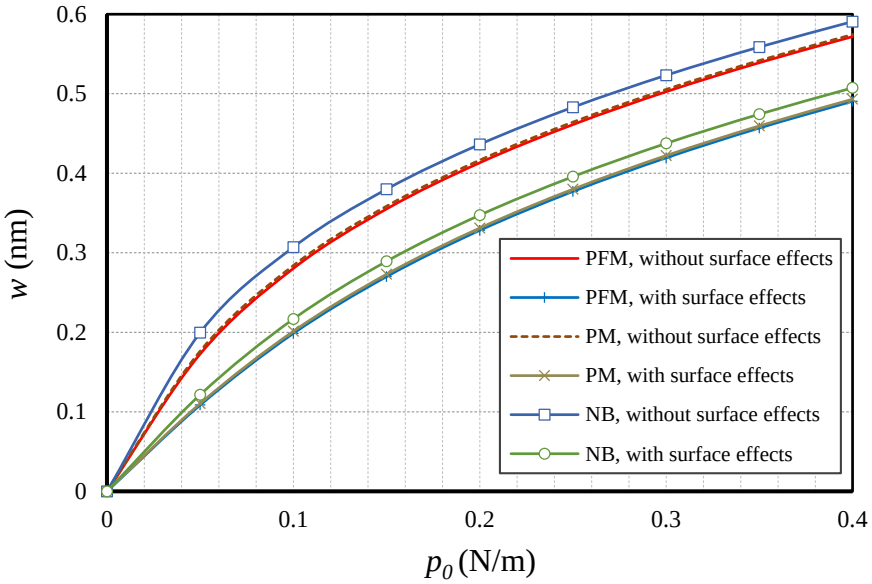

Fig. 5b. Static load vs. deflections for beams with and without surface effects (Ψ=1 mA, m=1, L/h=10, l=1 nm, e_0a=0.5 nm, SS)

At the end of the results section, by presenting two figures, Figs. 6a and 6b, which show the variations in the magnetic potential within the horizontal axis, we will evaluate any relationship between the surface effect and flexomagnetic at different values of the external magnetic

ampere. In the first figure, in the boundary conditions of two fixed edges, no serious result is obtained. However, by examining the second figure, which is related to the boundary conditions of two hinged edges, it can be seen that while the problem involves the surface effect, increasing the magnetic potential values leads to a very small reduction in the difference between results of PFM and PM. In fact, a very little effect resulted from magnetic potential variation on the flexomagnetic effect can be observed. Nevertheless, as a general conclusion, it can be stated that changes in the magnetic potential do not have a noteworthy impact on the relationship between the flexomagnetic behavior of the bulk and the surface layer effect. On the other hand, by comparing the two figures, it can be concluded that the downward trajectory of the results is faster due to the increase of the magnetic potential in the hinge boundary conditions.

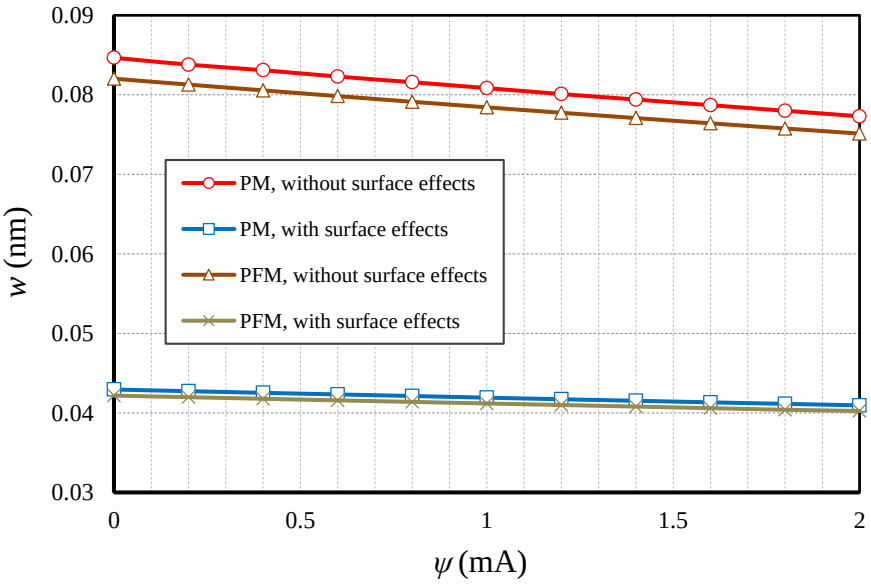

Fig. 6a. Magnetic ampere vs. deflections for beams with and without surface effects (m=1, L/h=10, l=1 nm, p_0=0.1 N/m, e_0a=0.5 nm, CC)

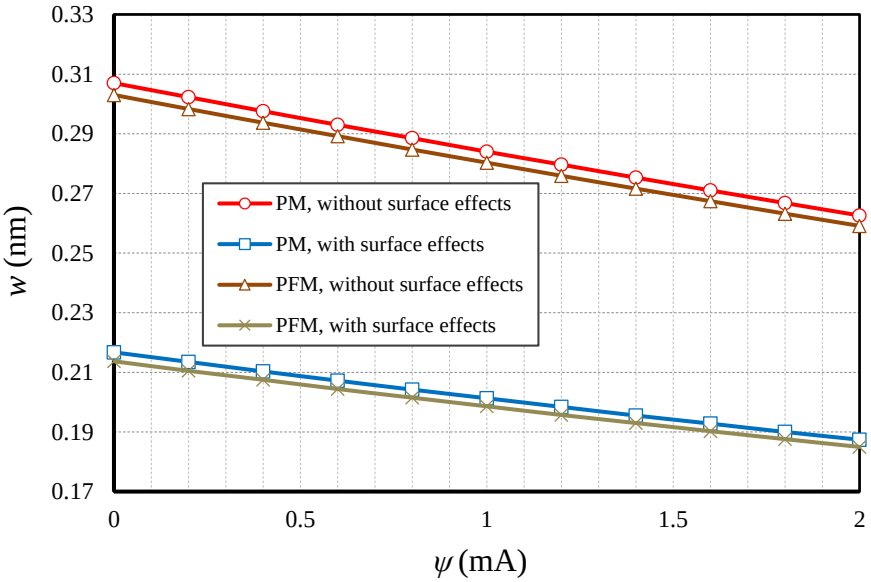

Fig. 6b. Magnetic ampere vs. deflections for beams with and without surface effects (m=1, L/h=10, l=1 nm, p_0=0.1 N/m, e_0a=0.5 nm, SS)

6 Conclusions

The work reported the effects of the surface layer on the various significance items included in a ferromagnetic structure for providing the flexomagnetic response. On the basis of the obtainable data of a flexoferroic material, an appropriate consideration was performed to predict the surface layer effect on the flexomagneticity. Euler-Bernoulli beam assumption was used to find out large deflections of clamped-clamped and pinned-pinned nanoscale beams. When the nonlocal strain gradient model is applied, it can generate the stress nonlocality and large gradient of atoms in the nanoscale. When the magnetic field gradient is applied, one can observe the converse flexomagnetic effect which was our case in this article. The contribution of the nonlinear von-Kármán strain aided us to mathematically model the problem. With the substitution of the differential quadrature method, which has been widely used and its precision has been entirely approved, the partial differential relations have been converted into algebraic equations. Thereafter, the algebraic relations were solved vis-à-vis the Newton-Raphson

technique to compute the large deflections. Further, investigations were warranted via a simple structure using a finite element commercial software before the results and discussion section. This study argued and demonstrated a huge potential in affecting the flexomagnetic effect based on the surface layer. The suitable concluded remarks developed by this research will help the designers of small scale actuators and sensors, where some of them are indicated below,

- If the end conditions are selected as less flexible, and values of nonlocal parameter or SGLS are respectively, big and small enough, the surface layer can affect and develop a further flexomagnetic response.

- In general, the more dominant the surface effect, the stiffer the material, then the less important the flexomagnetic effect.

- The less flexible the end conditions, the remarkable the surface effect and its coherency with flexomagnetic effect if the lateral load is increasing.

- There was found no evidence to show that the relationship between the effect of surface layer and the flexomagnetic influence can be affected by changes in values of the external magnetic ampere.

Acknowledgements

V.A.E acknowledges the support of the Government of the Russian Federation (contract No. 14.Z50.31.0046).

Data availability

The raw/processed data required to reproduce these findings cannot be shared at this time as the data also forms part of an ongoing study.

References

[1] W. Fahrner, Nanotechnology and Nanoelectronics, 1st ed.; Springer, Germany, 2005; pp. 269.

[2] P. Lukashev, R. F. Sabirianov, Flexomagnetic effect in frustrated triangular magnetic structures, Physical Review B 82 (2010) 094417.

[3] C. Pereira, A. M. Pereira, C. Fernandes, M. Rocha, R. Mendes, M. P. Fernández-García, A. Guedes, P. B. Tavares, J.-M. Grenèche, J. P. Araújo, and C. Freire, Superparamagnetic MFe_2O_4 (M = Fe, Co, Mn) Nanoparticles: Tuning the Particle Size and Magnetic Properties through a Novel One-Step Coprecipitation Route, Chemistry of Materials 24 (2012) 1496-1504.

[4] J. X. Zhang, R. J. Zeches, Q. He, Y. H. Chu, R. Ramesh, Nanoscale phase boundaries: a new twist to novel functionalities, Nanoscale 4 (2012) 6196-6204.

[5] H. Zhou, Y. Pei, D. Fang, Magnetic field tunable small-scale mechanical properties of nickel single crystals measured by nanoindentation technique, Scientific Reports 4 (2014) 1-6.

[6] S. Moosavi, S. Zakaria, C. H. Chia, S. Gan, N. A. Azahari, H. Kaco, Hydrothermal synthesis, magnetic properties and characterization of $CoFe_2O_4$ nanocrystals, Ceramics International 43 (2017) 7889-7894.

[7] E. A. Eliseev, A. N. Morozovska, V. V. Khist, V. Polinger, effective flexoelectric and flexomagnetic response of ferroics, In Recent Advances in Topological Ferroics and their Dynamics, Solid State Physics; Stamps, R. L., Schultheis, H.; Elsevier, Netherlands, 2019; Volume 70, pp. 237-289.

[8] A. F. Kabychenkov, F. V. Lisovskii, Flexomagnetic and flexoantiferromagnetic effects in centrosymmetric antiferromagnetic materials, Technical Physics, 64 (2019) 980-983.

[9] E. A. Eliseev, A. N. Morozovska, M. D. Glinchuk, R. Blinc, Spontaneous flexoelectric/flexomagnetic effect in nanoferroics, Physical Review B 79 (2009) 165433.

[10] J. E. Lennard-Jones, B. M. Dent, The change in lattice spacing at a crystal boundary.

Proceedings of the Royal Society A 121 (1928) 247-259.

[11] M. E. Gurtin, A. I. Murdoch, A continuum theory of elastic material surface, Archive for Rational Mechanics and Analysis 57 (1975) 291–323.

[12] M. E. Gurtin, A. I. Murdoch, Surface stress in solids, International Journal of Solids and Structures 14 (1978) 431–440.

[13] G.-L. Yu, H.-W. Zhang, Y.-X. Li, Modeling of magnetoelectric composite nano-cantilever beam with surface effect, Composite Structures 132 (2015) 65-74.

[14] Y. Yang, X.-F. Li, Bending and free vibration of a circular magnetoelectroelastic plate with surface effects, International Journal of Mechanical Sciences 157–158 (2019) 858-871.

[15] K. F. Wang, B. L. Wang, Nonlinear fracture mechanics analysis of nano-scale piezoelectric double cantilever beam specimens with surface effect, European Journal of Mechanics - A/Solids 56 (2016) 12-18.

[16] X. J. Xu, Z. C. Deng, K. Zhang, J.-M. Meng, Surface effects on the bending, buckling and free vibration analysis of magneto-electro-elastic beams, Acta Mechanica 227 (2016) 1557–1573.

[17] G. Sreenivasulu, S. K. Mandal, S. Bandekar, V. M. Petrov, and G. Srinivasan, Low-frequency and resonance magnetoelectric effects in piezoelectric and functionally stepped ferromagnetic layered composites, Physical Review B 84 (2011) 144426.

[18] C. Vazquez-Vazquez, M. A. Lopez-Quintela, M. C. Bujan-Nunez, J. Rivas, Finite size and surface effects on the magnetic properties of cobalt ferrite nanoparticles, Journal of Nanoparticle Research 13 (2011) 1663–1676.

[19] S. Sidhardh, M. C. Ray, Flexomagnetic response of nanostructures, Journal of Applied Physics 124 (2018) 244101.

[20] N. Zhang, Sh. Zheng, D. Chen, Size-dependent static bending of flexomagnetic nanobeams, Journal of Applied Physics 126 (2019) 223901.

[21] M. Malikan, V. A. Eremeyev, Free Vibration of Flexomagnetic Nanostructured Tubes Based on Stress-driven Nonlocal Elasticity. In Analysis of Shells, Plates, and Beams, 1st ed.; Altenbach, H., Chinchaladze, N., Kienzler R., Müller, W. H., Eds.; Springer Nature, Switzerland, 2020; Volume 134, pp. 215-226.

[22] M. Malikan, V. A. Eremeyev, On the geometrically nonlinear vibration of a piezo-flexomagnetic nanotube, Mathematical Methods in the Applied Sciences, (2020). https://doi.org/10.1002/mma.6758

[23] M. Malikan, N. S. Uglov, V. A. Eremeyev, On instabilities and post-buckling of piezomagnetic and flexomagnetic nanostructures, International Journal of Engineering Science 157 (2020) Article no 103395.

[24] M. Malikan, V. A. Eremeyev, K. K. Żur, Effect of Axial Porosities on Flexomagnetic Response of In-Plane Compressed Piezomagnetic Nanobeams, Symmetry 12 (2020) 1935.

[25] M. Malikan, T. Wiczenbach, V. A. Eremeyev, On thermal stability of piezo-flexomagnetic microbeams considering different temperature distributions, Continuum Mechanics and Thermodynamics, (2021). https://doi.org/10.1007/s00161-021-00971-y

[26] M. Malikan, V. A. Eremeyev, Flexomagnetic response of buckled piezomagnetic composite nanoplates, Composite Structures, 267 (2021) 113932.

[27] M. Malikan, R. Dimitri, F. Tornabene, Transient response of oscillated carbon nanotubes with an internal and external damping, Composites Part B: Engineering 158 (2019) 198-205.

[28] M. Malikan, V. B. Nguyen, Buckling analysis of piezo-magnetoelectric nanoplates in hygrothermal environment based on a novel one variable plate theory combining with higher-order nonlocal strain gradient theory, Physica E: Low-dimensional Systems and Nanostructures 102 (2018) 8-28.

[29] M. Malikan, M. Krasheninnikov, V. A. Eremeyev, Torsional stability capacity of a nano-composite shell based on a nonlocal strain gradient shell model under a three-dimensional magnetic field, International Journal of Engineering Science 148 (2020) 103210.

[30] L. Lu, X. Guo, J. Zhao, Size-dependent vibration analysis of nanobeams based on the

nonlocal strain gradient theory, International Journal of Engineering Science 116 (2017) 12–24.

[31] X. Xu, B. Karami, M. Janghorban, On the dynamics of nanoshells, International Journal of Engineering Science 158 (2021) 103431.

[32] X. Xu, B. Karami, D. Shahsavari, Time-dependent behavior of porous curved nanobeam, International Journal of Engineering Science 160 (2021) 103455.

[33] L. Li, Y. Hu, Buckling analysis of size-dependent nonlinear beams based on a nonlocal strain gradient theory, International Journal of Engineering Science 97 (2015) 84-94.

[34] X. Zhu, L. Li, Closed form solution for a nonlocal strain gradient rod in tension, International Journal of Engineering Science 119 (2017) 16-28.

[35] S. Sahmani, B. Safaei, Nonlocal strain gradient nonlinear resonance of bi-directional functionally graded composite micro/nano-beams under periodic soft excitation, Thin-Walled Structures 143 (2019) 106226.

[36] F. Mehralian, Y. Tadi Beni, M. Karimi Zeverdejani, Nonlocal strain gradient theory calibration using molecular dynamics simulation based on small scale vibration of nanotubes, Physica B: Condensed Matter 514 (2017) 61-69.

[37] A. Cemal Eringen, On differential equations of nonlocal elasticity and solutions of screw dislocation and surface waves, Journal of Applied Physics 54 (1983) 4703.

[38] Sh. Dastjerdi, M. Malikan, R. Dimitri, F. Tornabene, Nonlocal elasticity analysis of moderately thick porous functionally graded plates in a hygro-thermal environment, Composite Structures 255 (2021) 112925.

[39] F. Zare Jouneghani, R. Dimitri, F. Tornabene, Structural response of porous FG nanobeams under hygro-thermo-mechanical loadings, Composites Part B: Engineering 152 (2018) 71-78.

[40] R. Gholami, R. Ansari, A unified nonlocal nonlinear higher-order shear deformable plate model for postbuckling analysis of piezoelectric-piezomagnetic rectangular nanoplates with

various edge supports, Composite Structures 166 (2017) 202-218.

[41] R. D. Mindlin, Second gradient of train and surface-tension in linear elasticity, International Journal of Solids and Strucutres 1 (1965) 417-438.

[42] R. D. Mindlin, N. N. Eshel, On first strain-gradient theories in linear elasticity, International Journal of Solids and Strucutres 4 (1968) 109-124.

[43] M. Malikan, Electro-mechanical shear buckling of piezoelectric nanoplate using modified couple stress theory based on simplified first order shear deformation theory, Applied Mathematical Modelling 48 (2017) 196-207.

[44] A. Skrzat, V. A. Eremeyev, On the effective properties of foams in the framework of the couple stress theory, Continuum Mechanics and Thermodynamics 32 (2020) 1779-1801.

[45] M. Akbarzadeh Khorshidi, The material length scale parameter used in couple stress theories is not a material constant, International Journal of Engineering Science 133 (2018) 15-25.

[46] R. Barretta, S. A. Faghidian, R. Luciano, C. M. Medaglia, R. Penna, Free vibrations of FG elastic Timoshenko nano-beams by strain gradient and stress-driven nonlocal models, Composites Part B: Engineering 154 (2018) 20-32.

[47] G.-L. She, H.-B. Liu, B. Karami, Resonance analysis of composite curved microbeams reinforced with graphene nanoplatelets, Thin-Walled Structures 160 (2021) 107407.

[48] M. Malikan, V. A. Eremeyev, On nonlinear bending study of a piezo-flexomagnetic nanobeam based on an analytical-numerical solution, Nanomaterials 10 (2020) 1-22.

[49] R. C. Cammarata, Surface and interface stress effects in thin films, Progress in Surface Science 46 (1994) 1–38.

[50] R. E. Miller and V. B. Shenoy, Size-dependent elastic properties of nanosized structural elements, Nanotechnology 11 (2000) 139–147.

[51] S. Cuenot, C. Fretigny, S. Demoustier-Champagne, and B. Nysten, Surface tension effect on the mechanical properties of nanomaterials measured by atomic forcemicroscopy, Physical Review B 69 (2004) Article ID 165410.

[52] G.-F. Wang and X.-Q. Feng, Effects of surface elasticity and residual surface tension on the natural frequency of microbeams, Applied Physics Letters 90 (2007) Article ID 231904.

[53] J. He and C. M. Lilley, Surface effect on the elastic behavior of static bending nanowires, Nano Letters 8 (2008) 1798–1802.

[54] D.-H. Wang, G.-F. Wang, Surface Effects on the Vibration and Buckling of Double-Nanobeam-Systems, Journal of Nanomaterials, Volume 2011, Article ID 518706, 7 pages.

[55] M. Malikan, V. A. Eremeyev, Post-critical buckling of truncated conical carbon nanotubes considering surface effects embedding in a nonlinear Winkler substrate using the Rayleigh-Ritz method, Materials Research Express 7 (2020) 025005.

[56] R. Gholami, R. Ansari, Nonlinear resonance responses of geometrically imperfect shear deformable nanobeams including surface stress effects, International Journal of Non-Linear Mechanics 97 (2017) 115-125

[57] R. Bellman, B. G Kashef, J. Casti, Differential quadrature: A technique for the rapid solution of nonlinear partial differential equations, Journal of Computational Physics 10 (1972) 40-52.

[58] R. Bellman, J. Casti, Differential quadrature and long-term integration, Journal of Mathematical Analysis and Applications 34 (1971) 235-238.

[59] C. Shu, Differential quadrature and its application in engineering. Berlin: Springer; 2000.

[60] R. Ansari, S. Sahmani, B. Arash, Nonlocal plate model for free vibrations of single-layered graphene sheets, Physics Letters A 375 (2010) 53-62.

[61] L. Behera, S. Chakraverty, Application of Differential Quadrature method in free vibration analysis of nanobeams based on various nonlocal theories, Computers & Mathematics with Applications 69 (2015) 1444-1462.

[62] M. E. Golmakani, J. Rezatalab, Nonlinear bending analysis of orthotropic nanoscale plates in an elastic matrix based on nonlocal continuum mechanics, Composite Structures 111 (2014) 85-97.

[63] M. Malikan, M. Jabbarzadeh, S. Dastjerdi, Non-linear static stability of bi-layer carbon nanosheets resting on an elastic matrix under various types of in-plane shearing loads in thermo-elasticity using nonlocal continuum, Microsystem Technologies 23 (2017) 2973–2991.

[64] M. Malikan, M. N. Sadraee Far, Differential Quadrature Method for Dynamic Buckling of Graphene Sheet Coupled by a Viscoelastic Medium Using Neperian Frequency Based on Nonlocal Elasticity Theory, Journal of Applied and Computational Mechanics 4 (2018) 147-160.

[65] A.J.M. Ferreira, E. Carrera, M. Cinefra, E. Viola, F. Tornabene, N. Fantuzzi, A.M. Zenkour, Analysis of thick isotropic and cross-ply laminated plates by generalized differential quadrature method and a Unified Formulation, Composites Part B: Engineering, 58 (2014) 544-552.

[66] F. Tornabene, N. Fantuzzi, E. Viola, E. Carrera, Static analysis of doubly-curved anisotropic shells and panels using CUF approach, differential geometry and differential quadrature method, Composite Structures, 107 (2014) 675-697.

[67] E. Carrera, A. Pagani, R. Augello, et al. Large deflection and post-buckling of thin-walled structures by finite elements with node-dependent kinematics, Acta Mechanica, 232 (2021) 591–617.

[68] A. Pagani, E. Carrera, Large-deflection and post-buckling analyses of laminated composite beams by Carrera Unified Formulation, Composite Structures, 170 (2017) 40-52.

[69] Z.-l. Lu, P.-z. Gao, R.-x. Ma, J. Xu, Z.-h. Wang, E. V. Rebrov, Structural, magnetic and thermal properties of one-dimensional CoFe2O4 microtubes, Journal of Alloys and Compounds 665 (2016) 428-434.

[70] A. Balsing Rajput, S. Hazra, N. Nath Ghosh, Synthesis and characterisation of pure single-phase CoFe2O4 nanopowder via a simple aqueous solution-based EDTA-precursor route, Journal of Experimental Nanoscience 8 (2013) 629-639.

[71] V. P. Senthil, J. Gajendiran, S. Gokul Raj, T. Shanmugavel, G. Ramesh Kumar, C. Parthasaradhi Reddy, Study of structural and magnetic properties of cobalt ferrite (CoFe2O4) nanostructures, Chemical Physics Letters 695 (2018) 19-23.

[72] L. Li, Y. Hu, L. Ling, Wave propagation in viscoelastic single-walled carbon nanotubes with surface effect under magnetic field based on nonlocal strain gradient theory, Physica E: Low-dimensional Systems and Nanostructures 75 (2016) 118-124.

Postprint for: Malikan, M, Eremeyev, VA. Flexomagneticity in buckled shear deformable hard-magnetic soft structures. Continuum Mechanics and Thermodynamics. https://doi.org/10.1007/s00161-021-01034-y

Flexomagneticity in buckled shear deformable hard-magnetic soft structures

Mohammad Malikan[*1], Victor A. Eremeyev[1,2,3]

[1] Department of Mechanics of Materials and Structures, Faculty of Civil and Environmental Engineering, Gdansk University of Technology, 80-233 Gdansk, Gdansk, Poland

[2] Don State Technical University, Gagarina sq., 1, Rostov on Don 344000, Russia

[3] DICAAR, Università degli Studi di Cagliari, Via Marengo, 2, 09123, Cagliari, Italy

*Corresponding author: mohammad.malikan@pg.edu.pl, mohammad.malikan@yahoo.com

Abstract

This research work performs the first time exploring and addressing the flexomagnetic property in a shear deformable piezomagnetic structure. The strain gradient reveals flexomagneticity in a magnetization phenomenon of structures regardless of their atomic lattice is symmetrical or asymmetrical. It is assumed that a synchronous converse magnetization couples both piezomagnetic and flexomagnetic features into the material structure. The mathematical modeling begins with the Timoshenko beam model to find the governing equations and non-classical boundary conditions based on shear

deformations. Flexomagneticity evolves at a small scale and dominant at micro/nanosize structures. Meanwhile, the well-known Eringen's-type model of nonlocal strain gradient elasticity is integrated with the mathematical process to fulfill the scaling behavior. From the viewpoint of the solution, the displacement of the physical model after deformation is carried out as the analytical solution of the Galerkin weighted residual method (GWRM), helping us obtain the numerical outcomes on the basis of the simple end conditions. The best of our achievements display that considering shear deformation is essential for nanobeams with larger values of strain gradient parameter and small amounts of the nonlocal coefficient. Furthermore, we showed that the flexomagnetic (FM) effect brings about more noticeable shear deformations' influence.

Keywords: Flexomagneticity; Buckling analysis; Timoshenko nanobeam; NSGT; GWRM

Nomenclature:

ε_{xx} : Axial strain

γ_{xz} : Shear strain

η_{xxz} : Gradient of the axial elastic strain

C_{11} : Elastic modulus

σ_{xx} : Axial stress

τ_{xz} : Shear stress

f_{31} : Component of the fourth-order flexomagnetic coefficients tensor

a_{33} : Component of the second-order magnetic permeability tensor

q_{31} : Component of the third-order piezomagnetic tensor

ξ_{xxz} : Component of the higher-order hyper-stress tensor

B_z : Magnetic flux

H_z : Component of magnetic field

g_{31} : Influence of the sixth-order gradient elasticity tensor

q : Third-order piezomagnetic tensor
a : Second-order magnetic permeability tensor
g : sixth-order gradient elasticity tensor
C : Fourth-order elasticity coefficient tensor
f : Fourth-order flexomagnetic tensor
r : Fifth-order tensor
u_i (i=1,3): Displacement in the x- and z- directions
u and w: Axial and transverse displacements of the mid-plan
ϕ : Rotation of beam elements around the y-axis
z: Thickness coordinate
ψ : External magnetic potential
Ψ : Magnetic potential function
$l(nm)$: Strain gradient length scale parameter
$\mu(nm)^2 = (e_0 a)^2$: Nonlocal parameter
X_m : Residue of the equations
k_s : Shear correction factor
N_x : Axial stress resultant
Q_x : Shear stress resultant
M_x : Moment stress resultant
T_{xxz} : Hyper stress resultant

1. Introduction

Magnetic properties are divided into different categories: diamagnetic, paramagnetic, ferrimagnetic, ferromagnetic materials, etc. Ferromagnetic materials are magnetic structures with high permeability, such as cobalt and iron. Ferromagnetic materials are divided into hard (e.g., $CoFe_2O_4$) and soft groups (e.g., Fe_3O_4). Hard magnetic materials are materials that become magnetized hardly ever; That is, a strong magnetic field is required to create magnetism in them. As these materials become magnetized hardly, they also lose scarcely ever their magnetic properties. These structures are suited to be used as a steady magnetic state, such as sensors and measuring

instruments. Conversely, soft magnetic structures are easily magnetized and just as easily lose their magnetic properties [1-5].

$CoFe_2O_4$ magnetic nanostructures have received particular attention among different spinel ferrites, such as exclusive physical features, excellent mechanical hardness, significant magnetostrictive coefficient, high coercivity, moderate saturation magnetization, etc. [6, 7]. From a technological perspective, these characteristic properties cause the structure described above entirely significant, leading to its application in gas sensors, magnetic hyperthermia, biosensors, ferrofluid technology, and high-density magnetic media [8-11].

A lot of practical applications can be observed from the phenomenological magneto-mechanical coupling of crystals. Structures with reduced dimensions functioning as nano configurations are affected principally and importantly from this type of coupling. It is already known that the connection between induced magnetization and strain gradient is mainly significant among small-size structures. Flexomagneticity (FM) is a phenomenon that exists during the magneto-mechanical coupling regarding the magnetic field and strain gradient [12-14]. Compared to the flexomagneticity, flexoelectricity influence appears in crystalline structures between the electric field and strain gradient (converse effect) [15-33]. The physical action of FM makes it competent to the economic outlook. The advantage of FM property gives a possible way of improving biosensor efficiency.

The contemporary decade has been witnessed plenty of research work performed on the mechanics of piezomagnetic (PM) nano configurations [34-42]. However, the availability of FM in scientific papers is seen hardly and scarcely [43-52]. In the

aforementioned reports presented on FM for PM structures, in order to model the domain displacement field, all available references employed the concept of the Euler-Bernoulli (EB) approach regardless of shear deformation. By contrast, in the present research work, we analyze the transverse shear deformation on the basis of utilizing the Timoshenko beam approach. As long as the domain is a nanoscale volume, the size-dependent mechanical response should be considered. The literature in [43, 44] used the surface elasticity hypothesis to address this scale-dependent reaction. Oppositely, in the current paper and similar to [45-52], we handle stress/strain-driven non-classical elasticity models conforming to the nonlocal strain gradient size-dependent approach. Using this approach leads to investigating two concurrent size-dependent nanomaterials' behaviors: inhomogeneity distribution of atoms (material particles) and long-range lattice interactions. The first one occurs due to a large surface to the volume of atoms, and the second one arises concerning the long-range interatomic interaction among the whole atoms of the domain. It is germane to note that the [43, 44] applied both direct and converse magnetic fields; however, [45-52] and the present article have taken the converse effect only. We keep the ends of the magnetic nanobeam mathematically in simply-supported boundary conditions through a numerical solving procedure. Up to our knowledge, the literature has confirmed that FM behavior is completely size-dependent.

Moreover, the crucial achievements of [45-52] approved that the FM can cause more material stiffness. Therefore, we aim to investigate the relevance between transverse shear deformation and the FM, which is a novel study in the present scientific work and what follows. In a point of fact, until now, the FM has been investigated on thin beam models only regardless of shear deformation [43-52]. Furthermore, the linear

mathematical model which is obtained by this study is solved through the medium of the Galerkin weighted residual method. The numerical results have appeared in line with the graphical figures and detailed parametric diagrams.

2. Mathematical modeling

2.1 Fundamental calculations of the piezomagnetic-flexomagnetic (PFM) media

We begin the fundamental formulation of a PFM solid by assuming some restrictions acting as minute deformations in an isothermal environment, referencing [12-14]. Thus, the magnetic field H and displacement u are variables in the vector framework.

$$u=u\left(x\right),\ H=H\left(x\right) \tag{1}$$

in which x defines a position vector.

We introduce the free energy density U defined within the flexomagneticity as follows

$$U=U\left(\varepsilon,\eta,H\right)=-\frac{1}{2}H\cdot a\cdot H+\frac{1}{2}\varepsilon:C:\varepsilon+\frac{1}{2}\eta\vdots g\vdots\eta+\varepsilon:r\vdots\eta \\ -H\cdot q:\varepsilon-H\cdot f\vdots\eta \tag{2}$$

in which "$\vdots$", "$:$", and "$\cdot$" depict the inner (scalar) products in the spaces of third-order tensor, second-order tensor, and vectors, respectively.

The elastic strain and its gradient are expressed as

$$\varepsilon=\frac{1}{2}\left(\nabla u+\nabla u^{T}\right),\ \eta=\nabla\varepsilon \tag{3}$$

where ∇ is the 3D nabla operator.

In what follows, we use the magnetic potential ψ related with H as

$$H=-\nabla\psi \tag{4}$$

To study the FM on a static PM model, based on the virtual work principle, one can use the variational approach

$$\int_V \delta U dV = \delta A \tag{5}$$

where δA is dedicated for performing the work of outer loads, V exhibits the domain volume occupied by FM solid.

For simplicity, a standard relation for δA is introduced as

$$\delta A = \int_V F \cdot \delta u + \int_{\partial V} t \cdot \delta u ds \tag{6}$$

in which t and F display the surface traction and external mass forces, respectively.

We illustrate the following equations based on Eq. (5) and calculus of variations

$$\nabla \cdot \left(\sigma - \nabla \cdot \xi \right) + F = 0 \tag{7a}$$

$$\nabla \cdot B = 0 \tag{7b}$$

where B is a magnetic induction vector, and the constitutive relations of a PFM media can be established as

$$\sigma = \frac{\partial U}{\partial \varepsilon} \equiv C : \varepsilon + r \vdots \eta - H \cdot q \tag{8a}$$

$$\xi = \frac{\partial U}{\partial \eta} \equiv g : \eta + \varepsilon : r - H \cdot f \tag{8b}$$

$$B = -\frac{\partial U}{\partial H} = a \cdot H + q : \varepsilon + f \vdots \eta \tag{8c}$$

2.2 The PFM hard magnetic soft one-dimensional structure

This research tries to develop the FM studies on PM solids by accounting for the shear deformation of the structure while both ends of the one-dimensional beam-shaped

configuration are held in simple supports. Regarding Fig. 1, a one-dimensional figured beam bridged by simple ends can be detected. Dimensions of the beam are respectively assigned in the parametric framework by *h* and *L* for its thickness and effective length.

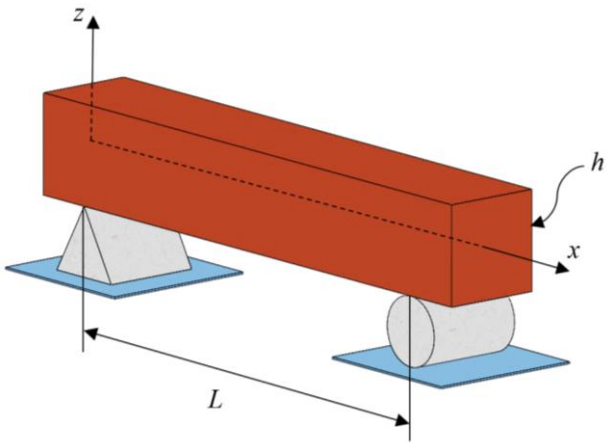

Fig. 1. Geometrical details of a simply supported square figured beam

While a beam incorporates FM properties, the constitutive relations (Eq. (8)) are re-defined as follows [43, 44]

$$\sigma_{xx} = C_{11}\varepsilon_{xx} - q_{31}H_z \tag{9}$$

$$\xi_{xxz} = g_{31}\eta_{xxz} - f_{31}H_z \tag{10}$$

$$B_z = a_{33}H_z + q_{31}\varepsilon_{xx} + f_{31}\eta_{xxz} \tag{11}$$

As the main scope of this paper is exerting transverse shear deformation in the PFM solid, we use the Timoshenko model as follows [53, 54]

$$u_1(x,z) = u(x) + z\phi(x) \tag{12a}$$

$$u_3(x,z) = w(x) \tag{12b}$$

In view of Lagrangian strain and as the present study addresses the linear stability of PFM nanoscale beams, thus

$$\varepsilon_{ij} = \frac{1}{2}\left(\frac{\partial u_i}{\partial x_j} + \frac{\partial u_j}{\partial x_i} \right) \tag{13}$$

On developing Eq. (13) based on Eq. (12), one obtains

$$\varepsilon_{xx} = \frac{du}{dx} + z\frac{d\phi}{dx} \tag{14a}$$

$$\gamma_{xz} = \phi + \frac{dw}{dx} \tag{14b}$$

$$\eta_{xxz} = \frac{d\varepsilon_{xx}}{dz} = \frac{d\phi}{dx} \tag{14c}$$

Modifying the Lagrange principle (5), we came to

$$\delta \int \left(\Pi_W + \Pi_U \right) = 0 \tag{15}$$

where the given letters Π_U and Π_W state respectively the internal strain energy originated from mechanical and magnetic sections, and mechanical work of external elements accomplished on the system.

The following relation can depict the whole strain energy of the beam

$$\delta\Pi_U = \int_V \left(\sigma_{xx}\delta\varepsilon_{xx} + \tau_{xz}\delta\gamma_{xz} + \xi_{xxz}\delta\eta_{xxz} - B_z\delta H_z \right) dV \tag{16}$$

Equilibrium equations and non-classical end supports conditions can be obtained after imposing the variational method on Eq. (16) as follows

$$\delta\Pi_{U_1}^{Mech} = -\int_0^L \left(\frac{dN_x}{dx}\delta u + \frac{dQ_x}{dx}\delta w - Q_x\delta\varphi + \frac{dM_x}{dx}\delta\varphi + \frac{dT_{xxz}}{dx}\delta\varphi \right) dx \tag{17a}$$

$$\delta\Pi_{U_2}^{Mag} = -\int_0^L \int_{-h/2}^{h/2} \frac{dB_z}{dz}\delta\Psi\, dz dx \tag{17b}$$

$$\delta\Pi_{U_1}^{Mech} = \left(N_x\delta u + Q_x\delta w + M_x\delta\varphi + T_{xxz}\delta\varphi \right)\Big|_0^L \tag{18a}$$

$$\delta\Pi_{U_2}^{Mag}=\int_0^L\left(B_z\delta\Psi\right)\Big|_{-h/2}^{h/2}dx \tag{18b}$$

where indices 1 and 2, respectively associated with the mechanical and magnetic parts, furthermore

$$N_x=\int_{-h/2}^{h/2}\sigma_{xx}dz \tag{19}$$

$$M_x=\int_{-h/2}^{h/2}\sigma_{xx}zdz \tag{20}$$

$$Q_x=k_s\times\int_{-h/2}^{h/2}\tau_{xz}dz \tag{21}$$

$$T_{xxz}=\int_{-h/2}^{h/2}\xi_{xxz}dz \tag{22}$$

Taking external items such as loads and environmental effects results in mechanical work in the solid, hence [55-58]

$$\Pi_W=\frac{1}{2}\int_0^L N_x^0\left(\frac{dw}{dx}\right)^2dx \tag{23}$$

Then, the first variation of Eq. (23) can be produced as

$$\delta\Pi_W=\int_0^L\left(N_x^0\frac{d\delta w}{dx}\frac{dw}{dx}\right)dx \tag{24}$$

where N_x^0 reveals in-plane pre-buckling force.

There is only a transverse component for the present media for the magnetic field determined as [59, 60]

$$H_z+\frac{d\Psi}{dz}=0 \tag{25}$$

Let us match the literature and embed the beam in a magnetic potential difference circuit so that the maximum and minimum magnetic potentials are at the uppermost and lowest surfaces, respectively. Therefore, the magnetic boundary conditions for a reverse PM impact besides closed-circuit yields [43, 44]

$$\Psi\left(+\frac{h}{2}\right)=\psi,\ \Psi\left(-\frac{h}{2}\right)=0 \tag{26a-b}$$

By combining Eqs. (11), (17b), (18b), (25), and (26) together and making some mathematical processes give the magnetic potential distribution in line with the thickness and component of the magnetic field as

$$\Psi=\frac{q_{31}}{2a_{33}}\left(z^2-\frac{h^2}{4}\right)\frac{d\phi}{dx}+\frac{\psi}{h}\left(z+\frac{h}{2}\right) \tag{27}$$

$$H_z=-z\frac{q_{31}}{a_{33}}\frac{d\phi}{dx}-\frac{\psi}{h} \tag{28}$$

The study of the structural properties of nanodomains, especially the accurate measurement of their mechanical response, has required complex tools. The ultrasmall size space is transferred into a continuum solid media through some mathematical theorems to avoid using complicated equipment. These theoretical models can act in two forms, integral or differential operators. However, we here employ a differential framework of one of these models, which is famed as nonlocal strain gradient elasticity theory (NSGT) [61]

$$\left(1-\mu\frac{d^2}{dx^2}\right)\sigma_{ij}=C_{ijkl}\left(1-l^2\frac{d^2}{dx^2}\right)\varepsilon_{ij} \tag{29}$$

In other words, in constitutive relations for stress tensor (8a), we consider C as an integro-differential operator related to Eq. (29).

The right side of the NSGT relation is assumed to project the strain gradient role. This part is significant in the mechanics of micro/nanoscale deformable materials [62]. Further, the left side is considered to render the nonlocality of atoms. Both parts involve extra parameters, respectively μ as a nonlocal parameter and l as a strain gradient parameter. It should be reminded that $\mu(nm)^2=(e_0a)^2$ where e denotes a nonlocal quantity and a indicates a characteristic internal length which can be the distance between the center of two neighbor atoms. It should be remembered that the values of small-scale parameters that existed in NSGT vary in light of several cases, such as the type of end supports. In general, the values of these factors are not constant or an associated value for each material [63-66].

Putting Eq. (14) and (27, 28) into Eqs. (9-11), and combining the obtained relations with Eq. (29), then, respectively, the components of magnetic induction, axial stress, and shear stress can be obtained as

$$\left(1-\mu\frac{d^2}{dx^2}\right)\xi_{xxz}=\left(1-l^2\frac{d^2}{dx^2}\right)\left[\left(g_{31}+\frac{q_{31}f_{31}z}{a_{33}}\right)\frac{d\phi}{dx}+\frac{f_{31}\psi}{h}\right] \tag{30}$$

$$\left(1-\mu\frac{d^2}{dx^2}\right)\sigma_{xx}=\left(1-l^2\frac{d^2}{dx^2}\right)\left[C_{11}\frac{du}{dx}+z\left(C_{11}+\frac{q_{31}^2}{a_{33}}\right)\frac{d\phi}{dx}+\frac{q_{31}\psi}{h}\right] \tag{31}$$

$$\left(1-\mu\frac{d^2}{dx^2}\right)\tau_{xz}=\left(1-l^2\frac{d^2}{dx^2}\right)\left[GA\left(\phi+\frac{dw}{dx}\right)\right] \tag{32}$$

Nonlocal stress resultants can be obtained by substituting Eqs. (30-32) into Eqs. (19-22) [67-75]

$$\left(1-\mu\frac{d^2}{dx^2}\right)N_x=\left(1-l^2\frac{d^2}{dx^2}\right)\left\{I_1\frac{du}{dx}+I_4\right\} \tag{33}$$

$$\left(1-\mu\frac{d^2}{dx^2}\right)M_x=\left(1-l^2\frac{d^2}{dx^2}\right)\left\{\left(I_2+I_3\right)\frac{d\phi}{dx}\right\} \tag{34}$$

$$\left(1-\mu\frac{d^2}{dx^2}\right)Q_x=\left(1-l^2\frac{d^2}{dx^2}\right)\left\{H_{44}\left(\phi+\frac{dw}{dx}\right)\right\} \tag{35}$$

$$\left(1-\mu\frac{d^2}{dx^2}\right)T_{xxz}=\left(1-l^2\frac{d^2}{dx^2}\right)\left\{I_5\frac{d\phi}{dx}+I_6\right\} \tag{36}$$

in which the numerical expressions bring about

$$\left\{I_1,I_2\right\}=\int_{-h/2}^{h/2}C_{11}\left\{1,z^2\right\}dz,\ I_3=\int_{-h/2}^{h/2}\frac{q_{31}^2z^2}{a_{33}}dz,I_4=\int_{-h/2}^{h/2}\frac{\psi q_{31}}{h}dz,$$

$$I_5=\int_{-h/2}^{h/2}g_{31}dz,\ I_6=\int_{-h/2}^{h/2}\frac{\psi f_{31}}{h}dz,\ H_{44}=k_s\int_{-h/2}^{h/2}GAdz$$

After implementing Eq. (17a) and (24) in Eq. (15), the equations which govern the PFM beam-shaped solid can be developed by which the beam behaves statically in a local domain

$$\frac{dN_x}{dx}=0 \tag{37}$$

$$\frac{dQ_x}{dx}+N_x^0\frac{d^2w}{dx^2}=0 \tag{38}$$

$$\frac{dM_x}{dx}+\frac{dT_{xxz}}{dx}-Q_x=0 \tag{39}$$

This is the time to simplify Eqs. (33-36) in the nonlocal domain. To do this, by way of Eqs. (37-39), one can derive

$$N_x=\left(1-l^2\frac{d^2}{dx^2}\right)\left\{I_1\frac{du}{dx}+I_4\right\} \tag{40}$$

$$M_x=-\mu\left(I_5\frac{d^3\phi}{dx^3}+N_x^0\frac{d^2w}{dx^2}\right)+\left(1-l^2\frac{d^2}{dx^2}\right)\left\{\left(I_2+I_3\right)\frac{d\phi}{dx}\right\} \tag{41}$$

$$Q_x = -\mu\left(N_x^0 \frac{d^3 w}{dx^3} \right) + \left(1 - l^2 \frac{d^2}{dx^2} \right)\left\{ H_{44}\left(\phi + \frac{dw}{dx} \right) \right\} \tag{42}$$

$$T_{xxz} = \left(1 - \mu \frac{d^2}{dx^2} \right)\left(I_5 \frac{d\phi}{dx} + I_6 \right) \tag{43}$$

Let us re-write Eqs. (37-39) based on Eqs. (40-42) as

$$\left(1 - l^2 \frac{d^2}{dx^2} \right)\left\{ I_1 \frac{d^2 u}{dx^2} \right\} = 0 \tag{44}$$

$$\left(1 - \mu \frac{d^2}{dx^2} \right)\left\{ N_x^0 \frac{d^2 w}{dx^2} \right\} + \left(1 - l^2 \frac{d^2}{dx^2} \right)\left\{ H_{44}\left(\frac{d\phi}{dx} + \frac{d^2 w}{dx^2} \right) \right\} = 0 \tag{45}$$

$$\left(1 - \mu \frac{d^2}{dx^2} \right)\left\{ I_5 \frac{d^2 \phi}{dx^2} \right\} - \left(1 - l^2 \frac{d^2}{dx^2} \right)\left\{ -\left(I_2 + I_3 \right)\frac{d^2 \phi}{dx^2} + H_{44}\left(\phi + \frac{dw}{dx} \right) \right\} = 0 \tag{46}$$

It is quite clear that Eq. (44) is independent of Eqs. (45) and (46). Therefore, to compute the system's stability capacity, Eqs. (45) and (46) will be solved. It is vital to remember that if we consider $\mu = l$, or $\mu = 0,\ l = 0$, the local analysis is performed.

Now, the pre-buckling compressive axial forces can be written as

$$N_x^0 = N^{Mech} + N^{Mag} \tag{47}$$

for which one can dedicate the magnetic and mechanical parts as N^{Mag} and N^{Mech} respectively.

$$N^{Mech} = -P_{cr} \tag{48}$$

$$N^{Mag} = -q_{31}\psi \tag{49}$$

3. Solution process

Buckling equations are solved based on various methods. In between these solution techniques, well-known ones can refer to the Galerkin weighted residual method (GWRM), which is a simple one involving a fast solution time [56]. To proceed with this method, the unknown functions $w(x)$ and $\phi(x)$ can be chosen as

$$w(x)=\sum_{m=1}^{N} a_m(x) \tag{50}$$

$$\phi(x)=\sum_{m=1}^{N} b_m(x) \tag{51}$$

The existed functions $a_m(x)$ and $b_m(x)$ based on the GWRM are expanded as

$$a_m=\int_0^L W_m(x)\,X_m dx \tag{52}$$

$$b_m=\int_0^L \Phi_m(x)\,X_m dx \tag{53}$$

Pertained to simple end conditions (SS), W_m and Φ_m are trigonometric functions as

$$W_m(x)=\sin\left(\frac{\pi}{L}x\right) \tag{54}$$

$$\Phi_m(x)=\cos\left(\frac{\pi}{L}x\right) \tag{55}$$

Manipulating and simplifying Eqs. (45) and (46) and combining it with Eq. (23), then based on Eqs. (50) and (51) and associating m=1, the linear analytical stability equation of the PFM beam-like nano solid can be achieved.

4. Discussion and numerical results

4.1. Results validation

The verification section is here conducted to devote the exactness of the solution process. This part of the study is divided into two divisions. The first validation (Table 1) corresponds to Euler-Bernoulli (EB) and Timoshenko (TB) common nanobeams based on nonlocal effects only. The TB results are then compared with the EB ones in Table 2 owing to the PFM nanoscale beams by comparing results of EB small size beam with TB on the basis of substituting physical quantities in Table 3 [43, 44].

The listed results in Table 1 represent that the difference between TB with EB tends to be shorter while increasing the value of the nonlocal parameter. What is more, no one can see any conflicts between present TB with those of [76]. In another investigation adjusted by Table 2, it is mentionable that the difference between the stability amounts of TB versus EB has become smaller. This smaller difference is observed while μ is increasing and the structure is PFM. In fact, the nonlocal parameter effect except decreasing the stiffness of the nanostructure deactivates the influence of shear deformations and then brings the EB and TB close to each other. Ultimately, on the basis of these prepared Tables, one can say that a very good accuracy and agreement are revealed for the employed solving technique.

Table 1. Comparison of critical buckling load (C_{11} =1TPa, υ= 0.3, l=0 nm, ψ=0 mA, SS, $\overline{P_{Cr}} = \frac{P_{Cr}L^2}{C_{11}I_c}$)

	$\overline{P_{Cr}}$									
	e_0a=0 nm		e_0a=0.5 nm		e_0a=1 nm		e_0a=1.5 nm		e_0a=2 nm	
L/h	EB[76], TB[76]	TB-Present	EB[76], TB[76]	TB-Present	EB[76], TB[76]	TB-Present	EB[76], TB[76]	TB-Present	EB[76], TB[76]	TB-Present
10	2.4674 2.4056	2.4056	2.4079 2.3477	2.3477	2.2457 2.1895	2.1895	2.0190 1.9685	1.8685	1.7690 1.7247	1.7247

30	2.4674 2.4603	2.4603	2.4606 2.4536	2.4536	2.4406 2.4336	2.4336	2.4079 2.4011	2.4011	2.3637 2.3569	2.3569

Table 2. Comparison of the critical buckling load of the piezomagnetic-flexomagnetic CFO nanostructure for EB and TB (l=1 nm, ψ=1 mA, SS)

L/h	P_{Cr} (nN)					
	μ=0 nm^2		μ=1 nm^2		μ=2 nm^2	
	EB	TB	EB	TB	EB	TB
10	3.2828	3.2111	3.0489	2.9832	2.8536	2.7928
12	2.4074	2.3734	2.2946	2.2627	2.1954	2.1652
14	1.9007	1.8825	1.8398	1.8225	1.7845	1.7679
16	1.5803	1.5697	1.5446	1.5344	1.5115	1.5016
18	1.3645	1.3579	1.3422	1.3358	1.3212	1.3150
20	1.2121	1.2078	1.1974	1.1933	1.1835	1.1794
22	1.1003	1.0974	1.0903	1.0875	1.0807	1.0779
24	1.0159	1.0139	1.0089	1.0069	1.0021	1.0001
26	0.9506	0.9491	0.9455	0.9440	0.9405	0.9390
28	0.8990	0.8978	0.8951	0.8941	0.8914	0.8903
30	0.8575	0.8566	0.8546	0.8537	0.8517	0.8509

Table 3. Properties of the magnetic nanoparticle

$CoFe_2O_4$ (CFO)
C_{11} =286 GPa
ν=0.32
q_{31} =580.3 N/A.m
a_{33} =1.57×10^{-4} N/A^2

4.2. Buckling analysis

In this article, the static linear buckling analysis of a piezo-flexomagnetic (PFM) nanobeam is probed to understand the flexomagnetic property more. We will determine the effectiveness of FM for a shear deformable structure in the ultrasmall size. The values of small scale parameters have been gotten as 0.5 nm$<e_0a<$0.8 nm [77], and $0<e_0a\leq$2 nm

[78, 79]. The value of the strain gradient parameter has been estimated as same as the lattice number of the examined nanostructure as l=1 nm.

In the results section, by maneuvering on the dimensionless relationship of length to beam thickness (L/h), we try to evaluate the difference between the results of EB and TB beams in both local and nonlocal phases. Since this dimensionless ratio directly determines the importance of shear deformations (It was seen that in small values of this coefficient, the beam is thicker and the shear deformations are further important), the aim is to determine the effect of shear deformations on beams with FM property to know whether FM will be more important considering the shear deformation.

First, in order to evaluate the different cases, Figs. 2 and 3 represent the problem by focusing on the nonlocal parameter and the strain gradient, respectively. With the help of Fig. 2, it is quite obvious that the thinner the beam, the less important the shear deformation in the smart beam. However, the process of reducing the results in the local beam (e_0a=0) will be on a steep slope. In fact, the nonlocal parameter and the shear deformation effect directly impressed each other. When the value of the nonlocal coefficient is other than zero (e_0a=2nm), the difference between the results of EB and TB decreases. Thus, it can be stated that the local solution (e_0a=0) of the nanostructures will lead to a more gap in the difference between the results of EB and TB. In Fig. 3, it can be seen that by increasing the value of the strain gradient parameter, the stiffer the material, the greater the difference between the EB and TB results. From these two diagrams, it can be concluded that the stiffer the material and its structure, the more important the shear deformations seem.

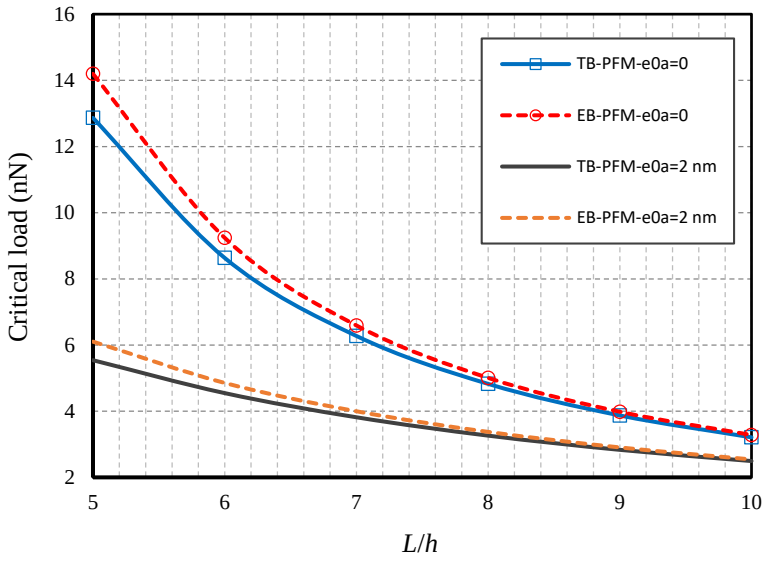

Fig. 2. Nonlocal parameter vs. EB and TB for COF nanostructure (l=1 nm, ψ=1 mA)

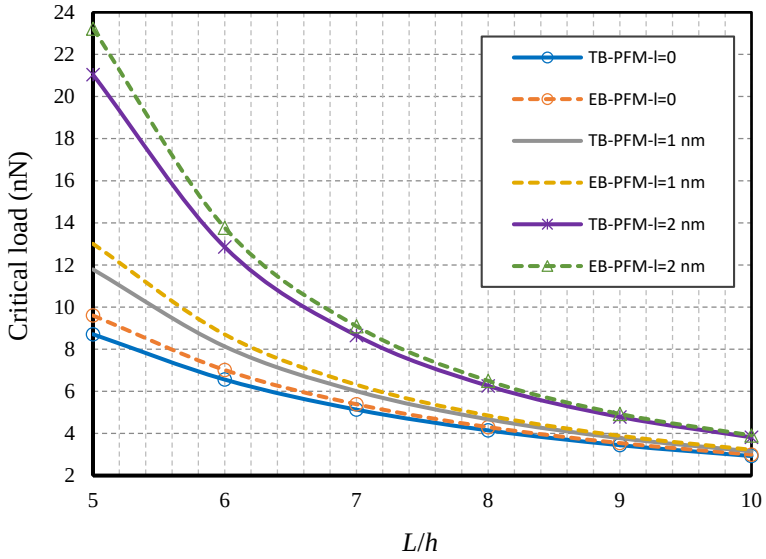

Fig. 3. Strain gradient parameter vs. EB and TB for COF nanostructure (e_0a =0.5 nm, ψ=1 mA)

Fig. 4 is based on changes in the value of the strain gradient parameter. Both EB and TB consist of two modes. The first mode is the PM beam, and the second mode is the PFM

beam. The result of the critical load for the EB-PFM at l = 0 is 2.836 nN and at l = 2nm is 3.6876 nN. Also, for TB-PFM is 2.7757 nN and 3.6055 nN, respectively. But we see that for PM beam in EB mode is 2.7373 nN and 3.5889 nN, respectively, and in TB mode is 2.6821 nN and 3.5119 nN. Therefore, considering the large values of the strain gradient parameter, we see that the difference between the results of EB-PM and TB-PM will be less than those of the EB-PFM with TB-PFM. It can be said that the strain gradient parameter affects the PFM beam more than the PM beams. A physical reason may be that the piezo-flexomagnetic material is stiffer than the piezo material.

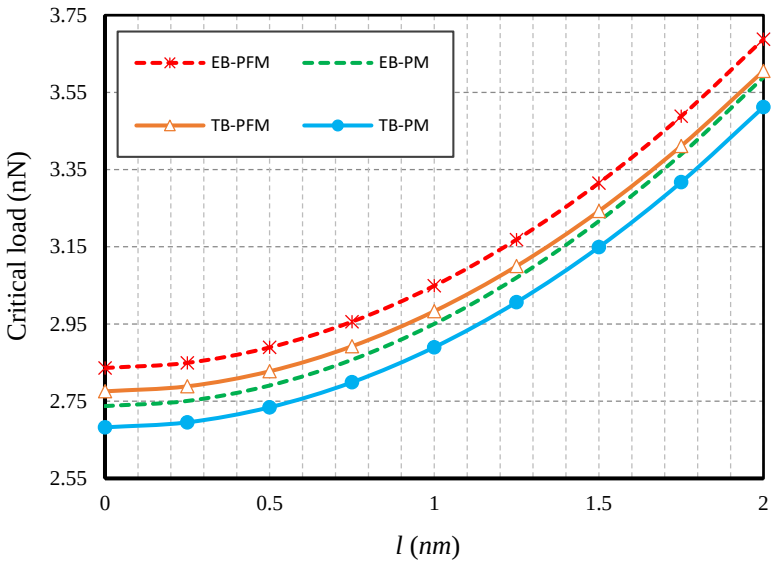

Fig. 4. Strain gradient parameter vs. EB and TB for COF nanostructure (e_0a=1 nm, L=10h, ψ=1 mA)

According to Fig. 5, we have tried to compare EB and TB in piezo and piezo-flexomagnetic modes by considering the numerical changes of the slenderness parameter (L/h). For this purpose, we assessed the beam in the thicker zone. It shall be reminded that the results of TB are not accurate enough in the very thick range, and TB theory is

often suitable for beams with 6<L/h, and also in the case of EB for 10<L/h. According to the diagram and in the thicker mode of the beams, it is observed that the critical load for the EB-PM beam is 12.615 nN and for the TB-PM is 11.471 nN, in contrast to EB-PFM is 13.009 nN and for TB-PFM beam is 11.793 nN. Therefore, it can be stated that the difference between the results of EB and TB in piezo-flexomagnetic mode is greater than those of piezomagnetic mode. Of course, the literature [43-52] reported that FM is dominant in thinner structures. However, as a result of this study, one can conclude that the flexomagnetic effect will lead to the greater importance of shear deformations in thicker nanobeams.

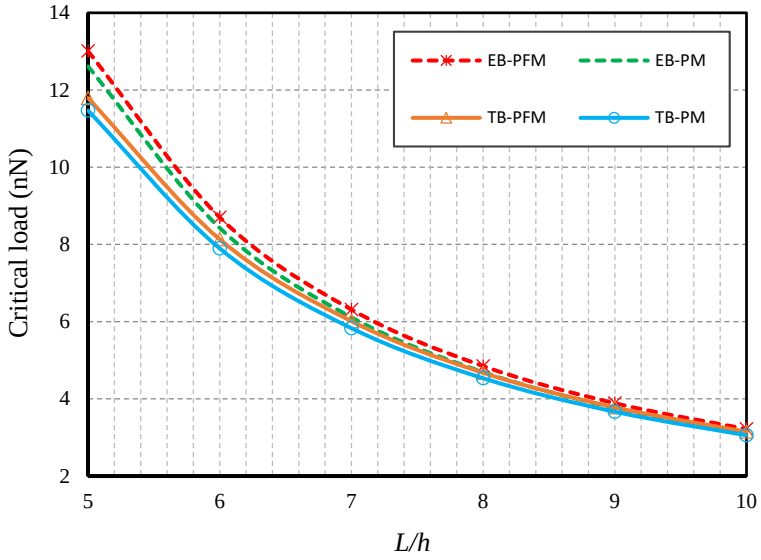

Fig. 5. Slenderness ratio vs. EB and TB for COF nanostructure (l=1 nm, e_0a=0.5 nm, ψ=1 mA)

Fig. 6 is drawn to show a pure mechanical response of the nanoscale beam (NB) compared with PM and PFM for both EB and TB. The NB excludes magnetic and also the FM properties. It is tried to sketch the beams from a thick beam up to a moderately thick

beam. As seen, the NB has the least mechanical stability in comparison with the PM and PFM nanobeams. Interestingly, in an analogy between NB with PFM, and PM, it can be observed that the results of the EB-NB would be matched with those of TB-NB sooner than other cases. From L/h=11, the results of EB and TB for NB are so closed to each other. However, this does not apply to magnetic cases. It means the importance of shear deformation will be increased in piezomagnetic-flexomagnetic domains.

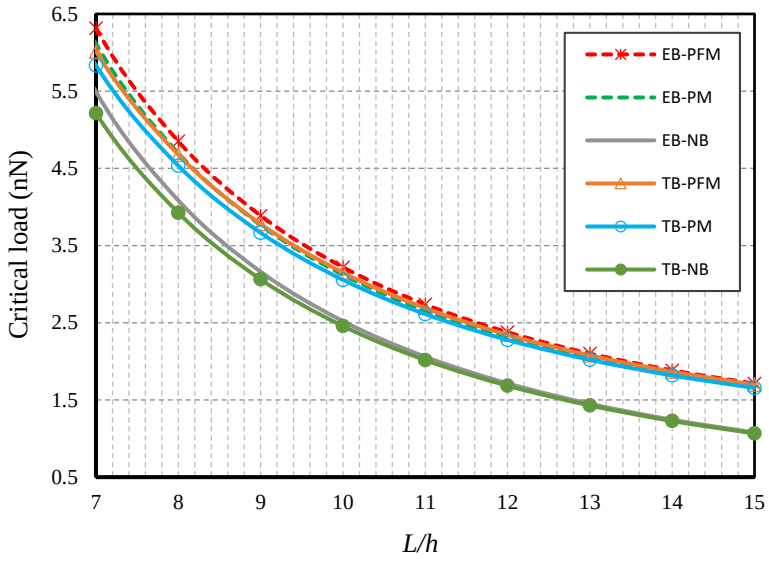

Fig. 6. Slenderness ratio vs. EB and TB for different nanostructure (l=1 nm, e_0a=0.5 nm, ψ=1 mA)

5. Conclusions

This work aimed to extend the shear deformation effect on the flexomagneticity response of a piezomagnetic ultrasmall scale elastic beam. We established the governing equations by using the Timoshenko beam. The nonlocal mechanics of the nanobeam was concerned with the nonlocal strain gradient approach by which we are able to transfer the discretize atomic lattice into a continuum region. The solution of the obtained equations

corresponded to a closed-form solution within which the numerical results were reported for simply supported end support. We organized some tabulated verifications to corroborate the numerical results. Based on the detailed parametric study and from an engineering perspective, this work provides some new attainments and outcome remarks as

- The stiffer structure leads to the further remarkable of shear deformations.
- The lesser the values of the nonlocal parameter, the more marked the shear deformations.
- The larger the values of the strain gradient parameter, the more considerable the shear deformations.
- For the smart nanobeams, the FM will affect the existence of shear deformations, and the effect is to increase its importance.

Acknowledgments

V.A. Eremeyev acknowledges the support of the Government of the Russian Federation (contract No. 14.Z50.31.0046).

References

[1] L. L.-P. Diandra, R. D. Rieke, Magnetic properties of nanostructured materials, Chemistry of materials 8 (1996) 1770-1783.

[2] C. Fei, Y. Zhang, Z. Yang, Y. Liu, R. Xiong, J. Shi, X. Ruan, Synthesis and magnetic properties of hard magnetic (CoFe2O4)–soft magnetic (Fe3O4) nano-composite ceramics by SPS technology, Journal of Magnetism and Magnetic Materials 323 (2011) 1811-1816.

[3] V. Reddy, N. P. Annapu, Pathak, R. Nath, Particle size dependent magnetic properties and phase transitions in multiferroic BiFeO3 nano-particles, Journal of Alloys and Compounds 543 (2012) 206-212.

[4] Z. Karimi, Y. Mohammadifar, H. Shokrollahi, Sh. Khameneh Asl, Gh. Yousefi, L. Karimi, Magnetic and structural properties of nano sized Dy-doped cobalt ferrite synthesized by co-precipitation, Journal of Magnetism and Magnetic Materials 361 (2014) 150-156.

[5] I. Obaidat, I. Bashar, Y. Haik, Magnetic properties of magnetic nanoparticles for efficient hyperthermia, Nanomaterials 5 (2015) 63-89.

[6] P. C. Rajath, R. S. Manna, D. Banerjee, M. R. Varma, K. G. Suresh, A. K. Nigam, Magnetic properties of CoFe2O4 synthesized by solid state, citrate precursor and polymerized complex methods: A comparative study, Journal of Alloys and Compounds 453 (2008) 298-303.

[7] J. Wang, T. Deng, Y. Dai, Comparative study on the preparation procedures of cobalt ferrites by aqueous processing at ambient temperatures, Journal of Alloys and Compounds 419 (2006) 155-161.

[8] M. S. Khandekar, R. C. Kamble, J. Y. Patil, Y. D. Kolekar, S. S. Suryavanshi, Effect of calcination temperature on the structural and electrical properties of cobalt ferrite synthesized by combustion method, Journal of Alloys and compounds 509 (2011) 1861-1865.

[9] D. H. Kim, D. E. Nikles, D. T. Johnson, C. S. Brazel, Heat generation of aqueously dispersed CoFe2O4 nanoparticles as heating agents for magnetically activated drug delivery and hyperthermia, Journal of Magnetism and Magnetic Materials 320 (2008) 2390-2396.

[10] P. C. Morais, Photoacoustic spectroscopy as a key technique in the investigation of nanosized magnetic particles for drug delivery systems, Journal of Alloys and Compounds 483 (2009) 544-548.

[11] N. M. Deraz, Glycine-assisted fabrication of nanocrystalline cobalt ferrite system, Journal of Analytical and Applied Pyrolysis 88 (2010) 103-109.

[12] A. F. Kabychenkov, F. V. Lisovskii, Flexomagnetic and flexoantiferromagnetic effects in centrosymmetric antiferromagnetic materials, Technical Physics 64 (2019) 980-983.

[13] E. A. Eliseev, A. N. Morozovska, M. D. Glinchuk, R. Blinc, Spontaneous flexoelectric/flexomagnetic effect in nanoferroics, Physical Review B 79 (2009) 165433.

[14] P. Lukashev, R. F. Sabirianov, Flexomagnetic effect in frustrated triangular magnetic structures, Physical Review B 82 (2010) 094417.

[15] W. Ma, Flexoelectricity: strain gradient effects in ferroelectrics, Physica Scripta T129 (2007) 180-183.

[16] D. Lee, A. Yoon, S. Y. Jang, J.-G. Yoon, J.-S. Chung, M. Kim, J. F. Scott, and T. W. Noh, Giant Flexoelectric Effect in Ferroelectric Epitaxial Thin Films, Physical Review Letters 107 (2011) 057602.

[17] T. D. Nguyen, S. Mao, Y.-W. Yeh, P. K. Purohit, M. C. McAlpine, Nanoscale Flexoelectricity, Advanced Materials 25 (2013) 946-974.

[18] P. Zubko, G. Catalan, A. K. Tagantsev, Flexoelectric Effect in Solids, Annual Review of Materials Research 43 (2013) 387-421.

[19] P. V. Yudin, A. K. Tagantsev, Fundamentals of flexoelectricity in solids, Nanotechnology 24 (2013) 432001.

[20] A. S. Yurkov, A. K. Tagantsev, Strong surface effect on direct bulk flexoelectric response in solids, Applied Physics Letters 108 (2016) 022904.

[21] B. Wang, Y. Gu, S. Zhang, L.-Q. Chen, Flexoelectricity in solids: Progress, challenges, and perspectives, Progress in Materials Science 106 (2019) 100570.

[22] L. Cross, Flexoelectric effects: charge separation in insulating solids subjected to elastic strain gradients, Journal of Materials Science 41 (2006) 53–63.

[23] W. Ma, L. E. Cross, Observation of the flexoelectric effect in relaxor Pb ($Mg_{1/3}Nb_{2/3}$)O_3 ceramics, Applied Physics Letters 78 (2001) 2920–21.

[24] W. Ma, L. E. Cross, Flexoelectricity of barium titanate, Applied Physics Letters 88 (2006) 232902.

[25] P. Zubko, G. Catalan, A. Buckley, P. R. L. Welche, J. F. Scott, Strain-gradient-induced polarization in SrTiO3 single crystals, Physical Review Letters 99 (2007) 167601.

[26] V. A. Eremeyev, J.-F. Ganghoffer, V. Konopinska-Zmysłowska, N. S. Uglov, Flexoelectricity and apparent piezoelectricity of a pantographic micro-bar, International Journal of Engineering Science 149 (2020) 103213.

[27] M. Esmaeili, Y. Tadi Beni, Vibration and Buckling Analysis of Functionally Graded Flexoelectric Smart Beam, Journal of Applied and Computational Mechanics 5 (2019) 900-917.

[28] M. Malikan, V. A. Eremeyev, On the Dynamics of a Visco–Piezo–Flexoelectric Nanobeam, Symmetry 12 (2020) 643.

[29] A. Singhal, H.-M. Sedighi, F. Ebrahimi, I. Kuznetsova, Comparative study of the flexoelectricity effect with a highly/weakly interface in distinct piezoelectric materials (PZT-2, PZT-4, PZT-5H, LiNbO3, BaTiO3), Waves in Random and Complex Media, (2019).

[30] N. Mawassy, H. Reda, J.-F. Ganghoffer, V. A. Eremeyev, H. Lakiss, A variational approach of homogenization of piezoelectric composites towards piezoelectric and flexoelectric effective media, International Journal of Engineering Science 158 (2021) 103410.

[31] M. S. Ebnali Samani, Y. Tadi Beni, Size dependent thermo-mechanical buckling of the flexoelectric nanobeam, Materials Research Express 5 (2018) 085018.

[32] A. Ghobadi, Y. Tadi Beni, H. Golestanian, Nonlinear thermo-electromechanical vibration analysis of size-dependent functionally graded flexoelectric nano-plate exposed magnetic field, Archive of Applied Mechanics 90 (2020) 2025-2070.

[33] A. Ghobadi, Y. Tadi Beni, H. Golestanian, Size dependent thermo-electro-mechanical nonlinear bending analysis of flexoelectric nano-plate in the presence of magnetic field, International Journal of Mechanical Sciences 152 (2019) 118-137.

[34] M. Arefi, A. M. Zenkour, Thermo-electro-magneto-mechanical bending behavior of size-dependent sandwich piezomagnetic nanoplates, Mechanics Research Communications 84 (2017) 27–42.

[35] F. Ebrahimi, M. R. Barati, Porosity-dependent vibration analysis of piezo-magnetically actuated heterogeneous nanobeams, Mechanical Systems and Signal Processing 93 (2017) 445-459.

[36] A. M. Zenkour, M. Arefi, N. A. Alshehri, Size-dependent analysis of a sandwich curved nanobeam integrated with piezomagnetic face-sheets, Results in Physics 7 (2017) 2172-2182.

[37] X.-P. Sun, Y.-.Z. Hong, H.-L. Dai, L. Wang, Nonlinear frequency analysis of buckled nanobeams in the presence of longitudinal magnetic field, Acta Mechanica Solida Sinica 30 (2017) 465-473.

[38] K.R. Balasubramanian, S.P. Sivapirakasam and R. Anand, Linear Buckling and Vibration Behavior of Piezoelectric/Piezomagnetic Beam under Uniform Magnetic Field, Applied Mechanics and Materials 592-594 (2014) 2071-2075.

[39] B. Alibeigi, Y. T. Beni, On the size-dependent magneto/electromechanical buckling of nanobeams, The European Physical Journal Plus 133 (2018) 398.

[40] M. Arefi, M. Kiani, O. Civalek, 3-D magneto-electro-thermal analysis of layered nanoplate including porous core nanoplate and piezomagnetic face-sheets, Applied Physics A 126 (2020) 76.

[41] M. Saadatfar, Stress Redistribution Analysis of Piezomagnetic Rotating Thick-Walled Cylinder with Temperature-and Moisture-Dependent Material Properties, Journal of Applied and Computational Mechanics 6 (2020) 90-104.

[42] M. Marin, A. Öchsner, An initial boundary value problem for modeling a piezoelectric dipolar body, Continuum Mechanics and Thermodynamics 30 (2018) 267–278.

[43] S. Sidhardh, M. C. Ray, Flexomagnetic response of nanostructures, Journal of Applied Physics 124 (2018) 244101.

[44] N. Zhang, Sh. Zheng, D. Chen, Size-dependent static bending of flexomagnetic nanobeams, Journal of Applied Physics 126 (2019) 223901.

[45] M. Malikan, V. A. Eremeyev, Free Vibration of Flexomagnetic Nanostructured Tubes Based on Stress-driven Nonlocal Elasticity, Analysis of Shells, Plates, and Beams. Advanced Structured Materials 134 (2020) 215-226.

[46] M. Malikan, V. A. Eremeyev, On the geometrically nonlinear vibration of a piezo-flexomagnetic nanotube, Mathematical Methods in the Applied Sciences, 2020. https://doi.org/10.1002/mma.6758

[47] M. Malikan, V. A. Eremeyev, On Nonlinear Bending Study of a Piezo-Flexomagnetic Nanobeam Based on an Analytical-Numerical Solution, Nanomaterials 10 (2020) 1762.

[48] M. Malikan, N. S. Uglov, V. A. Eremeyev, On instabilities and post-buckling of piezomagnetic and flexomagnetic nanostructures, International Journal of Engineering Science 157 (2020) 10339.

[49] M. Malikan, T. Wiczenbach, V. A. Eremeyev, On thermal stability of piezo-flexomagnetic microbeams considering different temperature distributions. Continuum Mechanics and Thermodynamics 33 (2021) 1281-1297.

[50] M. Malikan, V. A. Eremeyev, K. K. Żur, Effect of Axial Porosities on Flexomagnetic Response of In-Plane Compressed Piezomagnetic Nanobeams, Symmetry 12 (2020) 1935.

[51] M. Malikan, V. A. Eremeyev, Flexomagnetic response of buckled piezomagnetic composite nanoplates, Composite Structures 267 (2021) 113932.

[52] M. Malikan, V. A. Eremeyev, Effect of surface on the flexomagnetic response of ferroic composite nanostructures; nonlinear bending analysis, Composite Structures (2021).

[53] J. N. Reddy, Nonlocal nonlinear formulations for bending of classical and shear deformation theories of beams and plates, International Journal of Engineering Science 48 (2010) 1507-1518.

[54] G.-L. She, H.-B. Liu, B. Karami, Resonance analysis of composite curved microbeams reinforced with graphene nanoplatelets, Thin-Walled Structures 160 (2021) 107407.

[55] M. Malikan, V. A. Eremeyev, H. M. Sedighi, Buckling analysis of a non-concentric double-walled carbon nanotube, Acta Mechanica 231 (2020) 5007-5020.

[56] M. Malikan, V. A. Eremeyev, A new hyperbolic-polynomial higher-order elasticity theory for mechanics of thick FGM beams with imperfection in the material composition, Composite Structures 249 (2020) 112486.

[57] E. Turco, Numerically driven tuning of equilibrium paths for pantographic beams, Continuum Mechanics and Thermodynamics 31 (2019) 1941–1960.

[58] M. Marin, A. Öchsner, D. Taus, On structural stability for an elastic body with voids having dipolar structure, Continuum Mechanics and Thermodynamics 32 (2020) 147–160.

[59] R. Gholami, R. Ansari, A unified nonlocal nonlinear higher-order shear deformable plate model for postbuckling analysis of piezoelectric-piezomagnetic rectangular nanoplates with various edge supports, Composite Structures 166 (2017) 202-218.

[60] R. Gholami, R. Ansari, Nonlocal free vibration in the pre- and post-buckled states of magneto-electro-thermo elastic rectangular nanoplates with various edge conditions, Smart Materials and Structures 25 (2016) 095033.

[61] C. W. Lim, G. Zhang, J. N. Reddy, A Higher-order nonlocal elasticity and strain gradient theory and Its Applications in wave propagation, Journal of the Mechanics and Physics of Solids 78 (2015) 298-313.

[62] D.C.C. Lam, F. Yang, A.C.M. Chong, J. Wang, P. Tong, Experiments and theory in strain gradient elasticity, Journal of the Mechanics and Physics of Solids 51 (2003) 1477-1508.

[63] R. Ansari, S. Sahmani, B. Arash, Nonlocal plate model for free vibrations of single-layered graphene sheets, Physics Letters A 375 (2010) 53-62.

[64] M. Akbarzadeh Khorshidi, The material length scale parameter used in couple stress theories is not a material constant, International Journal of Engineering Science 133 (2018) 15-25.

[65] H. Yang, D. Timofeev, I. Giorgio, et al. Effective strain gradient continuum model of metamaterials and size effects analysis, Continuum Mechanics and Thermodynamics, (2020). https://doi.org/10.1007/s00161-020-00910-3

[66] B. E. Abali, Revealing the physical insight of a length-scale parameter in metamaterials by exploiting the variational formulation, Continuum Mechanics and Thermodynamics 31 (2019) 885–894.

[67] B. Karami, D. Shahsavari, M. Janghorban, L. Li, On the resonance of functionally graded nanoplates using bi-Helmholtz nonlocal strain gradient theory, International Journal of Engineering Science 144 (2019) 103143.

[68] M. Malikan, V. B. Nguyen, F. Tornabene, Damped forced vibration analysis of single-walled carbon nanotubes resting on viscoelastic foundation in thermal environment using nonlocal strain gradient theory, Engineering Science and Technology, an International Journal 21 (2018) 778–786.

[69] M. Malikan, R. Dimitri, F. Tornabene, Transient response of oscillated carbon nanotubes with an internal and external damping, Composites Part B: Engineering 158 (2019) 198-205.

[70] M. Malikan, M. Krasheninnikov, V. A. Eremeyev, Torsional stability capacity of a nano-composite shell based on a nonlocal strain gradient shell model under a three-dimensional magnetic field, International Journal of Engineering Science 148 (2020) 103210.

[71] S. Kumar Jena, S. Chakraverty, F. Tornabene, Dynamical behavior of nanobeam embedded in constant, linear, parabolic, and sinusoidal types of Winkler elastic foundation using first-Order nonlocal strain gradient model, Materials Research Express 6 (2019) 0850f2.

[72] M. Malikan, V. A. Eremeyev, Post-critical buckling of truncated conical carbon nanotubes considering surface effects embedding in a nonlinear Winkler substrate using the Rayleigh-Ritz method, Materials Research Express 7 (2020) 025005.

[73] B. Karami, M. Janghorban, T. Rabczuk, Dynamics of two-dimensional functionally graded tapered Timoshenko nanobeam in thermal environment using nonlocal strain gradient theory, Composites Part B: Engineering 182 (2020) 107622.

[74] S. Sahmani, B. Safaei, Nonlocal strain gradient nonlinear resonance of bi-directional functionally graded composite micro/nano-beams under periodic soft excitation, Thin-Walled Structures 143 (2019) 106226.

[75] F. Fan, B. Safaei, S. Sahmani, Buckling and postbuckling response of nonlocal strain gradient porous functionally graded micro/nano-plates via NURBS-based isogeometric analysis, Thin-Walled Structures 159 (2021) 107231.

[76] M. Simsek, H. H. Yurtcu, Analytical solutions for bending and buckling of functionally graded nanobeams based on the nonlocal Timoshenko beam theory, Composite Structures 97 (2013) 378–386.

[77] R. Ansari, S. Sahmani, H. Rouhi, Rayleigh–Ritz axial buckling analysis of single-walled carbon nanotubes with different boundary conditions, Physics Letters A 375 (2011) 1255–1263.

[78] W. H. Duan, C. M. Wang, Exact solutions for axisymmetric bending of micro/nanoscale circular plates based on nonlocal plate theory, Nanotechnology 18 (2007) 385704.

[79] W. H. Duan, C. M. Wang, Y. Y. Zhang, Calibration of nonlocal scaling effect parameter for free vibration of carbon nanotubes by molecular dynamics, Journal of Applied Physics 101 (2007) 24305.

Postprint for: Malikan, M, Wiczenbach T., Eremeyev, VA. Thermal buckling of functionally graded piezomagnetic micro- and nanobeams presenting the flexomagnetic effect. Continuum Mechanics and Thermodynamics. https://doi.org/10.1007/s00161-021-01038-8

Thermal buckling of functionally graded piezomagnetic nanobeams presenting the flexomagnetic effect

Mohammad Malikan[1], Tomasz Wiczenbach[1], Victor A. Eremeyev[1,2,3*]

[1] Department of Mechanics of Materials and Structures, Gdansk University of Technology, 80-233 Gdansk, Poland

[2] Research and Education Center "Materials" Don State Technical University, Gagarina sq., 1, 344000 Rostov on Don, Russia

[3] DICAAR, Università degli Studi di Cagliari, Via Marengo, 2, 09123, Cagliari, Italy

*Corresponding author:
Email: victor.eremeev@pg.edu.pl, eremeyev.victor@gmail.com

Abstract

Galerkin weighted residual method (GWRM) is applied and implemented to analytically address the axial stability and bifurcation point of thermal buckling of a functionally graded (FG) piezomagnetic structure containing flexomagneticity (FM). The continuum specimen involves an exponential mass distributed in a heterogeneous media with a constant square cross-section. The physical neutral plan is investigated to factually mark the postulated functionally graded material (FGM). Mathematical formulations are concerning the Timoshenko shear deformation theory. Small scale and atomic interactions are shaped as maintained by the nonlocal strain gradient elasticity approach.

Since there is no bifurcation point for FGMs, whenever both boundary conditions are rotational and neutral surface does not match the mid-plan, the clamp configuration is examined only. The fourth-order ordinary differential stability equations will be converted into the sets of algebraic ones by means of the GWRM, which its accuracy was proved before. Thereafter, by simply solving the achieved polynomial constitutive relation, the parametric study can be started due to various predominant and overriding factors. It was found that the flexomagneticity is further visible if the ferric nanobeam is constructed by FGM technology. In addition to this, shear deformations are also efficacious to make the FM detectable.

Nomenclature

σ_{xx} Stress component	k Material property variation
τ_{xz} Shear stress	I_z Area moment of inertia
ξ_{xxz} Hyper stress	u Axial displacement of the midplane
η_{xxz} Hyper strain	w Transverse displacement of the midplane
ε_{xx} Strain component	ϕ Rotation of beam nodes around the y axis
γ_{xz} Shear strain	q_{31} Component of the third-order piezomagnetic tensor
E Elasticity modulus	g_{31} Component of the sixth-order gradient elasticity tensor
G Shear modulus	f_{31} Component of fourth-order flexomagnetic tensor
u_1 Displacement along x	a_{33} Component of the second-order magnetic permeability tensor
u_3 Displacement along z	A Area of the cross-section of the beam
ν Poisson's ratio	N_x Axial stress resultant
L Length of the beam	M_x Moment stress resultant
b Width of the beam	Q_x Shear stress resultant
z Thickness coordinate	T_{xxz} Hyper stress resultant
h Thickness of the beam	ψ Magnetic potential
k_s Shear correction factor	

1 Introduction

The progress in micro and nanoelectronic technologies is directly related to the achievements in the field of materials engineering. The wide range of currently tested Smart Magnetic Materials (SMM) provides opportunities to develop new, innovative components and devices. The physical and chemical properties of which will be sensitive to changes in environmental parameters, such as temperature, pressure, electric field, and magnetic fields. What is more, with the development of science, new properties are

obtained. One of the frequent discoveries is flexomagnetism (FM). The phenomenon is currently being examined by scientists by considering different boundary conditions and dynamic and static terms. The flexomagnetic effect is established with a strain field gradient. In other words, it may be named the direct flexomagnetic effect. Following the attendance of a magnetic external field gradient, the flexo-effect may be distinguished in reverse impact. These new-discovered phenomena may appear in all types of materials and crystalline structures [1-9].

Functionally Graded Materials (FGMs) are new and advanced materials with a heterogeneous structure. The mechanical properties of these materials are constantly changing from one level to another, and these changes are caused by a gradual change in the volume ratio of their constituent materials [10-19]. FG materials are typically made of both ceramic and metal. Since the structural material of ceramic has a low heat transfer coefficient and high resistance to temperature, it can withstand high heat, and on the other hand, another structural material, metal, provides the required flexibility and strength. Due to the continuous changes in mechanical properties, the discontinuity problems that exist in laminated composite structures do not arise in functional materials. These materials are widely used in thermal insulation, coatings for turbine blades, protection systems, biomedical materials, bone, and dental implants, and the aerospace industry. Another implementation of FGMs can be seen in spaceship walls and engine parts, including piezoelectric, thermoelectric devices, and micro/nano-electro-mechanical systems (MEMS/NEMS).

Piezomagnetic is defined as a linear electromechanical reaction between two magnetic and mechanical states in insulating materials and crystals that do not have central symmetry. In fact, piezomagnetic structures are materials that, when pressed or stressed, a magnetic charge appears on certain surfaces. This phenomenon is called the Direct Piezomagnetic Effect, which is a reversible process, meaning that when a substance with this property is in an electric field, its dimensions change (Reverse Piezomagnetic Effect). In recent years, the mechanical response of micro and nanostructures, mainly electrically and magneto-electrically operated, has set off to be an intensive and significant region of investigation [20-37]. In order to confirm the novelty of this article, a thorough literature review was realized. The study of the most important

published works precisely associated with the investigation in this manuscript is presented.

The smart nanobeams issue is well-known, and there are many papers according to this subject. Liang et al. [38, 39] performed an investigation related to flexoelectricity and its impact on static bending issues, considering the Euler-Bernoulli beam model with the piezoelectric effect. Tadi Beni [40, 41] carried out an analysis of the dynamic behaviour and static deflection of a nanobeam exposed to electrical and mechanical loads, following the Euler-Bernoulli and Timoshenko beam model theory. Arefi et al. [42] performed a study of bending and vibration of a piezomagnetic layered nanobeam exposed to magnetic and electric potential laying on a two-parameter foundation following nonlocal Eringen's theory. Another investigation performed by Tadi Beni et al. [43] considered Van der Waals forces and electric effect and their impact on nanobeam deflection, following the modified couple stress theory. Alibeigi et al. [44, 45] performed an investigation of piezomagnetic and piezoelectric nanobeams exposed to buckling on electrical, thermal, and mechanical loads, following the Euler-Bernoulli beam theory and modified strain gradient theory. Qi et al. [46] carried out a study of bending analysis and its impact on electro-elastic nanobeams based on Euler-Bernoulli beam theory and nonlocal strain gradient theory. Li et al. [47] performed an investigation of buckling analysis of bilayered piezoelectric nanobeams with imperfections under mechanical and electrical loads, following trigonometric shear, and Eringen's nonlocal elasticity theory. Sidhardh and Ray [48] carried out a study of deflection analysis of pinned-roller supported nanobeams, including the flexoelectric layer, using the finite element method (FEM). Baroudi et al. [49] established an analytical solution for free vibration and transverse deflection study of a piezoelectric nanobeam exposed to an electrical load, based on strain gradient theory. Mohtashami et al. [50] investigated buckling and vibration of piezoelectric nanobeams following Euler-Bernoulli beam theory.

The nano-electro-mechanical devices are widely made as functionally graded nanobeams (FGN). This area is being crucially developed and investigated. Esfahani et al. [51] investigated the vibration and deflection of FGNs exposed to the external electric voltage, following the nonlocal strain gradient and Euler-Bernoulli beam theory. Zhao et al. [52] analyzed the free vibration and bending of flexoelectric FGNs with axial porous

based on strain gradient and Euler-Bernoulli beam theory. Xiao et al. [53] carried out a study of elastic-electro-magneto-thermal functionally graded nanobeams with porosity, following Eringen's nonlocal elasticity and higher-order shear deformation theory.

Following the literature review made on the piezo-flexomagnetic mechanics of structures, theoretical studies may be found. So far, several studies have been performed on nanostructures considering the flexomagnetic effect. The pioneers in this subject were Zhang et al. [54] and Sidhardh et al. [55]. In their investigation, they presented studies about piezo-flexomagnetic nanostructures subjected to linear bending. Additionally, the assumption of small-displacement was made, and only the linear-elastic region was taken into account. In both investigations, the model of the structure was nanobeam, modelled following the Euler-Bernoulli beam theory. Furthermore, the two cases of magnetization influences were considered, the direct and reverse impact. In the first study, it was deemed to be different boundary conditions. However, [55] assumed a cantilever beam in his investigation. The static load acting on a beam was applied uniformly and vertically across the length of the nanobeam. In both analyses, there is a lack of consideration of the size-dependent effect. What is more, microstructure or nonlocal impact were not investigated too. Nevertheless, they checked the surface and flexomagnetic effects on the nanobeam. More recently, Malikan et al. [56] investigated a piezo-flexomagnetic nanobeam exposed to vibrational mode, following the Euler-Bernoulli beam theory. According to the nonlocal stress-driven elasticity method, the size-dependent effect was analyzed, and the structures were subjected to linear frequency analysis. Following the obtained results, it could be concluded that the size-dependent effect concerns the flexomagnetic feature.

Furthermore, according to the nonlinear model, Malikan and Eremeyev [57] investigated the natural frequencies of piezo-flexomagnetic nanostructures. Following the nonlocal strain gradient elasticity model, they confirmed the size-dependent effect. Another study performed by Malikan et al. [58] presented piezo-flexomagnetic nanobeams subjected to large deflections, following two-step analytical and numerical solution methods. They found out that nano-electro-mechanical systems (NEMS) subjected to nonlinear bending and piezo-flexomagnetic effects are crucial in designing these systems. In this article, they showed a significant influence of the flexomagnetic

effect and its impact on the reduction of nanobeam deflection. More recently, Malikan et al. [59] investigated magnetic nanoparticles with piezo and flexomagnetic effect. The study concerning smart nanosensors investigates the analysis of the post-buckling impact on these structures. The conclusions included in this paper are very significant in the field of nanostructures. Newly, Malikan et al. [60] presented the nanobeam with porous state and piezo-flexomagnetic effect and the impact of beam size. Obtained results show that the flexomagnetic effect of the structure is dependent on the porosity of the materials. Most recently, Malikan and Eremeyev [61] investigated the composite nanoplate with the piezo-flexomagnetic effect subjected to the one-dimensional magnetic field, following the nonlocal strain gradient and classical plate theory. The conclusion earned from this paper is that flexomagnetic response is more significant if the ratio of nanoplate size (aspect ratio) is less than one.

The purpose of this paper is to present a thermal buckling analysis and the thermal capacity approach to the problems of nano and microbeam functionally-graded structures with flexomagnetic effect. The issue has been examined according to the reverse magnetic solution. The primary investigation is concerned about the functionally graded material composition and its response to the practical flexomagnetic effect. The FGMs nanosensors are frequently exposed to contact with soft tissues that may be designed with elastic structures. The problem is modelled with constitutive relations following the nonlocal strain gradient theory (NSGT). Subsequent to Gauss's law and Maxwell's equation, a relevant magnetic potential distribution is obtained. Following the clamp support boundary conditions and Timoshenko beam theory, the interaction governing equations of the structure are derived with the terms of the piezo and flexomagnetic effect. The thermal stability problem is computed with the use of discretization of the equations following Galerkin's principle. To obtain the buckling values, the characteristics equations are calculated straightforwardly. In order to ensure the accuracy of the present approach, the answers received from the introduced method were presented on different diagrams. Concerning the static behavior of the system, the effect of various parameters is shown with some illustrations. The obtained results in the numerical section of the manuscript could be conducive to attain a significant and efficient nano actuators/sensors design.

2 Mathematical modeling

To start up, a FGM piezomagnetic nanobeam is shown in Fig. 1. As the beam is shaped by a square cross-section and a schematic grading of grains of the cross-section, the Cartesian coordinate system is installed on the model. The dimensions of the beam are associated with *L* that is length, and *h* that introduces the thickness.

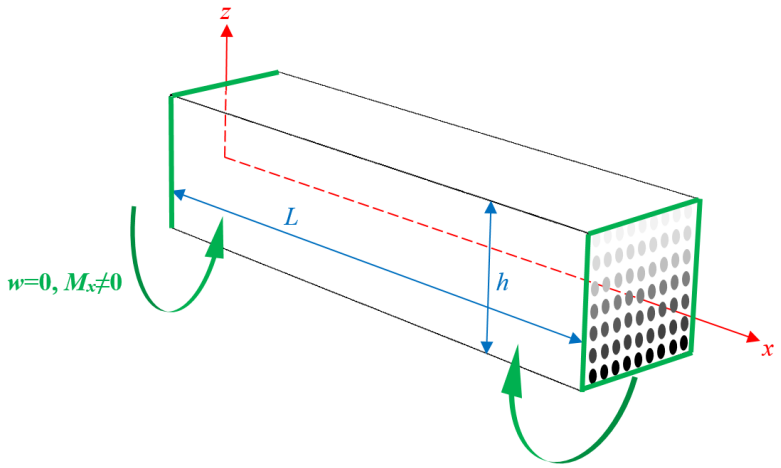

Fig. 1. A typical continuum model of FGM beam-like smart nano actuator having rectangular coordinates

Let us assume that it is essential to take into consideration the shear deformations for the FGM nanobeam. Accordingly, to concatenate the shear deformation throughout the thickness, this study utilizes the Timoshenko beam approach as [62],

$$u_1(x,z) = u(x) + (z - z_0)\phi(x) \tag{1a}$$

$$u_3(x,z) = w(x) \tag{1b}$$

The neutral plan's location is a crucial issue in FGMs with a physical concept. There is a minor deviation between the physical neutral surface and the mid-plan while appraising the FGMs due to the type of distribution of mechanical properties. The physical neutral plan's position can be described by [62-64],

$$z_0 = \frac{\int_{-h/2}^{h/2} zE(z)\,dz}{\int_{-h/2}^{h/2} E(z)\,dz} \tag{2}$$

in which z_0 defines the distance between the physical neutral plan and the geometric mid-surface.

The Voight estimate or rule of mixture interprets reasonably and continuously distribution of mechanical properties for FGMs in a heterogeneous schema. Pursuant to the volume fraction of the FGMs as composed materials, including functions of sigmoid, exponential, or power-law, the change in the material properties of FGMs is postulated to vary continuously along with the thickness. In this study, to describe the volume fraction, an exponential function is employed. Let us depict $P(z)$ which is a variable to define any property in the class of exponential functionality as [65],

$$P(z) = P_0 e^{kz} \tag{3}$$

in which an index for the property of the material is shown by *k* and P_0 represents any property related to mid-plane (*z*=0). It is requisite to remind that all these properties are varied along with the thickness. The shift from the heterogeneous beam to a homogeneous one corresponds to *k*=0. It is germane to note that the Poisson's ratio is taken as constant and independent of thickness because the difference in the values is negligible.

Lagrangian linear strain's relation layouts the following axial, shear, and hyper strains with the help of Eq. (1) as,

$$\varepsilon_{xx} = \frac{du}{dx} + (z - z_0)\frac{d\phi}{dx} - \alpha(z)\Delta T \tag{4}$$

$$\gamma_{xz} = \phi + \frac{dw}{dx} \tag{5}$$

$$\eta_{xxz} = \frac{d\varepsilon_{xx}}{dz} = \frac{d\phi}{dx} \tag{6}$$

Here, by expressing the principle of Lagrange, one can present the energy relation as,

$$\delta(W + U) = 0 \tag{7}$$

To define the internal strain energy and thermodynamic work of external forces, the letters U and W are dedicated.

It is necessary to expand the strain energy based on the description of variational calculus as,

$$\delta U = \int_V \left(\sigma_{xx} \delta \varepsilon_{xx} + \tau_{xz} \delta \gamma_{xz} + \xi_{xxz} \delta \eta_{xxz} - B_z \delta H_z \right) dV \tag{8}$$

By doing Eq. (8), we obtain single and double integrals which respectively correlate with non-classical end conditions and governing equations as follows,

$$\delta U^{Mech} = -\int_0^L \left(\frac{dN_x}{dx} \delta u + \frac{dQ_x}{dx} \delta w - Q_x \delta \phi + \frac{dM_x}{dx} \delta \phi + \frac{dT_{xxz}}{dx} \delta \phi \right) dx \tag{9a}$$

$$\delta U^{Mag} = -\int_0^L \int_{-h/2}^{h/2} \frac{dB_z}{dz} \delta \Psi dz dx \tag{9b}$$

$$\delta U^{Mech} = \left(N_x \delta u + Q_x \delta w + M_x \delta \phi + T_{xxz} \delta \phi \right) \Big|_0^L \tag{10a}$$

$$\delta U^{Mag} = \int_0^L \left(B_z \delta \Psi \right) \Big|_{-h/2}^{h/2} dx \tag{10b}$$

in which

$$N_x = \int_{-h/2}^{h/2} \sigma_{xx} dz \tag{11}$$

$$M_x = \int_{-h/2}^{h/2} \sigma_{xx} z dz \tag{12}$$

$$Q_x = k_s \times \int_{-h/2}^{h/2} \tau_{xz} dz \tag{13}$$

$$T_{xxz} = \int_{-h/2}^{h/2} \xi_{xxz} dz \tag{14}$$

Let us here attend to the work of external forces which can be formulated as,

$$W = \frac{1}{2} \int_0^L N_x^0 \left(\frac{dw}{dx} \right)^2 dx \tag{15}$$

Then, the variational method approximates the following relation,

$$\delta W = \int_0^L \left(N_x^0 \frac{d\delta w}{dx} \frac{dw}{dx} \right) dx \tag{16}$$

where the total critical buckling force is denoted with N_x^0.

It is postulated that a transverse magnetic field exists, which lets us retain the electrodes on the bottom and top surfaces of the thickness while a poling direction is kept transverse. Thus, the relation of magnetic field's lateral component corresponds to,

$$H_z + \frac{d\Psi}{dz} = 0 \tag{17}$$

The starting point of our study and the motivation is assessing flexomagneticity in smart functionally graded structures. The converse flexomagneticity is generated because of the magnetic field's strain gradient. Let us deem a closed-circuit through the thickness for which the topmost surface of the thickness contains the maximum potential, and the lowest surface involves the null of potential. To this, one can write

$$\Psi\left(+\frac{h}{2}\right) = \psi, \ \Psi\left(-\frac{h}{2}\right) = 0 \tag{18a,b}$$

The transverse magnetic field's formulas and the magnetic potential across the beam can be achieved by joining Eqs. (6, 9b, 10b, 17, and 18) with one another and the more-or-less mathematical efforts,

$$\Psi = \frac{q_{31}(z)}{2a_{33}(z)} \left((z - z_0)^2 - \frac{h^2}{4} \right) \frac{d\phi}{dx} + \frac{\psi}{h} \left((z - z_0) + \frac{h}{2} \right) \tag{19}$$

$$H_z = -(z - z_0) \frac{q_{31}(z)}{a_{33}(z)} \frac{d\phi}{dx} - \frac{\psi}{h} \tag{20}$$

According to Eringen's nonlocal theory, the stress at a reference point inside the body, such as *x*, depends not only on the strain of the point *x* but also on the strains of all points inside the body [66, 67]. This theory is consistent with predictions derived from the atomic theory of molecular lattice dynamics and observations of molecular dispersion. In the limit, the classical theory of elasticity will be derived when the effects of strain are ignored at points other than point *x*. For homogeneous and isotropic objects, the linear theory of nonlocal elasticity leads to a set of partial integro-differential equations for the displacement field that is generally difficult to solve. For certain classes of integral, these equations are reduced to a set of single partial differential equations. On the other hand, atoms consist of

a large strain gradient on a small scale. This is mathematically simulated by the strain gradient elasticity theory of Mindlin [60]. These two phenomena are unified, called nonlocal strain gradient elasticity theory [68], by which a small scale is transferred into a continuum media based on a differential model. The relation of NSGT is available below,

$$\left(1-\mu\frac{d^2}{dx^2}\right)\sigma_{ij}=C_{ijkl}\left(1-l^2\frac{d^2}{dx^2}\right)\varepsilon_{ij} \tag{21}$$

in which the additional and higher-order parameters demonstrated by μ and, l respectively, exhibit a nonlocal parameter and a strain gradient length scale parameter (SGLS). Amounts of these non-classical parameters are already determined for some classes of materials only [69].

Thereupon, infliction of Eq. (21) on Eqs. (11-14) causes Eqs. (22-24),

$$\left(1-\mu\frac{d^2}{dx^2}\right)\xi_{xxz}=\left(1-l^2\frac{d^2}{dx^2}\right)\left[\left(g_{31}(z)+\frac{q_{31}(z)\,f_{31}(z)(z-z_0)}{a_{33}(z)}\right)\frac{d\phi}{dx}+\frac{f_{31}(z)\psi}{h}\right] \tag{22}$$

$$\left(1-\mu\frac{d^2}{dx^2}\right)\sigma_{xx}=\left(1-l^2\frac{d^2}{dx^2}\right)\left[E(z)\frac{du}{dx}+(z-z_0)\left(E(z)+\frac{q_{31}^2(z)}{a_{33}(z)}\right)\frac{d\phi}{dx}+\frac{q_{31}(z)\psi}{h}-\alpha(z)E(z)\Delta T\right] \tag{23}$$

$$\left(1-\mu\frac{d^2}{dx^2}\right)\tau_{xz}=\left(1-l^2\frac{d^2}{dx^2}\right)\left[G(z)A\left(\phi+\frac{dw}{dx}\right)\right] \tag{24}$$

Later, Eqs. (11-14) will be written in the framework of Eq. (21). Thus, one can obtain

$$\left(1-\mu\frac{d^2}{dx^2}\right)N_x=\left(1-l^2\frac{d^2}{dx^2}\right)\left[I_1\frac{du}{dx}+(I_2+I_3)\frac{d\phi}{dx}+I_4-N^T\right] \tag{25}$$

$$\left(1-\mu\frac{d^2}{dx^2}\right)M_x=\left(1-l^2\frac{d^2}{dx^2}\right)\left[I_5\frac{du}{dx}+(I_6+I_7)\frac{d\phi}{dx}+I_8\right] \tag{26}$$

$$\left(1-\mu\frac{d^2}{dx^2}\right)Q_x=\left(1-l^2\frac{d^2}{dx^2}\right)\left[H_{44}\left(\phi+\frac{dw}{dx}\right)\right] \tag{27}$$

$$\left(1-\mu\frac{d^2}{dx^2}\right)T_{xxz}=\left(1-l^2\frac{d^2}{dx^2}\right)\left[(I_9+I_{10})\frac{d\phi}{dx}+I_{11}\right] \tag{28}$$

in which the established variables are expanded as follows,

$$\left\{I_1, I_2\right\} = \int_{-h/2}^{h/2} E(z)\left\{1,(z-z_0)\right\}dz,\ I_3 = \int_{-h/2}^{h/2} (z-z_0)\frac{q_{31}^2(z)}{a_{33}(z)}dz,\ I_4 = \int_{-h/2}^{h/2} \frac{\psi q_{31}(z)}{h}dz,$$

$$\left\{I_5, I_6\right\} = \int_{-h/2}^{h/2} E(z)\left\{(z-z_0),(z-z_0)^2\right\}dz,\ I_7 = \int_{-h/2}^{h/2} (z-z_0)^2\frac{q_{31}^2(z)}{a_{33}(z)}dz, I_8 = \int_{-h/2}^{h/2} (z-z_0)\frac{\psi q_{31}(z)}{h}dz,$$

$$I_9 = \int_{-h/2}^{h/2} g_{31}(z)dz,\ I_{10} = \int_{-h/2}^{h/2} (z-z_0)\frac{q_{31}(z) f_{31}(z)}{a_{33}(z)}dz, I_{11} = \int_{-h/2}^{h/2} \frac{\psi f_{31}(z)}{h}dz,\ H_{44} = k_s \int_{-h/2}^{h/2} G(z)Adz \tag{29}$$

It should be reminded that the pyromagnetic effect has been neglected in this work. The equilibrium equations can be pulled out from Eqs. (9, 10), moreover, mixed with Eq. (16),

$$\frac{dN_x}{dx} = 0 \tag{30}$$

$$\frac{dQ_x}{dx} + N_x^0 \frac{d^2 w}{dx^2} = 0 \tag{31}$$

$$\frac{dM_x}{dx} + \frac{dT_{xxz}}{dx} - Q_x = 0 \tag{32}$$

Ensuingly, Eqs. (25-28) can be taken out of complexity based on Eqs. (30-32) as follows,

$$N_x = \left(1 - l^2 \frac{d^2}{dx^2}\right)\left\{I_1 \frac{du}{dx} + \left(I_2 + I_3\right)\frac{d\phi}{dx} + I_4 - N^T\right\} \tag{33}$$

$$M_x = -\mu\left[\left(I_9 + I_{10}\right)\frac{d^3\phi}{dx^3} + N_x^0 \frac{d^2 w}{dx^2}\right] + \left(1 - l^2 \frac{d^2}{dx^2}\right)\left\{I_5 \frac{du}{dx} + \left(I_6 + I_7\right)\frac{d\phi}{dx} + I_8\right\} \tag{34}$$

$$Q_x = -\mu N_x^0 \frac{d^3 w}{dx^3} + \left(1 - l^2 \frac{d^2}{dx^2}\right)\left\{H_{44}\left(\phi + \frac{dw}{dx}\right)\right\} \tag{35}$$

$$T_{xxz} = \mu \frac{d^2 T_{xxz}}{dx^2} + \left(1 - l^2 \frac{d^2}{dx^2}\right)\left\{\left(I_9 + I_{10}\right)\frac{d\phi}{dx} + I_{11}\right\} \tag{36}$$

Eqs. (30-32) can be recasted with the aid of Eqs. (33-36) as,

$$\left(1 - l^2 \frac{d^2}{dx^2}\right)\left\{I_1 \frac{d^2 u}{dx^2} + \left(I_2 + I_3\right)\frac{d^2\phi}{dx^2}\right\} = 0 \tag{37}$$

$$\left(1-\mu\frac{d^2}{dx^2}\right)\left\{N_x^0\frac{d^2w}{dx^2}\right\}+\left(1-l^2\frac{d^2}{dx^2}\right)\left\{H_{44}\left(\frac{d\phi}{dx}+\frac{d^2w}{dx^2}\right)\right\}=0 \tag{38}$$

$$\left(1-\mu\frac{d^2}{dx^2}\right)\left\{\left(I_9+I_{10}\right)\frac{d^2\phi}{dx^2}\right\}+\left(1-l^2\frac{d^2}{dx^2}\right)\left\{I_5\frac{d^2u}{dx^2}+\left(I_6+I_7\right)\frac{d^2\phi}{dx^2}\right.$$
$$\left.-H_{44}\left(\phi+\frac{dw}{dx}\right)\right\}=0 \tag{39}$$

The above-coupled equations should be solved towards determining the thermal stability capacity of the postulated structure.

The total axial force is divided into the mechanical load, and a longitudinal magnetic load originated from the magnetic field,

$$N_x^0=N^T+N^{Mag} \tag{40}$$

where

$$N^T=\frac{1}{1-\nu}\int_{-h/2}^{h/2}\alpha_0E_0\Delta Tdz \tag{40}$$

$$N^{Mag}=\int_{-h/2}^{h/2}q_{31}\psi dz \tag{40}$$

where

$$\Delta T=T_{cr}-273.15K \tag{40}$$

3 Solving proceeding

A structure can be mathematically analyzed by implementing different edge/end conditions. But, [70] endorsed that if a FGM structure is considered, taking the physics of the structure into account, incorporating a shift of neutral surface (z_0), the bifurcation cannot occur while some supports, particularly simply-supported end conditions, are modelled. In this manner, the specimen tends to bend instead of buckling. Thereby, in continue, the fully fixed end conditions are analytically formed as

$$u\left(x\right)=\sum_{m=1}^{\infty}\frac{d}{dx}\left[\sin^2\left(\frac{m\pi}{L}x\right)\right]\exp\left(i\omega_nt\right) \tag{41}$$

$$w\left(x\right)=\sum_{m=1}^{\infty}\sin^2\left(\frac{m\pi}{L}x\right)\exp\left(i\omega_nt\right) \tag{42}$$

$$\phi(x)=\sum_{m=1}^{\infty}\cos^2\left(\frac{m\pi}{L}x\right)\exp(i\omega_n t) \tag{43}$$

in which t relates to time in dynamic systems.

With respect to the Galerkin weighted residual method, the clamped end conditions can be satisfied by the foregoing series. To calculate the residuals in the technique, the pursuing integrals assist us,

$$\int_0^L R_1(x)u(x)dx=0 \tag{44}$$

$$\int_0^L R_2(x)w(x)dx=0 \tag{45}$$

$$\int_0^L R_3(x)\phi(x)dx=0 \tag{46}$$

in which the residuals are illustrated by $R_i(x)(i=1,..,3)$.

Arranging the terms of Eqs. (44-46) with respecting unknown parameters $u, w,$ and ϕ in a matrix form leads to

$$\begin{bmatrix} K_{11} & K_{12} & K_{13} \\ K_{21} & K_{22} & K_{23} \\ K_{31} & K_{32} & K_{33} \end{bmatrix}\begin{Bmatrix} u \\ w \\ \phi \end{Bmatrix}=0 \tag{47}$$

Then, the determinant of the coefficient matrix gives a polynomial characteristic equation of axial stability of the smart FGM structure consisting of flexomagneticity,

$$\det\left[K_{ij}\right]=0 \tag{48}$$

Subsequently, solving the attained polynomial equation results in having values of the critical buckling temperature (T_{cr}).

4 Results and discussions

The fabrication of a piezomagnetic functionally graded structure with exponential functionality is deemed to evaluate and study its flexomagnetic response inside the illustration of a complete parametric study. Thence, Table 1 [71-73] detailedly indicates the structural properties needed for this section. Let us here see that the FGM can emboss the role of flexomagneticity or not. Therefore, a scientific interpretation is observed based

on Figures 2-5. Pursuing this, it is urgent to note that two states are considered, which are the piezomagnetic FGM encompassing flexomagneticity (FG-PFM) and piezomagnetic FGM that does not incorporate the flexomagneticity (FG-PM). Let us note that in all figures, the horizontal axis is the index *k*, and the vertical axis is the amount of heat stability capacity of the nanobeam. We must also confirm that the results were calculated only for the first buckling mode. The values of the other variables are included next to the titles of the figures.

Table 1. Available material properties

$CoFe_2O_4$
E_0=286GPa
$f_{31}=10^{-9}$ N/A
q_{31}=580.3 N/A.m
$a_{33}=1.57\times10^{-4}$ N/A^2
$\alpha_0=11.80\times10^{-6}$ 1/K
(room temperature)

We start presenting the results by changing the nonlocal coefficient in Figure 2. The most obvious possible consequence from the diagram is that increasing the coefficient *k* will increase the thermal stability of the nanobeams, and more importantly, the higher the value of *k*, the more significant the difference between the curve of the FG-PFM nanobeam and the FG-PM one. Of course, this distance between the results is crucial in the larger value of the nonlocal coefficient. Therefore, a significant outcome that can be deduced from this figure is that producing a piezomagnetic material in the skeleton of a FGM structure, while the cross-sectional FG properties follow an exponential function, increases the flexo-effect, and this will be even more momentous when the nonlocality parameter is larger.

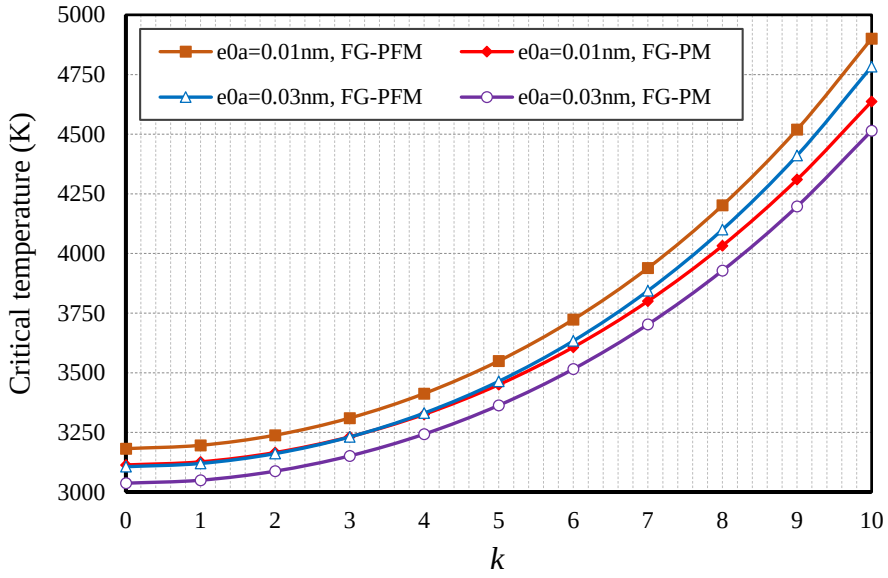

Fig. 2. FGM variation index vs. critical temperature for various cases (Ψ=1mA, l=0.05nm, L/h=10)

Many references have shown that the presence of the nonlocal coefficient in the relationships and modeling of the small-scale problems leads to a reduction in material stiffness and vice versa, the presence of the length scale strain gradient parameter (SGLS) existed in the couple stress relations and the first and second Mindlin gradients helps to increase the material stiffness. Therefore, regardless of Figure 3, we must conclude that the results of Figure 2 in Figure 3 will be obtained when the SGLS parameter has smaller values. That is, here, a smaller value of the SGLS enhances the importance of flexo. Of course, the most substantial result remains in place, which means in Figure 3, we again find that increasing k has raised the importance of the flexo-effect. If we examine and compare Figures 2 and 3 more carefully, we will come to the important conclusion that the increase in the difference between the FG-PFM and FG-PM results for l=0.01nm in Figure 3 is greater than e_0a=0.03nm in Figure 2. Therefore, it can be said that the SGLS parameter is more effective than the nonlocal parameter in this part.

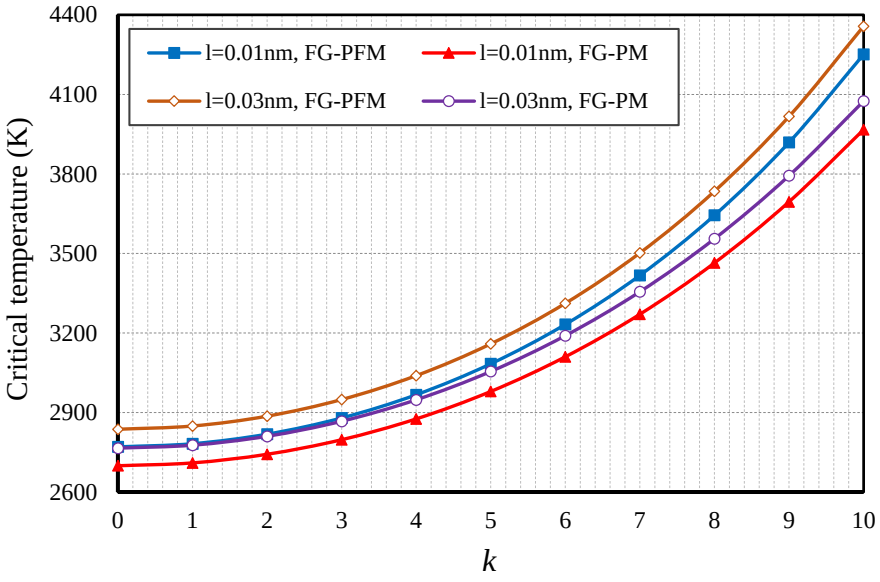

Fig. 3. FGM variation index vs. critical temperature for various cases (Ψ=1mA, e_0a=0.05nm, L/h=10)

Figure 4 is drawn to investigate the effect of the magnetic field. Following the previous diagrams, increasing k will develop the critical temperature stability. The amount of magnetic potential produced by the magnetic field is given in milliamperes. The point to consider in this figure is that, unlike the previous figures, the results initially differ for two different potential values, namely one and two milliamperes. On the other hand, it is crystal clear that the difference in the results obtained after increasing k is greater than the previous two figures. That is, the difference between FG-PM and FG-PFM is more pronounced than in Figures 2 and 3. This figure shows that the role of magnetic potential in magnetic FGMs will be more prominent. Also, the difference in the results of PFM and PM at k=10 is the same for both magnetic potentials, thus showing that different values of the magnetic potential have the same effect on the behavior of the flexomagneticity.

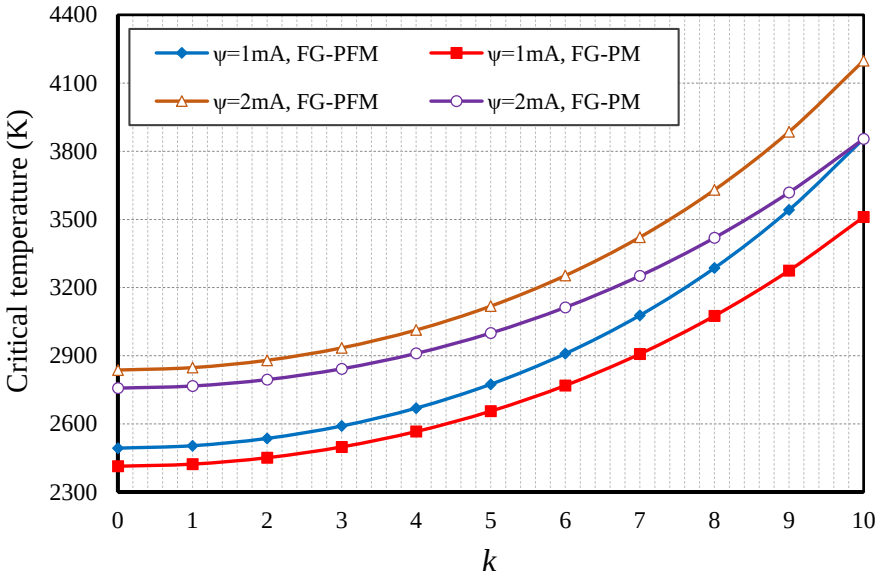

Fig. 4. FGM variation index vs. critical temperature for various cases (l=0.05nm, e_0a=0.1nm, L/h=10)

Let us measure the results and the relevant discussion by showing the effectiveness of changes in length to thickness coefficient (slenderness ratio). The nanobeam is designed in two modes, relatively thick (L/h=10) and relatively thin (L/h=20). At first glance, the point to be evaluated is that the results are increasing for three modes (FG-PM for L/h=10 and L/h=20, and FG-PFM for L/h=20) with almost the same slope, but in the relatively thick beam manner, the model FG-PFM, L/h=10, will have a greater slope and a more considerable increase. At k=10, this model distinguishes itself more than other models. This is an excellent argument to confirm that although the shear deformation is serious in relatively thick and thick beams, it will be doubly important if the flexomagnetic effect is analyzed in these beams.

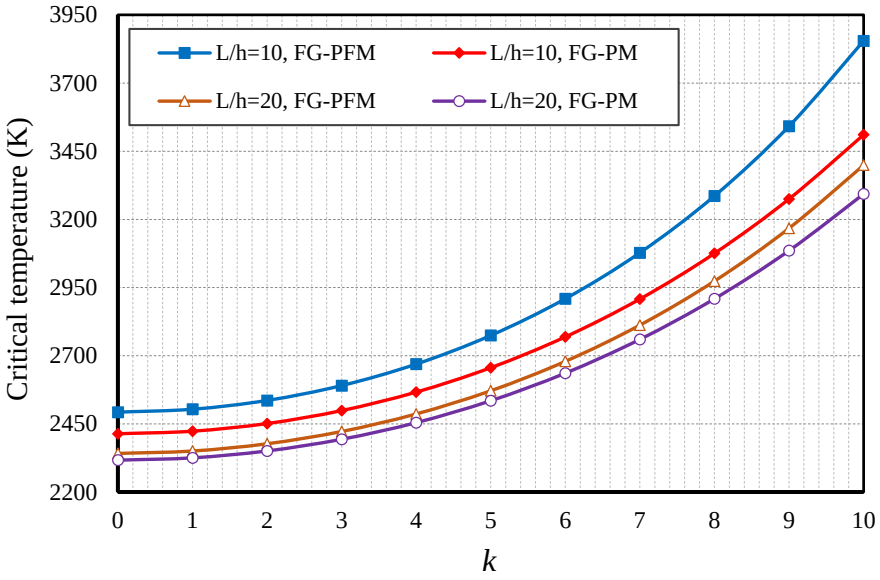

Fig. 5. FGM variation index vs. critical temperature for various cases (Ψ=1mA, l=0.05nm, e_0a=0.1nm)

5 Conclusions

It was observed that flexomagneticity (FM) could be even stronger in a ferroic functionally graded material (FGM). The Galerkin weighted residual method (GWRM) warranted the numerical results in the framework of analytical solutions for fully fixed ends conditions. The beam's behavior depended on the shear deformations; therefore, the Timoshenko beam was taken into the model. The nanoscale examination was revealed by exerting both stress nonlocality and strain gradient in the circumstance of the nonlocal strain gradient approach. The implementation of the material composition was presumed as exponential functionality concerning the rule of mixture. Inclusive of flexomagneticity was performed in terms of reverse field effect. Under the axially compressed conditions of the system, the critical buckling temperature was explored. Notwithstanding that the FGMs can be correctly analyzed in a way that the mid-plan plays the role of the neutral surface, this research took into account the physical neutral plan that differs from the mid-surface. Furthermore, one observed that the FM would be more visible in FGMs while shear deformations exist. This study provides and offers new principal aspects that suit the designing of a small-scale actuator/sensor.

Acknowledgements

V.A. Eremeyev acknowledges the support of the Government of the Russian Federation (contract No. 14.Z50.31.0046).

References

1. Fahrner, W.R.; Hilleringmann, U.; Horstmann, J.T.; Job, R.; Neitzert, H.C.; Scheer, H.C.; Ulyashin, A.; Wieck, A.D. *Nanotechnology and Nanoelectronic* **2005**, doi:10.1007/b137771.

2. Lukashev, P.; Sabirianov, R.F. Flexomagnetic Effect in Frustrated Triangular Magnetic Structures. *Phys Rev B* **2010**, *82*, 094417, doi:10.1103/PhysRevB.82.094417.

3. Pereira, C.; Pereira, A.M.; Fernandes, C.; Rocha, M.; Mendes, R.; Fernández-García, M.P.; Guedes, A.; Tavares, P.B.; Grenèche, J.-M.; Araújo, J.P.; et al. Superparamagnetic MFe 2 O 4 (M = Fe, Co, Mn) Nanoparticles: Tuning the Particle Size and Magnetic Properties through a Novel One-Step Coprecipitation Route. *Chem Mater* **2012**, *24*, 1496–1504, doi:10.1021/cm300301c.

4. Zhang, J.X.; Zeches, R.J.; He, Q.; Chu, Y.-H.; Ramesh, R. Nanoscale Phase Boundaries: A New Twist to Novel Functionalities. *Nanoscale* **2012**, *4*, 6196, doi:10.1039/c2nr31174g.

5. Zhou, H.; Pei, Y.; Fang, D. Magnetic Field Tunable Small-Scale Mechanical Properties of Nickel Single Crystals Measured by Nanoindentation Technique. *Sci Rep* **2015**, *4*, 4583, doi:10.1038/srep04583.

6. Moosavi, S.; Zakaria, S.; Chia, C.H.; Gan, S.; Azahari, N.A.; Kaco, H. Hydrothermal Synthesis, Magnetic Properties and Characterisation of CoFe2O4 Nanocrystals. *Ceram Int* **2017**, *43*, 7889–7894, doi:10.1016/j.ceramint.2017.03.110.

7. Eliseev, E.A.; Glinchuk, M.D.; Khist, V.; Skorokhod, V. V.; Blinc, R.; Morozovska, A.N. Linear Magnetoelectric Coupling and Ferroelectricity Induced by the Flexomagnetic Effect in Ferroics. *Phys Rev B* **2011**, *84*, 174112, doi:10.1103/PhysRevB.84.174112.

8. Kabychenkov, A.F.; Lisovskii, F. V. Flexomagnetic and Flexoantiferromagnetic Effects in Centrosymmetric Antiferromagnetic Materials. *Tech Phys* **2019**, *64*, 980–983, doi:10.1134/S1063784219070144.

9. Eliseev, E.A.; Morozovska, A.N.; Glinchuk, M.D.; Blinc, R. Spontaneous Flexoelectric/Flexomagnetic Effect in Nanoferroics. *Phys Rev B* **2009**, *79*, 165433, doi:10.1103/PhysRevB.79.165433.

10. Hadj Mostefa, A.; Merdaci, S.; Mahmoudi, N. An Overview of Functionally Graded Materials «FGM». In *Proceedings of the Third International Symposium on Materials and Sustainable Development*; Springer International Publishing: Cham, 2018; pp. 267–278.

11. Loh, G.H.; Pei, E.; Harrison, D.; Monzón, M.D. An Overview of Functionally Graded Additive Manufacturing. *Addit Manuf* **2018**, *23*, 34–44, doi:10.1016/j.addma.2018.06.023.

12. Udupa, G.; Rao, S.S.; Gangadharan, K.V. Functionally Graded Composite Materials: An Overview. *Procedia Mater Sci* **2014**, *5*, 1291–1299, doi:10.1016/j.mspro.2014.07.442.

13. Vasiliev, A.S.; Volkov, S.S.; Belov, A.A.; Litvinchuk, S.Y.; Aizikovich, S.M. Indentation of a Hard Transversely Isotropic Functionally Graded Coating by a Conical Indenter. *Int J Eng Sci* **2017**, *112*, 63–75, doi:10.1016/j.ijengsci.2016.12.002.

14. Malikan, M.; Eremeyev, V.A. A New Hyperbolic-Polynomial Higher-Order Elasticity Theory for Mechanics of Thick FGM Beams with Imperfection in the Material Composition. *Compos Struct* **2020**, *249*, 112486, doi:10.1016/j.compstruct.2020.112486.

15. Liu, T.-J.; Yang, F.; Yu, H.; Aizikovich, S.M. Axisymmetric Adhesive Contact Problem for Functionally Graded Materials Coating Based on the Linear Multi-Layered Model. *Mech Based Des Struct Mach* **2021**, *49*, 41–58, doi:10.1080/15397734.2019.1666721.

16. Zhang, J.; Zheng, W. Elastoplastic buckling of FGM beams in thermal environment. *Contin Mech Thermodyn* **2021**, *33*, 151–161, doi:10.1007/s00161-020-00895-z.

17. Huang, H.; Rao, D. Thermal buckling of functionally graded cylindrical shells with temperature-dependent elastoplastic properties. *Contin Mech Thermodyn* **2020**, *32*, 1403–1415, doi:10.1007/s00161-019-00854-3.

18. Roghani, M.; Rouhi, H. Nonlinear stress-driven nonlocal formulation of Timoshenko beams made of FGMs, *Contin Mech Thermodyn* **2021**, *33*, 343–355, doi:10.1007/s00161-020-00906-z.

19. Golmakani, M.E.; Malikan, M.; Pour, S.G. et al. Bending analysis of functionally graded nanoplates based on a higher-order shear deformation theory using dynamic

relaxation method, *Contin Mech Thermodyn* **2021**, doi:10.1007/s00161-021-00995-4.

20. Volkov, S.S.; Vasiliev, A.S.; Aizikovich, S.M.; Mitrin, B.I. Axisymmetric Indentation of an Electroelastic Piezoelectric Half-Space with Functionally Graded Piezoelectric Coating by a Circular Punch. *Acta Mech* **2019**, *230*, 1289–1302, doi:10.1007/s00707-017-2026-x.

21. Malikan, M. Electro-Thermal Buckling of Elastically Supported Double-Layered Piezoelectric Nanoplates Affected by an External Electric Voltage. *Multidiscip Model Mater Struct* **2019**, *15*, 50–78, doi:10.1108/MMMS-01-2018-0010.

22. Malikan, M.; Nguyen, V.B. Buckling Analysis of Piezo-Magnetoelectric Nanoplates in Hygrothermal Environment Based on a Novel One Variable Plate Theory Combining with Higher-Order Nonlocal Strain Gradient Theory. *Phys E Low-dimensional Syst Nanostructures* **2018**, *102*, 8–28, doi:10.1016/j.physe.2018.04.018.

23. Zenkour, A.M.; Aljadani, M.H. Porosity Effect on Thermal Buckling Behavior of Actuated Functionally Graded Piezoelectric Nanoplates. *Eur J Mech - A/Solids* **2019**, *78*, 103835, doi:10.1016/j.euromechsol.2019.103835.

24. Sobhy, M.; Zenkour, A.M. Porosity and Inhomogeneity Effects on the Buckling and Vibration of Double-FGM Nanoplates via a Quasi-3D Refined Theory. *Compos Struct* **2019**, *220*, 289–303, doi:10.1016/j.compstruct.2019.03.096.

25. Numanoğlu, H.M.; Akgöz, B.; Civalek, Ö. On Dynamic Analysis of Nanorods. *Int J Eng Sci* **2018**, *130*, 33–50, doi:10.1016/j.ijengsci.2018.05.001.

26. Farokhi, H.; Ghayesh, M.H. Nonlinear Mechanics of Electrically Actuated Microplates. *Int J Eng Sci* **2018**, *123*, 197–213, doi:10.1016/j.ijengsci.2017.08.017.

27. Zenkour, A.M.; Alghanmi, R.A. Hygro-Thermo-Electro-Mechanical Bending Analysis of Sandwich Plates with FG Core and Piezoelectric Faces. *Mech Adv Mater Struct* **2021**, *28*, 282–294, doi:10.1080/15376494.2018.1562134.

28. Abazid, M.A.; Zenkour, A.M.; Sobhy, M. Wave Propagation in FG Porous GPLs-Reinforced Nanoplates under in-Plane Mechanical Load and Lorentz Magnetic Force via a New Quasi 3D Plate Theory. *Mech Based Des Struct Mach* **2020**, 1–20, doi:10.1080/15397734.2020.1769651.

29. Zenkour, A.M.; Aljadani, M.H. Buckling Analysis of Actuated Functionally Graded Piezoelectric Plates via a Quasi-3D Refined Theory. *Mech Mater* **2020**, *151*, 103632, doi:10.1016/j.mechmat.2020.103632.

30. Arefi, M.; Kiani, M.; Rabczuk, T. Application of Nonlocal Strain Gradient Theory to Size Dependent Bending Analysis of a Sandwich Porous Nanoplate Integrated with Piezomagnetic Face-Sheets. *Compos Part B Eng* **2019**, *168*, 320–333, doi:10.1016/j.compositesb.2019.02.057.

31. Akgöz, B.; Civalek, Ö. Buckling Analysis of Functionally Graded Microbeams Based on the Strain Gradient Theory. *Acta Mech* **2013**, *224*, 2185–2201, doi:10.1007/s00707-013-0883-5.

32. Li, Y.S.; Cai, Z.Y.; Shi, S.Y. Buckling and Free Vibration of Magnetoelectroelastic Nanoplate Based on Nonlocal Theory. *Compos Struct* **2014**, *111*, 522–529, doi:10.1016/j.compstruct.2014.01.033.

33. Zhang, D.P.; Lei, Y.J.; Shen, Z.B. Thermo-Electro-Mechanical Vibration Analysis of Piezoelectric Nanoplates Resting on Viscoelastic Foundation with Various Boundary Conditions. *Int J Mech Sci* **2017**, *131–132*, 1001–1015, doi:10.1016/j.ijmecsci.2017.08.031.

34. Kim, J.; Reddy, J.N. Modeling of Functionally Graded Smart Plates with Gradient Elasticity Effects. *Mech Adv Mater Struct* **2017**, *24*, 437–447, doi:10.1080/0145935X.2016.1199188.

35. Li, Y.S.; Pan, E. Static Bending and Free Vibration of a Functionally Graded Piezoelectric Microplate Based on the Modified Couple-Stress Theory. *Int J Eng Sci* **2015**, *97*, 40–59, doi:10.1016/j.ijengsci.2015.08.009.

36. Mehralian, F.; Tadi Beni, Y.; Ansari, R. Size Dependent Buckling Analysis of Functionally Graded Piezoelectric Cylindrical Nanoshell. *Compos Struct* **2016**, *152*, 45–61, doi:10.1016/j.compstruct.2016.05.024.

37. Civalek, Ö.; Dastjerdi, S.; Akbaş, Ş.D.; Akgöz, B. Vibration Analysis of Carbon Nanotube-reinforced Composite Microbeams. *Math Methods Appl Sci* **2021**, mma.7069, doi:10.1002/mma.7069.

38. Liang, X.; Hu, S.; Shen, S. Effects of Surface and Flexoelectricity on a Piezoelectric Nanobeam. *Smart Mater Struct* **2014**, *23*, 035020, doi:10.1088/0964-1726/23/3/035020.

39. Liang, X.; Hu, S.; Shen, S. Size-Dependent Buckling and Vibration Behaviors of Piezoelectric Nanostructures Due to Flexoelectricity. *Smart Mater Struct* **2015**, *24*, 105012, doi:10.1088/0964-1726/24/10/105012.

40. Tadi Beni, Y. Size-Dependent Analysis of Piezoelectric Nanobeams Including Electro-Mechanical Coupling. *Mech Res Commun* **2016**, *75*, 67–80, doi:10.1016/j.mechrescom.2016.05.011.

41. Tadi Beni, Y. A Nonlinear Electro-Mechanical Analysis of Nanobeams Based on the Size-Dependent Piezoelectricity Theory. *J Mech* **2017**, *33*, 289–301, doi:10.1017/jmech.2016.65.

42. Arefi, M.; Zenkour, A.M. Size-Dependent Vibration and Bending Analyses of the Piezomagnetic Three-Layer Nanobeams. *Appl Phys A* **2017**, *123*, 202, doi:10.1007/s00339-017-0801-0.

43. Tadi Beni, Y.; Karimipöur, I.; Abadyan, M. Modeling the Effect of Intermolecular Force on the Size-Dependent Pull-in Behavior of Beam-Type NEMS Using Modified Couple Stress Theory. *J Mech Sci Technol* **2014**, *28*, 3749–3757, doi:10.1007/s12206-014-0836-5.

44. Alibeigi, B.; Tadi Beni, Y. On the Size-Dependent Magneto/Electromechanical Buckling of Nanobeams. *Eur Phys J Plus* **2018**, *133*, 398, doi:10.1140/epjp/i2018-12208-6.

45. Alibeigi, B.; Tadi Beni, Y.; Mehralian, F. On the Thermal Buckling of Magneto-Electro-Elastic Piezoelectric Nanobeams. *Eur Phys J Plus* **2018**, *133*, 133, doi:10.1140/epjp/i2018-11954-7.

46. Qi, L.; Zhou, S.; Li, A. Size-Dependent Bending of an Electro-Elastic Bilayer Nanobeam Due to Flexoelectricity and Strain Gradient Elastic Effect. *Compos Struct* **2016**, *135*, 167–175, doi:10.1016/j.compstruct.2015.09.020.

47. Li, Y.-D.; Bao, R.; Chen, W. Buckling of a Piezoelectric Nanobeam with Interfacial Imperfection and van Der Waals Force: Is Non-local Effect Really Always Dominant? *Compos Struct* **2018**, *194*, 357–364, doi:10.1016/j.compstruct.2018.04.031.

48. Sidhardh, S.; Ray, M.C. Effect of Nonlocal Elasticity on the Performance of a Flexoelectric Layer as a Distributed Actuator of Nanobeams. *Int J Mech Mater Des* **2018**, *14*, 297–311, doi:10.1007/s10999-017-9375-4.

49. Baroudi, S.; Najar, F.; Jemai, A. Static and Dynamic Analytical Coupled Field Analysis of Piezoelectric Flexoelectric Nanobeams: A Strain Gradient Theory Approach. *Int J Solids Struct* **2018**, *135*, 110–124, doi:10.1016/j.ijsolstr.2017.11.014.

50. Mohtashami, M.; Tadi Beni, Y. Size-Dependent Buckling and Vibrations of Piezoelectric Nanobeam with Finite Element Method. *Iran J Sci Technol Trans Civ Eng* **2019**, *43*, 563–576, doi:10.1007/s40996-018-00229-9.

51. Esfahani, S.; Esmaeilzade Khadem, S.; Ebrahimi Mamaghani, A. Nonlinear Vibration Analysis of an Electrostatic Functionally Graded Nano-Resonator with Surface Effects Based on Non-local Strain Gradient Theory. *Int J Mech Sci* **2019**, *151*, 508–522, doi:10.1016/j.ijmecsci.2018.11.030.

52. Zhao, X.; Zheng, S.; Li, Z. Effects of Porosity and Flexoelectricity on Static Bending and Free Vibration of AFG Piezoelectric Nanobeams. *Thin-Walled Struct* **2020**, *151*, 106754, doi:10.1016/j.tws.2020.106754.

53. Xiao, W.; Gao, Y.; Zhu, H. Buckling and Post-Buckling of Magneto-Electro-Thermo-Elastic Functionally Graded Porous Nanobeams. *Microsyst Technol* **2019**, *25*, 2451–2470, doi:10.1007/s00542-018-4145-2.

54. Zhang, N.; Zheng, S.; Chen, D. Size-Dependent Static Bending of Flexomagnetic Nanobeams. *J Appl Phys* **2019**, *126*, 223901, doi:10.1063.

55. Sidhardh, S.; Ray, M.C. Flexomagnetic Response of Nanostructures. *J Appl Phys* **2018**, *124*, 244101, doi:10.1063/1.5060672.

56. Malikan, M.; Eremeyev, V.A. Free Vibration of Flexomagnetic Nanostructured Tubes Based on Stress-driven Nonlocal Elasticity. In *Advanced Structured M* **2020**, *134*, 215-226, doi:10.1007/978-3-030-47491-1_12.

57. Malikan, M.; Eremeyev, V.A. On the Geometrically Nonlinear Vibration of a Piezo-Flexomagnetic Nanotube. *Math Methods Appl Sci* **2020**, doi: 10.1002/mma.6758.

58. Malikan, M.; Uglov, N.S.; Eremeyev, V.A. On Instabilities and Post-Buckling of Piezomagnetic and Flexomagnetic Nanostructures. *Int J Eng Sci* **2020**, 157, 103395, doi:10.1016/j.ijengsci.2020.103395.

59. Malikan, M.; Eremeyev, V.A.; Żur, K.K. Effect of Axial Porosities on Flexomagnetic Response of In-Plane Compressed Piezomagnetic Nanobeams. *Symmetry (Basel)* **2020**, *12*, 1–16, doi:10.3390/sym12121935.

60. Malikan, M.; Wiczenbach, T.; Eremeyev, V.A. On Thermal Stability of Piezo-Flexomagnetic Microbeams Considering Different Temperature Distributions. *Contin Mech Thermodyn* **2021**, doi:10.1007/s00161-021-00971-y.

61. Malikan, M.; Eremeyev, V.A. Flexomagnetic Response of Buckled Piezomagnetic Composite Nanoplates. *Compos Struct* **2021**, *267*, 113932, doi:10.1016/j.compstruct.2021.113932.

62. Thanh Tran, T.; Nguyen, P.-C.; Pham, Q.-H. Vibration analysis of FGM plates in thermal environment resting on elastic foundation using ES-MITC3 element and prediction of ANN. *Case Stud Therm Eng* **2021**, *24*, 100852. doi:10.1016/j.csite.2021.100852.

63. Chu, L.; Dui, G.; Ju, Ch. Flexoelectric effect on the bending and vibration responses of functionally graded piezoelectric nanobeams based on general

modified strain gradient theory. *Compos Struct* **2018**, *186*, 39-49. doi:10.1016/j.compstruct.2017.10.083.

64. Ahmed Hassan, A.H.; Kurgan, N. Bending analysis of thin FGM skew plate resting on Winkler elastic foundation using multi-term extended Kantorovich method. *Eng Sci Technol an Int J* **2020**, *23*, 788-800. doi:10.1016/j.jestch.2020.03.009.

65. Ait Atmane, H.; Tounsi, A.; Ahmed Meftah, S.; Abdesselem Belhadj, H. Free Vibration Behavior of Exponential Functionally Graded Beams with Varying Cross-section. *J Vib Control* **2011**, *17*, 311. doi:10.1177/1077546310370691.

66. Dastjerdi, Sh.; Malikan, M.; Dimitri, R.; Tornabene, F. Nonlocal elasticity analysis of moderately thick porous functionally graded plates in a hygro-thermal environment. *Compos Struct* **2021**, *255*, 112925. doi:10.1016/j.compstruct.2020.112925.

67. Eringen, A.C. On differential equations of nonlocal elasticity and solutions of screw dislocation and surface waves. *J Appl Phys* **1983**, *54*, 4703–4710. doi:10.1063/1.332803.

68. Lim, C.W.; Zhang, G.; Reddy, J.N. A higher-order nonlocal elasticity and strain gradient theory and its applications in wave propagation. *J Mech Phys Solids* **2015**, *78*, 298-313. doi:10.1016/j.jmps.2015.02.001.

69. Ansari, R.; Sahmani, S.; Arash, B. Nonlocal plate model for free vibrations of single-layered graphene sheets. *Phys Lett A* **2010**, *375*, 53-62. doi:10.1016/j.physleta.2010.10.028.

70. Karamanli, A.; Aydogdu, M. Bifurcation buckling conditions of FGM plates with different boundaries. *Compos Struct* **2020**, *245*, 112325. doi:10.1016/j.compstruct.2020.112325

71. Lu, Z.-l.; Gao, P.-z.; Ma, R.-x.; Xu, J.; Wang, Z.-h.; Rebrov, E. V. Structural, magnetic and thermal properties of one-dimensional CoFe2O4 microtubes. *J Alloy Comp* **2016**, *665*, 428-434. doi:10.1016/j.jallcom.2015.12.262.

72. Balsing Rajput, A.; Hazra, S.; Nath Ghosh, N. Synthesis and characterisation of pure single-phase CoFe2O4 nanopowder via a simple aqueous solution-based EDTA-precursor route. *J Exp Nanosci* **2013**, *8*, 629-639. doi:10.1080/17458080.2011.582170.

73. Senthil, V.P.; Gajendiran, J.; Gokul Raj, S.; Shanmugavel, T.; Ramesh Kumar, G.; Parthasaradhi Reddy, C. Study of structural and magnetic properties of cobalt ferrite (CoFe2O4) nanostructures. *Chem Phys Lett* **2018**, *695*, 19-23. doi:10.1016/j.cplett.2018.01.057.

International Journal of Engineering Science 148 (2020) 103210

Contents lists available at ScienceDirect

International Journal of Engineering Science

journal homepage: www.elsevier.com/locate/ijengsci

Torsional stability capacity of a nano-composite shell based on a nonlocal strain gradient shell model under a three-dimensional magnetic field ☆

Mohammad Malikan [a], Maxim Krasheninnikov [b], Victor A. Eremeyev [a,b,*]

[a] Department of Mechanics of Materials and Structures, Faculty of Civil and Environmental Engineering, Gdansk University of Technology, 80-233 Gdansk, Poland

[b] R. E. Alekseev Nizhny Novgorod Technical University, Minin St., 24, Nizhny Novgorod, 603950 Russia

ARTICLE INFO

Article history:
Received 19 December 2019
Accepted 25 December 2019
Available online 10 January 2020

Keywords:
Single-walled composite nano-shell
Torsional buckling
Three-dimensional magnetic field
Nonlocal strain gradient shell model
Analytical solution

ABSTRACT

This paper considers a single-walled composite nano-shell (SWCNS) exposed in a torsional critical stability situation. As the magnetic field affects remarkably nanostructures in the small size, a three-dimensional magnetic field is assessed which contains magnetic effects along the circumferential, radial and axial coordinates system. Based on the results of the nonlocal model of strain gradient small-scale approach and the first-order shear deformation shell theory (FSDST), the problem is estimated. Afterward, the numerical results are taken analytically and compared with other existing literature. Hereafter, the influences of various factors, such as the magnetic field, are discussed deeply. It is observed that when the magnetic field is studied in three dimensions, the transverse magnetic effect is the most serious factor that affects fundamentally the torsional stability of the shell.

1. Introduction

Due to the urgent need of industries for high strength structures with low weight, nano-composite shells are a good choice for this field. Over the years, nano-composite materials have been found from laboratory to commercial and industrial applications and have also many applications in various industries such as aerospace, defense, offshore and automotive. Some nano-composite structures which have been made, e.g. magnetic nano-composite structures, have received further attention over the previous years. These materials present impressive properties that outweigh the properties of conventional composite materials. The magnetic nano-composite structures are useful for producers of actuators and small motors, especially computer hardware, audio and video (Elimelech, Gregory, Jia & Williams, 1995).

To design different structures, analyzes such as static, dynamic, vibrational, fracture and buckling ones are performed. Since cylindrical nano-shell/tube structures are more susceptible to buckling loads, stability analysis is one of the most

☆ Preprint submitted to International Journal of Engineering Science December 19, 2019

* Corresponding author at: Department of Mechanics of Materials and Structures, Faculty of Civil and Environmental Engineering, Gdansk University of Technology, 80-233 Gdansk, Poland.

E-mail addresses: mohammad.malikan@pg.edu.pl (M. Malikan), maxim.krasheninnikov@mail.ru (M. Krasheninnikov), victor.eremeev@pg.edu.pl (V.A. Eremeyev).

https://doi.org/10.1016/j.ijengsci.2019.103210

serious analyses of these types of structures. Among the nano-shell structures, the carbon nanotubes (CNTs) are the most customary nano-shells that have been greatly investigated. Han and Lu (2003) based on the local continuum mechanics, studied the torsional stability of a double-walled carbon nanotube (DWCNT) based on considering an elastic substrate. They employed the classical shell model and solved the gained equations by means of the Navier solution technique. Wang, Yang and Dong (2005) considered multi-walled carbon nanotubes (MWCNTs) under a torsional stability condition based on the local classical continuum shell model. Lu and Wang (2006) combined torsional and axial stability conditions in order to estimate the local continuum shell MWCNTs. Zhang and Shen (2006) examined a single-walled carbon nanotube (SWCNT) with the help of molecular dynamics (MD) simulation subjected to torsion, axial and external pressures by assuming a thermal surrounding. In some valuable research works, other researchers have also studied CNTs in the case of torsional stability (Jeong, Lim & Sinnott, 2007; Wang, Quek & Varadan, 2007; Yang & Wang, 2007; Zhang & Wang, 2008). Later, Shen and Zhang (2010) modeled a DWCNT by using first-order shear deformation shell theory (FSDST) and in conjunction with nonlocal elasticity and also considering the thermal environment. Hao, Guo and Wang (2010), Natsuki, Tsuchiya, Ni and Endo (2010), on the other hand, worked on the shell model of DWCNTs based on the nonlocal elasticity theory. Khademolhosseini, Rajapakse and Nojeh (2010) used a modified Timoshenko shell model to evaluate a SWCNT in a shell domain based on the nonlocal theory of Eringen. In various conditions and cases, some other studies have been done on the CNTs exposed to torsional stability (Chowdhurry, Wang & Koh, 2014; Parvaneh, Shariati, Torabi, Masood & Sabeti, 2012; Song & Zha, 2011; Zhang & Li, 2015). More newly, Xiaohu, Yugang and Hanzhou (2013) carried out an electric and thermal field around the CNTs exposed to torsion by examining size effects. Ghorbanpour Arani, Abdollahian, Kolahchi and Rahmati (2013) analyzed a DWCNT subjected to the torsional critical force and thermal effects with considering piezoelectricity impact. They applied the FSDST and also assumed a matrix outer the system. The piezoelectric field was assumed in one direction. They solved the harvested stability relations regarding the Navier approach. In an effective paper, Mehralian, Tadi Beni and Karimi Zeverdejani (2017) simulated natural frequencies of a shell FSDST-CNTs by using MD based on different small-scale theories, namely modified couple stress theory (CST), nonlocal elasticity theory (NT), strain gradient theory (ST) and nonlocal strain gradient theory (NSGT). Their numerical outcomes approved more conformity of the results of nonlocal strain gradient theory with MD. More recently, however, Shojaeefard, Mahinzare, Safarpour, Saeidi Googarchin and Ghadiri (2018) presented the natural frequencies of a Timoshenko nano-composite shell by taking electric-magnetic and thermal environments into account. They assumed that the shell was under an ultra-fast rotation and was inserted in an elastic substrate. To capture the small-scale effects, the modified couple stress theory was discussed. Finally, they calculated the natural frequencies of the shell in the mentioned conditions based on the Navier analytical method and also generalized differential quadrature (GDQ) numerical method. Sahmani and Aghdam (2018) established the nonlocal strain gradient approach to study axial stability and post-stability responses of a nano-shell incorporating electric and magnetic field effects. They used the classical shell model in employing the cartesian coordinate system. To give their results numerically, they applied an improved perturbation technique.

Until the date, no paper has been recorded on an analysis of the torsional stability of nano-composite shells regarding a three-dimensional magnetic field based on the NSGT. Therefore, this paper studies a nano-composite material, i.e. $BaTiO_3$-$CoFe_2O_3$ in a shell-like structure. As this material is a smart piezomagnetic structure, it could be utilized in several nano-electro/magneto-mechanical systems. Hence, torsional stability analysis of such the nanostructure can be significant resulting in many advantages. This motivated authors to assess the torsional stability of the nano-composite shell while the magnetic field has three-dimensional influences. To predict the motion of the model's nodes, the first-order shear deformation shell hypothesis is employed. To address the size effects, the nonlocal theory of strain gradient is practiced. To attain the graphs based on the numerical outcomes, an analytical solution technique is exploited. In the results section, different key factors, such as the magnetic field and small-scale act, are taken into the investigation.

2. Basic formulation

A schematic picture of the SWCNS is below presented in which the radius, length, and thickness of the model are respectively, *R, L*, and *h* Figure 1.

In this research, concerning the cylindrical shape of the nano-shell, the first-order shear deformation shell theory (FSDST) is given by Ghorbanpour Arani et al. (2013), Mehralian et al. (2017), Shojaeefard et al. (2018)

$$\begin{Bmatrix} u_1(x,\theta,z) \\ u_2(x,\theta,z) \\ u_3(x,\theta,z) \end{Bmatrix} = \begin{Bmatrix} u(x,\theta)+z\varphi_x(x,\theta) \\ v(x,\theta)+z\varphi_\theta(x,\theta) \\ w(x,\theta) \end{Bmatrix} \tag{1}$$

in which $u_i(i=1,2,3)$ represents the displacement components of each point of the nano-shell along axial, circumferential and radial axes, respectively, $u(x,\theta)$, $v(x,\theta)$ and $w(x,\theta)$ correspond to the mid-plan displacements along with axial, circumferential and radial directions, φ_x and φ_θ display the rotation around the axial and circumferential axes. Furthermore, a coordinate for the thickness of the nano-shell is chosen as *z*.

Based on the Lagrangian strain, a continuum nonlinear strain-displacement equation can be written as

$$\{\varepsilon_{ij}\} = \frac{1}{2}\left\{\frac{\partial u_i}{\partial x_j}+\frac{\partial u_j}{\partial x_i}+\frac{\partial u_k}{\partial x_i}\frac{\partial u_k}{\partial x_j}\right\} \tag{2}$$

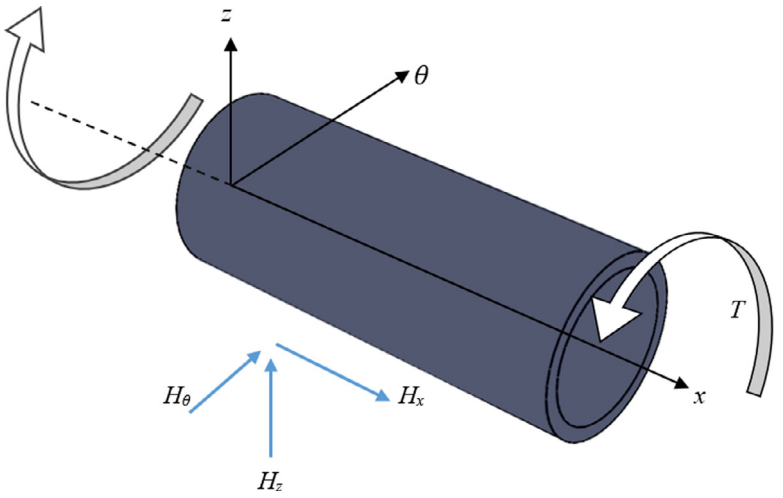

Fig. 1. A SWCNS under a three-dimensional magnetic field exposed to the torsional force.

Regarding the principle of curvilinear derivation and also the model of cylindrical shell, the components of strain for the shell SWCNS based on the Eq. (2) can be expanded as below

$$\begin{Bmatrix} \varepsilon_{xx} \\ \varepsilon_{\theta\theta} \\ \gamma_{xz} \\ \gamma_{x\theta} \\ \gamma_{\theta z} \end{Bmatrix} = \begin{Bmatrix} \frac{\partial u}{\partial x} + z\frac{\partial \varphi_x}{\partial x} + \frac{1}{2}\left(\frac{\partial w}{\partial x}\right)^2 \\ \frac{1}{R}\left(w + \frac{\partial v}{\partial \theta}\right) + \frac{1}{2R^2}\left(\frac{\partial w}{\partial \theta}\right)^2 + \frac{z}{R}\frac{\partial \varphi_\theta}{\partial \theta} \\ \varphi_x + \frac{\partial w}{\partial x} \\ \frac{\partial v}{\partial x} + \frac{1}{R}\left(\frac{\partial u}{\partial \theta} + \frac{\partial w}{\partial \theta}\frac{\partial w}{\partial x}\right) + z\left(\frac{\partial \varphi_\theta}{\partial x} + \frac{1}{R}\frac{\partial \varphi_x}{\partial \theta}\right) \\ \frac{1}{R}\left(\frac{\partial w}{\partial \theta} - v\right) + \varphi_\theta \end{Bmatrix} \tag{3}$$

The tensor of classical stresses of an element of the nano-shell along axial, circumferential and radial directions that includes the terms of magnetic and mechanic can be written as (Ghorbanpour Arani et al., 2013; Mehralian et al., 2017; Shojaeefard et al., 2018)

$$\begin{Bmatrix} \sigma_{xx} \\ \sigma_{\theta\theta} \\ \tau_{x\theta} \\ \tau_{xz} \\ \tau_{\theta z} \end{Bmatrix} = \begin{bmatrix} \overline{C}_{11} & \overline{C}_{12} & 0 & 0 & 0 \\ \overline{C}_{12} & \overline{C}_{22} & 0 & 0 & 0 \\ 0 & 0 & \overline{C}_{44} & 0 & 0 \\ 0 & 0 & 0 & \overline{C}_{55} & 0 \\ 0 & 0 & 0 & 0 & \overline{C}_{66} \end{bmatrix} \begin{Bmatrix} \varepsilon_{xx} \\ \varepsilon_{\theta\theta} \\ \gamma_{x\theta} \\ \gamma_{xz} \\ \gamma_{\theta z} \end{Bmatrix} - \begin{bmatrix} 0 & 0 & \overline{q}_{31} \\ 0 & 0 & \overline{q}_{32} \\ 0 & 0 & 0 \\ \overline{q}_{15} & 0 & 0 \\ 0 & \overline{q}_{24} & 0 \end{bmatrix} \begin{Bmatrix} \overline{H}_x \\ \overline{H}_\theta \\ \overline{H}_z \end{Bmatrix} \tag{4}$$

where the H_k is the magnetic field. Moreover, $\overline{q}_{ij}$ depicts piezomagnetic moduli related to the magnetic property of the nano-shell. Also, σ_{ij} and ε_{ij} are respectively the static stress and strain fields. Additionally, $C_{ijkl}(i, j = 1, ..., 6)$ is the stiffness matrix defined as follows

$$\begin{Bmatrix} \overline{C}_{11} \\ \overline{C}_{12} \\ \overline{C}_{22} \\ \overline{C}_{44} \\ \overline{C}_{55} \\ \overline{C}_{66} \end{Bmatrix} = \begin{Bmatrix} C_{11} - \frac{C_{13}^2}{C_{33}} \\ C_{12} - \frac{C_{13}C_{23}}{C_{33}} \\ C_{22} - \frac{C_{23}^2}{C_{33}} \\ C_{44} \\ C_{55} \\ C_{66} \end{Bmatrix} \tag{5}$$

The Hamilton's principle is utilized to derive the equilibrium equations as (Mikhasev, Eremeyev, Wilde & Maevskaya, 2019)

$$\delta\Pi = \int_{t_1}^{t_2} (\delta K - (\delta U - \delta W))dt = 0 \tag{6}$$

in which the variated kinetic and strain energies are respectively δK and δU. On the other hand, the work of outer loads is δW. Note that, in this paper, the effects of mass moment of inertia are removed.

The variated strain energy is presented below

$$\delta U = \iiint_v \left(\sigma_{ij}\delta\varepsilon_{ij} - B_k\delta H_k\right)dV = 0 \tag{7}$$

where the B_k is the magnetic induction which can be formulated as follows

$$\begin{Bmatrix} \overline{B}_x \\ \overline{B}_\theta \\ \overline{B}_z \end{Bmatrix} = \begin{bmatrix} 0 & 0 & 0 & \overline{q}_{15} & 0 \\ 0 & 0 & 0 & 0 & \overline{q}_{24} \\ \overline{q}_{31} & \overline{q}_{32} & 0 & 0 & 0 \end{bmatrix} \begin{Bmatrix} \varepsilon_{xx} \\ \varepsilon_{\theta\theta} \\ \gamma_{x\theta} \\ \gamma_{xz} \\ \gamma_{\theta z} \end{Bmatrix} + \begin{bmatrix} \overline{\eta}_{11} & 0 & 0 \\ 0 & \overline{\eta}_{22} & 0 \\ 0 & 0 & \overline{\eta}_{33} \end{bmatrix} \begin{Bmatrix} \overline{H}_x \\ \overline{H}_\theta \\ \overline{H}_z \end{Bmatrix} \tag{8}$$

in which $\overline{\eta}_{ij}$ shows a magnetic quantity. The magnetic constants can be expressed as

$$\begin{Bmatrix} \overline{q}_{31} \\ \overline{q}_{32} \\ \overline{q}_{15} \\ \overline{q}_{24} \end{Bmatrix} = \begin{Bmatrix} q_{31} - \frac{C_{13}q_{33}}{C_{33}} \\ q_{32} - \frac{C_{23}q_{33}}{C_{33}} \\ q_{15} \\ q_{24} \end{Bmatrix}; \begin{Bmatrix} \overline{\eta}_{11} \\ \overline{\eta}_{22} \\ \overline{\eta}_{33} \end{Bmatrix} = \begin{Bmatrix} \eta_{11} \\ \eta_{22} \\ \eta_{33} + \frac{q_{33}^2}{C_{33}} \end{Bmatrix} \tag{9}$$

Based on the available magnetic potential, the following linear function can be employed (Ghorbanpour Arani et al., 2013; Mehralian et al., 2017; Shojaeefard et al., 2018)

$$\overline{\Psi}(x,\theta,z) = -\cos\left(\frac{\pi z}{h}\right)\Psi(x,\theta) + \frac{2z\psi_0}{h} \tag{10}$$

in which the initial magnetic potential is symbolized with Ψ(x, y), and the magnetic potential is ψ_0.

By means of Eq. (10), the magnetic field can be indicated in three dimensions as below

$$\begin{Bmatrix} \overline{H}_x \\ \overline{H}_\theta \\ \overline{H}_z \end{Bmatrix} = \begin{Bmatrix} -\frac{\partial\overline{\Psi}}{\partial x} \\ -\frac{1}{R+z}\frac{\partial\overline{\Psi}}{\partial\theta} \\ -\frac{\partial\overline{\Psi}}{\partial z} \end{Bmatrix} = \begin{Bmatrix} \cos\left(\frac{\pi z}{h}\right)\frac{\partial\Psi}{\partial x} \\ \frac{1}{R+z}\cos\left(\frac{\pi z}{h}\right)\frac{\partial\Psi}{\partial\theta} \\ -\frac{\pi}{h}\sin\left(\frac{\pi z}{h}\right)\Psi - \frac{2\psi_0}{h} \end{Bmatrix} \tag{11}$$

Assuming an element of the nano-shell in an equilibrium condition gives us the stress resultants as

$$\{N_{xx}, N_{\theta\theta}, N_{x\theta}, M_{xx}, M_{x\theta}, M_{\theta\theta}, Q_{xz}, Q_{\theta z}\} = \int_{-0.5h}^{0.5h} \{\sigma_{xx}, \sigma_{\theta\theta}, \sigma_{x\theta}, \sigma_{xx}z, \sigma_{x\theta}z, \sigma_{\theta\theta}z, k\tau_{xz}, k\tau_{\theta z}\}dz \tag{12}$$

where the moment stress resultants (M_{xx}, $M_{x\theta}$, $M_{\theta\theta}$), the transverse shear stress resultants (Q_{xz}, $Q_{\theta z}$), and the axial stress resultants (N_{xx}, $N_{\theta\theta}$, $N_{x\theta}$) are shown. In addition, k defines a shear correction factor by which the value of the transverse shear stress along the thickness of the model can be refined.

Hence, based on Eq. (4), Eq. (12) can be developed as below

$$\begin{Bmatrix} \mathrm{N_{xx}} \\ \mathrm{N_{\theta\theta}} \\ \mathrm{N_{x\theta}} \\ \mathrm{M_{xx}} \\ \mathrm{M_{\theta\theta}} \\ \mathrm{M_{x\theta}} \\ \mathrm{Q_{xz}} \\ \mathrm{Q_{\theta z}} \end{Bmatrix} = \begin{bmatrix} \mathrm{A_{11}} & \mathrm{A_{12}} & 0 & 0 & 0 & 0 & 0 & 0 \\ \mathrm{A_{21}} & \mathrm{A_{22}} & 0 & 0 & 0 & 0 & 0 & 0 \\ 0 & 0 & \mathrm{A_{44}} & 0 & 0 & 0 & 0 & 0 \\ 0 & 0 & 0 & \mathrm{D_{11}} & \mathrm{D_{12}} & 0 & 0 & 0 \\ 0 & 0 & 0 & \mathrm{D_{21}} & \mathrm{D_{22}} & 0 & 0 & 0 \\ 0 & 0 & 0 & 0 & 0 & \mathrm{D_{66}} & 0 & 0 \\ 0 & 0 & 0 & 0 & 0 & 0 & kA_{55} & 0 \\ 0 & 0 & 0 & 0 & 0 & 0 & 0 & kA_{66} \end{bmatrix} \times \begin{Bmatrix} \frac{\partial u}{\partial x} + \frac{1}{2}\left(\frac{\partial w}{\partial x}\right)^2 \\ \frac{1}{R}\left(w + \frac{\partial v}{\partial\theta}\right) + \frac{1}{2R^2}\left(\frac{\partial w}{\partial\theta}\right)^2 \\ \frac{\partial v}{\partial x} + \frac{1}{R}\left(\frac{\partial u}{\partial\theta} + \frac{\partial w}{\partial\theta}\frac{\partial w}{\partial x}\right) \\ \frac{\partial\varphi_x}{\partial x} \\ \frac{1}{R}\frac{\partial\varphi_\theta}{\partial\theta} \\ \frac{\partial\varphi_\theta}{\partial x} + \frac{1}{R}\frac{\partial\varphi_x}{\partial\theta} \\ \varphi_x + \frac{\partial w}{\partial x} \\ \frac{1}{R}\left(\frac{\partial w}{\partial\theta} - v\right) + \varphi_\theta \end{Bmatrix} + \begin{Bmatrix} 2\bar{q}_{31}\psi_0 \\ 2\bar{q}_{32}\psi_0 \\ 0 \\ X_{35}\Psi \\ X_{63}\Psi \\ 0 \\ -X_{21}\frac{\partial\Psi}{\partial x} \\ -X_{23}\frac{\partial\Psi}{\partial\theta} \end{Bmatrix} \tag{13}$$

in which

$$A_{ij} = \int_{-\frac{h}{2}}^{\frac{h}{2}} \bar{\mathrm{C}}_{\mathrm{ij}}dz{:}(i,j=1,2,4,6), D_{ij} = \int_{-\frac{h}{2}}^{\frac{h}{2}} \bar{\mathrm{C}}_{\mathrm{ij}}z^2dz{:}(i,j=1,2,6) \tag{14}$$

By doing $\delta\Pi$i=0, the equilibrium equations can be obtained as

$$\delta u_1 = 0 : \frac{\partial N_{xx}}{\partial x} + \frac{1}{R}\frac{\partial N_{x\theta}}{\partial\theta} = 0 \tag{15a}$$

$$\delta u_2 = 0 : \frac{1}{R}\frac{\partial N_{\theta\theta}}{\partial\theta} + \frac{\partial N_{x\theta}}{\partial x} + \frac{Q_{\theta z}}{R} = 0 \tag{15b}$$

$$\delta u_3 = 0 : \frac{\partial}{\partial x}\left(N_{xx}\frac{\partial w}{\partial x}\right) + \frac{1}{R}\frac{\partial}{\partial\theta}\left(N_{\theta\theta}\frac{1}{R}\frac{\partial w}{\partial\theta}\right) + \frac{1}{R}\frac{\partial}{\partial\theta}\left(N_{x\theta}\frac{\partial w}{\partial x}\right) + \frac{1}{R}\frac{\partial}{\partial x}\left(N_{x\theta}\frac{\partial w}{\partial\theta}\right)$$

$$-\frac{N_{\theta\theta}}{R}+\frac{\partial Q_{xz}}{\partial x}+\frac{1}{R}\frac{\partial Q_{\theta z}}{\partial \theta}=0 \tag{15c}$$

$$\delta\varphi_x=0:\frac{\partial M_{xx}}{\partial x}+\frac{1}{R}\frac{\partial M_{x\theta}}{\partial \theta}-Q_{xz}=0 \tag{15d}$$

$$\delta\varphi_\theta=0:\frac{1}{R}\frac{\partial M_{\theta\theta}}{\partial \theta}+\frac{\partial M_{x\theta}}{\partial x}-Q_{\theta z}=0 \tag{15e}$$

$$\delta\Psi=0;\int_{-h/2}^{h/2}\left[\frac{\partial \bar{B}_x}{\partial x}\cos\left(\frac{\pi z}{h}\right)+\frac{1}{R+z}\frac{\partial \bar{B}_\theta}{\partial \theta}\cos\left(\frac{\pi z}{h}\right)+\frac{\pi}{h}\bar{B}_z\sin\left(\frac{\pi z}{h}\right)\right]dz=0 \tag{15f}$$

where

$$\begin{Bmatrix}\bar{B}_x\\ \bar{B}_\theta\\ \bar{B}_z\end{Bmatrix}=\int_{-h/2}^{h/2}\begin{Bmatrix}B_x\cos\left(\frac{\pi z}{h}\right)\\ B_\theta\frac{1}{R+z}\cos\left(\frac{\pi z}{h}\right)\\ B_z\frac{\pi}{h}\sin\left(\frac{\pi z}{h}\right)\end{Bmatrix}dz=\begin{Bmatrix}X_{21}\left(\varphi_x+\frac{\partial w}{\partial x}\right)+Y_{11}\frac{\partial \Psi}{\partial x}\\ X_{23}\left(\frac{1}{R}\left(\frac{\partial w}{\partial \theta}-v\right)+\varphi_\theta\right)+Y_{22}\frac{\partial \Psi}{\partial \theta}\\ X_{34}\frac{\partial u}{\partial x}+X_{35}\frac{\partial \varphi_x}{\partial x}+X_{63}\frac{1}{R}\left(\frac{\partial v}{\partial \theta}+w\right)+X_{64}\frac{1}{R}\frac{\partial \varphi_\theta}{\partial \theta}-Y_{33}\Psi\end{Bmatrix} \tag{16}$$

The additional parameters in Eqs. (13) and (16) are

$$\begin{Bmatrix}X_{21}\\ X_{23}\\ X_{34}\\ X_{35}\\ X_{63}\\ X_{64}\end{Bmatrix}=\int_{-h/2}^{h/2}\begin{Bmatrix}\bar{q}_{15}\cos\left(\frac{\pi}{h}z\right)\\ \bar{q}_{24}\frac{1}{R+z}\cos\left(\frac{\pi}{h}z\right)\\ \bar{q}_{31}\frac{\pi}{h}\sin\left(\frac{\pi}{h}z\right)\\ \bar{q}_{31}\frac{\pi}{h}z\sin\left(\frac{\pi}{h}z\right)\\ \bar{q}_{32}\frac{\pi}{h}\sin\left(\frac{\pi}{h}z\right)\\ \bar{q}_{32}\frac{\pi}{h}z\sin\left(\frac{\pi}{h}z\right)\end{Bmatrix}dz;\begin{Bmatrix}Y_{11}\\ Y_{22}\\ Y_{33}\end{Bmatrix}=\int_{-h/2}^{h/2}\begin{Bmatrix}\bar{\eta}_{11}\cos^2\left(\frac{\pi}{h}z\right)\\ \bar{\eta}_{22}\left(\frac{1}{R+z}\right)^2\cos^2\left(\frac{\pi}{h}z\right)\\ \bar{\eta}_{33}\left(\frac{\pi}{h}\right)^2\sin^2\left(\frac{\pi}{h}z\right)\end{Bmatrix}dz \tag{17}$$

Following on from the application of small-scale theories, such as (Eringen, 1983; Farajpour, Ghayesh & Farokhi, 2019; Mikhasev & Nobili, 2019; Reddy, 2007), couple stress (Akbarzadeh Khorshidi, 2018; Akgöz & Civalek, 2012; Malikan, 2017) and the strain gradient (Gholami, Darvizeh, Ansari & Sadeghi, 2016; Lurie & Solyaev, 2019a; Lurie and Solyaev, 2019b; Solyaev, Lurie, Koshurina, Dobryanskiy & Kachanov, 2019; Solyaev & Lurie, 2019), a new theory has been proposed (Lim, Zhang & Reddy, 2015) that presents two different properties of nanomaterials (stiffness-hardening and stiffness-softening), namely nonlocal theory of strain gradient with which much research works have been demonstrated (Arefi, Kiani & Rabczuk, 2019; Karami, Shahsavari & Janghorban, 2019; Malikan & Nguyen, 2018; Malikan, Dimitri & Tornabene, 2019; Sahmani & Aghdam, 2017; She, Yuan, Karami, Ren & Xiao, 2019). This theory in its differential form is formulated as

$$\left(1-\mu\nabla^2\right)\sigma_{ij}=\mathrm{C}_{ijkl}\left(1-l^2\nabla^2\right)\varepsilon_{kl} \tag{18}$$

in which the $\nabla^2=\frac{\partial^2}{\partial x^2}+\frac{1}{R^2}\frac{\partial^2}{\partial \theta^2}$ is the Laplace operator in cylindrical coordinates, l, and μ exhibit the small scale parameters which respectively define two independent effects for nanostructures. The first one assigns hardening effect resulted from reducing the size from macro to nano and the second one defines the interaction between atoms in an atomic lattice which means stress nonlocality.

According to Eq. (18), Eq. (13) in the NSGT form becomes

$$\left[N_{xx}-\mu\left(\frac{\partial^2 N_{xx}}{\partial x^2}+\frac{1}{R^2}\frac{\partial^2 N_{xx}}{\partial \theta^2}\right)\right]=\left(1-l^2\nabla^2\right)\left\{\mathrm{A}_{11}\left[\frac{\partial u}{\partial x}+\frac{1}{2}\left(\frac{\partial w}{\partial x}\right)^2\right]+\mathrm{A}_{12}\left[\frac{1}{R}\left(w+\frac{\partial v}{\partial \theta}\right)+\frac{1}{2R^2}\left(\frac{\partial w}{\partial \theta}\right)^2\right]\right\}+2\bar{q}_{31}\psi_0 \tag{19a}$$

$$\left[N_{\theta\theta}-\mu\left(\frac{\partial^2 N_{\theta\theta}}{\partial x^2}+\frac{1}{R^2}\frac{\partial^2 N_{\theta\theta}}{\partial \theta^2}\right)\right]=\left(1-l^2\nabla^2\right)\left\{\mathrm{A}_{21}\left[\frac{\partial u}{\partial x}+\frac{1}{2}\left(\frac{\partial w}{\partial x}\right)^2\right]+\mathrm{A}_{22}\left[\frac{1}{R}\left(w+\frac{\partial v}{\partial \theta}\right)+\frac{1}{2R^2}\left(\frac{\partial w}{\partial \theta}\right)^2\right]\right\}+2\bar{q}_{32}\psi_0 \tag{19b}$$

$$\left[N_{x\theta}-\mu\left(\frac{\partial^2 N_{x\theta}}{\partial x^2}+\frac{1}{R^2}\frac{\partial^2 N_{x\theta}}{\partial \theta^2}\right)\right]=\mathrm{A}_{44}\left(1-l^2\nabla^2\right)\left[\frac{\partial v}{\partial x}+\frac{1}{R}\left(\frac{\partial u}{\partial \theta}+\frac{\partial w}{\partial \theta}\frac{\partial w}{\partial x}\right)\right] \tag{19c}$$

$$\left[M_{xx}-\mu\left(\frac{\partial^2 M_{xx}}{\partial x^2}+\frac{1}{R^2}\frac{\partial^2 M_{xx}}{\partial\theta^2}\right)\right]=\left(1-l^2\nabla^2\right)\left(\mathrm{D}_{11}\frac{\partial\varphi_x}{\partial x}+\mathrm{D}_{12}\frac{1}{R}\frac{\partial\varphi_\theta}{\partial\theta}\right)+X_{35}\Psi \tag{19d}$$

$$\left[M_{\theta\theta}-\mu\left(\frac{\partial^2 M_{\theta\theta}}{\partial x^2}+\frac{1}{R^2}\frac{\partial^2 M_{\theta\theta}}{\partial\theta^2}\right)\right]=\left(1-l^2\nabla^2\right)\left(\mathrm{D}_{21}\frac{\partial\varphi_x}{\partial x}+\mathrm{D}_{22}\frac{1}{R}\frac{\partial\varphi_\theta}{\partial\theta}\right)+X_{63}\Psi \tag{19e}$$

$$\left[M_{x\theta}-\mu\left(\frac{\partial^2 M_{x\theta}}{\partial x^2}+\frac{1}{R^2}\frac{\partial^2 M_{x\theta}}{\partial\theta^2}\right)\right]=\mathrm{D}_{66}\left(1-l^2\nabla^2\right)\left(\frac{\partial\varphi_\theta}{\partial x}+\frac{1}{R}\frac{\partial\varphi_x}{\partial\theta}\right) \tag{19f}$$

$$\left[Q_{xz}-\mu\left(\frac{\partial^2 Q_{xz}}{\partial x^2}+\frac{1}{R^2}\frac{\partial^2 Q_{xz}}{\partial\theta^2}\right)\right]=A_{55}\left(1-l^2\nabla^2\right)\left(\varphi_x+\frac{\partial w}{\partial x}\right)-X_{21}\frac{\partial\Psi}{\partial x} \tag{19g}$$

$$\left[Q_{\theta z}-\mu\left(\frac{\partial^2 Q_{\theta z}}{\partial x^2}+\frac{1}{R^2}\frac{\partial^2 Q_{\theta z}}{\partial\theta^2}\right)\right]=A_{66}\left(1-l^2\nabla^2\right)\left(\frac{1}{R}\left(\frac{\partial w}{\partial\theta}-v\right)+\varphi_\theta\right)-X_{23}\frac{\partial\Psi}{\partial\theta} \tag{19h}$$

By substituting Eq. (19) into Eq. (15), and based on Eq. (13), and also by linearizing the obtained equations, we derive the stability equations as below

$$\left(1-l^2\nabla^2\right)\left\{\left[\mathrm{A}_{11}\frac{\partial^2 u}{\partial x^2}+\mathrm{A}_{12}\frac{1}{R}\left(\frac{\partial w}{\partial x}+\frac{\partial^2 v}{\partial x\partial\theta}\right)\right]+\mathrm{A}_{44}\frac{1}{R}\left(\frac{\partial^2 v}{\partial x\partial\theta}+\frac{1}{R}\frac{\partial^2 u}{\partial\theta^2}\right)\right\}=0 \tag{20a}$$

$$\left(1-l^2\nabla^2\right)\left\{\mathrm{A}_{44}\left(\frac{\partial^2 v}{\partial x^2}+\frac{1}{R}\frac{\partial^2 u}{\partial x\partial\theta}\right)+\left[\frac{\mathrm{A}_{21}}{R}\frac{\partial^2 u}{\partial x\partial\theta}+\frac{\mathrm{A}_{22}}{R^2}\left(\frac{\partial w}{\partial\theta}+\frac{\partial^2 v}{\partial\theta^2}\right)\right]+\frac{A_{66}}{R}\left[\frac{1}{R}\left(\frac{\partial w}{\partial\theta}-v\right)+\varphi_\theta\right]\right\}-\frac{X_{23}}{R}\frac{\partial\Psi}{\partial\theta}=0 \tag{20b}$$

$$\begin{aligned}&\left(1-\mu\nabla^2\right)\left(N^0_{xx}\frac{\partial^2 w}{\partial x^2}+\frac{2}{R}N^0_{x\theta}\frac{\partial^2 w}{\partial x\partial\theta}\right)+\left(1-l^2\nabla^2\right)\left\{A_{55}\left(\frac{\partial\varphi_x}{\partial x}+\frac{\partial^2 w}{\partial x^2}\right)+A_{66}\left[\frac{1}{R^2}\left(\frac{\partial^2 w}{\partial\theta^2}-\frac{\partial v}{\partial\theta}\right)+\frac{1}{R}\frac{\partial\varphi_\theta}{\partial\theta}\right]\right.\\&\left.-\frac{1}{R}\left[\mathrm{A}_{21}\frac{\partial u}{\partial x}+\mathrm{A}_{22}\frac{1}{R}\left(w+\frac{\partial v}{\partial\theta}\right)\right]\right\}-X_{21}\frac{\partial^2\Psi}{\partial x^2}-\frac{X_{23}}{R}\frac{\partial^2\Psi}{\partial\theta^2}=0\end{aligned} \tag{20c}$$

$$\left(1-l^2\nabla^2\right)\left\{\left(\mathrm{D}_{11}\frac{\partial^2\varphi_x}{\partial x^2}+\mathrm{D}_{12}\frac{1}{R}\frac{\partial^2\varphi_\theta}{\partial x\partial\theta}\right)+\frac{\mathrm{D}_{66}}{R}\left(\frac{\partial^2\varphi_\theta}{\partial x\partial\theta}+\frac{1}{R}\frac{\partial^2\varphi_x}{\partial\theta^2}\right)-A_{55}\left(\varphi_x+\frac{\partial w}{\partial x}\right)\right\}+X_{35}\frac{\partial\Psi}{\partial x}+X_{21}\frac{\partial\Psi}{\partial x}=0 \tag{20d}$$

$$\begin{aligned}&\left(1-l^2\nabla^2\right)\left\{\mathrm{D}_{66}\left(\frac{\partial^2\varphi_\theta}{\partial x^2}+\frac{1}{R}\frac{\partial^2\varphi_x}{\partial x\partial\theta}\right)+\left(\frac{\mathrm{D}_{21}}{R}\frac{\partial^2\varphi_x}{\partial x\partial\theta}+\mathrm{D}_{22}\frac{1}{R^2}\frac{\partial^2\varphi_\theta}{\partial\theta^2}\right)-A_{66}\left[\frac{1}{R}\left(\frac{\partial w}{\partial\theta}-v\right)+\varphi_\theta\right]\right\}\\&+\frac{X_{63}}{R}\frac{\partial\Psi}{\partial\theta}+X_{23}\frac{\partial\Psi}{\partial\theta}=0\end{aligned} \tag{20e}$$

$$\begin{aligned}&X_{21}\left(\frac{\partial\varphi_x}{\partial x}+\frac{\partial^2 w}{\partial x^2}\right)+X_{23}\left[\frac{1}{R}\left(\frac{\partial^2 w}{\partial\theta^2}-\frac{\partial v}{\partial\theta}\right)+\frac{\partial\varphi_\theta}{\partial\theta}\right]+Y_{22}\frac{\partial^2\Psi}{\partial\theta^2}+Y_{11}\frac{\partial^2\Psi}{\partial x^2}+X_{34}\frac{\partial u}{\partial x}+X_{35}\frac{\partial\varphi_x}{\partial x}\\&+X_{63}\frac{1}{R}\left(\frac{\partial v}{\partial\theta}+w\right)+X_{64}\frac{1}{R}\frac{\partial\varphi_\theta}{\partial\theta}-Y_{33}\Psi=0\end{aligned} \tag{20f}$$

in which the axial membrane magnetic and torsional membrane mechanical forces are as [33–35]

$$\text{Magnetic force}: N^0_{xx}=N^{mag}_{xx}=\int_{-h/2}^{h/2}\bar{q}_{31}\frac{2\psi_0}{h}dz \tag{21a}$$

$$\text{Torsional mechanical force}: T=2\pi R^2 N^0_{x\theta} \tag{21b}$$

where T denotes the torsional mechanical critical force, which should be dependent on the radius (Han & Lu, 2003), which determines the torsional stability condition of the SWCNS.

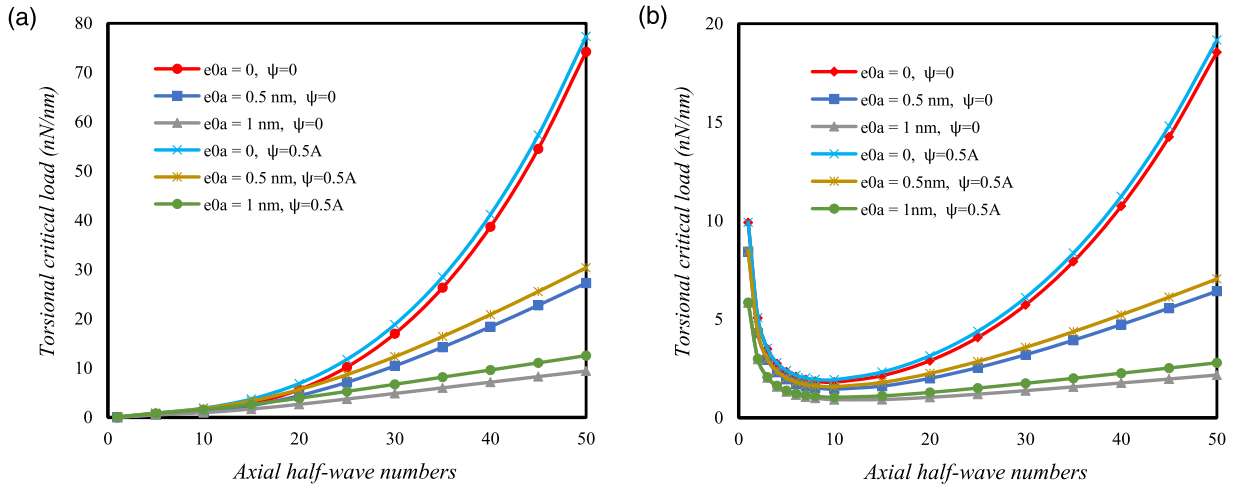

Fig. 2. **(a)** The axial half-wave number vs. stress nonlocality ($l = 0.5$ nm, $n = 1$). **(b)** The axial half-wave number vs. stress nonlocality ($l = 0.5$ nm, $n = 5$).

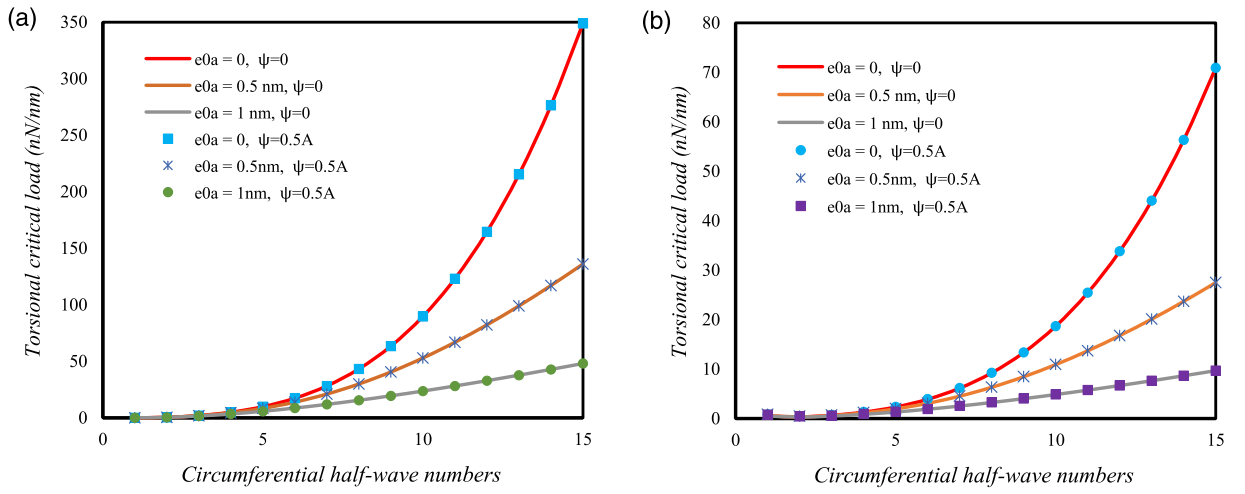

Fig. 3. **(a)** The circumferential half-wave number vs. stress nonlocality ($l = 0.5$ nm, $m = 1$). **(b)** The circumferential half-wave number vs. stress nonlocality ($l = 0.5$ nm, $m = 5$).

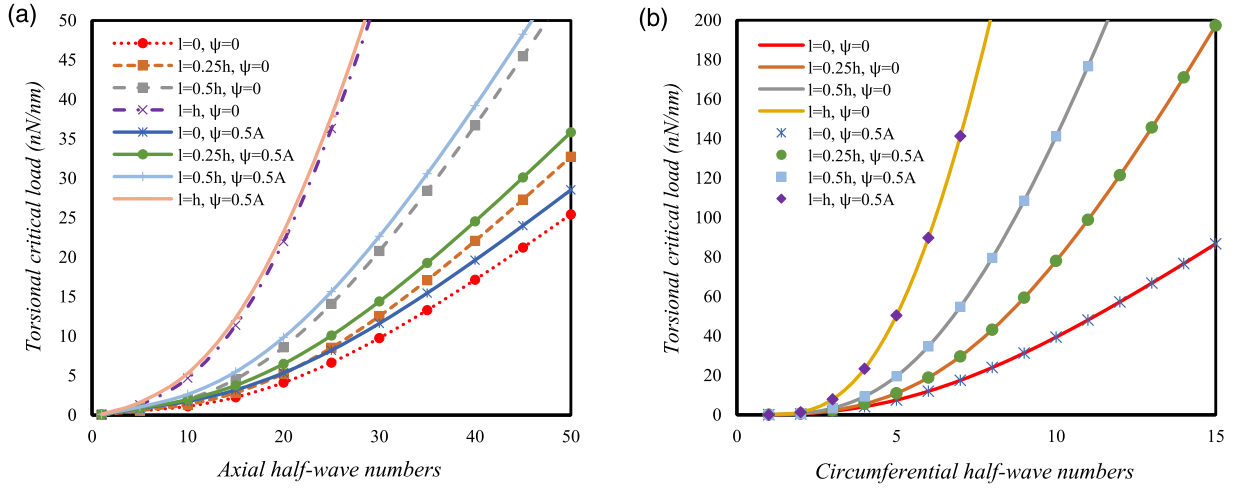

Fig. 4. **(a)** The axial half-wave number vs. strain gradient parameter (e_0a=0.5 nm, $n = 1$). **(b)** The circumferential half-wave number vs. strain gradient parameter (e_0a=0.5 nm, $m = 1$).

3. Solution of equations

In this section, the obtained Eq. (20) is considered to be solved with both ends simply-supported edge conditions. To do this, the below trigonometric displacement functions are utilized (Mehralian et al., 2017).

$$u(x,\theta,t)=\sum_{m=1}^{\infty}\sum_{n=1}^{\infty}U_{mn}\cos\left(\frac{m\pi}{L}x\right)\cos\left(n\theta\right) \tag{22a}$$

$$v(x,\theta,t)=\sum_{m=1}^{\infty}\sum_{n=1}^{\infty}V_{mn}\sin\left(\frac{m\pi}{L}x\right)\sin\left(n\theta\right) \tag{22b}$$

$$w(x,\theta,t)=\sum_{m=1}^{\infty}\sum_{n=1}^{\infty}W_{mn}\sin\left(\frac{m\pi}{L}x\right)cos(n\theta) \tag{22c}$$

$$\varphi_x(x,\theta,t)=\sum_{m=1}^{\infty}\sum_{n=1}^{\infty}\Phi_{xmn}\cos\left(\frac{m\pi}{L}x\right)\cos\left(n\theta\right) \tag{22d}$$

$$\varphi_\theta(x,\theta,t)=\sum_{m=1}^{\infty}\sum_{n=1}^{\infty}\Phi_{\theta mn}\sin\left(\frac{m\pi}{L}x\right)\sin\left(n\theta\right) \tag{22e}$$

$$\Psi(x,\theta,t)=\sum_{m=1}^{\infty}\sum_{n=1}^{\infty}\Theta_{mn}\sin\left(\frac{m\pi}{L}x\right)cos(n\theta) \tag{22f}$$

in which the axial and circumferential half-wave numbers are defined with m and n. By embedding Eq. (22) into Eq. (20), manipulating and also simplifying, we get

$$\begin{bmatrix} K_{11} & K_{12} & K_{13} & 0 & 0 & 0 \\ K_{21} & K_{22} & K_{23} & 0 & K_{25} & K_{26} \\ K_{31} & K_{32} & K_{33} & K_{34} & K_{35} & K_{36} \\ 0 & 0 & K_{43} & K_{44} & K_{45} & K_{46} \\ 0 & K_{52} & K_{53} & K_{54} & K_{55} & K_{56} \\ 0 & K_{62} & K_{63} & K_{64} & K_{65} & K_{66} \end{bmatrix} \begin{Bmatrix} U_{mn} \\ V_{mn} \\ W_{mn} \\ \Phi_{xmn} \\ \Phi_{\theta mn} \\ \Theta_{mn} \end{Bmatrix} = \begin{Bmatrix} 0 \\ 0 \\ 0 \\ 0 \\ 0 \\ 0 \end{Bmatrix} \tag{23}$$

where the matrix K_{ij} is the coefficients one (The elements of the matrix are presented in Appendix A). Setting the determinant of the coefficients matrix to zero gives the characteristic equation of the torsional stability of the SWCNS.

4. Numerical results

4.1. Verification of results

As far as no literature has been reported till now on the torsional buckling of a nano-composite shell inserted in a three-dimensional magnetic field, therefore, the formulation would be reduced into a nano-shell/tube under torsion with removing magnetic effects. On the other hand, in order to compare the results of the torsional buckling of the nano-shell, the molecular dynamics (MD) simulation as Table 1 in which the comparable results are found, is taken into validation (Chowdhurry et al., 2014). As can be observed, outcomes of the FSDT shell model while the size-dependent approach is NSGT, are in good agreement with those of MD. Although the numerical results originated from NSGT completely depend on the correct values of the parameters e_0a and l, these factors should be obligatory obtained in an experiment.

4.2. Parametric study

To proceed with the parametric solution for the nano-composite shell, the properties mentioned in Table 2 are employed.

To make the numerical outcomes, first, the effect of stress nonlocality versus magnetic field by variations in axial half-wave numbers is depicted. To do this, Figure 2a is for $n = 1$ and Figure 2b is drawn for $n = 5$. As it is shown, the increase of axial half-wave numbers tends to increase the torsional capacity. In addition to this, an increase in the magnetic field enlarges the torsional capacity. It is also worthy to note that an increase in axial half-wave numbers remarkably increases the effect of stress nonlocality. This is due to the increase in the distance of curves of the results of various nonlocal parameters. It is also observed that the increase of axial half-wave numbers makes the torsional stability noticeably larger in a local condition than while the stress nonlocality is considered. This is due to the softening effect of the nonlocality. That's why the slope of the results of e_0a=0 in both cases is much steeper. Besides these, it can be conducted that for higher axial half-wave numbers, the impact of magnetic potential in a nonlocal domain is more than a local one. This is because of more gaps between the results of cases e_0a=0.5 nm, ψ=0, with e_0a=0.5 nm, ψ=0.5 A, and also another one. Based on the

Table 1
Results of torsional buckling (nN/nm) of MD for single-walled carbon nanotubes.

SWCNT ($^{*}a = 5, b = 5$)			SWCNT (10, 10)			SWCNT (15, 15)			SWCNT (20, 20)		
d = 0.678 nm			d = 1.356 nm			d = 2.034 nm			d = 2.713 nm		
L/d	MD	Present**	L/d	MD	Present	L/d	MD	Present	L/d	MD	Present
2	16	16	1	43.6	43.6	1	53.3	53.3	1.5	46	46
3.1	11.2	11.2	1.5	30.6	30.6	1.4	43.8	43.8	1.8	42	42
4.2	8.9	8.9	2.1	24.6	24.6	1.6	39.1	39.1	2	39.2	39.2
4.9	8	8	2.4	22.9	22.9	2	35.3	35.3	2.2	38.7	38.7
6	7.2	7.2	3	20.2	20.2	2.4	31	31	2.6	36.8	36.8
7	6.7	6.7	3.5	19.5	19.5	2.7	27.8	27.8	3	31.7	31.7
8.1	6.5	6.5	4.1	18.5	18.5	3	26.7	26.7	3.5	29	29
8.9	6.3	6.3	4.4	16.8	16.8	3.3	24.6	24.6	3.8	28.4	28.4
9.9	6.2	6.2	5	14.8	14.8	4	22.6	22.6	4	27.7	27.7
			6.1	12.5	12.5	4.6	21.8	21.8	4.5	26.3	26.3
			7	11.2	11.2	5	20.9	20.9			
			7.5	10.8	10.8	5.4	20.8	20.8			
			8	10.4	10.4	6	19	19			
			9	9.9	9.9	6.7	16.8	16.8			
			10	9.6	9.6						
			20	8.4	8.4						

* $d(nm) = \frac{2.46}{\pi}\sqrt{a^2 + ab + b^2}$ (Kok & Wong, 2016).
** FSDT shell theory in conjunction with NSGT ($0 < e_0 a \leq 1.5$ nm, $0 < l \leq 8$ nm).

Table 2
Mechanical and magnetic characteristics of Barium Titanate–Cobalt Ferrite nano-composite shell (Gholami & Ansari, 2017; Ghorbanpour Arani et al., 2013; Mehralian et al., 2017; Shojaeefard et al., 2018).

	Elastic properties (GPa)
$BaTiO_3$–$CoFe_2O_4$	C_{11}=C_{22}=226, C_{12}=125, C_{13}= C_{23}=124, C_{33}=216, C_{44}= C_{55}=44.2, C_{66}=50.5 Piezomagnetic quantities ($N/A.m$) q_{15}= q_{24}=275, q_{31}= q_{32}=290.1, q_{33}=349.9 Magnetic quantities ($N.s^2/C^2$) η_{11}= η_{22}=−297e-6, η_{33}=83.5e-6 Sundry quantities h = 4 nm, R = 6 nm, L = 10R, l^{*}=l/h

second figure, it is clear that while the circumferential half-wave number is greater than one, the increase of axial half-wave numbers does not make the increasing effect only for the numerical results of torsional buckling. And the buckling results would be initially decreased and then increased. Plus, there has been found that when the circumferential half-wave number is bigger than one, the effect of stress nonlocality is remarkable even at lower values of the half-waves. But according to the first figure, the effect is not noticeable for the lower values of the half-waves.

To consider the influence of stress nonlocality and magnetic field more deeply, Figure 3a,b as similar as the previous ones are indicated, however by changes in circumferential half-wave numbers. Regarding both presented figures, it can be witnessed that the increase of the circumferential half-wave numbers makes the torsional stability fundamentally further than axial ones. It is noteworthy that the increase of circumferential half-wave numbers even if the axial wave number is chosen as greater than one, leads to a steadily increasing trend for buckling loads. The important point of these two figures, however, can be the fact that for larger circumferential half-wave numbers, there has never been seen any major impact on variations of the magnetic potential.

To clarify the influences of the strain gradient scale parameter, Fig. 4a and b are revealed, respectively. Based on these figures it can be remarked that the increase of the strain gradient parameter leads to decreasing the effect of the magnetic field. This is in light of the distances between results of $l = 0$, ψ=0 and $l = 0$, ψ=0.5A with $l = h$, ψ=0 and $l = h$, ψ=0.5A. In fact, the distance is lower for the second case leads to this conclusion that the increase of torsional buckling loads which resulted from the increase of the magnetic potential is lower in the larger values of the strain gradient parameter. It can be somehow stated that if the material is stiffer, the increase of magnetic potential does not affect outstandingly the stability. On the other hand, as is clear, the increase of the axial half-wave numbers when the strain gradient parameter is chosen as larger, results in a greater impact of the waves on the torsional stability. This means the larger the values of the strain gradient factor, the greater the impact of the axial half-wave numbers.

To study the effect of an increase of magnetic potential on the torsional stability response of the nano-composite shell, the Fig. 5a–c is displayed, respectively. The first two figures are plotted for changes of axial half-wave numbers and the third figure shows the role of changes of circumferential half-wave numbers. For the first figure, the circumferential half-wave is chosen as $n = 1$ and subsequently the $n = 10$ for the second figure. As shown by the first figure, the increase of

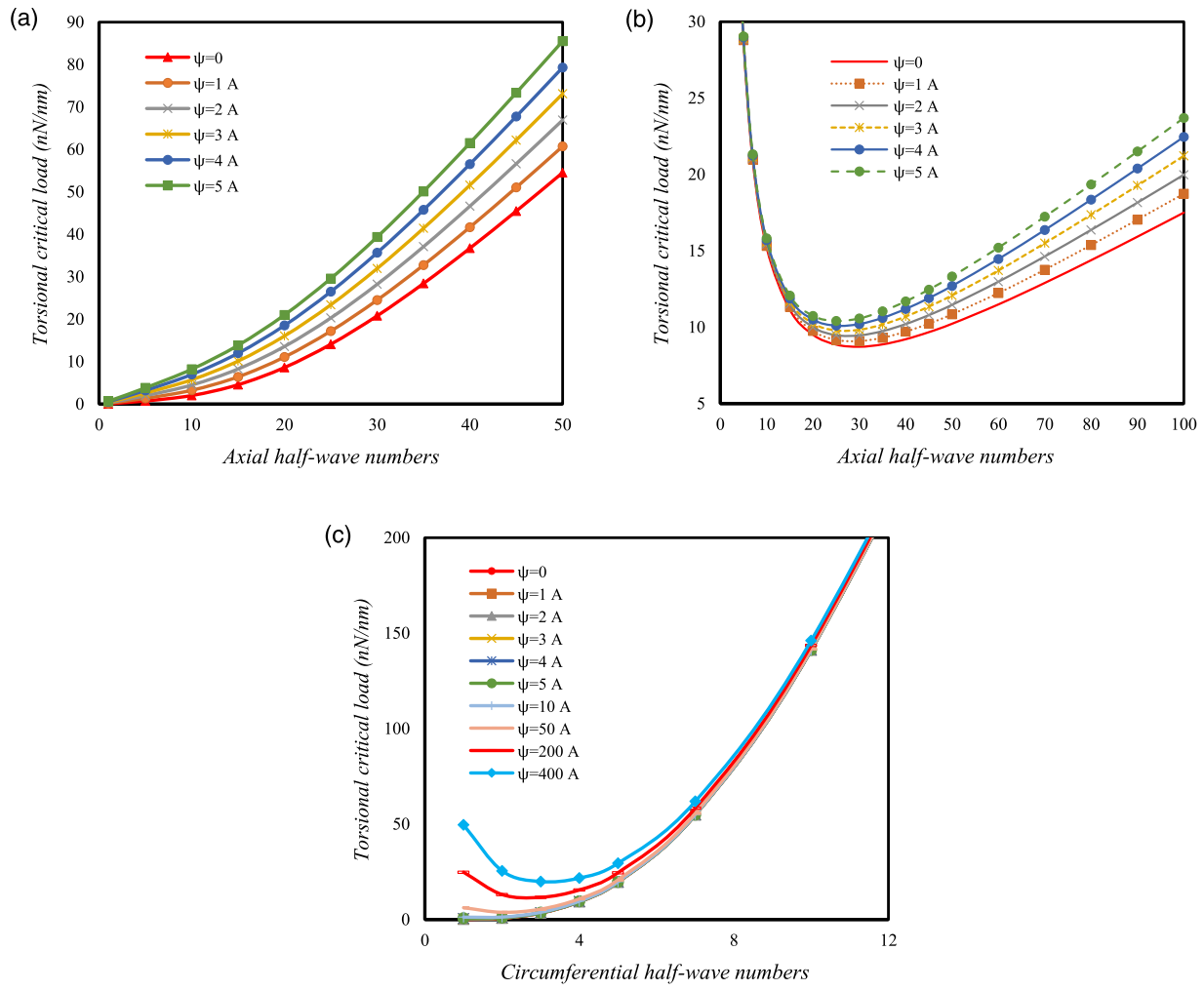

Fig. 5. **(a)** The axial half-wave number vs. magnetic influences (e_0a=0.5 nm, l^*=0.5, $n = 1$). **(b)** The axial half-wave number vs. magnetic influences (e_0a=0.5 nm, l^*=0.5, $n = 10$). **(c)** The circumferential half-wave number vs. magnetic influences (e_0a=0.5 nm, l^*=0.5, $m = 1$).

the magnetic potential increases further the torsional stability by an increase of the axial half-wave numbers. This result is also achieved for the second figure. Additionally, by comparing Figs. 2b and 5b, it is interesting to say that whenever the circumferential half-wave number is selected bigger, the negative slope of curves of results which is related to the lower axial wave numbers, is steeper. On the other side, Fig. 5c illustrates that even powerful and high magnetic environments cannot affect the torsional stability of the nano-composite shell while the circumferential half-wave number is large. Either way, about the effect of the magnetic surrounding on the circumferential wave numbers, it can be said that the strong magnetic field affects the shell's stability if and only if the circumferential half-wave number is small.

In order to consider the effect of a three-dimensional magnetic field versus other magnetic fields, initially, the axial half-wave number is investigated while the magnetic potential is for two cases, weak and powerful magnetic fields which are shown by Fig. 6a and b respectively. From the first figure, as it is vividly seen, when the magnetic field three-dimensionally affected the model, the torsional stability capacity of the shell is lower. But, on the other hand, when the effect is two-dimensional as well as while the transverse effect (B_z=0) is neglected, the highest stability for the nano-shell is predicted. This means that the transverse magnetic effect makes weaker the composite shell under torsional conditions. By comparing the results of three cases of one-dimensional magnetic effect, one can find that on the torsional stability of nano-shells, the transverse magnetic effect (B_z=0), circumferential magnetic effect (B_θ=0) and axial magnetic effect (B_x=0) respectively are making the model weaker under torsion. This can prove that the effect of transverse magnetic is more significant than the others. It is also worth mentioning that when we have a three-dimensional magnetic effect; the stability is further than when there is a two-axis effect by assuming B_x=0. It is also interesting to note that by the increase of the axial half-wave numbers the importance of analysis of magnetic effect in various directions can be demonstrated. In fact, this can be in light of the increase in the distances between the results of various cases in the diagram by the increase of the wave numbers. Moreover, after looking into the second plotted figure, it can be clearly seen that the second diagram also approves the

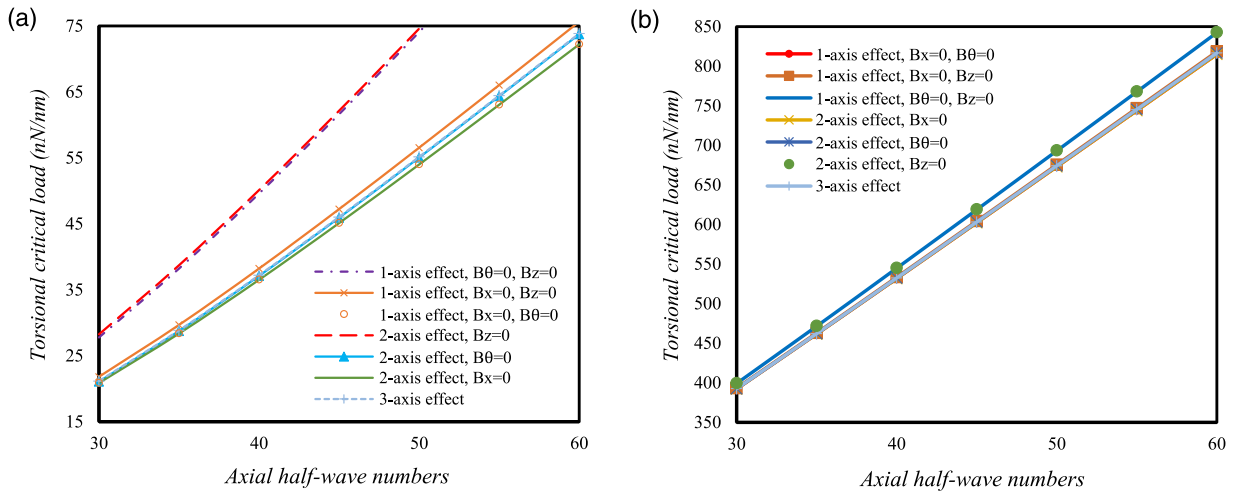

Fig. 6. **(a)** The axial half-wave number vs. three-axis magnetic influences (e_0a=0.5 nm, l^*=0.5, n = 1, ψ=0.1A). **(b)** The axial half-wave number vs. three-axis magnetic influences (e_0a=0.5 nm, l^*=0.5, n = 1, ψ=100A).

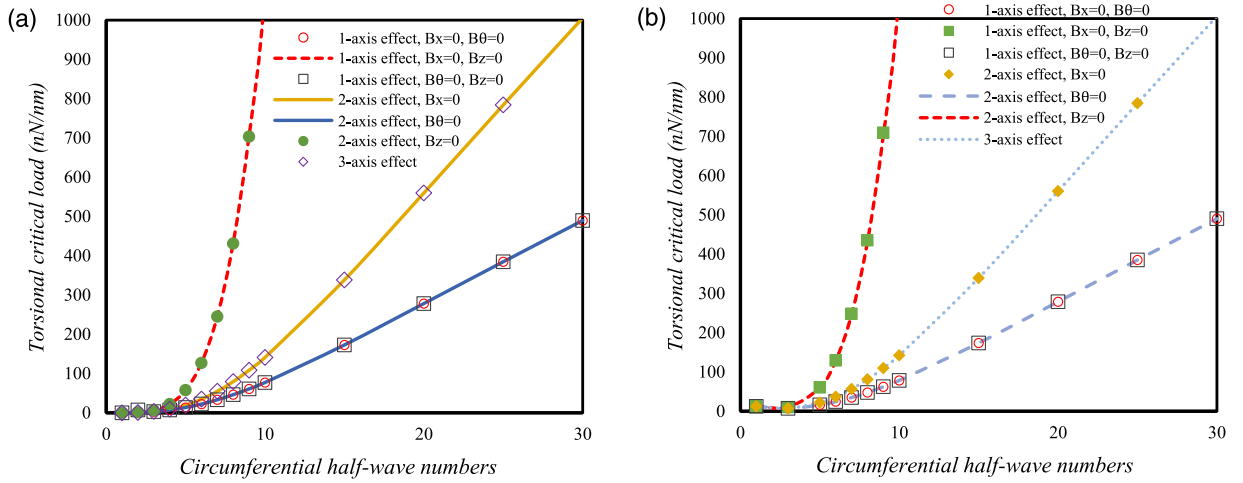

Fig. 7. **(a)** The circumferential half-wave number vs. three-axis magnetic influences (e_0a=0.5 nm, l^*=0.5, m = 1, ψ=0.1A). **(b)** The circumferential half-wave number vs. three-axis magnetic influences (e_0a=0.5 nm, l^*=0.5, m = 1, ψ=100A).

significance of the transverse magnetic effect in a magneto-elastic analysis. The analysis of the high magnetic environment which is appeared by the second figure presents that in a high potential magnetic field, the effect of direction for magnetic potential is lesser. To conclude, these two figures confirmed that even in a nanoscale the direction of magnetic influences is very important.

Fig. 7a and b respectively exhibit the influence of an increase of the circumferential half-wave number under different cases of the magnetic field, first, in a weak magnetic condition and second for a high magnetic condition. First off, in comparison of these two figures with the Fig. 6a and b, one can find that the increase of the circumferential half-wave numbers increases dramatically the importance of the different magnetic fields. In other words, whatever the circumferential wave numbers increased, the results in the figures have become far from each other by a very steep slope. Consequently, in very large circumferential wave numbers, the direction of the magnetic field is seriously important. Furthermore, as shown in the figures, for lower circumferential half-wave numbers, the directions of the magnetic field cannot be considerable.

5. Conclusions

This paper performed a study on the torsional resistance of the nano-composite shell under a three-dimensional magnetic field based on the first-order shear deformation shell approach in combining with the nonlocal theory of strain gradient. In order to take the numerical findings, an analytical approach was used. After validation of numerical outcomes, the role of key parameters was investigated on the torsional behavior of the shell. According to the remarkable findings, some notes are summarized as below

- In a three-dimensional magnetic analysis of the nano-composite shell, the most important magnetic effect can be for the transverse effect.
- While the larger amounts of circumferential half-wave numbers are considered, it is very important to study the three-dimensional magnetic field.
- The influence of the magnetic environment is more remarkable for the larger axial half-wave numbers.
- The larger amounts of the strain gradient parameter, the smaller the effect of magnetic potential.
- The higher values of the axial half-wave number, the higher the impact of the magnetic potential in a nonlocal domain.

Acknowledgements

The second and third authors acknowledge the support by grant 14.Z50.31.0036 awarded to R. E. Alekseev Nizhny Novgorod Technical University by Department of Education and Science of the Russian Federation.

Appendix A

$$K_{11} = -\mathrm{A}_{11}\left(\frac{m\pi}{L}\right)^2 - \frac{\mathrm{A}_{44}n^2}{R^2}$$
$$K_{12} = \frac{\mathrm{A}_{12}}{R}\frac{m\pi\, n}{L} + \frac{\mathrm{A}_{44}}{R}\frac{m\pi\, n}{L}$$
$$K_{13} = \frac{\mathrm{A}_{12}}{R}\frac{m\pi}{L}$$

$$K_{21} = \frac{\mathrm{A}_{44}}{R}\frac{m\pi\, n}{L} + \frac{\mathrm{A}_{21}}{R}\frac{m\pi\, n}{L} + \frac{\mathrm{A}_{44}l^2 n}{R}\left(\frac{m\pi}{L}\right)^3 + \frac{\mathrm{A}_{21}l^2 n}{R}\left(\frac{m\pi}{L}\right)^3 + \frac{\mathrm{A}_{44}l^2 n^3}{R^3}\frac{m\pi}{L} + \frac{\mathrm{A}_{21}l^2 n^3}{R^3}\frac{m\pi}{L}$$
$$K_{22} = -\mathrm{A}_{44}\left(\frac{m\pi}{L}\right)^2 - \frac{\mathrm{A}_{22}n^2}{R^2} - \frac{A_{66}}{R^2} - \mathrm{A}_{44}l^2\left(\frac{m\pi}{L}\right)^4 - \frac{\mathrm{A}_{22}l^2n^2}{R^2}\left(\frac{m\pi}{L}\right)^2 - \frac{l^2A_{66}}{R^2}\left(\frac{m\pi}{L}\right)^2$$
$$- \frac{\mathrm{A}_{44}l^2n^2}{R^2}\left(\frac{m\pi}{L}\right)^2 - \frac{\mathrm{A}_{22}l^2n^4}{R^4} - \frac{l^2A_{66}n^2}{R^4}$$
$$K_{23} = -\frac{\mathrm{A}_{22}n}{R^2} - \frac{l^2\mathrm{A}_{22}n}{R^2}\left(\frac{m\pi}{L}\right)^2 - \frac{l^2\mathrm{A}_{22}n^3}{R^4} - \frac{A_{66}n}{R^2} - \frac{l^2A_{66}n}{R^2}\left(\frac{m\pi}{L}\right)^2 - \frac{l^2A_{66}n^3}{R^4}$$
$$K_{25} = \frac{A_{66}}{R} + \frac{l^2A_{66}}{R}\left(\frac{m\pi}{L}\right)^2 + \frac{l^2A_{66}n^2}{R^3}$$
$$K_{26} = \frac{X_{23}n}{R}$$

$$K_{31} = \frac{\mathrm{A}_{21}}{R}\frac{m\pi}{L} + \frac{l^2\mathrm{A}_{21}}{R}\left(\frac{m\pi}{L}\right)^3 + \frac{l^2\mathrm{A}_{21}n^2}{R^3}\frac{m\pi}{L}$$
$$K_{32} = -\frac{A_{66}n}{R^2} - \frac{A_{66}l^2n}{R^2}\left(\frac{m\pi}{L}\right)^2 - \frac{A_{66}l^2n^3}{R^4} - \frac{\mathrm{A}_{22}n}{R^2} - \frac{\mathrm{A}_{22}l^2n}{R^2}\left(\frac{m\pi}{L}\right)^2 - \frac{\mathrm{A}_{22}l^2n^3}{R^4}$$
$$K_{33} = -N^0_{xx}\left(\frac{m\pi}{L}\right)^2 - \mu N^0_{xx}\left(\frac{m\pi}{L}\right)^4 - \frac{\mu n^2}{R^2}N^0_{xx}\left(\frac{m\pi}{L}\right)^2 - \frac{2}{R}N^0_{x\theta}\frac{m\pi\, n}{L} - \frac{2\mu n}{R}N^0_{x\theta}\left(\frac{m\pi}{L}\right)^3$$
$$- \frac{2\mu n^3}{R^3}N^0_{x\theta}\frac{m\pi}{L} - A_{55}\left(\frac{m\pi}{L}\right)^2 - \frac{A_{66}n^2}{R^2} - A_{55}l^2\left(\frac{m\pi}{L}\right)^4 - \frac{A_{66}l^2n^2}{R^2}\left(\frac{m\pi}{L}\right)^2 - \frac{A_{55}l^2n^2}{R^2}\left(\frac{m\pi}{L}\right)^2$$
$$- \frac{A_{66}l^2n^4}{R^4} - \frac{\mathrm{A}_{22}}{R^2} - \frac{\mathrm{A}_{22}l^2}{R^2}\left(\frac{m\pi}{L}\right)^2 - \frac{\mathrm{A}_{22}l^2n^2}{R^4}$$
$$K_{34} = -A_{55}\frac{m\pi}{L} - A_{55}l^2\left(\frac{m\pi}{L}\right)^3 - \frac{A_{55}l^2n^2}{R^2}\frac{m\pi}{L}$$
$$K_{35} = \frac{A_{66}n}{R} + \frac{A_{66}l^2n}{R}\left(\frac{m\pi}{L}\right)^2 + \frac{A_{66}l^2n^3}{R^3}$$
$$K_{36} = X_{21}\left(\frac{m\pi}{L}\right)^2 + \frac{X_{23}n^2}{R}$$

$$\mathrm{K}_{43} = -A_{55}\frac{m\pi}{L}$$

$$K_{44} = -D_{11}\left(\frac{m\pi}{L}\right)^2 - \frac{D_{66}n^2}{R^2} - A_{55}$$
$$K_{45} = \frac{D_{12}n}{R}\frac{m\pi}{L} + \frac{D_{66}n}{R}\frac{m\pi}{L}$$
$$K_{46} = X_{35}\frac{m\pi}{L} + X_{21}\frac{m\pi}{L}$$

$$K_{52} = \frac{A_{66}}{R} + \frac{A_{66}l^2}{R}\left(\frac{m\pi}{L}\right)^2 + \frac{A_{66}l^2n^2}{R^3}$$
$$K_{53} = \frac{A_{66}n}{R} + \frac{A_{66}l^2n}{R}\left(\frac{m\pi}{L}\right)^2 + \frac{A_{66}l^2n^3}{R^3}$$
$$K_{54} = \frac{D_{66}n}{R}\frac{m\pi}{L} + \frac{D_{21}n}{R}\frac{m\pi}{L} + \frac{l^2D_{66}n}{R}\left(\frac{m\pi}{L}\right)^3 + \frac{l^2D_{21}n}{R}\left(\frac{m\pi}{L}\right)^3 + \frac{l^2D_{66}n^3}{R^3}\frac{m\pi}{L} + \frac{l^2D_{21}n^3}{R^3}\frac{m\pi}{L}$$
$$K_{55} = -D_{66}\left(\frac{m\pi}{L}\right)^2 - \frac{D_{22}n^2}{R^2} - A_{66} - l^2D_{66}\left(\frac{m\pi}{L}\right)^4 - \frac{l^2D_{22}n^2}{R^2}\left(\frac{m\pi}{L}\right)^2 - A_{66}l^2\left(\frac{m\pi}{L}\right)^2 - \frac{l^2D_{66}n^2}{R^2}\left(\frac{m\pi}{L}\right)^2 - \frac{l^2D_{22}n^4}{R^4} - \frac{A_{66}l^2n^2}{R^2}$$
$$K_{56} = -\frac{X_{63}n}{R} - X_{23}n$$

$$K_{61} = -X_{34}\frac{m\pi}{L}$$
$$K_{62} = \frac{X_{63}n}{R} - \frac{X_{23}n}{R}$$
$$K_{63} = -X_{21}\left(\frac{m\pi}{L}\right)^2 - \frac{X_{23}n^2}{R} + \frac{X_{63}}{R}$$
$$K_{64} = -X_{21}\frac{m\pi}{L} - X_{35}\frac{m\pi}{L}$$
$$K_{65} = X_{23}n + \frac{X_{64}}{R}n$$
$$K_{66} = -Y_{22}n^2 - Y_{11}\left(\frac{m\pi}{L}\right)^2 - Y_{33}$$

References

Akbarzadeh Khorshidi, M. (2018). The material length scale parameter used in couple stress theories is not a material constant. *International Journal of Engineering Science, 133*, 15–25.

Akgöz, B., & Civalek, Ö. (2012). Free vibration analysis for single-layered graphene sheets in an elastic matrix via modified couple stress theory. *Materials & Design, 42*, 164–171.

Arefi, M., Kiani, M., & Rabczuk, T. (2019). Application of nonlocal strain gradient theory to size dependent bending analysis of a sandwich porous nanoplate integrated with piezomagnetic face-sheets. *Composites Part B: Engineering, 168*, 320–333.

Chowdhurry, A. N. R., Wang, C. M., & Koh, S. J. A. (2014). Continuum shell model for buckling of armchair carbon nanotubes under compression or torsion. *International Journal of Applied Mechanics, 6*(1), 1450006.

Elimelech, M., Gregory, J., Jia, X., & Williams, R. A. (1995). Chapter 15 - Application of simulation techniques to colloidal dispersion systems. *Particle Deposition & Aggregation, Measurement, Modelling and Simulation*, 402–425. doi:10.1016/B978-075067024-1/50015-7.

Eringen, A. C. (1983). On differential equations of nonlocal elasticity and solutions of screw dislocation and surface waves. *Journal of Applied Physics, 54*(9), 4703–4710.

Farajpour, A., Ghayesh, M. H., & Farokhi, H. (2019). Nonlocal nonlinear mechanics of imperfect carbon nanotubes. *International Journal of Engineering Science, 142*, 201–215.

Gholami, R., & Ansari, R. (2017). A unified nonlocal nonlinear higher-order shear deformable plate model for postbuckling analysis of piezoelectric-piezomagnetic rectangular nanoplates with various edge supports. *Composite Structures, 166*, 202–218.

Gholami, R., Darvizeh, A., Ansari, R., & Sadeghi, F. (2016). Vibration and buckling of first-order shear deformable circular cylindrical micro-/nano-shells based on Mindlin's strain gradient elasticity theory. *European Journal of Mechanics - A/Solids, 58*, 76–88.

Ghorbanpour Arani, A., Abdollahian, M., Kolahchi, R., & Rahmati, A. H. (2013). Electro-thermo-torsional buckling of an embedded armchair DWBNNT using nonlocal shear deformable shell model. *Composites: Part B, 51*, 291–299.

Han, Q., & Lu, G. (2003). Torsional buckling of a double-walled carbon nanotube embedded in an elastic medium. *European Journal of Mechanics A/Solids, 22*(6), 875–883.

Hao, M. J., Guo, X. M., & Wang, Q. (2010). Small-scale effect on torsional buckling of multi-walled carbon nanotubes. *European Journal of Mechanics A/Solids, 29*(1), 49–55.

Jeong, B.-W., Lim, J.-K., & Sinnott, S. B. (2007). Elastic torsional responses of carbon nanotube systems. *Journal of Applied Physics, 101*, 084309.

Karami, B., Shahsavari, D., & Janghorban, M. (2019). On the dynamics of porous doubly-curved nanoshells. *International Journal of Engineering Science, 143*, 39–55.

Khademolhosseini, F., Rajapakse, R. K. N. D., & Nojeh, A. (2010). Torsional buckling of carbon nanotubes based on nonlocal elasticity shell models. *Computational Materials Science, 48*(4), 736–742.

Kok, Z. K. J., & Wong, C. H. (2016). Molecular dynamics simulation studies of mechanical properties of different carbon nanotube systems. *Molecular Simulation, 42*(15), 1274–1280.

Lim, C. W., Zhang, H., & Reddy, J. N. (2015). A higher-order nonlocal elasticity and strain gradient theory and its applications in wave propagation. *Journal of the Mechanics and Physics of Solids, 78*, 298–313.
Lu, Y. J., & Wang, X. (2006). Combined torsional buckling of multi-walled carbon nanotubes. *Journal of Physics D: Applied Physics, 39*(15), 3380–3387.
Lurie, S., & Solyaev, Y. (2019a). On the formulation of elastic and electroelastic gradient beam theories. *Continuum Mechanics and Thermodynamics, 31*(6), 1601–1613.
Lurie, S., & Solyaev, Y. (2019b). Anti-plane inclusion problem in the second gradient electroelasticity theory. *International Journal of Engineering Science, 144*, 103129.
Malikan, M. (2017). Electro-mechanical shear buckling of piezoelectric nanoplate using modified couple stress theory based on simplified first order shear deformation theory. *Applied Mathematical Modelling, 48*, 196–207.
Malikan, M., Dimitri, R., & Tornabene, F. (2019). Transient response of oscillated carbon nanotubes with an internal and external damping. *Composites Part B: Engineering, 158*, 198–205.
Malikan, M., & Nguyen, V. B. (2018). Buckling analysis of piezo-magnetoelectric nanoplates in hygrothermal environment based on a novel one variable plate theory combining with higher-order nonlocal strain gradient theory. *Physica E: Low-dimensional Systems and Nanostructures, 102*, 8–28.
Mehralian, F., Tadi Beni, Y., & Karimi Zeverdejani, M. (2017). Nonlocal strain gradient theory calibration using molecular dynamics simulation based on small scale vibration of nanotubes. *Physica B: Physics of Condensed Matter, 514*, 61–69.
Mikhasev, G., & Nobili, A. (2019). On the solution of the purely nonlocal theory of beam elasticity as a limiting case of the two-phase theory. *International Journal of Solids and Structures*. doi:10.1016/j.ijsolstr.2019.10.022.
Mikhasev, G. I., Eremeyev, V. A., Wilde, K., & Maevskaya, S. S. (2019). Assessment of dynamic characteristics of thin cylindrical sandwich panels with magnetorheological core. *Journal of Intelligent Material Systems and Structures, 30*(18–19), 2748–2769.
Natsuki, T., Tsuchiya, T., Ni, Q. Q., & Endo, M. (2010). Torsional elastic instability of double-walled carbon nanotubes. *Carbon, 48*(15), 4362–4368.
Parvaneh, V., Shariati, M., Torabi, H., Masood, A., & Sabeti, M. (2012). Torsional buckling behavior of SWCNTs using a molecular structural mechanics approach considering vacancy defects. *Fullerenes, Nanotubes and Carbon Nanostructures, 20*(8), 709–720.
Reddy, J. N. (2007). Nonlocal theories for bending, buckling and vibration of beams. International Journal of Engineering Science, *45*(2–8), 288–307.
Sahmani, S., & Aghdam, M. M. (2017). Nonlinear instability of axially loaded functionally graded multilayer graphene platelet-reinforced nanoshells based on nonlocal strain gradient elasticity theory. *International Journal of Mechanical Sciences, 131–132*, 95–106.
Sahmani, S., & Aghdam, M. M. (2018). Nonlocal strain gradient shell model for axial buckling and postbuckling analysis of magneto-electro-elastic composite nanoshells. *Composites Part B: Engineering, 132*, 258–274.
She, G.-L., Yuan, F.-G., Karami, B., Ren, Y.-R., & Xiao, W.-S. (2019). On nonlinear bending behavior of FG porous curved nanotubes. *International Journal of Engineering Science, 135*, 58–74.
Shen, H.-S., & Zhang, C.-L. (2010). Torsional buckling and postbuckling of double-walled carbon nanotubes by nonlocal shear deformable shell model. *Composite Structures, 92*(5), 1073–1084.
Shojaeefard, M. H., Mahinzare, M., Safarpour, H., Saeidi Googarchin, H., & Ghadiri, M. (2018). Free vibration of an ultra-fast-rotating-induced cylindrical nano-shell resting on a Winkler foundation under thermo-electro-magneto-elastic condition. *Applied Mathematical Modelling, 61*, 255–279.
Solyaev, Y., & Lurie, S. (2019). Pure bending of a piezoelectric layer in second gradient electroelasticity theory. *Acta Mechanica, 230*(12), 4197–4211.
Solyaev, Y., Lurie, S., Koshurina, A., Dobryanskiy, V., & Kachanov, M. (2019). On a combined thermal/mechanical performance of a foam-filled sandwich panels. *International Journal of Engineering Science, 134*, 66–76.
Song, H.-Y., & Zha, X.-W. (2011). Molecular dynamics study of effects of nickel coating on torsional behavior of single-walled carbon nanotube. *Physica B, 406*(4), 992–995.
Wang, Q., Quek, S. T., & Varadan, V. K. (2007). Torsional buckling of carbon nanotubes. *Physics Letters A, 367*(1–2), 135–139.
Wang, X., Yang, H. K., & Dong, K. (2005). Torsional buckling of multi-walled carbon nanotubes. *Materials Science and Engineering A, 404*(1–2), 314–322.
Xiaohu, Y., Yugang, S., & Hanzhou, L. (2013). Combined torsional buckling of carbon nanotubes subjected to thermo-electro-mechanical loadings with consideration of scale effect. *Key Engineering Materials, 562-565*, 744–749.
Yang, H. K., & Wang, X. (2007). Torsional buckling of multi-wall carbon nanotubes embedded in an elastic medium. *Composite Structures, 77*(2), 182–192.
Zhang, C.-L., & Shen, H.-S. (2006). Buckling and postbuckling analysis of single-walled carbon nanotubes in thermal environments via molecular dynamics simulation. *Carbon, 44*(13), 2608–2616.
Zhang, Q. W., & Li, B. (2015). Torsional behavior of single-walled carbon nanotubes. *Carbon, 94*, 826–835.
Zhang, Y. Y., & Wang, C. M. (2008). Torsional responses of double-walled carbon nanotubes via molecular dynamics simulations. *Journal of Physics: Condensed Matter, 20*(45), 455214.